Jessica Llop Castelbou

"Rhodium nanoparticles stabilised by phosphorus based ligands. Synthesis, characterisation and application in selective hydrogenations"

DOCTORAL THESIS

Supervised by

Dr. Cyril Godard and Prof. Carmen Claver Cabrero

Departament de Química Física I Inorgànica

UNIVERSITAT ROVIRA I VIRGILI

Tarragona, 2014

**Universitat
ROVIRA I VIRGILI**

Departament de Química
Física i Inorgànica
Campus Sescelades
Carrer Marcel·lí Domingo s/n
43007 Tarragona
Tel. 977559575
Fax. 977559563

Dr. Cyril Godard,

Faig constar:

Que el present treball, titulat "Rhodium nanoparticles stabilized by phosphorus based ligands. Synthesis, characterisation and application in selective hydrogenations", que presenta Jessica Llop Castelbou per a l'obtenció del títol de Doctor, ha estat realitzat sota la meva direcció i la co- dirección de la Prof. Dra. Carmen Claver Cabrero, al Departament de Química Físca i Inorgànica i que acompleix els requeriments per poder optar a Menció Internacional.

Tarragona, 4 de juliol de 2014

Dr. Cyril Godard   Prof. Carmen Claver Cabrero

AGRAÏMENTS

La part més difícil de la tesi, intentaré ser breu, encara que ara que s'acaba aquesta etapa tan intensa crec que és necessari agraïr.

En primer lugar a Carmen, la que ha hecho posible que esté escribiendo esto. Gracias por darme la oportunidad de entrar en tu grupo y por enseñarme tanto. Siempre he pensado que eres todo un ejemplo que las mujeres podemos en este mundo de hombres. Siempre con tu vitalidad, energía, diplomacia, agilidad, capacidad resolutiva y positividad tan necesaria.

Cyril gracias por guiar y dirigir este proyecto. Gracias por la paciencia, por querer mirar más allá y buscar solución a todo lo que nos hemos ido encontrando. Por querer siempre un punto más, he aprendido mucho! Disfruta mucho de la bonita etapa que inicias.

Aitor gracias por ayudarme tanto! Al principio por enseñarme todo y después por estar siempre disponible para mis dudas hasta desde la otra punta, te deseo toda la suerte!

Ali, que suerte tenerte en el labo, gracias por tu amabilidad y comprensión siempre.

Al resto de profesores que también me han animado siempre que han tenido ocasión, Aurora, Elena, Anna Mª. Sergio, gracias por tu amabilidad siempre.

Merci aussi a LCOMS, pour les deux mois fantastiques que j'ai passé avec vous. Mostafa Taoufik merci pour la confiance et l'amabilité. Nicolas merci pour ta pacience et m'aider tellement! Teresa, mi bella portuguesa, gracias! També tenen un paper important els tècnics, gracies Ramón i Francesc per sempre mostrar interés. I als que es converteixen en amics, a la més bonica del servei, gràcies Rita! A la resta de l'unitat de microscopia Mercè, Núria, Mariana i Lukas.

Als meus estimats "veteranos", Javi siempre seré tu personaje, Oriol gràcies per l'amabilitat i paciencia sobre tot al principi, Cris Pubill la bateana més simpàtica. Vero la millor companya de vitrina que podia tenir, l'esforç i constancia personificat, tot un honor haver compartit tants moments dins i fora del labo. Angy mi nano-compañera, gracias por introducirme en el

mundo oscuro jeje un placer todo lo que hemos compartido! Amadeu, que al segon dia ja era la pebels i he passat per tots els apodos, gràcies pel carinyo! Cristy, quants anys ja! Per tantes coses, pels balls entre vitrines, pels ànims, per ser tant autèntica! Jessi, també molts anys, ara que el camí es bifurca, et desitjo molta sort. I la més veterana que tenim la sort de tenir encara, gracies Mercè, la nostra mami, sempre tant atenta amb mi i el meu voltant.

A tot el grup de Carmen, Fran benvingut al nanomón, espero que et porti alegries, Alberto ànims amb la síntesi i sort amb el que et queda de tesi. Nanette thanks to always offer your help and your attention, good luck! Al ctqc Bianca, Stefano, Dolores, Mónica, Jordi, por esas cenas autènticas i la coordialidad en lo científico. Jorge gracias por siempre estar dispuesto a ayudarme, ese colombiano bailarín, ánimo para la recta final.

A la Raquel, més que una tècnica, gràcies per la teva simpatia i disponibilitat.

A les noves incorporacions, sort en l'inici d'aquesta etapa, Marc, Núria, Maria, Olga, Toni i Jordi.

Als membres dels altres grups, perque convivim tant bé i feu el dia a dia més fantàstic! Gerard el recordador d'aniversaris jeje sort en la etapa final! Xavi ànims amb el bor! Enrico buona fortuna. Laia un encant de super crítica ;-). Marc gràcies per estar disposat sempre a xerrar de química o el que sigui, per l'interés, no tinc cap dubte que arribaras lluny, ets un gran químic i persona. Jessica la més bona del seminari, desbordes bones intencions, paciencia i ànims per la resta! Charly, la nostra assistent personal, gràcies pels consells i l'atenció, que be ens ho passem amb el gossip jiji. Emma la bondat en persona, ànims pel que ve i gràcies per les estones compartides. Miriam que també fa molts anys que ens coneixem, disfruta d'aquesta etapa tan bonica que viuras.

A mis estem a tope! Itziar, mi regalo de fin de año, porque coincidimos en la manera de pensar y ver las cosas muchas veces. Gracias por los ánimos, tu positivismo y cariño y por quererla también a mi tesis jeje. Ana que suerte tenerte! Que gran química y que gran persona, te deseo toda la suerte porque te la mereces toda, gracias!

Eli! Perque Zipi no seria res sense Zape, perque 10 anys una al costat de l'altra no ho pot dir qualsevol. Gracies per la paciencia, per aguantar-me fins i tot quan estic realment insoportable, perque Iknowyouloveme i espero tu també ho sapiguis. Saps que estaré aquí igual que ho has estat tu, gràcies!

Mi ismael! Quantes coses que hem passat, un honor compartir aquest tram final. Gràcies per ser tan autèntic, i estar també sempre que ho he necessitat. Creu-te tot el que vals que es molt!

Els no químics que m'han entés i han estat amb mi també.

Michelle cuantos años siendo amigas, por todo lo que hemos compartido porque sea por mucho tiempo más. Blanca, porque un abrazo tuyo vale todos los kilómetros que nos separan, porque seras una gran mami, y las bebitas ya pueden ser 2.0 porque no me pienso perder nada! Muchas gracias a las dos por estar ahí siempre. Anna la reusenca amb el cor més gran, perque fa "poc" que ens coneixem, però sembla que sigui de tota la vida, gracies per estar i entendrem tant!

La Dolce vita, gràcies Alma, Patricia, Maria i Marta. Perque ens coneixem tant i des de fa tant, encantada de reconectar amb vosaltres. Alba perque ets una amiga de les que sempre estan als dits de la mà, gràcies!

Las Premio Revelación Marta, Nerea i Anna, por muchas cenas y vivencias más.

A la meva tati, gràcies Sònia per estar sempre al meu costat, per tenir un gran home, Sergi gràcies per ser tant atent, un nen fantàstic, el Nil el més wapu del món, que em fa treure tants somriures, perque una part de la tesi també es teva ;-) Perque em viscut moltes coses i se que en viurem moltes més.

A mis floretes andaluzas, Laura y Gloria, que bien encontraros en el camino! Borja gracias por creer tanto en mi.

Als meus lyonnais! Nestor el meu veí, gràcies pels nostres sopars, per escoltar-me i recolzar-me, molts ànims si comences l'aventura! Marc, el meu brasiler, disfruta molt, gràcies per tenir sempre la porta oberta i creure tant amb mi!

També a la familia València, que tant de suport, carinyo i respecte m'ha demostrat sempre.

A la meva familia, que tant aprop està sempre de mi i que tant em valora. Gràcies per fer-me sentir que sempre us tinc, per no deixar que decaigui, m'heu demostrat molt en aquests anys una miqueta durs. Espero us hagi demostrat tot el que us estimo. Perque tinc la mare més autèntica, gràcies per poder-te parlar de tot i en qualsevol moment. Joan gràcies per cuidar tant bé de la mama i per ser tant comprensiu. Papa gràcies pel teu gran cor i demostrar-me que estas aquí encara que ens separin uns quilòmetres. Mapi ja saps que sempre dono gràcies que et creuessis al meu camí, ets un àngel. A la peque de casa, Inés, per ser tant atenta, espero que em sentis a prop encara que estigui lluny. Gràcies també a la padri més autèntica, per estar sempre en tots els passos de la meva vida. Als meus iaios, per demostrar-me el que vol dir estimar i fer-me sentir sempre lo orgullosos que esteu de mi, és un honor ser la vostra néta.

A mes grand-parents pour m'aider a grandir et me montrer tant de choses!

À ma famille française tata Sylvia et Thierry, Jean Michel qui sont toujours là mêmme si on est un peut loin.

A la familia Labaila- Barberán que sempre m'ha demostrat carinyo i m'heu fet sentir una més. Salvadora vas marxar massa d'hora i no estàvem preparats, jo només puc dedicar-te la tesis, se que també estas orgullosa de mi.

A la casa de les tres bessones, que m'ha aguantat lo inaguantable. Anna gràcies per tenir paciència amb mi i per intentar entendrem. Segueix així d'autèntica i persegueix el que somies. Raquel, gràcies per la atenció i per entendre el significat, per no necessitar explicacions, creu en tu i a menjar-te el futur. Al meu perrito que a vegades fa més que moltes persones i que m'acompanya en el meu dia a dia.

I gràcies a tu, que has aparegut per posar un asterisc, fer-me somriure, donar-me support i ensenyar-me que puc comptar amb tu.

A tots espero que us hagi demostrat, lo agraïda que em sento de tenir-vos!

TABLE OF CONTENTS

CHAPTER 1: Introduction and objectives

CHAPTER 2. Synthesis and characterisation of Rh-NPs stabilised by phosphine and phosphite ligands

CHAPTER 3. Catalytic hydrogenation of arenes using P-stabilised rhodium nanoparticles

CHAPTER 4: Hydrogenation of aromatic ketones using P-stabilised Ru and Rh nanoparticles

CHAPTER 5: Anchoring of organometallic Rh-NPs onto modified silica: a preliminary study

CHAPTER 6: Conclusions/Summary

CHAPTER 7: Appendix

List of abbreviations

NP: nanoparticle
NPs: nanoparticles
M-NPs: metal-nanoparticles
C-C: carbon-carbon
Nm: nanometers
ILs: ionic liquids
PVP: poly(N-vinyl-2-pyrrolidone)
THF: tetrahydrofuran
TEM: transmission electron microscopy
CNFs: carbon nanofibers
Atm: atmosphere
TON: turn over numbers
TOF: turn over frequencies
TTO: total turn overs
TOA: troctylamine
DOCEA: R-(-)-dioctylcyclohexyl-1-etylamine
Ar_3P: triarylphosphines
Alk_2ArP: dialkylphosphines
AlK_3P: trialkylphosphines
NHC: n- heterocyclic carbenes
HRTEM: High resolution transmission electron microscopy
TEM: transmission electron microscopy
HP-NMR: High pressure nuclear magnetic resonance
NMR: nuclear magnetic resonance
BINAP: 2,2'-bis(diphenylphosphino)-1,1'-binaphthyl)
FILS: functionalisaed ionic liquids
ICP: inductive coupled plasma
XRD: X- Ray diffraction
WAXS: wide angle X-ray scattering
RDF: Radial distribution function
XPS: X-ray photoelectron spectroscopy
TGA: thermogravimetric analysis
Nt: total number of atoms
Ns: number of surface atoms
Nb: number of bulk atoms
V: volumen

Na: number of avogadro
ρ: density
Fcc: face centered cubic
Hcp: hexagonal close packed
VHH: Van hardevel hartod
Dppb: diphenylphosphino butane
GC- Ms: gas phase mass spectroscopy
FTT: Fourier transform
IR: infra- red
TBA: tetrabutylammonium
HEA: N,N-dimethyl-N-cetyl-N-(2-hydroxyethyl)ammonium
BMI: 1-n-butyl-3-methylimidazolium
COD: cyclooctadiene
COT: cyclooctatriene
Sc: supercritic
PEG: polyethylene glicol
BMIM 1-butyl-3-methylimidazolium
CD cyclodextrins
SD substitution degree
EXAFS: extended X-ray absorption fine structure
Tf trifluoroethanesulfonamide
IPr: isopropyl
UHV: ultra high vacuum
SOMC: surface organometallic chemistry
SiO_2 : silica
CPMAS: Cross polarisation magic angle spinning
DRIFT: diffuse reflectance infrared fourier transform

A Salvadora

Chapter 1.

Introduction and objectives
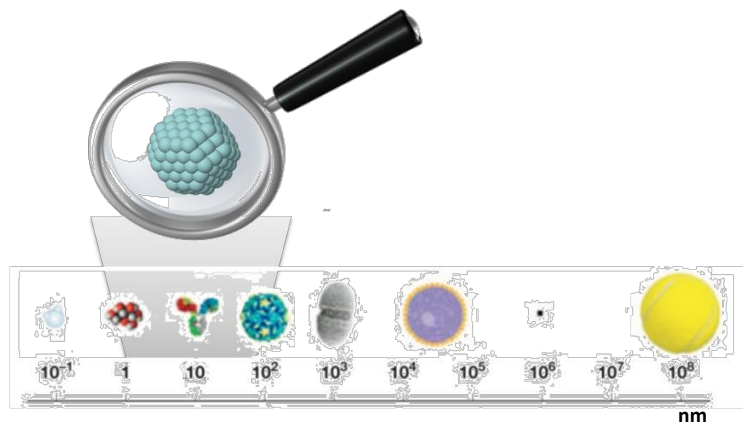
1.1 Soluble metal nanoparticles

Metal nanoparticles are currently an area of intense scientific research, due to a wide variety of potential applications in biomedical, optical, electronic and catalytic fields.[1,2] A metallic nanoparticle (M-NPs) is constituted by several metallic atoms and possesses a nanometric dimension, ranging between 1 and 100 nm of diameter. At nanometrical size, atoms and molecules work differently, and provide a variety of surprising and interesting properties that are significantly different from those of molecular species and of bulk materials.

In catalysis, soluble nanoclusters are considered at the frontier between homogeneous and heterogeneous catalysts since they could present the advantages of both: high selectivity by modulation of their surface and catalyst recovery and reuse.

Many types of reactions have already been reported using metal nanoparticles as catalysts such as redox reactions, hydrogenation, oxidation, C-C bond formation processes, etc...[3]

Soluble nanoparticles exhibit several advantages such as high surfaces areas that confer high activity and avoid internal mass transfer limitations. Moreover, these systems are freely rotational and three- dimensional in reaction systems. Therefore, their metal- surface active sites are much more accessible for the reactant molecules, which enhance their activity.[4]

1.2 Stabilisation of metal nanoparticles

Transition-metal nanoclusters are only kinetically stable, since the thermodynamic minimum is the bulk metal.[2] At short interparticle distances and in the absence of any repulsive effect, the Van der Waals forces will attract two metallic particles to each other. There is therefore a tendency for aggregation which leads to the loss of the properties associated with the colloidal state of these metallic particles. For this reason, the use of a stabilising agent is required during their synthesis.

In the next sections, nanocluster stabilisation is discussed in terms of two general categories, the electrostatic and the steric stabilisation.

1.2.1 Steric stabilisation

A schematic representation of the steric stabilisation is shown in Figure 1.1. This stabilisation is based on the steric repulsion of molecules presents at the surface of the particles. Such repulsion can be performed by organic molecules such as polymers or molecules containing coordinating groups in their molecular structure, as these species prevent the particle agglomeration by providing a protective layer at the metallic surface.
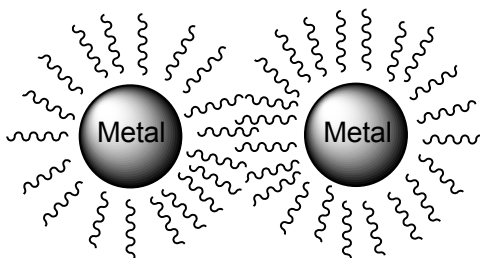
Figure 1.1 Schematic representation of steric stabilization of metal colloid particles.

By contrast with the electrostatic stabilisation, which is mainly used in aqueous media, the steric stabilisation can be used in organic or in aqueous phase.

1.2.2 Electrostatic stabilisation

This type of stabilisation is based on the creation of an ionic environment at the surface of the particles to reinforce the electrostatic repulsion that is represented in Figure 1.2. This is performed through the adsorption of compounds at the surface such as halides, carboxylates or polyoxoanions, dissolved generally in aqueous solution that can generate this stabilisation.[5]
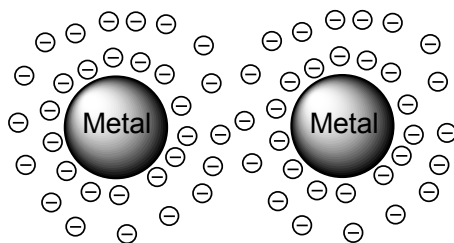
Figure 1.2 Schematic representation of electrostatic stabilization of metal colloid particles.

The presence of these compounds surrounding the metal surface generates an electrical double layer. If the electric potential associated with the double layer is high enough, the electrostatic repulsion will prevent particle agglomeration.

1.2.3 Stabilising agents

Several types of compounds have been reported as efficient stabilisers for soluble nanoparticles. A brief overview of these compounds is described below and some examples are displayed in Figure 1.3. [3]
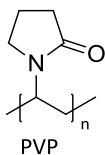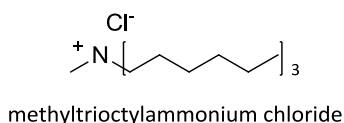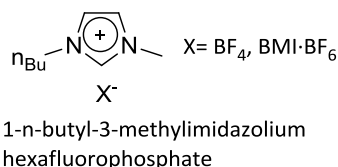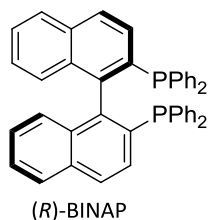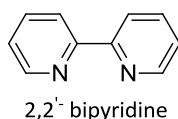
Figure 1.3 Examples of NPs stabilisers used in the literature.

Polymers

Polymers provide stabilisation of metal NPs through the steric bulk of their framework, but also by weakly binding to the NP surface through heteroatom that play the role of ligands. Poly (N-vinyl-2-pyrrolidone) (PVP) is the most used polymer for NP stabilisation.[3] The length of the PVP chains and the interaction with the solvent has an important influence on the particles aggregation.

Surfactants, micelles and microemulsions

The surfactants prevent agglomeration by forming a monomolecular layer around the M-NPs core. Lipophilic surfactants of cationic type such as tetraalkylammonium halides ($R_4N^+X^-$) can give very stable M-NPs.[6] Micelles can also be used as micro-reactors for the growth of particles, forming a confined environment that control their size and distribution.

Ionic liquids

Dupont and co-workers initiated the development of the synthesis of metal nanoparticles in ionic liquids as stabilisers.[7] The stabilisation of M-NPs by these species involves both steric and electrostatic interactions. Another interesting feature of these systems is that they play a double role, as both solvent and stabiliser.[8] M-NPs stabilised by these moieties are employed as catalysts for hydrogenation, oxidation, and C-C couplings reaction for example.[9] Ionic liquids present characteristic physicochemical properties such as ionic mobility, hydrophobicity, miscibility with other organic and inorganic compounds, low vapour pressure or non flammability that made them ideal media for various transformations in solution.[10]

Other small molecules

The introduction of small molecules, which are referred to as ligands in molecular chemistry, as NP stabilisers is of special interest since their properties and effects on the performance of metallic catalysts has been reported in detail for homogeneous systems. This type of stabilisation was reported using species such as phosphines, thiols, amines or carbon monoxide.[11,12] This stabilisation strategy could potentially allow the fine-tuning of the parameters that govern the performance of these nanocatalyst, and the introduction of a chiral protective layer that could open the door to applications in heterogeneous enantioselective catalysis.

1.3 Methods of synthesis of metal nanoparticles

Several synthetic methods for the formation of metallic nanoparticles have been reported and are summarised in the following section.

1.3.1 *Chemical reduction of metal salts*

This synthetic method is the most commonly used and involves the reduction of an ionic salt in an appropriate medium using a reducing agent.[13]

$$M^{n+} X^-_n \xrightarrow{\text{reducing agent}} M^0 \quad + \text{salts}$$
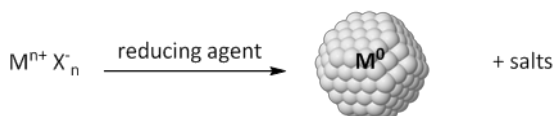
Figure 1.4 Formation of M-NPs by chemical reduction of metal salts.

Different reducing agents can be used to obtain colloidal materials: gases such as hydrogen or carbon monoxide, hydrides or salts such as sodium borohydride or sodium citrate, or even oxidable solvents such as alcohols. This latter case was applied for example by Hirai[14] or Delmas[15], using polymers or oligomers as stabilisers.

The use of metal salts as nanoparticles precursors present several advantages: they are easy to deal with, they are compatible with water and organic solvents and they allow the use of a large choice of stabilising agents and reduction pathways. However, the main disadvantage is the formation of by-products from the initial metal salt or reducing agent that often end up at the surface of the NPs and can modify and/or inhibit their catalytic properties.

1.3.2   Thermal, photochemical or sonochemical decomposition

Many organometallic compounds can be thermally decomposed to their respective zerovalent element.[5] For instance, the synthesis of Pd and Pt organosols by thermolysis of precursors such as palladium acetate, palladium acetylacetonate, or platinum halides have been reported using high boiling point solvents such as methyl-*iso*butylcetone and without stabilising agents, resulting in large particles with broad size distributions.[16] Methods involving photolabile ligands in organometallic complexes that dissociate under UV irradiation were also reported for the synthesis of a wide range of transition metal nanoparticles such as Ag, Au, Ir, Pt, Pd, or Cu NPs (Figure 1.5).[17]

active species generation

$$H_2O \xrightarrow{h\nu} H^{\cdot}, OH^{\cdot}, e^{-}_{s}, H_3O^{+}, H_2, H_2O_2$$

$$OH^{\cdot}(H^{\cdot}) + RH \longrightarrow R^{\cdot} + H_2O \ (H_2)$$

metal reduction

$$M^{n+} \ nR^{\cdot} \longrightarrow M^0 + nR^{\cdot} + nH^+$$

$$M^{n+} \ ne^{-}_{s} \longrightarrow M^0$$

NPs growth $nM^0 \longrightarrow$ **M-NPs**
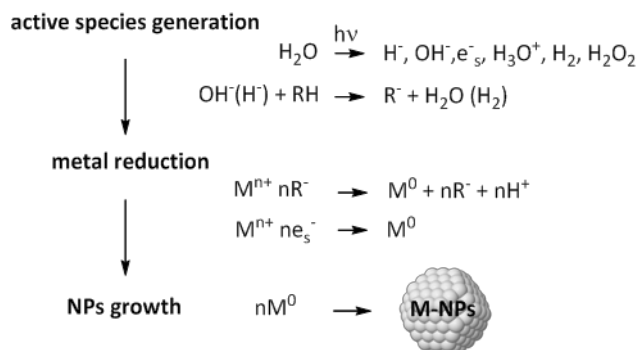
Figure 1.5 Schematic representation of the radiolytic formation of colloidal metals.

Organometallic compounds can also be decomposed into individual atoms in cavitation bubbles by sonication.[18] The main advantage of this method is that gram scale production of NPs can be achieved.

These methodologies afford the formation of M-NPs without the use of additional compounds. However, low control on the size and shape of the resulting nanoparticles is usually obtained using these techniques.

1.3.3   Metal vapour synthesis

The use of metal vapours to synthesise colloidal metals is a very old technique.[19] This method consists in the evaporation at reduced pressure of relatively volatile metals. Subsequent co-condensation of these metals with the vapours of organic solvents at low temperatures yields the M-NPs. In this case, the organic solvents can be considered as stabilising agents.

M
metal evaporation   condensation at low T
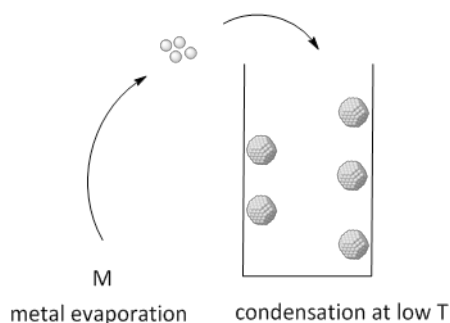
Figure 1.6 Schematic representation of the formation of M-NPs by metal vapour synthesis.[19]

One limitation to this method is that a special reactor is required, which can be either rotating or static. The main disadvantage of the application of this technique is the not control of the size.

1.3.4   Electrochemical method

In this method developed by Reetz and co-workers, the synthesis of metal nanoparticles is carried out with a sacrificial anode as the metal source and

a quaternary ammonium salt is used as electrolyte and stabilising agent.[20] The ions are then reduced at the cathode to yield the metal nanoparticles. Some of the solvents used are THF, acetonitrile or water. The main advantage of this procedure is that the size of the resulting particles can be easily controlled.
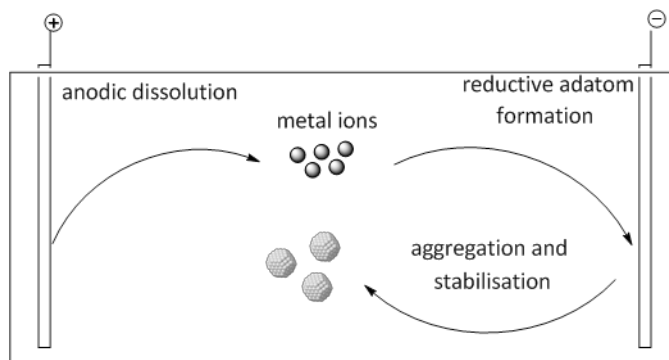
Figure 1.7 Schematic representation of electrochemical formation of M-NPs.[20]

1.3.5   The organometallic approach

This approach was reported by Chaudret and co-workers and takes advantage of the intrinsic reactivity of metal complexes towards ligand displacement or ligand reduction.[21] The ideal precursor is in this case a zerovalent olefinic complex able to be hydrogenated to provide a bare metal atom that condenses in the reaction medium.[22] Precursors such as $[Ru(COD)(COT)]$, $[Rh(\eta^3\text{-}C_3H_5)_3]$, $[Rh(acac)(C_8H_{12})]$, $[Pd(dba)_2]$ were reported for this methodology.[23] The use of a gas such as H_2 or CO in this method yields nanoparticles with "clean surfaces", when compared to other reducing agents such as $NaBH_4$.[24] In this case, the synthesis usually takes place under mild conditions and the size, the shape and the surface environment of the nanoparticle can be controlled. Ligand-protected nanoparticles are synthesised in the presence of substoichiometric quantity of stabiliser. A general scheme for this method is described in Figure 1.8.
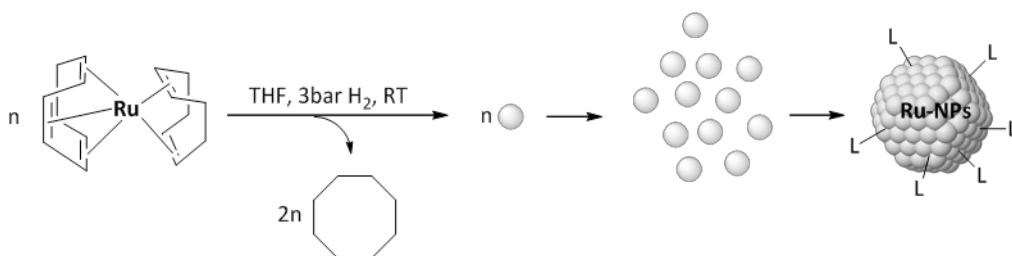
Figure 1.8 Schematic representation of the organometallic approach for the synthesis of metal NPs from [Ru(COD)(COT)].[21]

The main advantage of this method is the control of the metal surface. This synthesis prevents the formation of undesirable interactions at the surface that can affect the reactivity of the NPs and their catalytic properties.

This method was selected for the synthesis of the NPs presented in this work.

1.4 Methods for the anchoring of metal nanoparticles onto a solid support

1.4.1 Brief introduction

Supported metal catalysts can usually be easily separated from the reaction products and recycled and as such, are the most widely used catalysts in industry. For economical and environmental purposes, the catalyst recovery is of crucial importance for sustainable fine chemicals production. However, most of the industrial processes involve metal nanoparticles in a broad range of size and morphologies, which make difficult the subsequent rationalisation of the catalytic results.[25]

One of the aims in this field is therefore the preparation of well- defined supported metal catalysts controlling their size, morphology and composition, which are parameters that affect their catalytic activity.[26]

The main challenge is usually to obtain a highly dispersed catalyst and hence in a highly active form, when expressed as a function of the weight of the active component.[27] This feature of supported catalysts is especially

important with regard to precious metal catalysts, with a more effective use of the metal compared to bulk metal systems.

There are two ways to prepare supported nanoparticles. In one hand, a metal salt component could be dispersed on a support by impregnation adsorption from solution, co- precipitation, or deposition. Secondly, the supported metal salt is converted to a metallic or oxide state by calcinations or reduction.[28]

On the other hand, the nanoparticles could be prepared by the methodologies explained in the previous section and later be anchored onto a solid support through adsorption or grafting of the metal colloids onto supports, or a more sophisticated approach named the Langmuir-Blodgett technique.[29]
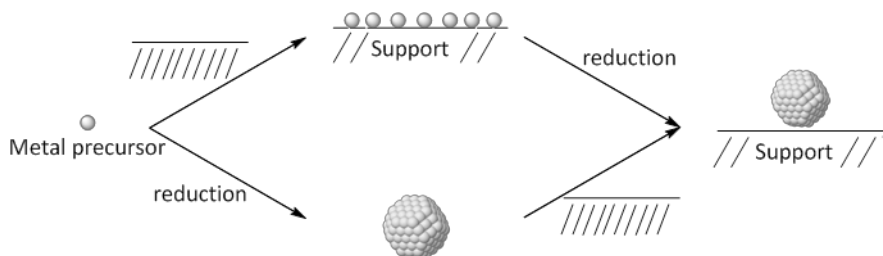
Figure 1.9 Schematic representation of common methodologies supporting of nanoparticles.

Some examples of the techniques reported in the literature for the anchoring of metal nanoparticles will be briefly described in the following section.

1.4.2   Impregnation: direct colloidal deposition

Impregnation is a preparation technique in which a solution containing the metal salt is brought in contact with the support.[30] The solvent is later removed to obtain the supported catalysts. It is the most used methodology to support metal nanoparticles due to the easy synthetic procedure and the

possibility to implement it for various supports and metals. Furthermore, the mild immobilisation conditions used in this approach ensure that nanoparticles retain their original shape and size.

Using this methodology, the dispersion of a pre-stabilised colloidal suspension of Rh-NPs onto silica by impregnation was for instance reported.[31] The nanoparticles were synthesised by reduction of the rhodium chloride precursor with sodium borohydride in the presence of the surfactant HEA- 16Cl as stabiliser (Figure 1.10). The nanoparticles solution was added to a silica suspension in water and after filtration and washing, the supported nanoparticles were obtained. ICP analysis showed that 0.08% Rh in weight was present in this material.
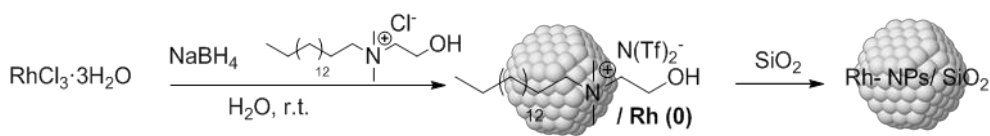
Figure 1.10 One- pot silica- supported Rh-NPs synthesis used by Chaudret and co-workers.[31]

These systems were analysed by TEM, observing an increase in the nanoparticles size from 2.4 to 5 nm after impregnation onto the silica. When used in catalysis, these systems exhibited high activity in the hydrogenation of toluene, anisole and *o*-xylene.

Li and co- workers reported an interesting study on the anchoring of chiral rhodium nanoparticles by impregnation on silica.[32] RhCl$_3$ was dissolved in a surfactant solution (TOAB) and reduced with sodium borohydride in the presence of the chiral phosphine BINAP. The Rh(0) NPs were impregnated on a silica support by stirring the NPs in dichloromethane in the presence of silica. The nanoparticles were uniformly dispersed with a mean diameter of 1.5-2nm. ^{31}P MAS NMR and CO-adsorption IR indicated that the diphosphine ligands were strongly adsorbed onto rhodium surface. These systems were used as catalysts in the hydroformylation of alkenes and exhibited high regioselectivity and chiral inductivities up to 26% and 59% when styrene and vinyl acetate were the substrates, respectively. The

authors proposed a surface mechanism where the active species coordinate and the enantioselective reaction is performed to yield the hydroformylated product. However, as it will be developed in section 1.6 of this thesis the real nature of the catalyst could be controversial. Philippot and co-workers explained that the observation of similar activities, compared to molecular complexes, and the effects produced by the addition of ligands or the variation of the reaction conditions could indicate the formation of homogeneous rhodium species during reaction.[33]

This methodology is also employed with other supports such as carbon materials.[34] For instance, Nagashima and co- workers reported the use of carbon nanofibers (CNFs) with controlled nanostructures consisting of stacked graphene sheets as support for Rh-NPs.[35]
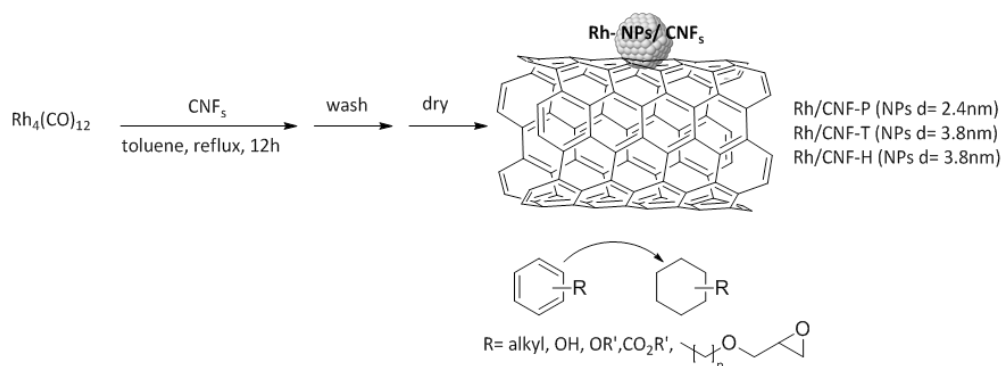
Figure 1.11 Synthetic methodology for the preparation of Rh/CNF$_s$ reported by Nagashima and co- workers.[35]

In this study, the Rh-NPs were synthesised in situ by thermal decomposition of $Rh_4(CO)_{12}$ in the presence of three types of carbon nanofibers (Figure 1.11). TEM microscopy showed the formation of small and well dispersed nanoparticles of 2.4-3.8 nm diameter at the surface in all the CNFs. The Rh-NPs were well anchored onto the support as observed by TEM and no leaching was observed during catalysis. These systems were used as catalysts in the hydrogenation of aromatic compounds under mild

conditions and the selective hydrogenation of the phenyl groups contained in aromatic epoxides was achieved.

1.4.3 Langmuir-Blodgett deposition

The Langmuir-Blodgett (LB) technique is one of the powerful tools for fabricating monolayers of nanoscopic structures on various supports.[29]
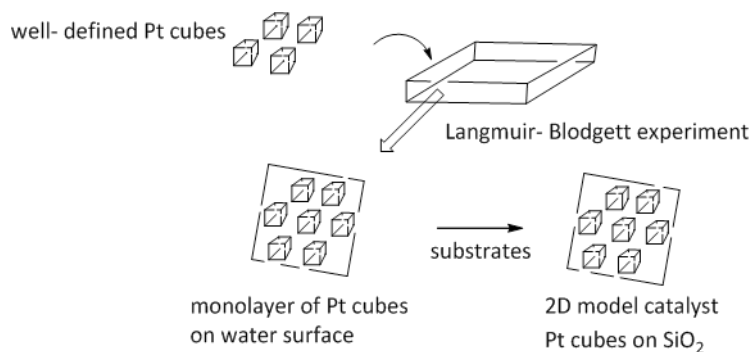
Figure 1.12 Schematic representation of Langmuir- Blodgett method.[36]

Using this technique, monodisperse NPs with uniform size and shape can be deposited as a two- dimensional film, which makes this technique optimal for technological application.

For instance, Somorjai and co- workers synthesised a series of Rh-NPs stabilised by polyvinylpyrrolidone (PVP) with narrow size distributions (2-11 nm) and deposited them on silicon wafers by Langmuir-Blodgett deposition and used as catalysts for CO oxidation.[36]

Both impregnation and Langmuir- Blodgett deposition techniques provide a successful anchoring of M-NPs onto various types of supports. However, impregnation can be easily applied for the simplicity of the synthetic procedure while the Langmuir-Blodgett deposition requires more sophisticated equipment.

1.5 Application of soluble metal nanoparticles in catalysis

As previously mentioned, the properties of soluble nanoparticles such as high surface area or increased substrate accessibility to the active sites due to their free rotation and three dimensional disposition make them of high interest and to date, metal nanoparticles revealed to be efficient catalysts in a large number of processes that were typically performed using homogeneous or supported catalysts. However, the nature of the "true" active catalytic specie remains in some cases controversial.[3,5,37,]

For instance, the use of Pd-NPs in C-C coupling reactions is nowadays extensively reported,[38,39] but in most cases, the true active species was shown to be molecular species[40,41] or small cluster catalysts[42] (Figure 1.13).
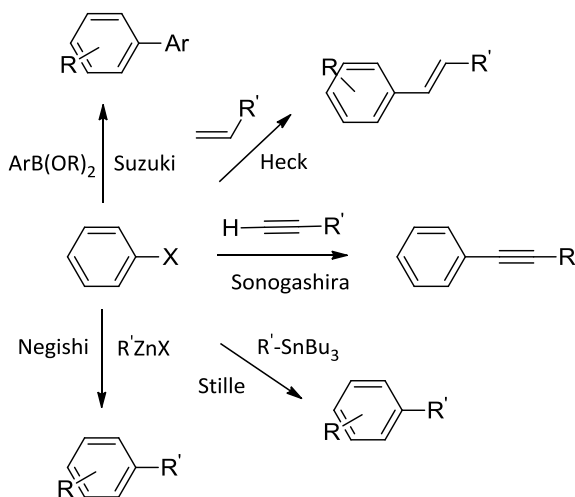
Figure 1.13 Pd-NPs catalysed C-C bond formation reactions.[38]

Nanoparticles are also applied in hydrosilylation reaction that is one of the most important ways to prepare silicone polymers.[5] For example, Schmid and co- workers used Pt-NPs to catalyse the hydrosilylation of oct-1-ene with heptamethyltrisiloxane (HMTS) (Figure 1.14).[43] The final product was obtained with a good selectivity after 24h. The results were compared with bimetallic Pt/Au and Pt/Pd supported on alumina.
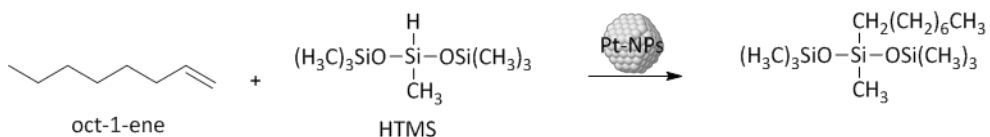
Figure 1.14 Hydrosilylation of oct-1-ene with Pt-NPs.[43]

The use of soluble M-NPs as catalysts for hydrogenation reactions of terminal, internal or cyclic olefins has been widely studied.[44] These systems have shown good activities in chemo-, regio-, stereo-, or enantioselective hydrogenations of various substrates. Catalytic hydrogenations of multiple carbon-carbon bonds are of special interest due to their high importance in bulk and fine chemical production.[45,46]

Product selectivity is essential for the development of sustainable catalytic processes in order to only produce the desired product(s) out of many thermodynamically stable molecules.[47] In view of the recent progress in the field of nanoscience, the design of selective nanocatalysts is nowadays becoming a reality. Somorjai and co-workers have identified seven molecular factors that affect selectivity such as surface structure, surface composition, charge transfer during catalysis or oxidation state of the catalyst, for instance.[48]

The synthetic techniques described in the previous sections provide metallic nanoparticles with controlled size, shape, oxidation states and composition, these parameters were all shown to influence the chemical selectivity in catalysis.[49] The type of stabilisers also affects the catalytic performances of NPs, acting as a surface poison that controls the reactivity of these catalysts.

In the following sections, a brief review on some of the main parameters reported to influence the selectivity of M- NPs in catalysis will be described.

Size effect

It is now well established that the size and shape of the NPs influence their catalytic performances.[50] The size dependence in catalysis was described as

a complex concept and there is no single theory that can explain all the behaviours observed.[48] The main structural changes involving the size of NPs are the relative surface area and the concentration of low coordinated sites (defect sites) which provide higher activities due to the lower activation barrier for reactant molecules.[51] Moreover, shape controlled synthesis of M-NPs allows the formation of a specific structure that exposes a certain facet.

In the case of Rh-NPs, these systems generally have a face- centered cubic structure, and are described in the literature as a hypothetical cubooctahedron.[52] Using this model, up to four different sites, types of surface atoms, are observed. Two different faces (100) and (111) are described for this model, in addition of corners and edges. These different atoms and the percentage of each type as a function of size are reflected in Figure 1.15.
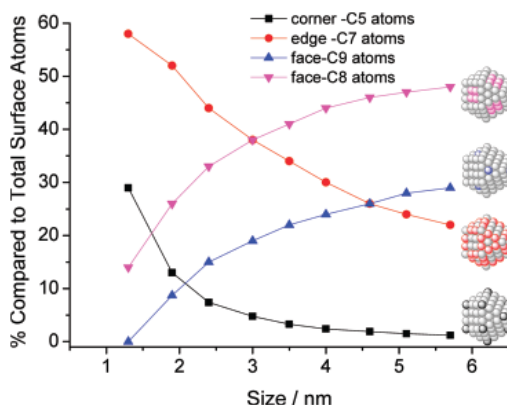
Figure 1.15 Types of surface atoms as a function of particle size (based on a cubooctahedron model).[52]

The number and properties of the metal atoms situated in corners and edges and faces directly affect the performance of NPs in catalysis since distinct reactivity could be expected at each specific site. For instance, a significant size effect is always observed in the hydrogenation of aromatic

substrates, where the adsorption of the planar moiety on the surface atoms of Rh-NPs is critical.[53] This reaction should take place in the faces of the nanoparticles where this coordination is possible. Subsequently, the nanoparticles systems must have the suitable size for the formation of faces required to perform the reaction.

One example of size effect with Rh-NPs as catalysts is the already mentioned PVP stabilised systems reported by Somorjai and co-workers.[36] Various interesting aspects can be extracted from this work. First, the effect of particle size on the activity of the Rh-NPs catalyst was evaluated. It was observed that a decrease of the particle size from 11 to 2nm, lead to a five-fold increase in TOF and a decrease in the activation energy for this process. Moreover, in situ XPS experiments demonstrated that the rhodium oxides were the active species and that the amount of these species formed increases when the particle size decreases. It was also mentioned that PVP may also play a role in the formation of the surface oxide layer.

Effect of the metal precursors and synthetic conditions

 It has been shown that the type of metal precursor and the conditions used to synthesise M-NPs also influence their activity and or/ selectivity. For instance, Dupont and co-workers described the synthesis of Ir NPs stabilised by ionic liquids (ILs).[54] The activity of the NPs prepared from an ionic Ir(I) precursor resulted almost twice as fast in the cyclohexene hydrogenation compared with NPs synthesised using a neutral Ir(I) precursor (Figure 1.16). In this case, the smaller size of the NPs prepared by the ionic precursor, which provides a greater surface area compared to the neutral Ir precursor, was proposed to explain these observations.
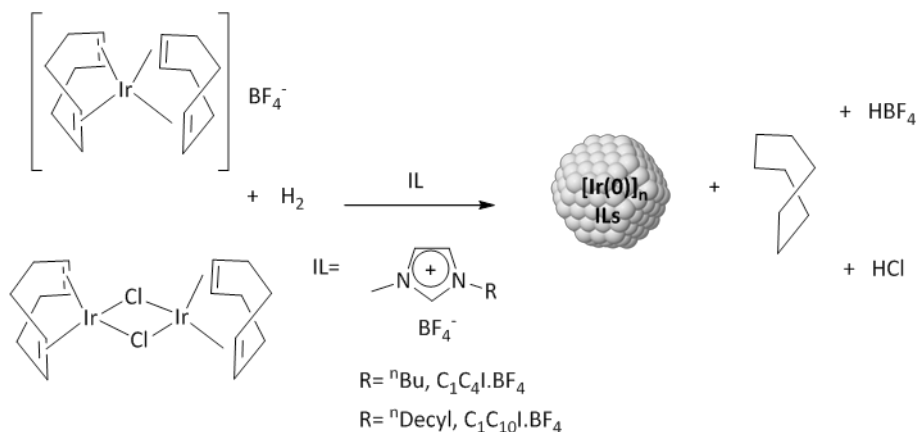
Figure 1.16 Ir NPs formation reported by Dupont and co-workers.[54]

Moores and co-workers reported the use of two rhodium precursors, namely $[Rh(\eta^3\text{-}C_3H_5)_3]$ and $RhCl_3 \cdot 3H_2O$, for the synthesis of nanoparticles stabilised by phosphine-functionalized imidazolium ionic liquids that were applied as catalysts in arene hydrogenation.[55] They observed considerably lower activity for the nanoparticles synthesised from the chloride precursor due to its lower solubility in the ionic liquid compared to the allyl precursor.[56]

Using $Rh(acac)_3$ as precursor and PVP as stabiliser, Somorjai and co-workers showed that modification of the reaction time, temperature and the precursor concentration provides Rh-NPs with different structures mainly exposing (111) faces.[57] Although the authors did not report catalytic applications of these NPs, it is known that the synthesis of NPs that expose a particular face should favour the selectivity of such nanocatalysts for specific catalytic transformations.[58] For instance, El-Sayed and co-workers, reported a study where the value of the activation energy and other kinetic parameters of a electron-transfer reaction were compared using Pt-NPs with three different structures, "near spherical", cubic and tetrahedral.[50] This study revealed that the tetrahedrical nanoparticles, that are composed entirely of (111) facets, were the most active systems.

To summarise, the methodology and parameters used during the synthesis of the nanoparticles was shown to affect their size, shape and chemical environment and consequently are of crucial importance in order to control their catalytic performances.

Stabilisers effect

The choice of the stabilising agent is often crucial for both the growth and the reactivity/selectivity of the NPs.

For instance, our group recently reported the comparison between PVP and lignins as stabilisers for Ru-NPs catalysts in Aqueous Fisher-Tropsch Synthesis and the properties of the stabilising polymers was observed to affect the hydrocarbon selectivity of the reaction.[59] The Ru-NPs stabilised by PVP produced more alkanes, slightly more oxygenates and less alkenes than those stabilised by lignin. These differences could be attributed to the distinct functional groups present in each polymer and their interactions at the NPs surface. In this example the election of the stabilising agent revealed an important role in the formation of the different products.
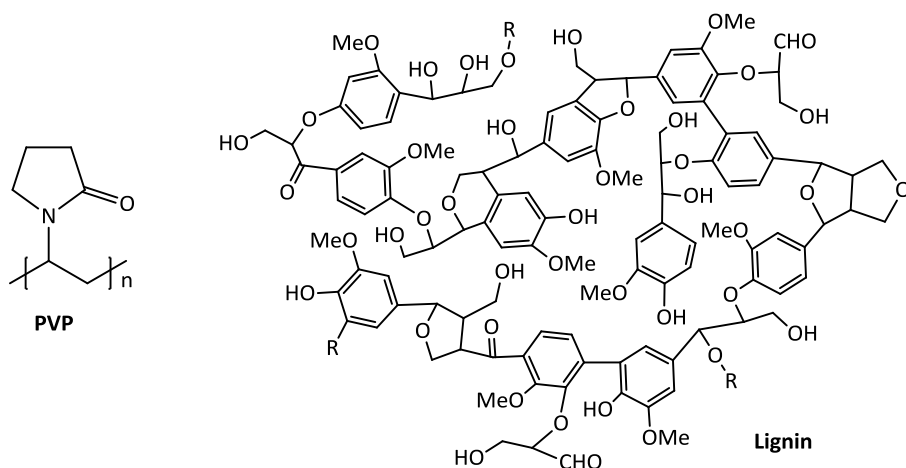
Figure 1.17 Structure of the polymers used as stabilising agent for Ru- NPs in the study of Claver and co-workers.[59]

Roucoux and co-workers intensively studied the use of surfactants as stabilising agents for the synthesis of metallic NPs and their application as catalysts in arene hydrogenation in biphasic liquid-liquid (water/substrate) media.[60,61,62,63,64,65,66] Some of the surfactants used as stabilisers are showed in Figure 1.18.
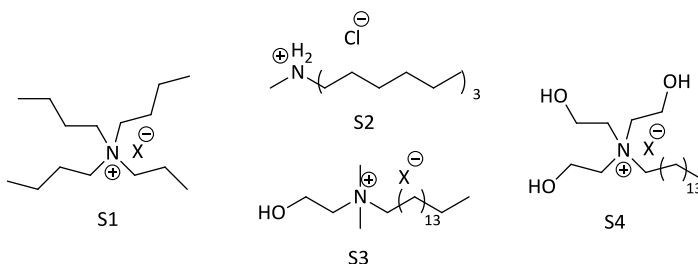
Figure 1.18 Surfactants used in the stabilisation of metal-NPs. (S1= tetrabutylammonium salts, S2= methyltrioctyammonium chloride, S3= N,N-dimethyl-N-cetyl-N-(2-hydroxyethyl)ammonium salts HEA-16-X, S4= N-hezadecyl-N-tris-(2-hydroxyethyl)ammonium salts THEA-16-X.

They reported the first example of efficient nanocatalysts under biphasic conditions for this reaction, using 1 atm of hydrogen pressure at room temperature and achieving the recycling of the catalysts.[5,61] They compared the results obtained with colloidal Rh-NPs stabilized by N,N-dimethyl-N-cetyl-N-(2-hydroxyethyl)ammonium bromide (HEA-16-Br) with those obtained with the standard Rh/C heterogeneous catalyst and with the classical water-soluble Rh/PVP and Rh/PVA systems synthesised in hydroalcoholic media and showed that the Rh/HEA-16-Br-NPs were the most active catalysts in the hydrogenation of anisole and toluene under these conditions.[67]

As an example of other stabilisers, Chaudret and Basset groups demonstrated that ILs act as an organised system formed through a self-assembling process resembling nanoreactor in which the size of nanoparticles generated in situ could be controlled.[68] In this study, the

synthetic conditions and the ILs used had an influence on the size of the resulting NPs. Ru NPs formed from the organometallic complex [Ru(COD)(COT)] stabilised by various ILs, [RMIm][Ntf$_2$](R= C$_n$H$_{2n+1}$ with n= 2, 4, 6, 8, 10), and [R$_2$Im][NTf$_2$] (R=Bu) and [BMMIm][NTf$_2$] were synthesised under hydrogen at room temperature or 0 °C with or without stirring. In all ILs, the size of RuNPs was smaller at lower temperature and the stirring induced agglomeration of the systems. Moreover, when the size of the non-polar domains was increased the size of the nanoparticles increased. In addition, as shown in Figure 1.19 a linear correlation between the size of the RuNPs generated in situ and the length of the alkyl chain could be established. The authors showed that at a specific temperature the hydrogen solubility in the ionic liquid has less influence on the reaction rate than in organic solvents (where under the conditions used in this study, aggregated clusters are formed) and so the variation of the mean size of the NPs can be directly related to the nature of IL.
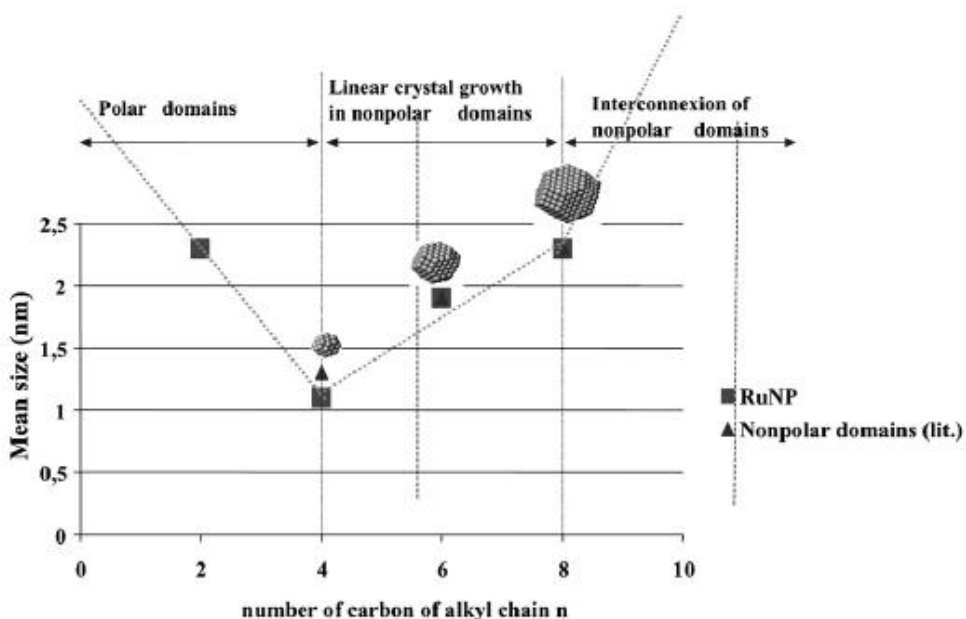
Figure 1.19 Correlation between the number of carbons in alkyl chains C$_n$H$_{2n+1}$ of [RMIm][NTf$_2$] and the RuNPs size (or the number of Ru atoms).[68]

These studies showed the tuneability of ionic liquids that make them excellent stabilisers to control the nanoparticles surface.

Other type of stabilisation was reported for instance by Finke and co-workers using polyoxoanion- tetrabutylamonium- as rhodium nanoparticles stabilisers.[69] The Rh-NPs were formed in situ from a polyoxoanion rhodium complex dissolved in acetone under 40 bar of hydrogen pressure. Up to 193.000 turnovers were obtained for the hydrogenation of cyclohexene. However, the systems detailed in this study presented some problems, such as the solubility of the catalyst into the substrate that forces the use of a solvent or the use of the catalyst at high temperatures.

Interestingly, these polyoxoanion stabilised Rh-NPs exhibited lifetimes approaching those of supported heterogeneous catalysts.

Small molecules also named ligands in organometallic chemistry can also be used as stabilisers and were shown to modulate both the electronic and steric environment at the surface of nanoparticles.[70] For instance, amines and aromatic imines are commonly used (Figure 1.20). Lemaire and co-workers showed that very active Rh- and Ru-catalysts for the hydrogenation of disubstituted arenes could be formed in the presence of amines such as trioctylamine (TOA) and *R*-(-)-dioctylcyclohexyl-1-ethylamine (DOCEA).[71] The mild conditions used in these studies and the chemoselectivity obtained were at this time surprising when compared with typical heterogeneous catalysts.
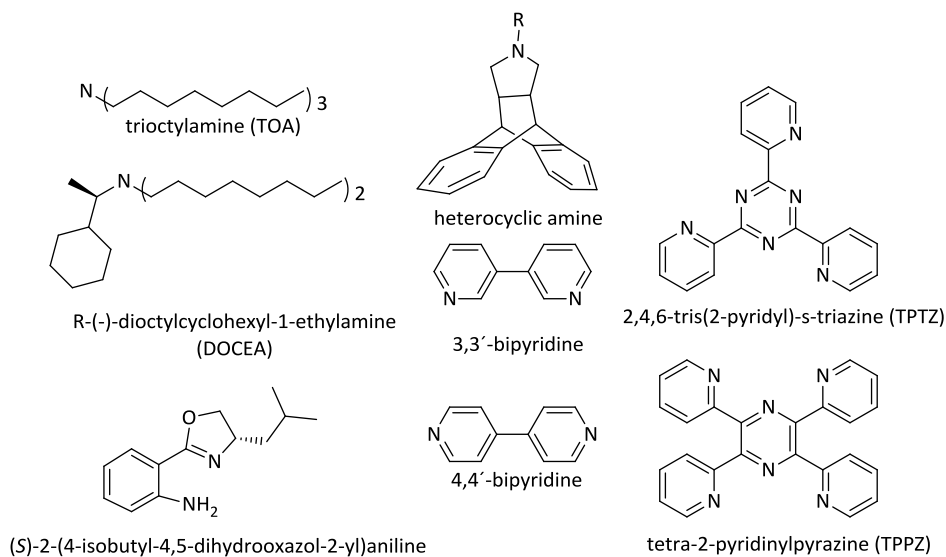
Figure 1.20 N-donor molecules used for the stabilization of M-NPs.[71]

Chaudret, co-workers extensively study ruthenium nanoparticles, especially with ligands as stabilisers.[70]

Chaudret and van Leeuwen and co-workers recently reported, the use of large bite angle diphosphine and carbene ligands as stabilisers for Ru-NPs and their application in the hydrogenation of arenes. Interesting ligand effects were observed.

In the first study, different mono and diphosphine with 0.1 and 0.2 equivalents (eq= ligand/ Ru ratio) during the synthesis were used as stabilisers (Figure 1.21).[72]
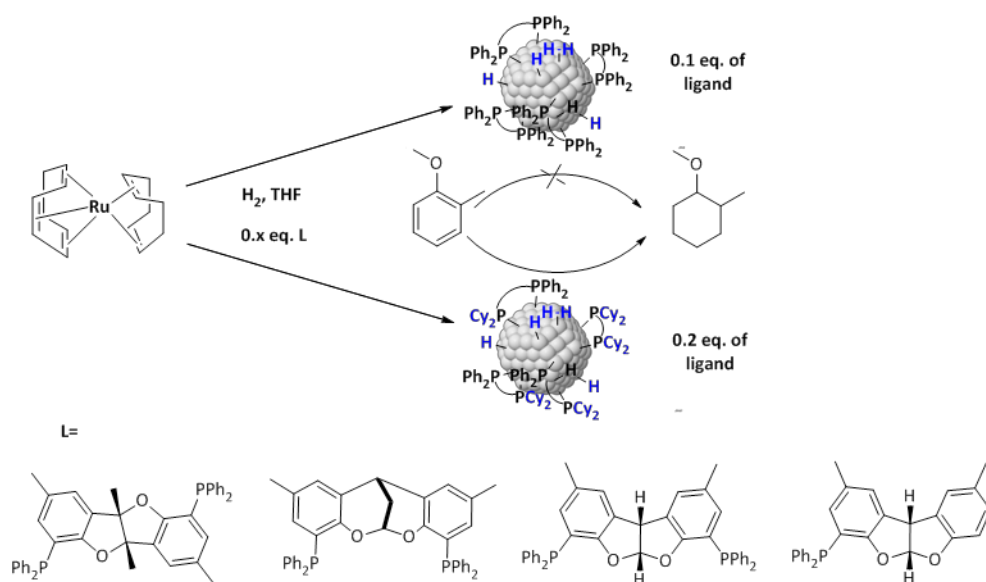
Figure 1.21 Phosphines used by Chaudret and van Leewen as Ru-NPs stabilisers.[72]

Small and soluble Ru NPs of 1.1-2.1 nm of mean diameter were obtained, the size and dispersion could be influenced by the structure of the phosphine and the number of equivalents used during the NP synthesis. Interestingly, in addition to the expected signals for triarylphosphines (Ar_3P), dialkylarylphosphines (Alk_2ArP) and trialkylphosphines (Alk_3P) were also detected by ^{31}P NMR, indicating that hydrogenation of the aromatic groups of the ligands had taken place during the synthesis of the Ru-NPs. The authors deduced that for the diphosphine stabilised systems, at low ligand ratio, the ligands first coordinate to the apexes, where they are not hydrogenated (Ar_3P was observed) while at higher ligand ratio the ligand can interact with the faces and thus can be hydrogenated (Alk_2ArP and Alk_3P were detected). Moreover, monophosphine can be more easily hydrogenated due to its flexibility. These systems were used in the hydrogenation of *o*- methylanisole revealing the crucial importance of the nature of the substituents on the phosphine for the catalytic activity.

Nanoparticles containing aryl moieties at phosphorus showed no or poor activity, while nanoparticles with the partially hydrogenated phosphines as stabilisers showed complete hydrogenation of the substrate. The poor activity obtained using the nanoparticles stabilised by the arylphosphines was explained by the interaction of these aryl groups with the surface, thus blocking the access of the substrate to the active site. Interestingly, the systems containing fully hydrogenated ligands were slower catalyst than those bearing partially hydrogenated ligands.

In the second study of these authors, ruthenium NPs were stabilised by the carbenes ligands showed in Figure 1.22.[73]
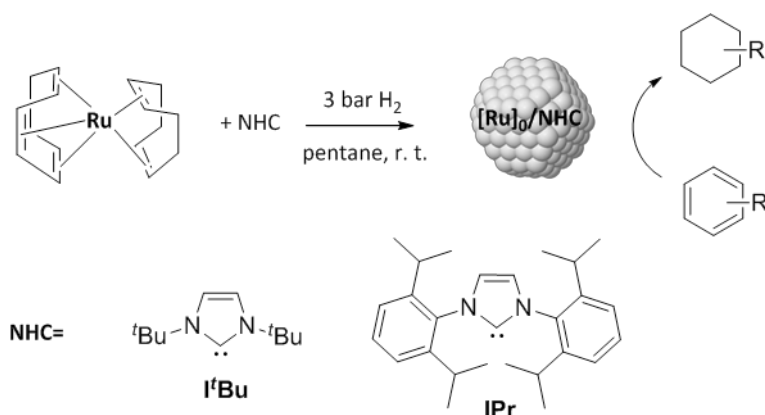
Figure 1.22 N- heterocyclic carbenes used for the synthesis of RuNHCs NPs.[73]

Small nanoparticles of 1.5-1.7 nm were obtained and applied as catalysts for arene hydrogenation, detecting significant differences depending on the ligands used as stabiliser. The nanoparticles synthesised with the I^{t}Bu carbene needed a higher content of ligand for their stabilisation than the analogous IPr and provided lower activity in the hydrogenation of *o*-anisole or acetophenone. The presence of the excess of ligand coordinated at the surface of the nanoparticle could explain this behaviour.

In this study, the coordination of the IPr ligand at the surface was examined and it was deduced that at low ligand concentration, the carbene may be coordinated either at the corner, edges and defects, while at higher concentration, the faces of the nanoparticle could be occupied as well. The

increased hindrance at the surface affects significantly the catalytic activity of the NPs in the hydrogenation of arenes since the reaction takes place at the faces of the catalysts. In reactions employing these carbene stabilised ruthenium nanoparticles, the solvent and catalytic conditions revealed to affect the catalytic performances. For instance, as a function of the competition between the solvent, the substrate and the product adsorption on the nanoparticles surface that could direct the selectivity towards a specific compound.

Philippot and co-workers reported the first use of water-soluble alkyl sulfonated diphosphines as stabilisers for Ru-NPs.[74] The NPs were formed by decomposition of [Ru(COD)(COT)] under hydrogen in THF and in presence of the alkyl sulfonated diphosphines containing different alkyl chain length and using different ligand/ metal ratios (0.1, 0.2 or 0.5) (Figure 1.23).
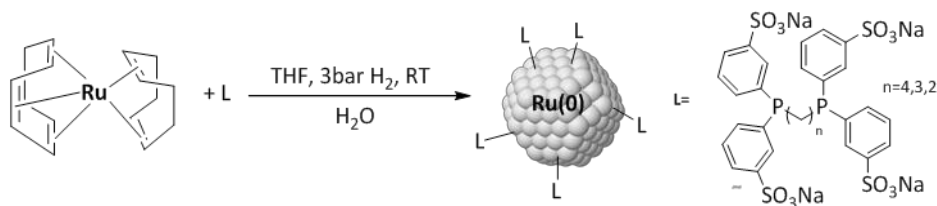
Figure 1.23 Sulphonated diphosphines used by Philippot and co-workers as stabilisers for Ru NPs.[74]

Nanoparticles of small size (1.2-1.5nm) were obtained and easily redispersed in water without changes in dispersion or size. The Ru-NPs were used as catalysts for the hydrogenation of styrene, tetradecene and acetophenone under biphasic conditions. Interestingly, increasing the alkyl chain length of the diphosphine used as stabiliser caused an increase in the activity in the styrene hydrogenation. The authors correlated this observation with the difference in flexibility of the chain that could facilitate the diffusion of the substrate towards the metal surface.
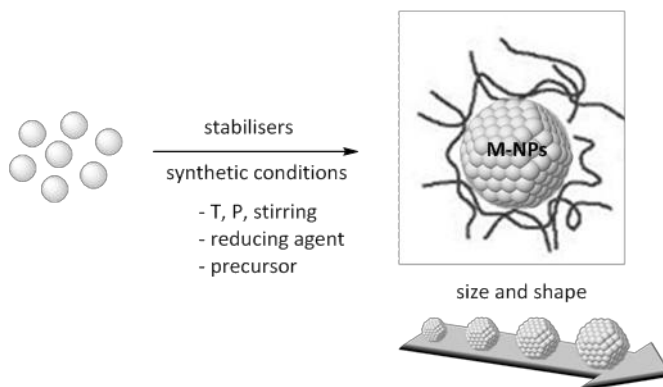
Figure 1.24 Schematic representation of the parameters that affect selectivity using soluble M-NPs as catalysts.

Nowadays, the selective production of a specific compound for a given transformation is one of the main challenges in nanocatalysts development. The examples described above show that their selectivity can be tuned through variations of several parameters. However, the effects observed in catalysis are often difficult to predict and there is still much to learn on how modulate the activity/selectivity of such active and reactive species.

1.6 Nature of the active catalyst: Homogeneous vs. Heterogeneous

As previously mentioned, the identification of the real active species is of critical importance in catalysis in order to design more efficient catalysts and processes. Several methods were reported in order to obtain indications of whether the active species is of homogeneous or heterogeneous nature.[75]

Different authors have made efforts in this field and their studies will be used in this section. For example, Finke and co-workers reported various reports on the identification of the catalyst nature in hydrogenation processes with platinum[76], ruthenium[77] or rhodium systems.[78,79] Dyson also reported in situ formation of heterogeneous catalysts from a metallic molecular pre-catalysts in arene hydrogenation, and determine the nature of the active species through the study of the reaction mechanism.[53] De

Vries and co-workers analysed the nature of the real catalyst in C-C coupling reactions using palladium systems and determined that PdNPs act as a reservoir of molecular species in these processes.[40]

In this context, the isolation and detailed characterisation of nanocatalysts is usually the first step to obtain information on the active catalyst.[80,81]

Moreover, the study of the kinetics of a reaction has also been used as a decisive factor to determine the nature of the active species.[82] When isolated NPs are used as catalyst, the observation of an induction period is usually attributed to the formation of heterogeneous species from homogeneous catalysts in solution. In this case, the correlation between substrate conversion versus time results in a sigmoidal-shaped kinetics curve, indicating the presence of a nucleation and then the autocatalytic surface growth step prior to the catalytic reaction.[78]
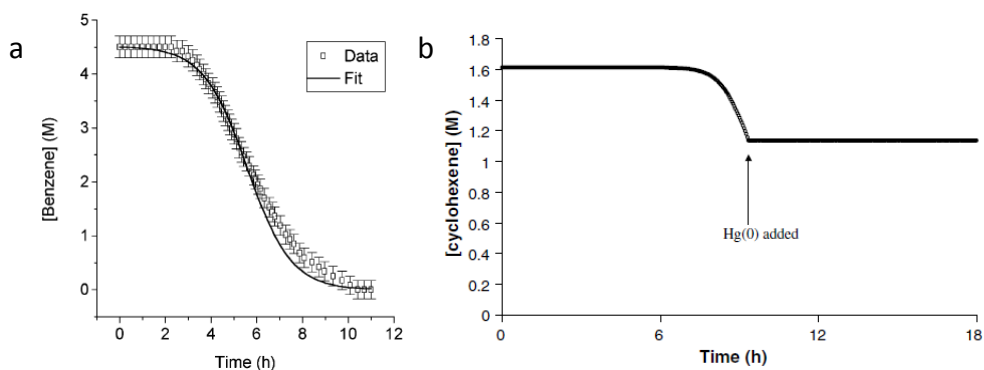
Figure 1.25 a) Data and curve- fit for typical benzene hydrogenation with a Ru pre-catalyst.[76] b) Example of Hg^0 poisoning a $Pt^{II}(1,5\text{-COD})Cl_2$ system.[76]

Figure 1.25 (a) showed the evolution of the concentration of benzene versus time during hydrogenation where the catalyst precursor was $Ru(II)(C_6(CH_3)_6)(OAc)_2$.[76] The typical sigmoidal curve can be observed with a *ca*. 3h induction period.

If the isolated nanoparticles species are the real catalysts, no induction period is expected and an exponential decay curve should be observed.[83]

However, the presence of an induction period can also be due to other processes such as catalyst activation for reactions occurring by composite mechanism for instance and can therefore not be considered as a definitive evidence.[84]

The main methodology employed to identify heterogeneous catalysts is the poisoning of the catalyst surface by the addition of reagents that binds to the heterogeneous catalyst and thus inhibit the catalytic reaction. The most reported method is the addition of mercury due to the ability of this compound to poison metal (0) by formation of amalgam or adsorption on metal surfaces.[85] In these tests, large excess of mercury is needed and good stirring to ensure contact of the Hg^0 with the preformed active catalyst.[86]

The poisoning metal is added after the initiation of the reaction, usually at *ca*. 30% of conversion. The suppression of the catalytic activity by addition of Hg^0 is considered an evidence for a heterogeneous catalyst, while if the catalytic activity is not suppressed, it implies that the catalysis is homogeneous. An example of the addition of mercury to a platinum system is shown in Figure 1.25 b, where the cyclohexene concentration versus the time is represented. No further cyclohexene hydrogenation took place after the addition of the poisoning metal.

The mercury poisoning experiment is easy to perform, but this metal can induce side reactions and also react with some molecular complexes. Consequently, the results obtained with this test are not enough to conclude about the catalyst nature.

Ligands such as CS_2, PPh_3 or thiols can also be used as poisons.[75] If less than one equivalent of ligand for surface atom stops the catalysis, this constitutes evidences of the presence of a heterogeneous catalyst. However, CS_2-poisoning has for instance the limitation that this dissociates from the heterogeneous catalyst at high temperatures.[87]

Carbon monoxide is also used in the literature as heterogeneous catalyst poisoning. For instance, Chaudret and co-workers have recently demonstrated that arene hydrogenation is inhibited after the adsorption of CO at the surface of the ruthenium nanoparticles stabilised by PVP and

dppb.[88] When the reaction temperature was increased, slow recovery of the active sites was observed by displacement of CO under hydrogen pressure.
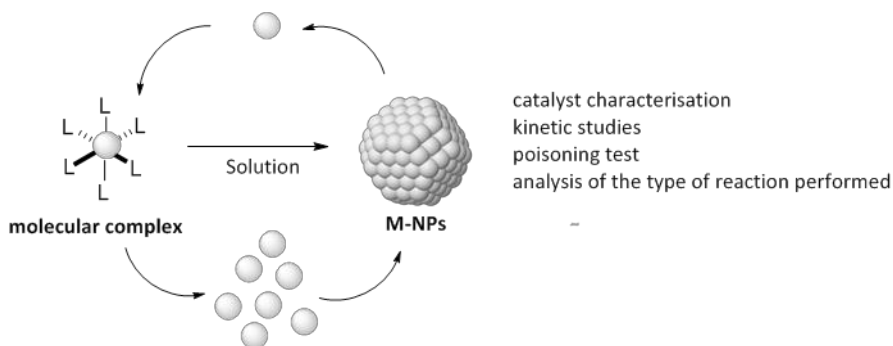
Figure 1.26 Schematic representation of the active species that can be formed in homogeneous catalysis.

Sometimes, the type of reactivity observed can be also considered as a direct evidence of the nature of the catalyst. Dupont and co-workers reported the use of imidazolium ionic liquids to stabilise Rh and Ir NPs that were used as catalysts in the hydrogenation of arenes.[89] In this study, hydrogenolysis of the C-O bond of anisole and acetophenone was observed, and described as a characteristic of surface metal catalyst.[90] The observation of the hydrogenolysis products that could only be formed through the nanoparticles and not by homogeneous systems evidences the real heterogeneous nature of the catalyst.[91]

These tests are useful to obtain information about the real nature of the catalyst (Figure 1.26). However, none of these experiments allow definitive conclusions and coherent information between all of them is needed to define the catalyst nature.

1.7 Selective hydrogenation reactions catalysed by soluble Rh-NPs

In this section a brief overview of the main hydrogenation processes reported using soluble rhodium nanoparticles will be described.

The hydrogenation of monocyclic arenes is an active area of research due to the high industrial interest in the production of cyclohexanes from the corresponding arenes (Figure 1.27).[92]
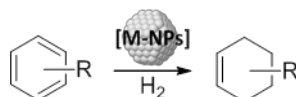
Figure 1.27 Formation of cyclohexenes from hydrogenation of arenes catalysed by M-NPs.

This reaction has been reported using soluble M-NPs as catalysts under various conditions.[93] The use of these catalysts is considered as a reference in this field due to the already mentioned advantages in terms of activity, selectivity and recovery. The mild conditions employed when dealing with M-NPs also present potential in order to overcome selectivity issues such as chemoselectivity when several groups are present in the substrates and stereoselectivity for substituted substrates.

The partial arene hydrogenation for the production of cyclohexenes derivatives is also a challenge in this area of catalysis.[94] The selective reduction of aromatic compounds to the partial hydrogenated products is typically performed in industry using supported Ru catalysts.[95] An example of this chemistry is the selective hydrogenation of benzene to cyclohexene, which is of synthetic and industrial interest since cyclohexene is a useful intermediate material in the synthesis of commercially important products, such as adipic acid, that is produced industrially by "Asahi Chemical company" in Japan.[96]

The use of soluble nanoclusters as catalysts for this selective reaction has received increased attention over the last years, mainly with ruthenium and rhodium catalysts.[97] This type of catalysts presents some advantages over traditional heterogeneous catalysts, such as their high activity under mild conditions that is important when dealing with substrates that are

temperature sensitive.[71] Moreover, soluble nanocatalysts are also more selective that the corresponding traditional heterogeneous catalysts for some reactions.[91]

A more detailed review of the literature on these processes will be described in Chapter 3.

Among the unsaturated molecules commonly used in selective hydrogenation, styrene has been used as a model substrate to determine the capability of nanocatalysts to reduce aromatic rings and/or vinylic C=C bonds. This type of chemoselectivity is of great interest when the substrates can not be reduced by classical homogeneous catalysts and are totally hydrogenated by purely heterogeneous systems (Figure 1.28).
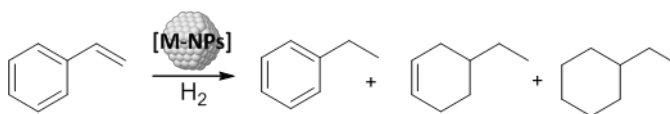
Figure 1.28 Products obtained from styrene hydrogenation catalysed by NPs.

The metals used for the selective hydrogenation of styrene with soluble nanoparticles as catalysts are ruthenium, rhodium and to a less extent Pd. The detailed examples will be also mentioned in Chapter 3.

Aromatic amines are generally produced by the hydrogenation of the corresponding nitro compounds with heterogeneous catalysts.[98] One of the challenges of this reaction is the selective reduction of the nitro group when other reducible groups are present in the same molecule (Figure 1.29). Functionalised anilines are industrially important intermediates for pharmaceuticals, polymers, herbicides or in fine chemistry.[99] This type of transformation can be carried out by stoichiometric methods such as Béchamp[100] with Fe/ HCl, or the sulfide reduction with H_2S or NaSH as reducing agents.[101] These processes are not environmentally sustainable and should be replaced since large amounts of waste are produced.
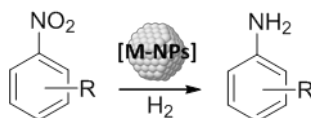
Figure 1.29 NPs catalysed hydrogenation of nitroaromatics into aromatic amines.

The most used metals for the hydrogenation of nitro groups are Pt and Pd, mostly supported on active carbon or alumina, and Raney Nickel. During the reduction of nitroarenes to aromatic amines, the accumulation of several reaction intermediates such as azo and azoxy derivatives or hydroxylamines results in low selectivity. Using soluble nanocatalysts, these products are not formed, which thus represents an advantage over classical heterogeneous catalysts.

In the field of soluble metal nanoparticles for this catalytic reaction, some studies are reported in the literature. As in the heterogeneous way one of the metals most used is Pt. However a wide range of metals are also applied for this transformation as it's going to be detailed in the following sections.

The group of Dyson reported the use of platinum nanoparticles synthesised by thermal decomposition and redispersed in PVP or ionic-liquid-like-copolymer (IP) (Figure 1.30).[102] These systems were used in various solvents and evaluated as catalytst for the hydrogenation of 2,4-dichloro-3–nitrophenol.
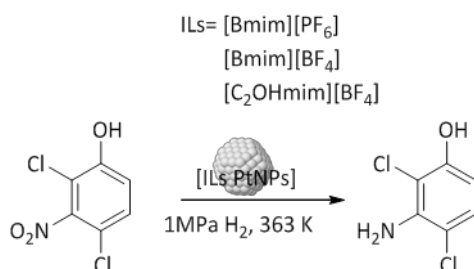
Figure 1.30 Hydrogenation of 2,4- dichloro-3-nitrophenol catalysed by Pt-NPs.[102]

Using organic solvents, low selectivity and dehalogenation were observed, so they performed the reaction in ILs media, improving the selectivity to quantitative yields and suppressing the side reactions. After an exploration of the conditions and the ILs counterions, high conversion and selectivity

was obtained with the IP protected Pt-NP in [C$_2$OHmim] [BF$_4$] at 363 K. So this system was used with other subtrates containing different substituent groups obtaining good results in all the cases. Moreover, this system was able to be recycled up to 9 runs maintaining good selectivity and conversion, reaching a turnover number (TON) of 2025, which is higher than the TON obtained using Raney Ni.[103]

More recently, the group of Chaudret reported the use of platinum nanoparticles stabilised by NHC carbenes and synthesised by the organometallic approach (Figure 1.31).[104] Nitrobenzene was used as model substrate and the reaction conditions were optimise to 30 °C, 1 bar H$_2$ and using 0.05-0.3 mol% of Pt. The catalytic performances of the nanoparticles stabilised by both carbenes and with different amount of stabiliser during the synthesis were tested for this reaction.
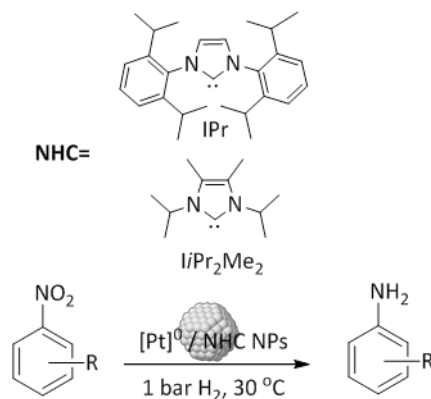
Figure 1.31 Reaction conditions and NHC ligands used by Chaudret and co-workers for the reduction of nitro arenes into nitro amines.[104]

As the best results were obtained with the system using IPr at 0.2 equivalents, a range of functionalised nitroarenes were studied with this catalyst. High activities and selectivity for the anilines derivatives were obtained under mil conditions in the absence of additives or promoters.

Bimetallic nanoparticles are also used for this transformation. Yu and co-workers reported the synthesis of Pt/Ru nanoparticles stabilised by the

polymer poly(N-vinyl-2-pyrrolidone) (PVP) by thermal decomposition in ethanol/ water system.[105] Nanoparticles with different metal ratios of the corresponding metal precursors $RuCl_3 \cdot nH_2O$ and $H_2PtCl_6 \cdot 6H_2O$ were synthesised and characterised.

These systems were used in the hydrogenation of ortho-chloronitrobenzene (o-CNB) to *ortho*-chloroaniline (o-CAN) (Figure 1.32).
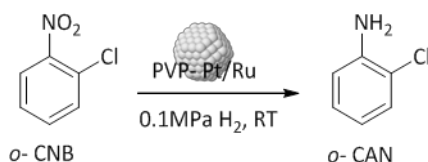
Figure 1.32 Hydrogenation of o- chloronitrobenzene by PVP- Pt/Ru NPs.[105]

They observed different catalytic results depending on the colloidal nanoparticles composition. The selectivity towards the o-CAN product increased with the increased proportion of Ru in Pt/Ru catalyst, being similar to PVP-Ru systems, indicating that Ru was rich on the surface of these PVP-Pt/ Ru nanoparticles. Moreover, they compared these results with PVP-Pt/ Ru synthesised by $NaBH_4$ reduction, in which the selectivity to o-CAN was similar to that of PVP-Pt, in agreement with their core- shell structure with more Ru atoms in the core, the opposite case. They demonstrated the importance of the composition either in the metal distribution into the core-shell structure or the ratio between the metals, in the catalytic performances for the selective hydrogenation of this nitro aromatic compound.

The same polymer stabiliser was used by Tsukuda and co-workers to synthesised two different systems.[106] In this case, iridium PVP nanoparticles were prepared reducing the precursor $H_2[IrCl_6] \cdot 6H_2O$ by $NaBH_4$ (system named A) or ethylene glycol (system named B), obtaining nanoparticles of 1.8 and 2.1nm of diameter respectively. Other metals such as Pd, Pt, Rh and Au were used for comparative purposes.
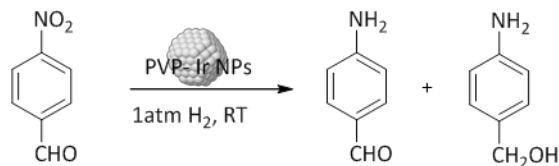
Figure 1.33 Catalytic hydrogenation of 4-nitrobenzaldehyde catalysed by Ir-PVP NPs.[106]

Both systems were applied in the hydrogenation of 4- nitrobenzaldehyde (Figure 1.33), obtaining higher conversions and selectivities for 4-aminobenzaldehyde than using other metal NPs. However, in the case of the system A, small amount (up to 7%) of the reduction of the aldehyde group was also detected. This selectivity was attributed to the nanoparticles size differences between the systems. The most selective catalyst (system B) was used in the hydrogenation of nitroaromatics containing ketone, nitriles and chloride functional groups obtaining high conversions and selectivities in all the cases. The authors postulated a correlation between the catalytic performances and the structural characterization by XPS, assuming a preferential adsorption of the NO_2 group onto the oxidised area found at the surface and activation of the hydrogen on the non-oxidised area. In conclusion, the high selectivity for the Ir NPs compared to the other metals used in this study could have a correlation with the partially oxidised area observed on the nanoparticles.

The same substrate 4-nitrobenzaldehyde was studied by Li and co-workers.[107] However, in this example a Rh/ Ni bimetallic system stabilised by a surfactant, octadecylamine (ODA) was used. Different ratios between the metals were employed, obtaining the best results in terms of activity and selectivity towards the 4-aminobenzaldehyde without reduction of the aldehyde moiety for the Rh_3Ni_1 nanoparticles at low catalyst loading (0.3 mol%) under mild conditions (atmospheric H_2 pressure and room temperature). The catalyst could be easily recycled by centrifugation or sedimentation, without loss in activity and selectivity for at least 5 cycles. This catalyst was used under the same conditions with a wide range of

substrates shown in Figure 1.34 with excellent isolated yields with high selectivity.
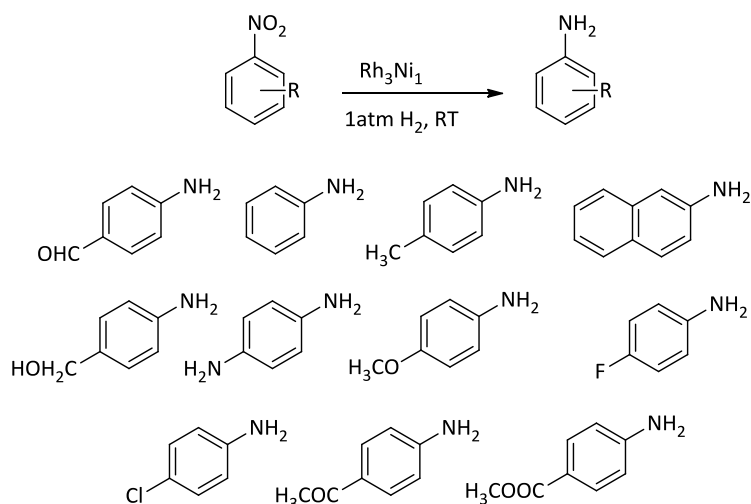
Figure 1.34 Substrates used for the reduction of nitro groups by Rh_3Ni_1 NPs.[107]

The group of Harrad also used a surfactant stabiliser, CMC, to synthesised nickel nanoparticles (Ni-CMC) by reduction with $NaBH_4$ (Figure 1.35).[108] Nitrobenzene was used as model substrate to optimise the reaction conditions such as solvent, temperature and pressure.
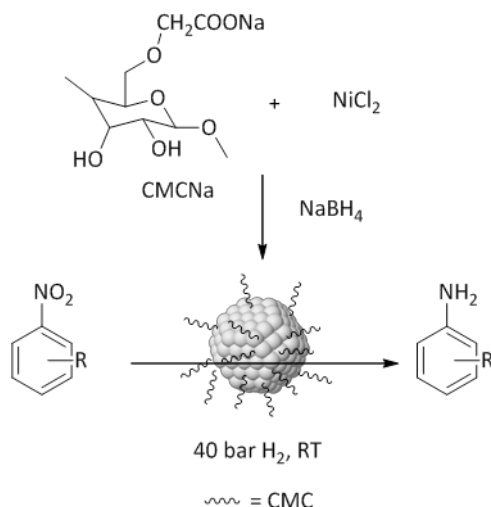
Figure 1.35 System used for the selective hydrogenation of nitro aromatic compounds.[108]

Full conversion was obtained using this system at room temperature, 40 bar H_2 pressure and with a solvent mixture of H_2O/methanol in an 8/2 proportion. With these conditions and catalyst, other functionalised nitrobenzenes with functional groups such as alcohol, esters or amines in different position, were tested obtaining high yields for the desired anilines derivatives.

The chemoselective hydrogenation of aromatic rings contained in ketones has also been reported using various M-NPs and acetophenone is usually used as a model substrate (Figure 1.36).
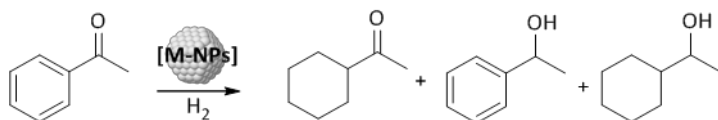
Figure 1.36 Products obtained in the hydrogenation of acetophenone catalysed by metal surfaces.

The use of Ru and Rh-NPs was mainly reported in these reactions, although a few examples of Pd- and Ir-NPs were also described.[109]

A more detailed review of the literature concerning these systems will be presented in the chapter 4 of this thesis.

In the selective hydrogenations of substrates bearing other functional groups such as esters or amides, less work has been reported so far due to the difficulty to hydrogenate these functional groups using metal nanoparticles.[110]

Nevertheless, Jessop and co-workers reported the use of soluble Rh-NPs for the selective hydrogenation of substrates containing ester groups.[111] Rh-NPs generated *in situ* from [Rh(μ-Cl)(COD)]$_2$ in aqueous/supercritical fluid biphasic media were applied as catalysts in the hydrogenation of ethyl benzoate and 96% of selectivity towards the hydrogenation of the aromatic ring was obtained.

96% of selectivity
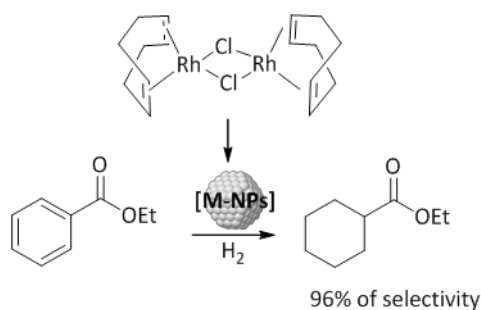
Figure 1.37 Hydrogenation of ethyl benzoate reported by Jessop and co-workers.[111]

Other substrates containing imide groups have also been tested as substrate in hydrogenation reaction using Rh-NPs as catalysts.[112] The nanoparticles where synthesised by reduction of the [Rh(acac)(CO$_2$] precursor under supercritical conditions and in presence of solid ammonium salts that formed ionic liquids in solution. With this simple procedure, well-defined rhodium nanoparticles were obtained in various ionic matrices at mild temperatures using three different ammonium bromide salts. The brownish solid particles could be re-dissolved under pressurised CO$_2$ to form homogeneous solutions. Even after storage of the solids over three months, the nanoparticles remained stable and no change in their catalytic behaviour was observed. The promising results obtained with the simple test reactions prompted them to evaluate the new materials as catalysts for more challenging substrates. The sterically encumbered (*E*)-2-(benzoylamino)-2-propenoic acid derivatives are precursors for non-natural amino acids and show interesting biological activities.[113] Their selective hydrogenation is thus of interest to increase the structural diversity of these substances. Several reducible groups are present in these substrates and selectivity is therefore required. In contrast to conventional catalysts, ammonium halide stabilised Rh-NPs were found to combine good catalytic activities with significant selectivity for the aromatic and olefinic moieties.
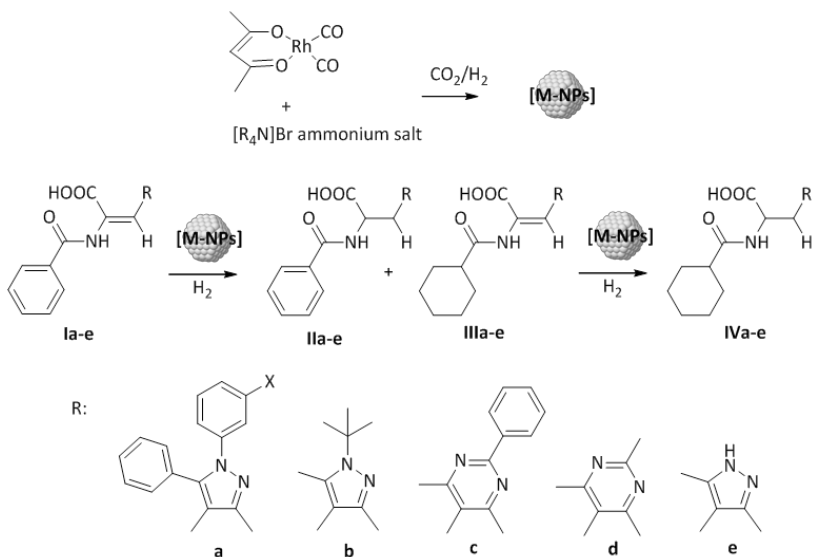
Figure 1.38 Selective hydrogenation of (*E*)-2-(benzoylamino)-2-propenoic acids using RhNPs stabilised by [Bu$_4$N]Br as catalyst.[112]

Indeed, for substrates **Ia-e**, all three possible hydrogenation products were formed via parallel and consecutive hydrogenation processes. Remarkably, product **IIIa-e** was formed preferentially over **IIb**, which indicated that hydrogenation of the aromatic moiety is faster than that of the olefinic double bond in this case. This trend is even more pronounced for the sterically more encumbered substrates **Ic-d**. Product **IIId** was obtained with excellent selectivity reaching up to 96% at 60% conversion. In contrast, the substrate **4e**, which contains a basic NH group in the heteroaromatic substituent, was hydrogenated exclusively at the double bond to provide the benzoyl amino acid **IIe** in good yields.

As previously detailed, hydrogenation using soluble nanoparticles as catalysts is widely explored in the literature. However, the formation of high yields of selective products employing this type of catalysts is still a challenge in some cases.

1.8 Objectives

The understanding of the parameters that influence the selectivity of metal nanoparticles in catalysis is crucial in order to design more efficient nanocatalysts. Among these parameters, the properties of the stabilising agent were shown to affect the performances of nanocatalysts and in this context, the use of ligands as stabilising agents presents several advantages. Indeed, ligands such as phosphine and phosphites have been used for decades in homogeneous catalysis and their properties and reactivity were investigated in depth. The systematic variations of their structure revealed a powerful methodology to better understand how these molecules control the catalytic properties of molecular catalysts and is also relevant for nanocatalysts.
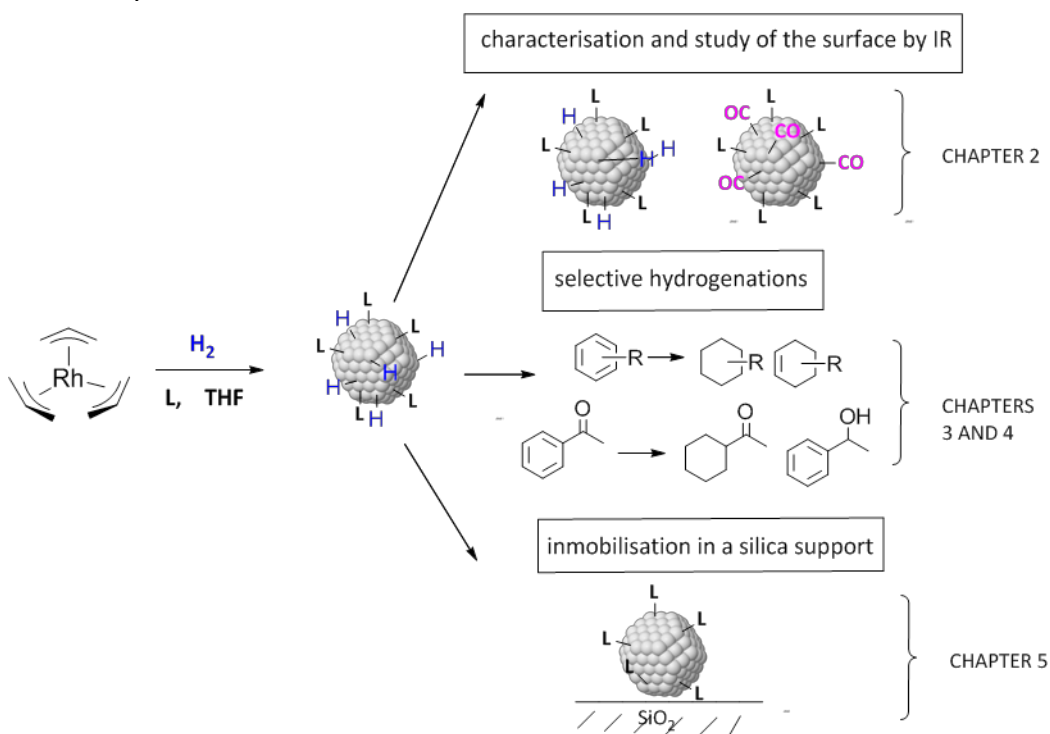
Figure 1.39 Schematisation of the objectives of this work.

The work described in this thesis deals with the synthesis and characterisation of Rh-nanoparticles stabilised by two families of P-based ligands, namely phosphines and phosphites and their application as catalysts in the hydrogenation of various substrates. A preliminary study on the immobilisation of Rh-NPs onto modified silica is also described in the last chapter.

The objectives of this work can thus be summarised as follow:

- Synthesis and characterisation of Rh-NPs stabilised by phosphine and phosphite ligands.
- Application of these NPs as catalysts in the hydrogenation of arenes
- Application of these NPs as catalysts in the hydrogenation of aromatic ketones
- Immobilisation of these NPs on modified silica via surface organometallic chemistry.

1.9 References

[1] G. Schmid, in *Nanoparticles: From Theory to Application*, Ed Wiley- VCH, Germany, **2004**, vol. 1, ch.2, pp 4- 44.

[2] J. D. Aiken III, R. G. Finke, *J. Mol. Catal. A: Chem*. **1999**, 145, 1-44.

[3] D. Astruc, F. Lu, J. Ruiz Aranzaes, *Angew. Chem. Int*. *Ed*. **2005**, *44*, 7852-7872.

[4] P. Wasserscheid, W. Keim, *Angew. Chem. Int. Ed*. **2000**, *39*, 3772-3789.

[5] A. Roucoux, J. Schulz, H. Patin, *Chem. Rev*. **2002**, *102*, 3757-3778.

[6] M. T. Reetz, R. Breinbauer, K. Wanninger, *Tetrahedron Lett*. **1996**, *37*, 4499-4502.

[7] J. Dupont, G.S. Fonseca, A.P. Umpierre, P.F.P. Fichtner, S. R. Teixiera, *J. Am. Chem. Soc.* **2002**, *124*, 4228-4229.

[8] J. D. Scholten, B. Caroline Leal, J. Dupont, *ACS Catal*. **2012**, *2*, 184-200.

[9] a) J. Dupont, J. D. Scholten, *Chem. Soc. Rev*. **2010**, *39*, 1780-1804. b) M. H. Prechtl, J. D. Scholten, J. Dupont, *Molecules* **2010**, *15*, 3441-3461. c) P. Migowski, J. Dupont, *Chem. Eur. J.* **2007**, *13*, 32-39.

[10] J. Dupont, P. A. Z. Suarez, *Phys. Chem. Chem. Phys*. **2006**, *8*, 2441-2452.

[11] R.G. Finke, S. Özkar, *Coord. Chem. Rev*. **2004**, *248*, 135-146.

[12] M. Brust, M. Walker, D. Bethell, D. J. Schiffrin, R. Whyman, *Chem. Commun*. **1994**, 801-802.

[13] H. Bönemman, G. Braun, W. Brijoux, R. Brinkmann, A. Schulze, K. Seevogel, K. Siepen, *J. Organomet. Chem*. **1996**, *520*, 143-162.

[14] H. Hirai, Y. Nakai, N. Toshima, *Chem. Lett*. **1978**, 545-548.

[15] A. Borsla, A. Wilhelm, H. Delmas, *Catal. Today* **2001**, *66*, 389-395.

[16] K. Esumi, O.Sadakane, K. Torigoe, K. Meguro, *Colloids Surf*. **1992**, *62*, 255-257.

[17] A. D. Belapurkar, S.Kapoor, S. K. Kulshreshtha, J. P. Mittal, *Mater. Res. Bull*. **2001**, *36*, 145-151.

[18] K. S. Suslick , M. Fang, T. Hyeon, *J. Am. Chem. Soc*. **1996**, *118*, 11960-11961.

[19] F. W. S. Benfield, M. Green, J. S. Odgen, D. J. Young, *J. Chem. Soc. Chem. Commun*. **1973**, 866-867.

[20] M. T. Reetz, W. Heilbig, *J. Am. Chem. Soc*. **1994**, 116, 7401-7402.

[21] B. Chaudret, K. Philippot, *Oil& Gas Science and Technology* **2007**, 62, 799-817.

[22] B. Chaudret, *C. R. Physique* **2005**, 6, 117-131.

[23] K. Philippot, B. Chaudret, *C. R. Chimie* **2003**, 6, 1019-1034.

[24] R. M. Crooks, *Acc. Chem. Res*. **2001**, 34, 181-190.

[25] J. A. Anderson, M. Fernández Garcia, *Supported metals in catalysis*, Imperial college Press, London, **2005**.

[26] eds. B. C. Gates, L. Guczi, H. Knozinger, *Metal Clusters in Catalysis*, Elsevier, Amsterdam, **1986**.

[27] L. M. Rossi, L. L. R. Vono, M. A. S. Garcia, T. L. T. Faria, J. S. Lopez- Sanchez, *Top. Catal* **2013**, *56*, 1228-1238.

[28] B. Delmon, P. Grange, P. A. Jacobs, G. Poncelet, ed., *Preparation of Catalysts II*, Elsevier, Amsterdam, **1979.**

[29] C.-J. Jia, F. Schüth, *Phys. Chem. Chem. Phys.* **2011**, *13*, 2457-2487.

[30] J. A. Anderson, M. Fernández García, Ed. *Supported metals in catalysis*, Imperial college press. , London, **2005**.

[31] L. Barthe, A. Denicourt- Nowicki, A. Roucoux, K. Philippot, B. Chaudret, M. Hemati, *Catalysis Communication* **2009**, *10*, 1235-1239.

[32] K. Li, Y. Wang, J. Jiang, Z. Jin, *Catalysis Communications* **2010**, *11*, 542-546.

[33] M. Guerrero, N. T. T. Chau, S. Noël, A. Denicourt- Nowicki, F. Hapiot, A. Roucoux, E. Monflier, K. Philippot, *Current organic chemistry* **2013**, *17*, 364-399.

[34] N. M. Rodriguez, *J. Mater. Res.* **1993**, *8*, 3233-3250.

[35] Y. Motoyama, M. Takasaki, S.- H. Yoon, I. Mochida, H. Nagashima, *Org. Lett.* **2009**, *11*, 5042-5045.

[36] M. E. Grass, y. Zhang, D. R. Butcher, J. Y. Park, Y. Li H. Bluhm, K. M. Bratlie, T. Zhang, G. A. Somorjai, *Angew. Chem. Int. Ed.* **2008**, *47*, 8893-8896.

[37] M. Moreno-Mañas, R. Pleixats, *Acc. Chem. Res.* **2003**, *36*, 638-643.

[38] A. Balanta, C. Godard, C. Claver, *Chem. Soc. Rev.* **2011**, *40*, 4973-4985.

[39] See for instance: B. C. Ranu, R. Dey, K. Chattopadhyay, *Tetrahedron Lett.* **2008**, *49*, 3430-3432 and references therein.

[40] M. T. Reetz, J. G. de Vries, *Chem. Commun.* **2004**, 1559-1563.

[41] D. Sanhes, E. Raluy, S. Rétory, N. Saffon, E. Teuma, M. Gómez, *Dalton Trans.* **2010**, *39*, 9719-9726.

[42] A. Leyva- Pérez, J. Oliver- Meseguer, P. Rubio- Marqués, A. Corma, *Angew. Chem. Int. Ed.* **2013**, *52*, 11554-11559.

[43] G. Schmid, H. West, H. Mehles, A. Lehnert, *Inorg. Chem.* **1997**, *36*, 891-895.

[44] a) M. Zhao, R. M. Crooks, *Angew. Chem. Int. Ed. Engl.* **1999**, *38*, 364-366. b) M. Zhao, L. Sun, R. M. Crooks, *Polym. Prepr.* **1999**, *40*, 400-401. c) V. Chechik, R. M. Crooks, *J. Am. Chem. Soc.* **2000**, *122*, 1243-1244.

[45] A. Molnar, A. Sarkany, M. Varga, *J. Mol. Catal. A: Chem.* **2001**, *173*, 185-221.

[46] B. Chen, U. Dingerdissen, J. G. E. Krauter, J. G. J. L. Rotgerink, K. Mobus, D. J. Ostgard, P. Panster, T. H. Riermeier, S. Seebald, T. Tacke, H. Trauthwein, *Appl. Catal. A*, **2005**, *280*, 17-46.

[47] G. A. Somorjai, R. M. Rioux, *Catal. Today* **2005**, *100*, 201-215.

[48] G. A. Somorjai, J. Y. Park, *Angew. Chem. Int. Ed*. **2008**, *47*, 9212-9228.

[49] G. A. Somorjai, H. Frei, J. Y. Park, *J. Am. Chem. Soc*. **2008**, *131*, 16589-16605.

[50] R. Narayanan, M. A. El- Sayed, *Nano. Letters* **2004**, *4*, 1343-1348.

[51] C. J. Weststrate, A. Resta, R. Westerström, E. Lundgren, A. Mikkelsen, J. N. Andersen, *J. Phys. Chem. C* **2008**, *112*, 6900-6906.

[52] Y. Yuan, N. Yan, P. Dyson, *ACS Catal*. **2012**, *2*, 1057-1069.

[53] P. J. Dyson, *Dalton Trans*. **2003**, 2964-2974.

[54] P. Migowski, D. Zanchet, G. Machado, A. M. Gelesky, S. R. Teixeira, J. Dupont, *Phys. Chem. Chem. Phys*. **2010**, *12*, 6826-6833.

[55] S. A. Stratton, K. L. Luska, A. Moores, *Catalysis Today* **2012**, *183*, 96-100.

[56] M. R. Axet, S. Castillón, C. Claver, K. Philippot, P. Lecante, B. Chaudret, *Eur. J. Inorg. Chem*. **2008**, 3460-3466.

[57] Y. Zhang, M. E. Grass, S. E. Habas, F. Tao, T. Zhang, P. Yang, G. A. Somorjai, *J. Phys. Chem. C*. **2007**, *111*, 12243-12253.

[58] Y. Xia, Y. Xiong, B. Lim, S. E. Skrabalak, *Angew. Chem. Int. Ed*. **2009**, *48*, 60-103.

[59] A. Gual, J. A. Delgado, C. Godard, S. Castillón, D. Curulla- Ferré, C. Claver, *Top. Catal*. **2013**, *56*, 1208-1219.

[60] J. Schulz, A. Roucoux, H. Patin, *Chem. Eur. J*. **2000**, *6*, 618-624.

[61] J. Schulz, S. Levigne, A. Roucoux, H. Patin, *Adv. Synth. Catal.* **2002**, *344*, 266-269.

[62] A. Roucoux, J. Schulz, H. Patin, *Adv. Synth. Catal.* **2003**, *345*, 222-229.

[63] V. Mévellec, A. Roucoux, E. Ramirez, K. Phillipot, B. Chaudret, *Adv. Synth. Catal*. **2004**, *346*, 72-76.

[64] A. Nowicki, V. Le Boulaire, A. Roucoux, *Adv. Synth. Catal,* **2007**, *349*, 2326-2330.

[65] C. Hubert, A. Denicourt-Nowicki, J. P. Guégan, A. Roucoux, *Dalton Trans*. **2009**, 7356-7358.

[66] V. Mévellec, A. Nowicki, A. Roucoux, C. Dujardin, P. Granger, E. Payen, K. Philippot, *New. J. Che,*. **2006**, *30*, 1214-1219.

[67] a) H. Hirai, Y. Nayao, N. Toshima, *J. Macromol. Sci. Chem.* **1978**, *A12*, 1117-1141; b) H. Hirai, Y. Nakao, N. Toshima, *J. Macromol. Chem*. **1979**, *A13*, 633-649; c) H. Hirai, Y. Nakao, N. Toshima, *J. Macromol. Chem*. **1979**, *A13*, 727-750.

[68] T. Gutel, C. Santini, K. Philippot, A. Padua, K. Pelzer, B. Chaudret, Y. Chauvin, J.- M. Basset, *J. Mater. Chem*. **2009**, *19*, 3624-3631.

[69] J. D. Aiken III, R. G. Finke, *J. Am. Chem. Soc*. **1999**, *121*, 8803-8810.

[70] P. Lara, K. Philippot, B. Chaudret, *Chem. Cat. Chem*. **2013**, *5*, 28-45.

[71] a) F. Fache, S. Lehuede, M. Lemaire, *Tetrahedron Letters* **1995**, *36*, 885-888. (b) K. Nasar, F. Fache, M. Lemaire, J. C. Béziat, M. Besson, P. Gallezot, *J. Molec. Catal.* **1994**, *87*, 107-115.

[72] D. Gonzalez- Galvez, P. Nolis, K. Philippot, B. Chadret, Piet W. N. M. van Leeuwen, *ACS catal.* **2012**, *2*, 317-321.

[73] D. Gonzalez-Galvez, P. Lara, O. Rivada-Wheelaghan, S. Conejero, B. Chaudret, K. Philippot, P.W.N.M. van Leeuwen, *Catal. Sci. Technol*. **2013**, *3*, 99-105.

[74] M. Guerrero, A. Roucoux, A. Denicourt- Novicki, H. Bricout, E. Monflier, V. Collière, K. Fajerwerg, K. Philippot, *Catal. Today* **2012**, *183*, 34-41.

[75] M. Gómez, I. Favier Chapter 31 in *Metal Nanoclusters in Catalysis and Materials Science: The issue of size control*. Elsevier, Amsterdam, **2008**, Ed. By B. Corain, G. Schmid, N. Toshima.

[76] E. E. Finney, R. G. Finke, *Inorg. Chim. Acta* **2006**, *359*, 2879-2887.

[77] J. A. Widegren, M. A. Bennett, R. G. Finke, *J. Am. Chem. Soc*. **2003**, *125*, 10301-10310.

[78] K. S. Weddle, J. D. Aiken III, R. G. Finke, *J. Am. Chem. Soc*. **1998**, *120*, 5653-5666.

[79] C. M. Hagen, J. A. Widefren, P. M. Maitlis, R. G. Finke, *J. Am. Chem. Soc*. **2005**, *127*, 4423-4432.

[80] J. S. Bradley, in G. Schmid (ed.) *Clusters and colloids: From theory to Applications*, *Chapter 6*, VCH, Weinheim, **1994**, 459.

[81] L. N. Lewis, *J. Am. Chem. Soc*. **1986**, *108*, 743-749.

[82] R. M. Laine, *J. Mol. Catal*., **1982** *14*, 137-169.

[83] M. A. Watzky, R. G. Finke, *J. Am. Chem. Soc*, **1997** *119*, 10382-10400.

[84] K. J. Laidler, *Chemical Kinetics*, Harper Collins publishers, New York, **1987**.

[85] G. M. Whitesides, M. Hackett, R. L. Brainard, J.- P. P. M. Lavalleye, A. F. Sowinski, A. N. Izumi, S. S. Moore, D. W. Brown, E. M. Staudt, *Organometallics* **1985**, *4,* 1819-1830.

[86] B. R. James, *Homogeneous Hydrogenation*, Wiley- Interscience, New York, **1973**.

[87] L- Gonzalez- Tejuca, K. Aika, S. Namba, J. Turkevich, *J. Phys. Chem.* **1977**, *81*, 1399-1406.

[88] F. Novio, D. Monahan, Y. Coppel, G. Antorrena, P. Lecante, K. Philippot, B. Chaudret, *Chem. Eur. J*. **2014**, *20*, 1287-1297.

[89] G. S. Fonseca, A. P. Umpierre, P. F. P. Fichtner, S. R. Teixeira, J. Dupont, *Chem. Eur. J.* **2003**, *9*, 3263-3269.

[90] a) G. W. Parshall, S. D. Ittel, *Homogeneous Catalysis*, Wiley-Interscience, New York, **1992**; b) *An Integrated Approach to Homogeneous, Heterogeneous and Industrial Catalysis* (Eds.: J. A. Moulijn, P. W. N. M. van Leeuwen, R. A. van Santen), Elsevier, Amsterdam, **1995**;

c) *Applied Homogeneous Catalysis with Organometallic compounds* (Eds.: B. Cornils, W. A. Herrmann), VCH, Weinheim, **1996**.

[91] J. D. Aiken, Y. Lin, R. G. Finke, *J. Mol. Catal. A Chem.* **1996**, *11*4, 29-51.

[92] A) J. A. Widegren, R. G. Finke, *J. Mol. Catal. A: Chem*. **2003**, *191*, 187-207.

[93] A. Gual, C. Godard, S. Castillón, C. Claver, *Dalton Trans*. **2010**, *39*, 11499-11512.

[94] K. Weissermel, H. J. Arpe, *Industrial Organic Chemistry*, 2nd edn, VCH, New York, **1993**; H. Nagahara, M. Ono, M. Konishi and Fukuoka, *Appl. Surf. Sci.*, **1997**, *121-122*, 448-451.

[95] Y. Zhao, J. Zhou, J. Zhang, S. Wang, *Catal. Commun*. **2008**, *9*, 459-464.

[96] H. Nagahara, M. Konishi, EP Patent 0220525, 1987, to Asahi Kasei Kogyo Kabushiki Kaisha

[97] D. Astruc, *Nanoparticles and catalysis*, Wiley-VCH, Weinheim, **2008**.

[98] H.U. Blaser, U. Siegrist, H. Steiner, M. Studer, *in Fine Chemicals through Heterogeneous Catalysis*, Wiley- VCH, Weinheim, **2001**, p.389.

[99] R. S. Downing, P. J. Kunkeler, H. van Bekkum, *Catal. Today* **1997**, *37*, 121-136.

[100] J. Butera, J. Bagli, WO Patent 91/09023, **1991.**

[101] F. Kovar, F. E. Armond, U.S. Patent 3,975,444, **1976.**

[102] X. Yuan, N. Yan, C. Xiao, C. Li, Z. Fei, Z. Cai, Y. Kou, P. Dyson, *Green Chem*. **2010**, *12*, 228-233.

[103] US Pat. 4129414, **1978.**

[104] P. Lara, A. Suárez, V. Collière, K. Philippot, B. Chaudret, *ChemCatChem*. **2014**, *6*, 87-90.

[105] M. Liu, J. Zhang, J. Liu, W. Yu, *Journal of Catalysis* **2011**, *278*, 1-7.

[106] Md. J. Sharif, P. Maity, S. Yamazoe, T. Tsukuda, *Chem. Lett*. **2013**, *42*, 1023-1025.

[107] S. Cai, H. Duan, H. Rong, D. Wang, L. Li, W. He, Y. Li, *ACS Catal*. **2013**, *3*, 608-612.

[108] M. A. Harrad, B. Boualy, L. Firdoussi, A. Mehdi, C. Santi, S. Giovagnoli, M. Nocchetti, M. A. Ali, *Cat. Commun.* **2013**, *32*, 92-100.

[109] a) G.S Fonseca, J.D Scholten, J. Dupont, *Synlett* **2004**, *9*, 1525-1528. b) F. Jutz, J.-M Andanson, A. Baiker, *J. Catal.* **2009**, *268*, 256-266.

[110] J. Zheng, H. Lin, T-N. Wang, X. Zheng, X. Duan, Y. Yuan, *Journal of Catal*. **2013**, *297*, 110-118.

[111] R. J. Bonilla, B. R. James, P. G. Jessop *Chem. Commun.* **2000**, 941-942.

[112] V. Cimpeanu, M. Kocevar, V. I. Parvulescu, W. Leitner, *Angew. Chem. Int. Ed*. **2009**, *48*, 1085-1088.

[113] a) U. Schmidt, A. Lieberknecht, J. Wild, *Synthesis* **1988**, 159-1972. b) C. Bonauer, T. Walenzyk, B. König, *Synthesis* **2006**, 1-20.

Chapter 2.

Synthesis and characterisation of Rh-NPs stabilised by phosphine and phosphite ligands
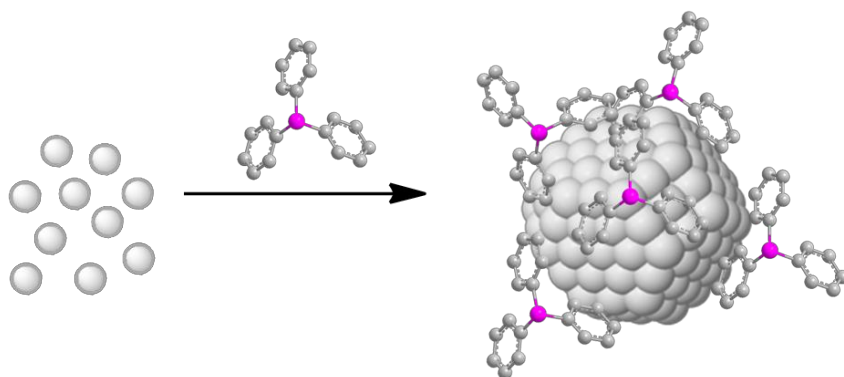
2.1 Introduction

2.1.1 *Synthetic methods reported for Rh-NPs*

As mentioned in Chapter 1, the formation of zero-valent metal nanocatalysts can be obtained through a variety of methods and in different media. For the synthesis of rhodium nanoparticles, several of these methods were reported.[1]

The methodology mainly used in the literature is the chemical reduction of metal salts using reducing agents such as sodium borohydride.[2] For instance, Roucoux and co- workers reported the preparation of rhodium(0) nanoparticles by reduction of rhodium trichloride with sodium borohydride in the presence of bipyridine and ILs (Figure 2.1).[3] The synthesis was performed under aerobic conditions and at room temperature, obtaining small nanoparticles of *ca*. 2.0-2.5nm.
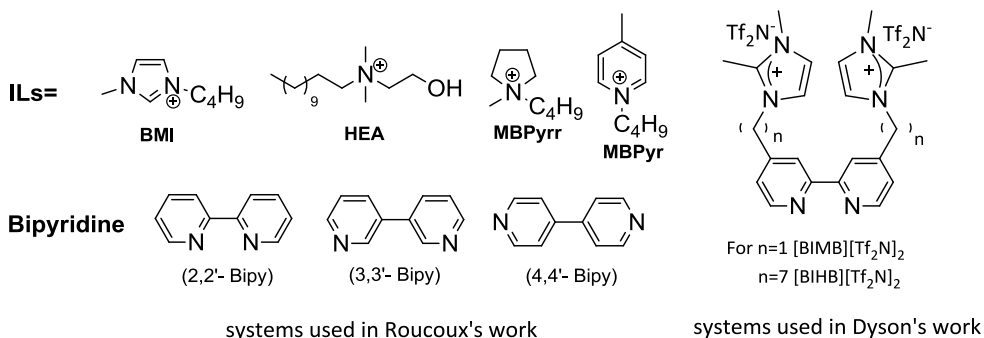
Figure 2.1 ILs and bipyridine ligands used in the study of Roucoux and Dyson.[3,4]

Similar approach was used by Dyson and co- workers a few years later using ILs containing imidazolium groups modified with bipyridine units.[4] The synthesis of these systems is described and correlated with the steric and electronic effects of the modified ligands. This study revealed that the functionalisation increases the catalytic activity of the systems and facilitates the subsequent separation of the products from the catalysts

through the retention of the NPs in the reaction medium during product extraction.

These systems were applied as catalysts in the hydrogenation of arenes, analysing the influence of the nature of the stabiliser on the catalytic activity.

Rhodium nanoparticles can also be formed by thermal decomposition. For instance, the group of Somorjai reported the decomposition of Rh(acac)$_3$ at 140 °C in 1,4- butanediol and with polyvinylpyrrolidone (PVP) as stabilising agent.[5] Nanoparticles with diameters between 7 and 12 nm were obtained and characterised using several techniques such as UV, FTIR or Raman spectroscopy. This report showed that spectroscopic techniques are a very effective tool to study the degradation of the PVP stabiliser, the electronic structure of the metal/PVP interface or the aggregation of the nanoparticles.

Metal vapour synthesis is less used in the literature for the synthesis of rhodium nanoparticles. However, Martra and co- workers successfully synthesised supported rhodium nanoparticles via this methodology.[6] Bulk rhodium and mesitylene were vaporised under vacuum and deposited on the frozen walls (-196 °C) of a glass reactor (Figure 2.2). HRTEM revealed the formation of small nanoparticles of *ca*. 2nm.
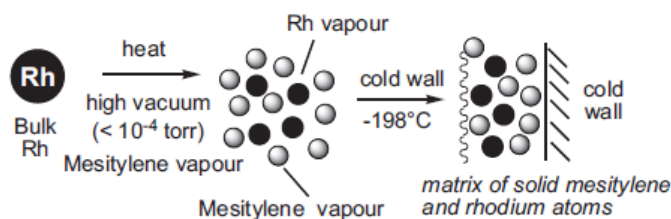
Figure 2.2 Methodology used by Martra and co- workers to synthesise Rh- NPs.[6]

The Rh-NPs were supported in organic and inorganic matrices and applied as catalysts in silylcarbocyclisation of alkynes reactions that generate β- lactones and β- lactams in high yields, showing a better specific activity than the corresponding commercial catalysts.

The organometallic approach was also reported for the synthesis of rhodium nanoparticles. An example was reported by our group, in collaboration with that of Prof. Chaudret, for the synthesis of rhodium nanoparticles stabilised by chiral diphosphite ligands.[7] Two organometallic precursors were used in this study: $[Rh(\eta^3\text{-}C_3H_5)_3]$ and $[Rh(\mu\text{-}OMe)(cod)]_2$. Both were reduced under hydrogen pressure with THF as solvent and with chiral diphosphites as stabilisers. In this work, the shape, size and dispersion of the nanoparticles were distinct depending on the precursor used. The decomposition of $[Rh(\eta^3\text{-}C_3H_5)_3]$ provided small rhodium nanoparticles of 2-3 nm, whereas sponge-like structures were obtained from $[Rh(\mu\text{-}OMe)(COD)]_2$ of 50 and 35nm depending on the ligand used as stabiliser. Both, the stabiliser and the precursor affected the nanoparticles size and shape. These Rh-NPs were active catalysts in the hydroformylation of styrene. However, high pressure NMR revealed the formation of molecular complexes under CO/H_2 pressure that could be the real catalysts, and it was concluded that these NPs could be considered as reservoir for molecular catalysts under hydroformylation conditions.

As its describe, rhodium is wide use in the literature as nanoparticles metal, the election of the synthetic methodology, the precursor and the stabilising agent could be crucial for a certain application of these type of systems.

2.1.2 *Synthetic methods for the preparation of Rh-NPs stabilised by P-based ligands*

Several studies are reported in the literature on the use of ligands to stabilise nanoparticles providing precise definition of the catalytic systems.[8] Phosphorus based ligands such as phosphines and phosphites are extensively used in homogeneous catalysis due to their broad coordination chemistry with transition metals and the possibility to fine-tune the electronic and steric properties of the catalysts through structural modifications of the ligands to obtain high activity and selectivity in catalytic processes.[9] In the last decade, these ligands were also shown to

efficiently stabilise metal nanoparticles that are catalysts in several catalytic reactions.[2,10] However, to date, the fine tuning of the properties of this type of catalysts to achieve specific selectivities remains a challenge.

Jin and co-workers reported the reduction of rhodium trichloride under hydrogen in presence of the thermoregulated ligand $Ph_2P(CH_2CH_2O)_nCH_3$ (n=16) using 1-butanol and water as solvent.[11] This type of ligands allow the system to transfer from aqueous phase to 1-butanol phase and vice versa by means of changing the temperature. Small nanoparticles of *ca.* 2.4± 0.3nm were obtained and used in the hydrogenation of olefins. The use of this type of ligands allows the efficient recycling of the catalyst and revealed to play an important role in the catalytic properties of the obtained systems.
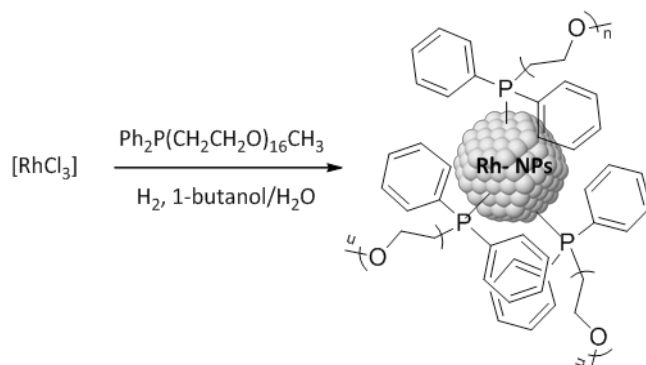
Figure 2.3 Synthetic methodology used for the preparation of Rh-NPs reported by Jin and co-workers.[11]

Li and co-workers reported the chemical reduction of rhodium trichloride by sodium borohydride employing the chiral (R)-BINAP ligand as stabiliser.[12] The nanoparticles were obtained following the strategy showed in Figure 2.4. These systems were used in the asymmetric hydroformylation of styrene and vinyl acetate and enantioinduction was achieved in some cases. The authors assumed that a heterogeneous process was taking place, although no mechanistic study nor poisoning tests were reported.
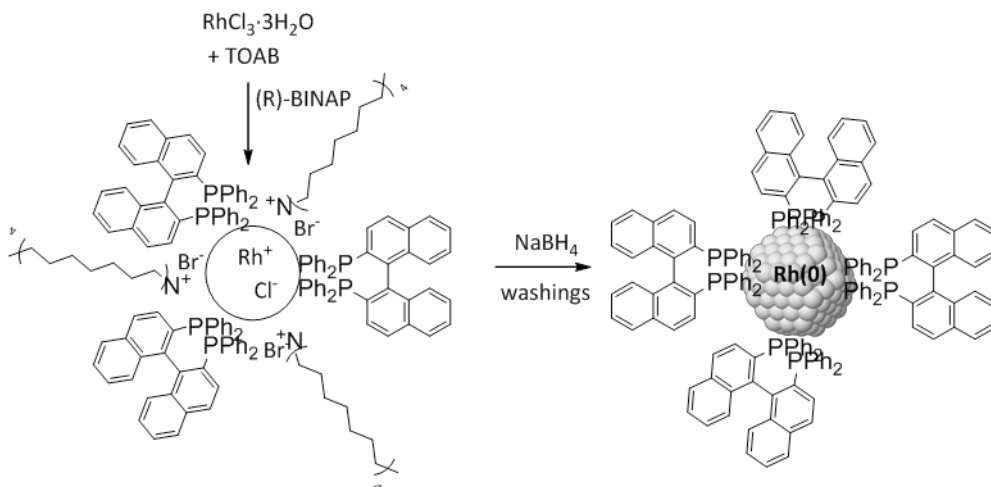
Figure 2.4 Synthetic approach used by Li and co-workers for the preparation of Rh-NPs stabilised by BINAP.[12]

However, Philippot and co-workers proposed the formation of molecular species acting as real catalysts for these systems.[13] Moreover, in our group, using rhodium nanoparticles stabilised by diphosphite ligands as catalysts in hydroformylation reactions the presence of homogeneous systems, was demonstrated by HP-NMR.[7]

Since the synthetic method used in this thesis for the preparation of NPs is the decomposition of an organometallic complex, the main reports using this methodology for the synthesis rhodium nanoparticles stabilised by P-based ligands are detailed as follows.

Masdeu-Bultó and Gómez reported the synthesis of Rh-NPs stabilised by triphenylphosphine and its fluorinated derivatives with the aim of increasing the affinity of M-NP to scCO$_2$.[14] The precursor [Rh(μ-OMe)(cod)]$_2$ was decomposed under H$_2$ in presence of the corresponding phosphine ligand. The nanoparticles were characterised by TEM revealing systems of *ca.* 2 nm and with tendency to agglomerate. IR was also performed to these samples, observing the band at *ca.* 802 cm^{-1}, characteristic of the C-P bond and elemental analysis revealed a content of 17% in rhodium for the nanoparticles stabilised by triphenylphosphine. These NPs were used as

catalysts for the hydrogenation of substrates containing aromatic groups. ScCO$_2$ and THF were used as solvent, showing different activities of the catalysts dealing with solubility issues. Moreover, the selectivity observed employing these systems, revealed a strong interaction between the phenyl groups of the substrates and the surface.

Moores and co- workers reported an interesting work in the use of phosphine functionalised imidazolium ionic liquid (FILs) as Rh-NPs stabilisers (Figure 2.5).[15]
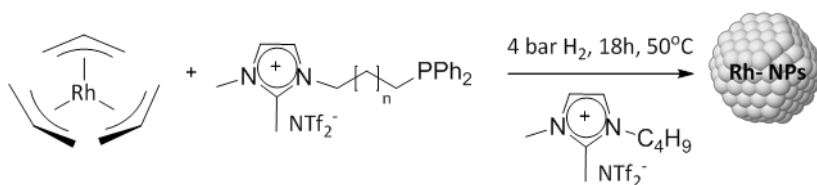
Figure 2.5 Method reported by Moores and co- workers for the synthesis of Rh-NPs.[15]

The influence of the chain length spacer of these FILs was also studied, compared with triphenylphosphine as stabiliser. The systems were only characterised by TEM, obtaining *ca.* 2 and 1.5 nm for the FILs and PPh$_3$ stabilised nanoparticles, respectively.

As previously mentioned, chiral diphosphites derived from carbohydrates were reported as stabilisers for Ru, Rh and Ir nanoparticles.[16] Modifications of the 1,2-O-isopropyliden-α- D- Xylofuranose and 1,2-O-isopropyliden-α-D-glucofuranose backbones were carried out and affected the size dispersion and shape of these systems.
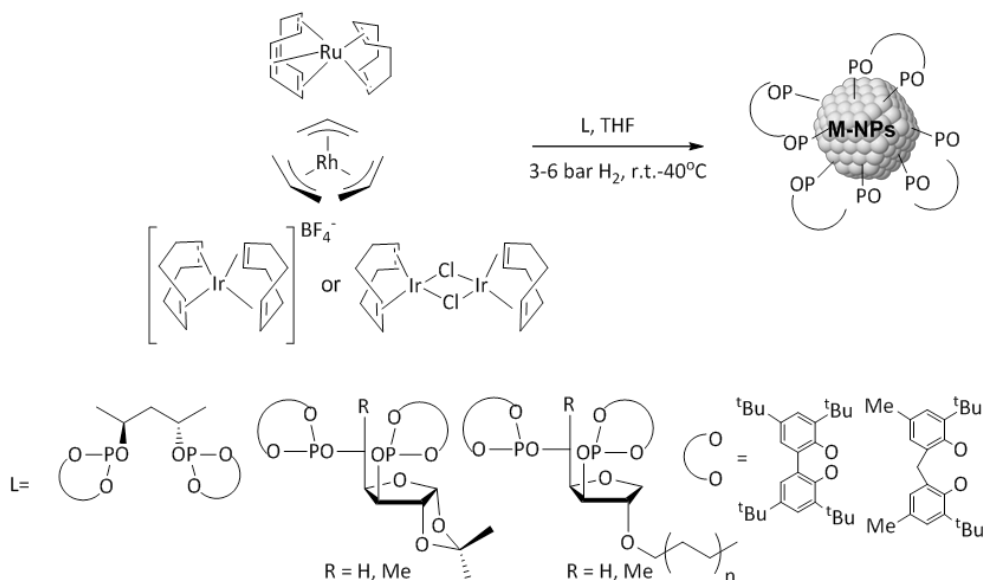
Figure 2.6 Synthesis of M-NPs through decomposition of organometallic precursors in the presence of diphosphite ligands.[16]

The rhodium nanoparticles were smaller (2.5nm) than their ruthenium (4nm) analogues using the same ligand. For the rhodium systems, increasing the steric hindrance of the ligand caused a decrease in size of the nanoparticles. However, no obvious effect of the metal precursor on the size and shape of the formed nanoparticles was observed. The systems were also characterised using elemental analysis by ICP obtaining a content of *ca.* 25% and 3-4% in weight of rhodium and phosphorus respectively. These nanoparticles were used as catalysts for the hydrogenation of *o-* and *m-* methylanisole. The structure of the stabilising ligand revealed to have an effect on the catalytic activity, indicating that through the utilization of the appropriate ligands, the activity and selectivity of such catalysts can be modulated.

Another interesting study was recently reported by Dyson and co-workers that involved PVP- stabilised Rh nanoparticles synthesised by alcoholic reduction of RhCl$_3$ in the presence of PVP.[17] After the formation of the nanoparticles, various phosphine ligands were added to investigate the

possible effects on the morphology of the systems and study how the modification of the surface properties of the nanoparticle are affected by the steric and electronic properties of these ligands. (Figure 2.7).
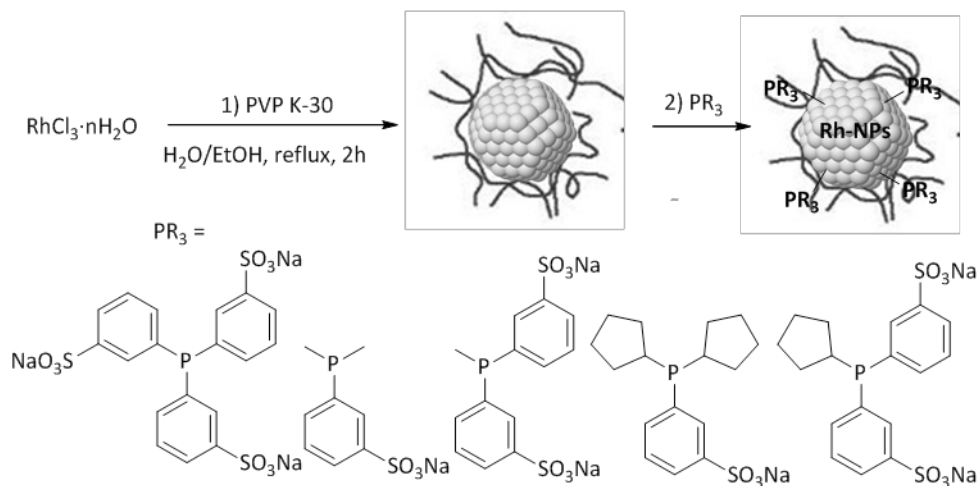
Figure 2.7 Synthetic methodology used in the study of Dyson and co- workers.[17]

TEM analysis revealed the formation of nanoparticles of 3-4 nm of diameter, and the addition of phosphine ligands had no significant effect on the nanoparticle size distribution. IR spectroscopy after CO exposure was showed the disappearance of a CO stretching band at *ca.* 2100 cm^{-1} when phosphines are added. It was deduced that upon addition of the ligands, a specific CO adsorption site was capped. These systems were applied in the hydrogenation of functionalised aromatic compounds. The authors reported that the phosphine ligands modified the properties of the nanoparticle surface and consequently influenced their catalytic performances such as the selectivity for arene vs ketone hydrogenation. In this study, the phosphine ligands were described as "selective poisons" for surface active sites.

These reports showed that P-donor ligands are able to efficiently stabilise Rh-NPs and could be used to modulate the activity/ selectivity of these NPs in catalysis. It is therefore important to gain information on their coordination and behaviour at their surface.

2.1.3 *Characterisation techniques*

Although various characterisation techniques are available for metal nanoparticles, the precise of metal nanoparticles, remains a challenge.[18]
In this thesis, various techniques were utilised to determine the size, structure, chemical composition and content of the nanoparticles synthesised (Figure 2.8). The fundamentals of these characterisation techniques are briefly described in the following sections.

TEM: size, morphology, dispersion   **XPS**: chemical environment at the surface

Rh(0)

XRD: crystallinity, packing, size   **TGA**: content of the NPs in % weight
WAXS:
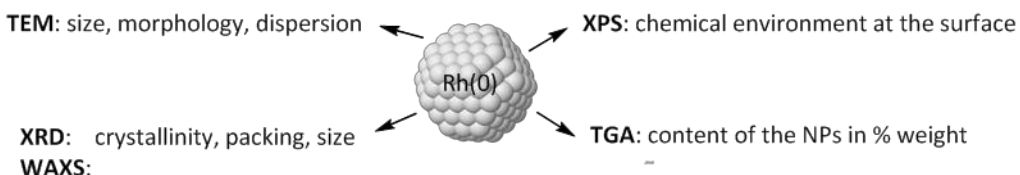
Figure 2.8 Characterisation techniques used in this study.

a) Transmission electron microscopy (TEM, HRTEM)

Transmission electron microscopy (TEM) is the most widely used technique to characterise metal nanoparticles. TEM has routine magnifications of 10^6 with a resolution of ± 4Å, this parameter can be improved to ± 2Å with a high resolution transmission electron microscopy (HRTEM). These techniques provide direct visual information by simple inspection of the high magnification images on the size, shape, dispersity, structure and morphology of the metallic nanoparticles.[19]

However, this technique presents some disadvantages such as the only two- dimensional interpretation and that the examination of the samples is performed under high- vacuum conditions, and no direct information on the nanoparticles under catalytic conditions can be obtained.

b) X- Ray diffraction (XRD)

X- Ray diffraction is a non destructive technique which can identify the crystal phase structure and composition for crystalline systems. The theory of XRD on single crystals was developed by Laue and Bragg in the early

1900s. However, dealing with nanomaterials instead of single crystals, XRPD (P= powder) is used. Powder is defined as a large amount of small crystallites randomly oriented in space.[20]

The peak position of X-ray powder diffractogram reflects the crystallographic symmetry, while the peak intensity is related to the unit cell composition. The diffraction line shape gives information about sample microstructure and defects distribution at the atomic level. For that reason, the analysis of nanoparticles samples that are deviated from the ideal crystalline structure produce broad XRPD lines.

c) Wide angle X- Ray Scattering (WAXS)

WAXS is an X- ray diffraction technique specifically analyses the Bragg Peaks scattered at wide angles, which (by Bragg's law) are caused by small crystalline structures. The samples are analysed in solid state, sealed in 1mm Lindemann glass capillaries. The diffused corrected intensity is due to the chemical composition, structure and the interaction between the nanoparticles. The radial distribution function is obtained by the Fourier transform of the intensity, and facilitates interpretation. The WAXS provides a distribution of the metal-metal bonds inside a homogeneous assembly of nanoparticles, since well- defined RDF indicates well-crystallised nanoparticles.

Using a model it is then possible to have information of the structure of the particle and to its coherence length, assuming that all particles adopt the same size and structure.

- Measurement of the nanoparticle size

Nanoparticle size could be obtained by the previous described techniques. TEM gives visual measurement of the size of the systems that by resolution issues is often reproduced as the approximate diameter of a sphere. XRD and WAXS provide a coherence length that if each particle in a powder sample is a single crystal, the distribution of size frequently has a lognormal distribution.

In order to compare estimates of the mean diameter derived from TEM, XRD and WAXS, it is essential to define the way in which the mean values are calculated.[21]
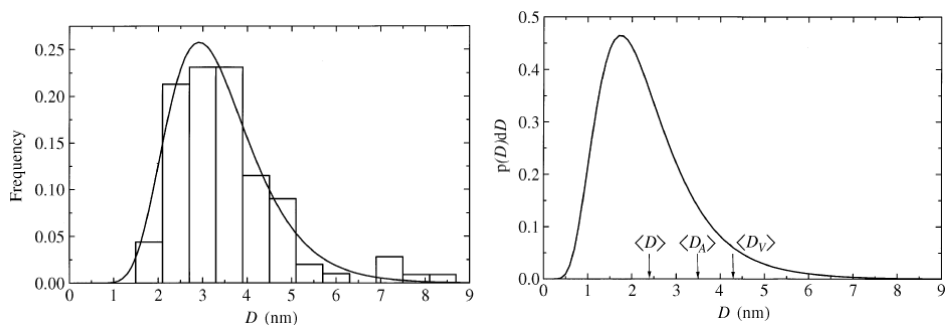
Figure 2.9 a) Crystallite size distribution from TEM data, with corresponding lognormal distribution. b) Lognormal distribution from least- squares fitting of XRD data.

TEM data are collected as average particle diameters, directly from the micrograph, the mean value and standard deviation is measured using a Gaussian approximation (Figure 2.9 a). For XRD, in the case of spherical crystallites for example, the equivalent volume- weighted mean diameter (D_v) and the area- weighted mean diameter shown in Figure 2.9 are calculated by equations described by Matyi and co-workers.[22]

Differences are observed between both methodologies, for instance if particles contain subgrains that are not revealed in the micrographs, the mean size obtained by XRD will be smaller. Moreover, it is important to note that the size of domains which diffract coherently is determined from XRD data and this may not be the quantity of interest in some applications, such as catalysis, if particles are not single crystals and the reaction is performed at the defects of the systems for instance.

For these reasons, it is important to specify which value is provided for the diameter and the approximation that was used to calculate it. The most common way to describe the size of a nanoparticle distribution is by the mean size (D), however, some techniques provide D_v which corresponds to the maximum size obtained for a given sample.

d)   X-Ray photoelectron spectroscopy (XPS)

The X- Ray photoelectron spectroscopy (XPS) is a technique used to investigate the chemical environment at the surface of a sample.

Basically, XPS counts electrons ejected from a sample surface when irradiated by X- rays. The chemical shift observed in XPS data is therefore a valuable source of information providing information on the nature of the atoms contained in the sample such as the oxidation state of a metal. A spectrum representing the number of electrons recorded at a sequence of energies includes both a contribution from a background signal and also resonance peaks characteristic of the bound states of the electrons in the surface atoms. The resonance peaks above the background are the significant features in an XPS spectrum.

XPS spectra are quantified in terms of peak intensities and peak positions. The peak intensities measure how much of a material is at the surface, while the peak positions indicate the elemental and chemical composition.

The theoretical peaks for the binding energies for rhodium species are reflected in Table 2.1.

Table 2.1 Binding energies for rhodium species.

	3d5/2	3d3/2
Rh(0)	307.2	311.9
Rh(I)	308.3	313.2
Rh(III)	309.4	314.8

e)   Thermogravimetric analysis (TGA)

Thermogravimetric analysis is defined as an experimental method for characterising a system (element, compound or mixture) by measuring changes in physic- chemical properties as a function of increasing temperature.[23]

The basic instrumental requirements for TGA are a precision balance and a furnace that is programmed for a linear rise of temperature with time. The results from a TGA run may be presented by weight versus temperature (or time) curve, referred to this type of analysis as thermogravimetric curve or by rate of loss of weight versus temperature curve, referred as the differential TGA curve.

f)   Solid state NMR spectroscopy
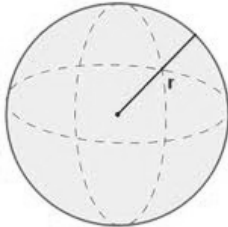
In recent years, gas phase and solid state NMR spectroscopy were also used for the surface characterisation of M-NPs, in particular Ru, has been demonstrated.[24,25,26,27] The group of Chaudret and co-workers first demonstrated the presence of hydride ligands by H/D exchange using gas phase NMR. Moreover, in recent years, the use of solid state ^{31}P and ^{13}C NMR has been employed to gain information on the location and dynamics of the stabilising ligands at the surface of small Ru-NPs. They for instance could demonstrate by ^{31}P NMR the coordination of polyphosphines to the surfaces of the particles through the P-atoms. More recently, they studied the coordination of NHC-carbene ligand on similar Ru-NPs. Similar studies were recently extended to other metals such as Au and bimetallic Ru-Pt system.[28,29]

2.1.4   *Theoretical considerations for the calculation of the number of atoms*

For the characterisation of metal nanoparticles, several models can be used to obtain further information on these nanoobjects such as the approximate total number of metal atoms contained in these compounds or the distribution of these atoms at the different sites of their surface. The main models reported in the literature will be summarised in the following section.

Sphere model

The most simple methodology to calculate the number of atoms contained in a nanoparticle involves considering this system as a sphere.[30] The volume of this structure is used to calculate total number (Nt) of atoms in a nanocluster of a given diameter using the equation showed in Figure 2.10.

Nt= (N$_A$ρV)/Mr
N$_A$= the number of Avogadro
ρ= the density
V= volume of the particle Mr the molecular weight
V= 3/4πr^3

Figure 2.10 Equations used by the sphere's model.

The number of total atoms is thus calculated directly from the diameter of the particle and does not take the structure of the systems into account.

"De Vrie's" model

De Vries and co- workers used the sphere model to calculate Nt in a nanoparticle but also included the density of the nanoparticles and of the metallic atoms.[31] With this methodology, the number of surface atoms (Ns) is calculated considering the NPs as a sphere. They for instance reported the calculations Nt and Ns for iron nanoparticles using this approximation (Figure 2.11).
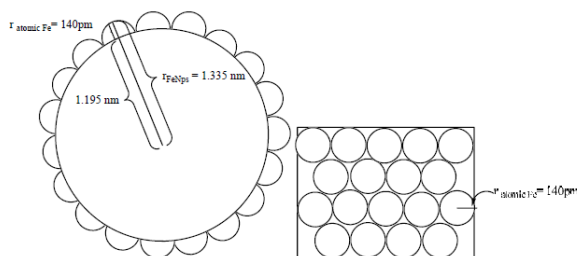
Figure 2.11 Methodology used by de Vries to calculate the number of surface atoms in NPs.

The radius and volume of the metallic atoms forming the nanoparticles are also considered with this method to obtain the number of surface atoms (Ns) of a nanoparticle.

To summarise, with these two models, the nanoparticles are considered as a sphere and the methodology reported by de Vries also includes the radius, the density and volume of the atomic metals that form the nanoparticles to calculate Nt and Ns.

Magic number

The "magic number" approach is based on the consideration that the formation of clusters containing certain numbers of atoms occurs much more frequently than others.[32] These magic numbers are 3, 4, 6 and 8 that are in fact the smallest nontrivial triangular, tetrahedral, octahedral and cubic numbers. The progression of these magic numbers, as a result of packing of atoms according to certain prescribed rules governed by electronic and/or steric principles, may be termed magic sequences. Magic numbers and sequences in cluster formation are intimately related to the nucleation and growth processes, which are governed by the often competing bonding and packing factors. Nt and Ns are calculated through the model building blocks that are distributed in layers for a given polyhedral such as for example an icosahedra (Figure 2.12).
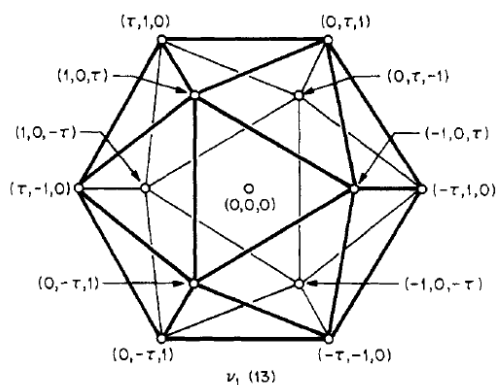
Figure 2.12 Icosahedra model used for the magic number approach.

The growth in size of these clusters, via either layer- by- layer or cluster-of-clusters growth pathways, form sequences of magic numbers as a result of filling the electronic or atomic shells or both. In many cases, these progressions correspond to the succession of high- frequency polyhedral clusters of increasing size while maintaining overall shape and symmetry.

The use of the "magic number" approach provide an accurate calculation of Nt and Ns of a given nanopaticle.

Van Hardevel Hartog
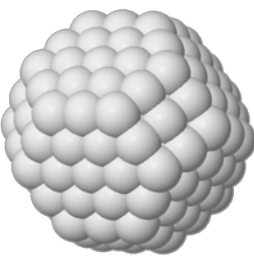
Van Hardevel Hartog published a model based on the principle that atoms at the surface of a metal crystal can be differentiated according to the number and arrangement of their nearest neighbours. The algebraic expressions for the populations of atomic site types with different coordination numbers were reported as a function of the cluster edge length m that is expressed as a number of atoms for several geometries. [33,34]

The total number of atoms (Nt) constituting a crystal is made of a number of bulk atoms (Nb) and of surface atoms (Ns). The number of total atoms (Nt) is extracted from the equation of the relative particle size $d_{rel} = b(Nt)^{1/3}$, where the diameter d_{rel} is provided by the observation of a sample some of the previously commented techniques and b is a constant that is equal to 1.105 for close packed crystallographic structures (fcc and hcp). This model proposes that the shape of nanosized particles can be represented by cubooctahedrons. However, there is no experimental evidence that all particles have such a shape or preserve such structure at any temperature.

Moreover two types of cubooctahedrons are described in the literature for Rh-NPs: standard and truncated cubooctahedrons.[35] The difference between these two structures relies on the distance (R), that is the longest distance in the cubooctahedron, and correspond the diagonal following the (110) direction.[36] When 0.87 < R < 1.73 (nm), the corresponding particles with exhibit a truncated octahedral structure containing both (100) and

(111) facets, if not the systems follows a standard cubocotahedral structure.

However, both the truncated and standard cubooctahedral structures provide very similar results since the same types of facets are present in both models and that only small differences can be observed in the number of atoms for each site.

The equations providing Nt and Ns are displayed in Figure 2.13. In this figure, the structure of a perfect cubooctaedron where m= 3 is represented, *m* being the number of atoms lying on an equivalent edge (corner atoms included).

		m		
		2	3	>3
Nt		38	201	$16m^3-33m^2+24m-6$
Nb		6	79	$16m^3-63m^2+84m-38$
Ns		32	122	$30m^2-60m+32$
N (corner)		24	24	24
N (edge)		0	12	$12(m-2)$
N (fase 100)		0	6	$6(m-2)$
N (fase111)		8	56	$8(3m^2-pm+7)$

Figure 2.13 Representation of Fcc perfect cubooctaedron m= 3 and values obtained for the different type atoms in this system.

For these model structures, the surface metal atoms are located on the (111) or (100) planes constituted by the faces (N_{face}), edges (N_{edge}) and corners (N_{corner}). The systems defined by this structure are regular, the number of metal atoms on each edge is the same for a given cubooctahedron.

The variations in Ns/ Nt ratios for corner, edge and face atoms as a function of the mean diameter of nanoparticles (1-10 nm) with fcc packing structure such as Rh NPs is represented in Figure 2.14.
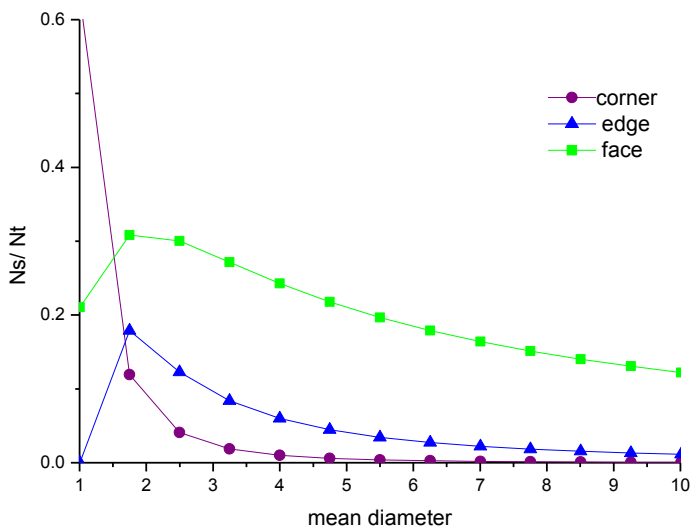
Figure 2.14 Number of atoms, distributed in corner, edges and faces depending on the mean diameter for fcc structures.

This graph indicates that the atoms on the faces predominate when the mean diameter is higher than *ca*. 2nm, and that this size corresponds to the the highest Ns/Nt.

Comparative study of the different modes

The previously commented methodologies were used to calculate Nt and Ns for a rhodium nanoparticle of 1.5nm of diameter with these 4 models. The results are reflected in Table 2.2.

Table 2.2 Values of Nt and Ns for a Rh-NPs of 1.5nm using the models previously described.

Model	Nt	Ns
Sphere	128	-
De Vries	130	77
Magic Numbers	136	87
VHH	130	82

As can be observed, only small differences in Nt and Ns are observed for these models.

In this PhD thesis, the VHH model was used to extract the approximate number of atoms in each specific position of the nanoparticle (corner, edge or face) using the structure and diameter of the nanoparticles determined by XRD, WAXS and TEM.

In this chapter, the synthesis and characterisation of two series of Rh-NPs stabilised by phosphines and phosphites are described.

2.2 **Results and discussion**

2.2.1 *Synthesis and characterisation of M-NPs stabilised by phosphorus based ligands*

In this work, series of mono- and bidentate phosphines and phosphites ligands were employed as stabilising agents for rhodium nanoparticles. The ligands were selected to determine the effect of variation of their steric and electronic properties on the structure of the resulting Rh- NPs and on their catalytic performances. The phosphorus based ligands used in this study are shown in Figure 2.15.
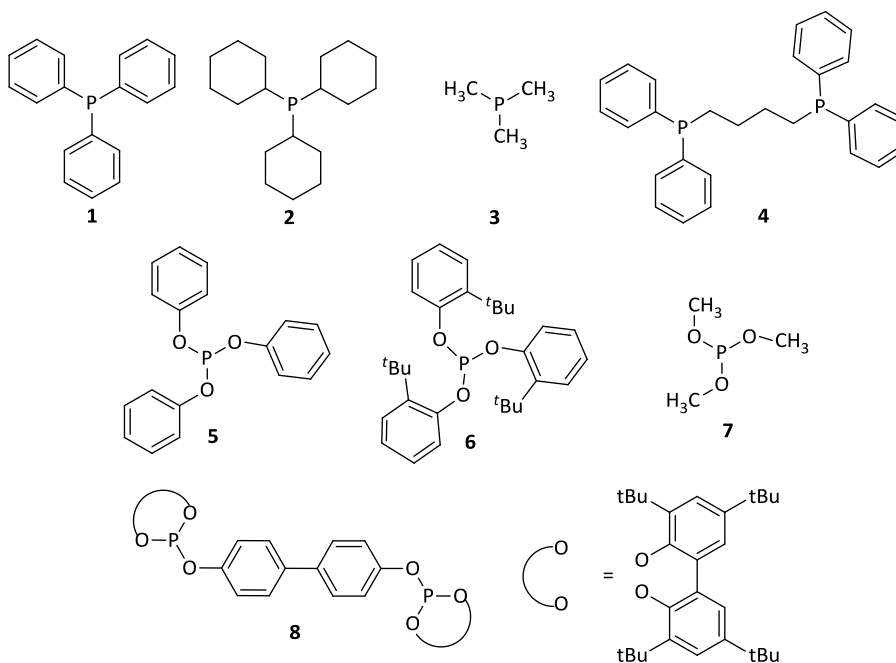
Figure 2.15 P- based ligands used to stabilise rhodium nanoparticles in this work.

In each family, a compound was used as model: for the phosphines, triphenylphosphine **1** was selected for that purpose. Tricyclohexylphosphine **2** and trimethylphosphine **3** were used to vary the properties of these mondentate stabilising ligands. The effect of the

hapticity of the phosphine was also tested through comparison with the bidentate ligand diphenylphosphinobutane (dppb) **4**.

A series of phosphite ligands were also tested as NP stabilisers. The stronger coordination of $P(OR)_3$ to low oxidation state Rh atoms, compared to PR_3, has been well established in molecular complexes.[37] It was thus thought that the comparison between these types of ligands could provide interesting information.

The triphenylphosphite ligand **5** was selected as a model for this family of ligands for comparison with triphenylphosphine **1**. The bulky phosphite **6** was tested as stabiliser. The presence of a tert-buthyl substituent in ortho position of the phenyl group could prevent the approach of the phenyl moiety towards the metallic surface in a planar manner. Furthermore, the trimethylphosphite **7** which is a less sterically demanding ligand was chosen for comparative purposes. The diphosphite ligand **8,** derived from the 4,4'dihydroxydiphenyl, was also tested.

As previously mentioned in Chapter 1, the synthesis of metal nanoparticles through the organometallic approach, by olefin reduction and displacement from organometallic compounds provides nanoparticles with small size and narrow distribution with a "clean surface" under mild conditions.[38]

In the work presented in this thesis, this synthetic methodology was followed in all cases and the rhodium nanoparticles were obtained by decomposition of the organometallic complex $[Rh(\eta^3\text{-}C_3H_5)_3]$ under H_2 atmosphere. This precursor was synthesised by reaction of $RhCl_3 \cdot 3H_2O$ in the presence of excess of allylmagnesium bromide, and purified by sublimation, according to reported methods.[39]

As a standard procedure, the decomposition of this organometallic precursor was carried out in a Fischer-Porter bottle using THF as the solvent under H_2 atmosphere in the presence of sub-stoichoimetric amounts of the corresponding P-donor ligand (L). In order to maintain the P/Rh ratio unchanged, 0.4 equivalent of L per Rh was used for the monodentate ligands and 0.2 equivalent for bidentate stabilisers in all standard syntheses.[7] The reaction mixture was usually heated at 40°C during 24h, the

initial pale yellow solution was observed to slowly turn black, confirming the decomposition of the complex. Finally, the NPs were isolated as black powders after precipitation with pentane.
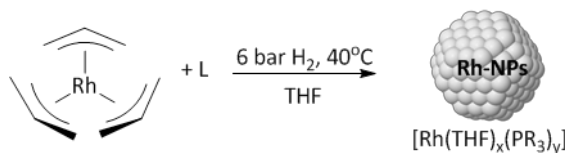
Figure 2.16 Synthetic method used for the preparation of rhodium nanoparticles stabilised by P donor ligands described in this work.

The remaining solution was analysed by NMR spectroscopy and GC-MS and the NPs were characterised by transmission electron microscopy (TEM), X-Ray diffraction (XRD), X- Ray photoelectron spectroscopy (XPS) and thermogravimetric analysis (TGA).

As a routine procedure, the purity of the P-stabilised nanoparticles was confirmed by ^{31}P NMR spectroscopy. Indeed, the non-detection of ^{31}P resonances corresponding to the coordinated ligands may be due to different factors that are described in several reports such as a Knight shift, the fast T_2 relaxation resulting from the slow tumbling of the particles in solution and to the surface anisotropy.[40] ^{31}P NMR was therefore used to confirm the absence of phosphorus based species such as free ligand, oxidised ligand, etc … through the absence of ^{31}P resonances.

This information was used as evidence of the purity of the systems prior to further characterisation and use in catalysis.

2.2.2 *Synthesis and characterisation of Rh- NPs stabilised by phosphine ligands*

To study the stabilisation of rhodium nanoparticles by phosphine ligand, the commercially available triphenylphosphine **1** was first used as a model, the nanoparticles were synthesised with 0.4 equivalents of ligand per rhodium as a standard procedure. Additionally, the synthesis was also performed

using 0.2 and 0.6 equivalents in order to analyse the effect of the amount of stabiliser on the structure of these nanoparticles.

Triphenylphosphine **1** is reported in the literature as stabilising ligand for gold[41], palladium[42,26], platinum[43] and ruthenium[14,44] nanoparticles. Two reports were found on the stabilisation by this ligand of rhodium nanoparticles.[14,15]

Synthesis of Rh- NPs Rh1 stabilised by triphenylphosphine 1

These nanoparticles were synthesised under 6 atm of H_2 at room temperature using THF as solvent during 16h (Figure 2.17). The resulting black solid was precipitated in pentane, washed and both the solid and the washings were analysed.
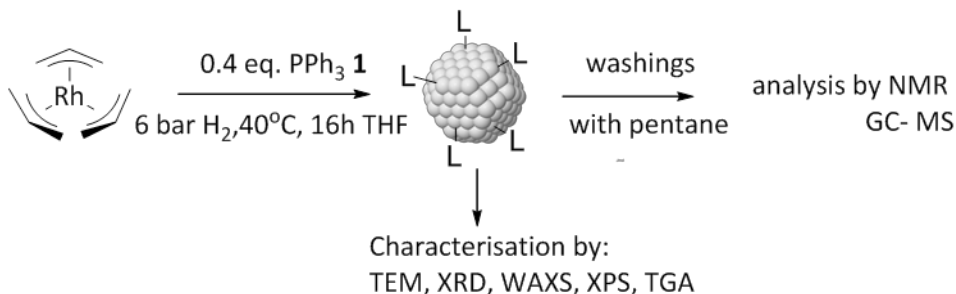
Figure 2.17 Schematic representation of the synthesis and characterisation performed to the **Rh1** NPs.

Initially, 0.4 equivalents of the monodentate ligand triphenylphosphine **1** per Rh were used. TEM microscopy confirmed the formation of the rhodium nanoparticles **Rh1** that exhibited spherical shape, a diameter of 1.52 ± 0.21 nm and a narrow size distribution (Figure 2.18a). The mean size obtained is in agreement with the already mentioned nanoparticles synthesised by Moores and co-workers using the same rhodium precursor[15] (1.5nm) and are slightly smaller than the reported using the [Rh(μ-OMe)(COD)]$_2$ precursor by Masdeu, Gómez and co-workers (2nm).[14]
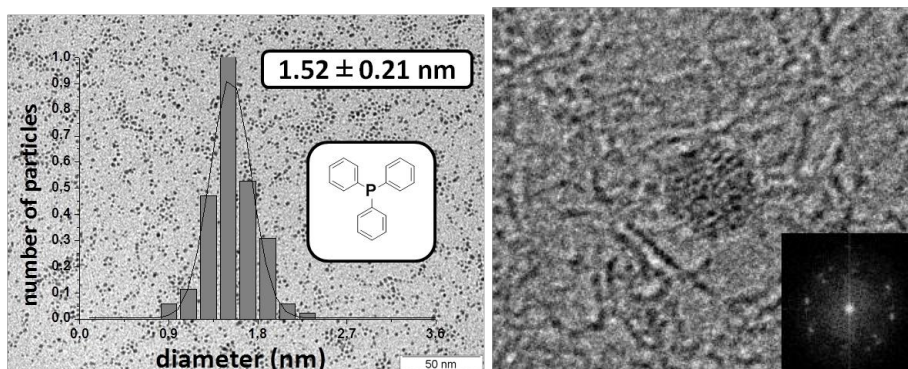
Figure 2.18 a) TEM micrograph and size distribution of the **Rh1** NPs; b) HR-TEM micrograph of **Rh1**.

These systems were also studied by high resolution transmission electron microscopy (Figure 2.18 b), which revealed that some of the single nanoparticles exhibit a "hexagonal type" shape and confirmed the high dispersion of these nanoparticles. The Fourier (FTT) analyses performed to these high resolution acquisitions provide a bond length between the rhodium atoms of 0.26 nm that is in agreement with an fcc structure. It was concluded from these results that the **Rh1** NPs exhibit an "hexagonal type" shape since HRTEM allows a more accurate visual observation of the sample.

After precipitation of **Rh1** with pentane, the solvent of the washings was evaporated and the resulting liquid analysed by ^{1}H and ^{31}P NMR and GC-MS. In the ^{1}H NMR spectrum, signals with low intensity were observed in the aromatic region (6-8 ppm) while intense resonances were detected in the alkylic region (1- 3 ppm), indicating that the majority of the products in solution did not contain aromatic rings. In the ^{31}P{H} spectrum, several signals were detected, indicating that the products in solution must be derivatives of the stabilising agent. Four singlet signals were observed at δ 50.7, 50.0, 45.5 and 34.5 ppm in ratio of *ca.* 1:1:4:1. After, comparison of these chemical shifts with literature values,[45] the signals at 50.7, 45.5 and 34.5 ppm were attributed to the compounds **9**, **11** and **12** described in Figure 2.19, which are the oxide derivatives of tricyclohexyl-,

dicyclohexylphenyl- and triphenylphosphine. These assignments are in agreement with the large alkylic signals detected in the ^{1}H spectra. In the case of compound **10**, no information was found in the literature and its assignment was based on its ^{31}P chemical shift, situated between those of tricyclohexylphosphine oxide **9** and dicyclohexylphenylphosphine oxide **11**. The formation of compound **10** could result from the partial hydrogenation of one of the phenyl rings with complete hydrogenation of the other two (Figure 2.19). This hypothesis was confirmed by GC-MS analysis, since a m/z value of 294 was detected for this species, which correspond to the loss of 2 hydrogen atoms compared to that of tricyclohexylphosphine oxide 9 (m/z= 296). In this analysis, the major compound was identified as the dicyclohexylphenylphosphine oxide **11**, which is in agreement with the ^{31}P NMR observations.

	9	**10**	**11**	**12**
^{31}P NMR (ppm)	50.7	50	45.45	34.5
GC-MS: m/z	296	294	290	277
retention time (min)	29.27	28.68	28.14	28.40
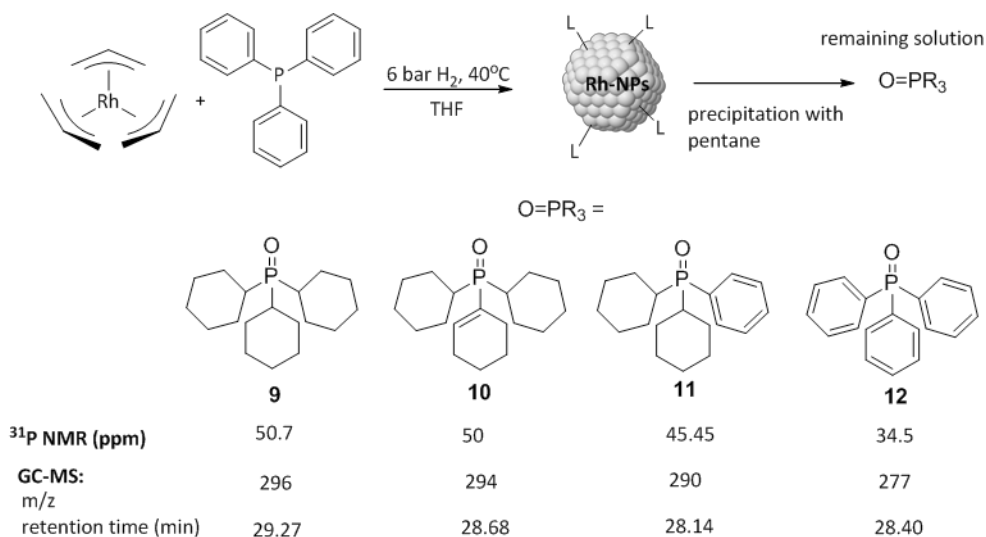
Figure 2.19 Products observed in the synthesis of **Rh1** NPs.

These results thus indicated that hydrogenation of the phenyl rings of the stabilising ligand **1** had occurred during the synthesis of the **Rh1**-NPs and that hydrogenated ligands could be stabilising these NPs. This behaviour was also observed for ruthenium nanoparticles stabilised by the same ligand **1**.[44] Chaudret and co- workers showed that synthesising the

nanoparticles with triphenylphosphine **1**, both PPh_3 and PCy_3 were present at the surface of the particles.

It is also interesting to note that the stabilising agent and hydrogenated derivatives were present in the washings in their oxidised form. This oxidation could have taken place either during the synthesis or during experimental manipulations posterior to the formation of NPs. However, since all experiments had been performed under inert atmosphere, this latter possibility was unlikely. The detection of phosphine oxides was previously reported during the synthesis of ruthenium NPs.[44] However, no information on the origin of the oxygen and the mechanism for the oxidation of the ligand has been reported so far.

To probe the ability of these NPs to hydrogenate such ligands, a test was performed where triphenylphosphine **1** was used as a substrate in the presence of **Rh1** as catalyst (2 mol%), under 40 bar of hydrogen pressure and at 80 °C during 16h (Figure 2.20). However, only the signal corresponding to the compound **1** was observed after reaction. The corresponding oxide product **12** was also used as substrate under the same conditions, in order to avoid the possible phosphorus coordination to the nanoparticles surface that could inhibit the hydrogenation of the phenyl rings.
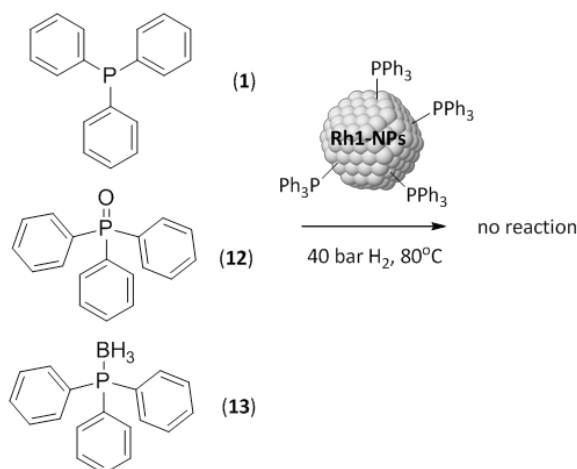
Figure 2.20 Attempts of hydrogenation reactions of PPh_3 and derivatives using **Rh1** as catalyst.

However, as in the previous case, only the substrate was detected after 16h under hydrogenation conditions. The same result was obtained using the triphenylphosphine boroprotected with BH_3 group **13**.

These results indicated that the hydrogenation of the stabilising ligands could take place at the early stages of the synthesis of the nanoparticles, and that the species responsible for these reactions might be smaller clusters.

The structure of the nanoparticles **Rh1** was investigated by several techniques.

First, the structural determination of **Rh1** was achieved by X- Ray diffraction (XRD) and the diffraction pattern obtained is shown in Figure 2.21. Strong Bragg's diffraction peaks were observed at 41.07°, 47.78°, 69.88°, 84.39° and 89.11°. These peaks correspond to the planes (111), (200), (220), (311) and (222), which are related to the facets of the face centered cubic (fcc) lattice of Rh-NPs.[46] These results were in good agreement with reported data for Rh nanoparticles supported on MgO of similar size.[47] No reflections due to rhodium oxide were observed. A crystallite size of 1.49± 0.034 nm was determined in this analysis, which is smaller than the average diameter previously determined from TEM analysis. Such discrepancy is frequently encountered in the case of metal nanoparticles, since the metal atoms at the surface exhibit disorder and as such do not contribute to the crystallite size.
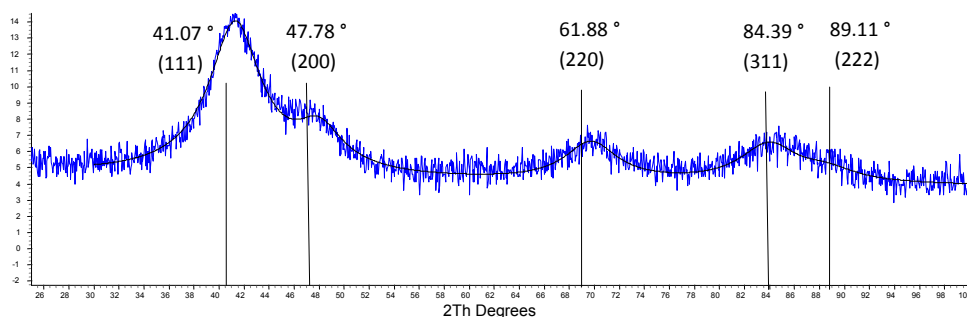
Figure 2.21 XRD pattern recorded for the nanoparticles **Rh1**.

Wide angle X-ray Scattering (WAXS) was performed to this sample (Figure 2.22). The WAXS measurements revealed the presence of highly crystalline rhodium domains displaying fcc structure, a coherence length of 2 nm and a bond length of 0.269 nm.
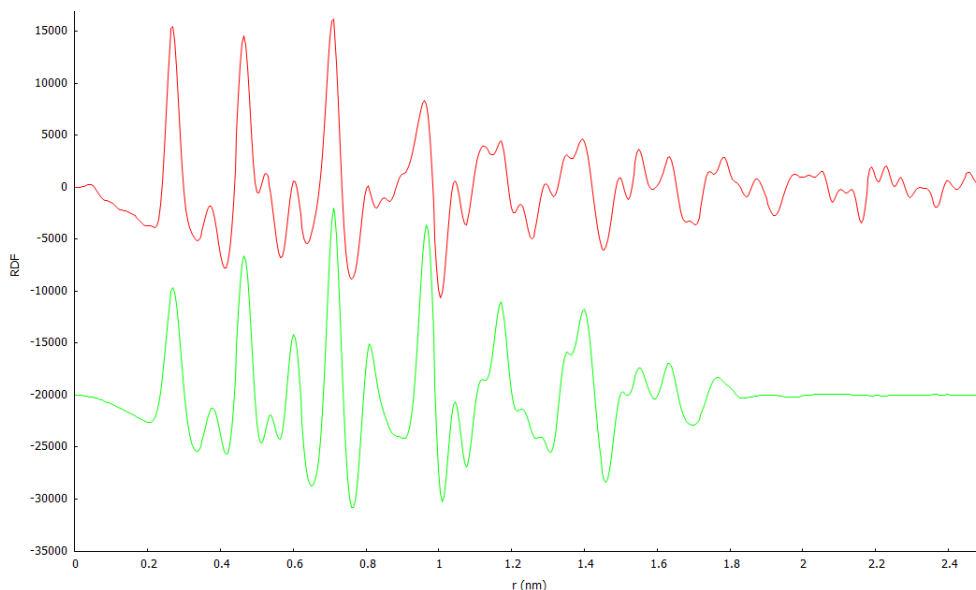
Figure 2.22 Experimental (red) RDF of **Rh1** and theoretical (green) RDF for Rh fcc.

The mean diameter is slightly higher than the measured by TEM and XRD, as previously reported.[48] Moreover, the mean size value can differ between the different techniques and depend on the approximation used for the calculations. However, the same packing was obtained by XRD and WAXS and the bond lengths are in agreement with the value obtained by the fourier (FTT) analyses performed on high resolution images, corresponding to fcc crystalline rhodium nanoparticles.

XPS measurements were also performed on freshly prepared samples to obtain information on the oxidation state of the Rh atoms at the surface of these NPs. In the spectrum corresponding to these NPs, the peaks expected for Rh^0 $3d_{3/2}$ and $3d_{5/2}$ were slightly displaced from theoretical values (see introduction section) and were observed at 308.32 eV and 313.02 eV. Such

behaviour is usually observed for supported particles or when metal particles are surrounded by organic ligands.[49] For instance, Dutta and co-workers reported the influence of the oxygen framework of the clay matrix for Rh- supported on montmorillonite, producing a similar shift.[50] For nanoparticles **Rh1**, this shift may be due to a strong interaction between the Rh surface atoms and the phosphorus centres of the stabilising agents. Using calculations based on the Monte-Carlo approximation and taking into account the parameters optimised for Rh surfaces,[51] the analysis revealed a $Rh^{\delta+}/Rh^{0}$ ratio of 40/60 at the surface of the nanoparticles **Rh1**.
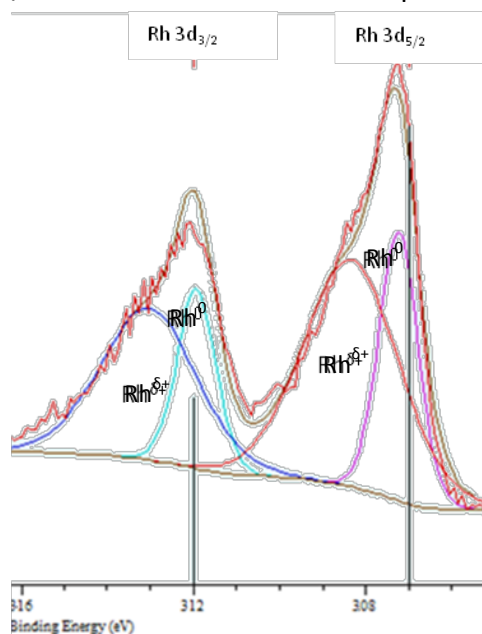
Figure 2.23 XPS spectra of Rh 3d for nanoparticles **Rh1**.

XPS analysis confirmed the presence of rhodium and that 40% of $Rh^{\delta+}$ was present at the surface of **Rh1**, while 60% of Rh in zero valent state was identified at the surface of the nanoparticles. Rh-NPs are reported to be prone to oxidation when small sizes are reached.[35] However, oxidation of the samples during measurements cannot be discarded.

The presence of phosphorus at the surface of the nanoparticles was confirmed by X-ray microanalysis performed with a SEM microscope, in which rhodium and phosphorus were detected as the main elements.

To evaluate the content in stabiliser of these nanoparticles, thermogravimetric analyses were performed during which the sample was heated from 30 °C to 900 °C under a flow of N_2, while the weight was recorded continuously. As a reference, the free ligand triphenylphosphine **1** was first analysed, and a unique weight loss at approximately 340 °C was observed (Figure 2.24). When the nanoparticles **Rh1** stabilised by this ligand were looked at, two main weight losses were observed, between 70 °C-100 °C and between 200 °C- 470 °C. The TGA curves obtained for **1** and **Rh1** are displayed in Figure 2.24.

In the curve corresponding to the nanoparticle **Rh1,** no relevant weight loss was observed at 340 °C, and it was concluded that no free ligand was contained in the sample, in agreement with the results obtained by solution ^{31}P NMR spectroscopy of these nanoparticles. The first weight loss (under 100 °C) was attributed to solvent loss, and that observed between 200 °C and 500 °C was assigned to the ligand coordinated at the surface of the NPs. The weight measured at the end of the experiments (900 °C) was attributed to the remaining metal, and thus provided the % of rhodium contained in these NPs.
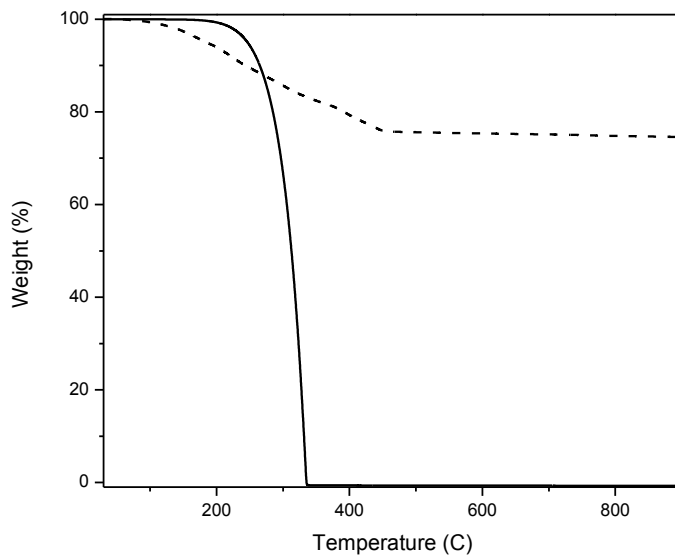
Figure 2.24 TGA curves of free ligand PPh$_3$ **1** (solid line) and the corresponding nanoparticle **Rh1** (dashed line) (10 °C min^{-1} in N$_2$).

The TGA analysis of **Rh1** therefore indicated that these NPs contained *ca*. in weight: 2% of solvent THF, 25% of phosphine ligands and 70% of rhodium.

To summarise, the nanoparticles **Rh1** stabilised by the triphenylphosphine ligand **1** exhibit a diameter of 1.52± 0.21 nm with hexagonal shape, are highly crystalline with fcc packing, with the majority of the surface in zerovalent state. Quantitatively, they contain 2% of solvent, 25% of organic part and 70% of rhodium.

Using these experimental data and the the VHH model, the approximate number of Rh atoms contained in these nanoparticles **Rh1** was calculated (Table 2.3). A P/Rh$_s$ ratio comprised between 0.2-0.3, which represents *ca*. 1 phosphorus ligand for 3-6 rhodium surface atoms. These data are in agreement with previous reports on Ru-NPs stabilised by P-donor ligands that describe P/Rhs of *ca*. 0.30.[25]

Table 2.3 Approximate structural features for systems **Rh1**. Calculations based on the diameter (nm) obtained by TEM and TGA analysis.

	1.31	1.52	1.73
Nt	83	132	194
Ns	59	86	118
Nt/ Ns	71	65	61
P/Rh$_s$	0.33	0.23	0.17

These results reflected that small differences in size produce significant changes in the total and surface number of atoms. However, the ratio of surface atoms per total atoms in the nanoparticle remains similar in all cases.

In an attempt to further characterise these NPs, indirect techniques were also used. The presence of hydrides at the surface of nanoparticles has been demonstrated by Chaudret and co- workers using NMR spectroscopy on ruthenium nanoparticles stabilised by hexadecylamine (HDA).[52] The authors demonstrated by direct NMR evidence the presence of mobile and reactive hydride coordinated to metal nanoparticles and published a methodology for the titration of these surface hydrides with olefins.[40] Ruthenium nanoparticles stabilised by HDA, PVP and dppb were used for these experiments with norbornene and 1- octene, obtaining in all the cases a hydride/ surface Ru ratio greater than 1.
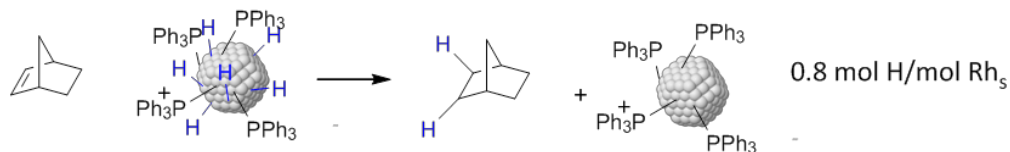
Figure 2.25 Scheme representing the titration experiments on Rh- NPs.

To quantify the presence of hydrides at the nanoparticles surface, the rhodium systems **Rh1** were reacted with norbornene following the same methodology. The quantity of norbornane produced was determined by GC- MS and these experiments revealed that *ca*. 0.8 hydride is present per

Rh surface atom in system **Rh1**. This value is thus lower than those reported for related P- ligand stabilised ruthenium nanoparticles.

Note that to check that experimental errors were not responsible for this lower value, the Ru-dppb nanoparticles were synthesised following the reported procedures and the hydride titration experiments carried out in our lab.[40] Since the literature value was reproduced in our hands, it was concluded that a lower hydride/hydrogen coverage is present at the surface of **Rh1** than in analogous ruthenium systems.

The characterisation of **Rh1** by solid state NMR spectroscopy was attempted several times and on various spectrometers during the course of this thesis. However, no signals were detected each time.

As already explained, no signals were detected when the nanoparticles were analysed by ^{31}P NMR at room temperature in d$_8$-THF (Figure 2.27a). However, when a ^{31}P{^{1}H} NMR spectrum was recorded at -80 °C (Figure 2.27b), one phosphorus signal was detected at 43.3 ppm. ^{31}P signals with similar chemical shifts were attributed to phosphine ligands bonded to the metallic atoms of ruthenium nanoparticles stabilised with these ligands.[25] However, based on the analysis of the washings, this signal was attributed to the diphenylcyclohexylphosphine oxide or derivatives. This result indicates that this species is involved in a dynamic process with the NPs.
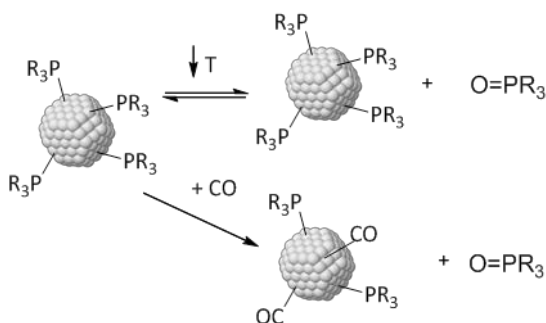
Figure 2.26 P-species observed by solution ^{31}P NMR at low temperature and under 30 bar of CO.
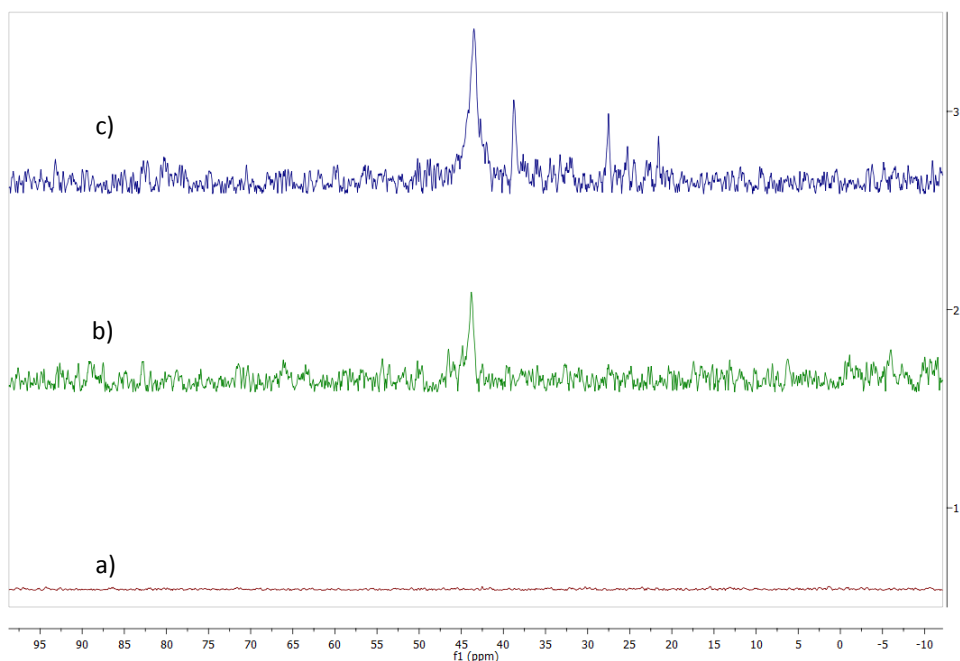
Figure 2.27 Solution ^{31}P{H} NMR spectra of **Rh1** NPs at a) room temperature, b) -80 °C, c) after 30 bar of CO pressure.

Next, the sample was placed in a high pressure sapphire tube and charged with 30 bar of CO pressure at room temperature. In the corresponding ^{31}P{^{1}H}, the signal previously detected at low temperature was again observed at 43.3 ppm, but with higher intensity and together with three other singlets at 37.7, 27.4 and 21.6 ppm. No signal for PPh$_3$ was detected. It was therefore concluded that under CO pressure, several P-based species were expulsed from the NP surface and as such are detected in solution. It can thus be concluded that the system **Rh1** therefore contains diphenylcyclohexylphosphine oxide at its surface. Further analyses are needed to identify the species giving rise to the smaller signals. This observation is in agreement with a recent report that demonstrated the adsorption of phosphine oxide at the surface of Ru-NPs by solid state NMR spectroscopy.[44]

Next, the nanoparticles **Rh1** were analysed by Infra-red spectroscopy using a KBr pellet. The spectrum obtained is shown in Figure 2.28.

First, the C-H stretching vibrations zone (*ca.* 3000 cm^{-1}) was analysed. At frequencies higher than 3000 cm^{-1}, only a small signal attributed to aromatic $\upsilon_{(C-H)}$ was observed. However, at lower frequencies (2900 cm^{-1}<υ< 3000 cm^{-1}), a set of signals attributed to $\upsilon_{(C-H)}$ of alkyl moieties was detected (Figure 2.28).
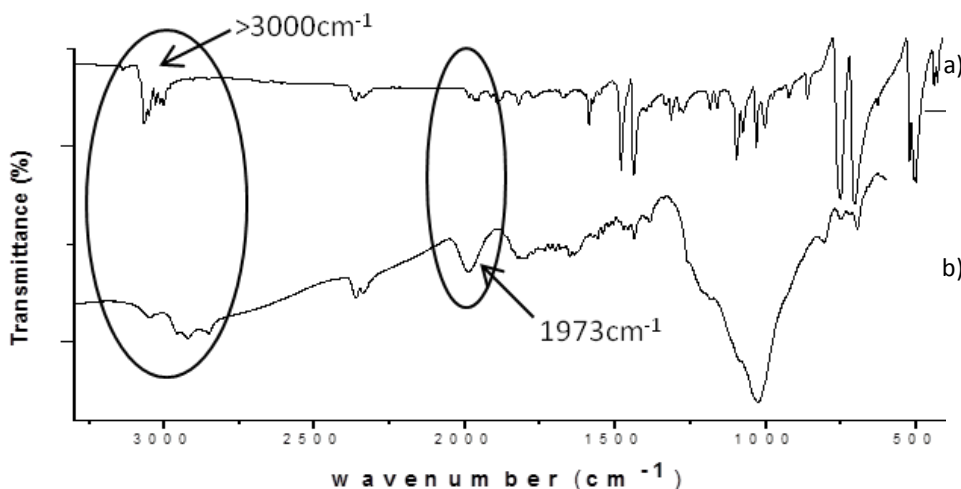
Figure 2.28 IR spectra of: a) PPh$_3$ **1**, b) **Rh1** NPs.

These signals were not present in the spectrum of PPh$_3$ **1** (Figure 2.28) and it was therefore concluded that some hydrogenation of the phenyl rings of the ligand had taken place during the synthesis of the NPs. These observations are in agreement with the NMR results obtained with the NPs **Rh1** in solution where dicyclohexylphenylphosphine derivatives were shown to be adsorbed at the surface.

At frequencies lower than 1500 cm^{-1}, no clear bands could be distinguished and only a broad signal centred at *ca.* 1000 cm^{-1} was observed.

However, at 1973 cm^{-1}, a broad and intense band was detected. Such a frequency value corresponds typically to a carbon monoxide ligand coordinated to a metal centre or a metal surface.[66] Chaudret and co workers reported the possible decarbonylation of the THF solvent at the

surface of the nanoparticles.[25] However, since very distinct spectra were obtained upon addition of CO to these NPs in the solid state (see Section 2.2.4 of this chapter), it was concluded that this signal could not be due to coordinated CO ligands.

In a study on a Rh/Al$_2$O$_3$ catalyst, Worley and co-workers attributed a similar band at 2013m^{-1} to rhodium hydride species at the surface when the samples was placed under H$_2$.[53] When the reaction was repeated under D$_2$, this band moved to 1441 cm^{-1}. Interestingly, they also detected a band at 1618 cm^{-1} that was attributed to adsorbed water on alumina surface.

Therefore, in order to clarify the origin of the signal observed at 1973cm^{-1}, an IR spectrum was recorded after norbornene titration, since no hydride should be present at the NPs surface after such a treatment. As shown in Figure 2.29 (spectra b), after titration with norbornene, no signal was detected at *ca.* 2000 cm^{-1}. Furthermore, the signals in the region 700-1300 cm^{-1} were sharper, probably indicating a modification of the NPs due to the treatment with norbornene.
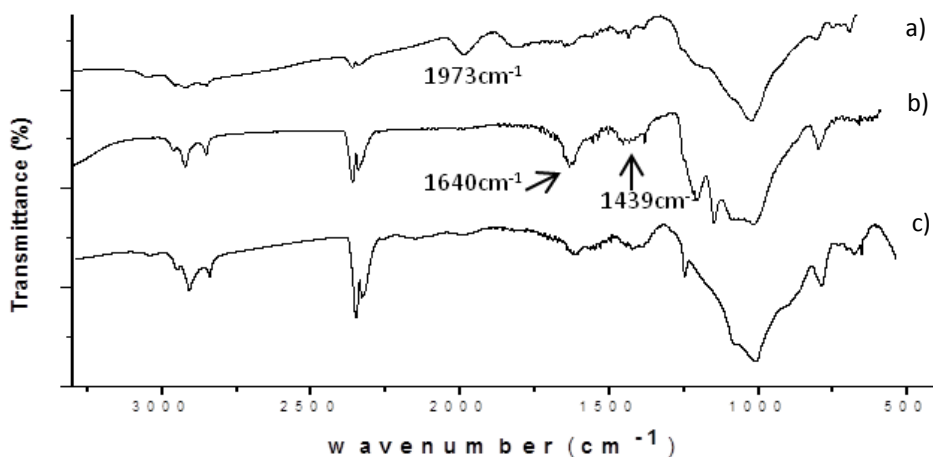
Figure 2.29 IR spectra of a) **Rh1**; b) **Rh1** after titration with norbornene; c) **Rh1**-D2.

To confirm this result, a fresh sample of these nanoparticles was synthesised using D$_2$ as the reducing agent instead of H$_2$. An IR spectrum of

Rh1-D$_2$ was recorded and compared to that of **Rh1** synthesised under H2 atmosphere (Figure 2.29, spectrum c vs a).

In the spectra of **Rh1-D2**, the intense band previously observed at 1973 cm^{-1} was not detected. In the already mentioned study of Worley and co-workers, a displacement of 572 cm^{-1} between the vibrations of Rh-H and Rh-D band was observed.[53] In our study, such a displacement could not be observed due to the presence of overlapping signals at these frequency values.

It was therefore concluded from these observations that the signal observed at 1973 cm^{-1} arises from the Rh-H stretching vibrations.

It should be noted that in the spectra b and c, two bands at 1640 and 1439 cm^{-1} were observed whereas in spectrum a, these signals are much weaker. These signals were observed in several occasions during the course of this study and appeared independently of the NPs. Based on literature reports, these bands were tentatively attributed to adsorbed carbonate species presumably formed by reaction of the NPs with atmospheric CO_2 and possibly H_2O. Very similar signals were previously detected by other groups when Rh-NPs supported on hydrotalcite were exposed to CO or CO_2 atmosphere.[54] It was therefore deduced that the presence of these signals could not be related to the presence or absence of hydride ligands at the surface of these NPs. Investigations to determine the origin of these signals are currently on going in our lab.

In an attempt to regenerate hydride species from the **Rh1** treated with norbornene, the sample was placed in a Fischer-Porter bottle in the solid state under 6 bar of hydrogen pressure at room temperature and a new spectrum was recorded. However, no relevant changes were observed before and after between the sample after titration and after the addition of hydrogen pressure. This result indicated that the signal could arise from hydride species that cannot be formed by treatment with H_2 under the conditions used in this study.

The characterisation of **Rh1** by NMR and IR spectroscopy therefore determined:

- The presence of hydrides at the surface was demonstrated through their titration and direct detection by IR spectroscopy. The hydride/Rh_s ratio was estimated to be 0.8 by titration with norbornene.
- The hydrogenation (partial or total) of the phenyl rings of the stabilisers was shown by NMR and IR spectroscopy.

Variation of the equivalents of triphenylphosphine 1

Variations of the amount of stabilising phosphines during the synthesis of the nanoparticles were previously reported for Ru systems.[25] Van Leeuwen and Chaudret used between 0.1 and 0.2 equivalent of phosphine during the synthesis of their Ru-NPs and study the effect of these variations on their performances in the hydrogenation of arenes. They observed that increasing the amount of ligand during their synthesis in the case of monodentate phosphine did not influence the size of the nanoparticles.

Here, the amount of the ligand **1** was varied from 0.2 equivalents per Rh to 0.6 during the synthesis of the nanoparticles using the procedure shown in Figure 2.30.
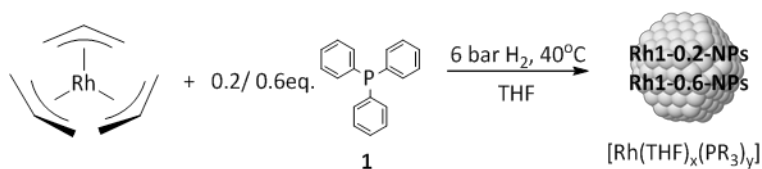
Figure 2.30 Method used for the synthesis of the **Rh1-0.2** and **Rh1-0.6** NPs.

The formation of the nanoparticles **Rh1-0.2** and **Rh1-0.6** was confirmed by TEM analysis (Figure 2.31). No relevant differences in size and shape were observed between the nanoparticles **Rh1** and the nanoparticles described in this section **Rh1-0.2** and **Rh1-0.6**.

It should be noted that when 0.1 equivalent of PPh_3 **1** per Rh was used during the synthesis, no NPs were formed and only bulk Rh was obtained, indicating that this amount of ligand was insufficient for the stabilisation of NPs under these conditions.
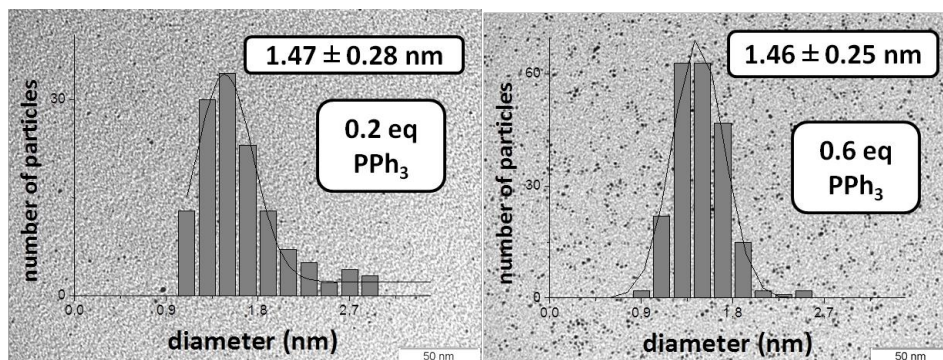
Figure 2.31 TEM micrographs and size distributions of the **Rh1-0.2** and **Rh1-0.6** NPs.

The characterisation of **Rh1-0.2** and **Rh1-0.6** was carried out by XRD, XPS and TGA analysis:

- XRD analysis revealed crystalline nanoparticles with fcc packing, as previously determined for **Rh1**.
- XPS reflected the presence of $Rh^{\delta+}$ at the surface, 48% for system **Rh1-0.2** and 40% for **Rh1-0.6**. The slightly higher oxidation detected at the surface for the nanoparticles **Rh1-0.2** could be due to the lower amount of stabilising ligand, although oxidation of the samples during the manipulation for the XPS measurements cannot be discarded.
- TGA analysis of these species revealed that **Rh1-0.2** contains 44% in weight of phosphine while for the systems **Rh1** and **Rh1-0.6**, the values are similar (27% and 30% respectively).

Consequently, after the correlation between the number of atoms at the surface and the TGA results, the P/Rh_s ratios was calculated to be between 0.3 and 0.8 ligand per rhodium surface atoms.

Table 2.4 Approximate structural features for systems **Rh1-0.2** and **Rh1-0.6**. Calculations based on the diameter (nm) obtained by TEM and TGA analysis.

	Rh1-0.2			Rh1-0.6		
	1.19	**1.47**	**1.75**	**1.21**	**1.46**	**1.71**
Nt	63	125	202	67	127	188
Ns	47	82	122	50	84	115
Nt/ Ns	75	66	61	74	66	61
P/Rh$_s$	0.82	0.47	0.32	0.43	0.25	0.19

In view of these results, no clear correlation could be established between the amount of phosphine **1** used during the synthesis of the nanoparticles and the weight losses observed by TGA.

These results were compared with the already mentioned work of van Leeuwen, Chaudret and co-workers in which the amount of ligands was varied for phosphine stabilised ruthenium nanoparticles.[25] In this study, differences in size were observed for the resulting NPs and higher degree of hydrogenation of the phosphines was observed by solid state NMR at lower ligand ratio.

Here, no differences in size were observed when the amount of **1** was varied. The degree of hydrogenation of the ligand was investigated using Infra-red spectroscopy and Figure 2.32 shows the spectra recorded for the systems **Rh1**, **Rh1-0.2** and **Rh-0.6** and that of the free ligand **1**. As in the previous case, no significant information could be extracted from the signals observed under 1500 cm^{-1}. At *ca*. 2000 cm^{-1}, a very weak band previously attributed to Rh-hydride was observed for system **Rh1-0.2**. This signal was more pronounced in the spectrum of **Rh1-0.6**, although the most intense of the series was observed for **Rh1** synthesised with 0.4 eq of ligand per rhodium. No correlation between the intensity of this signal and the amount of PPh$_3$ **1** used in the synthesis could be deduced from these results.
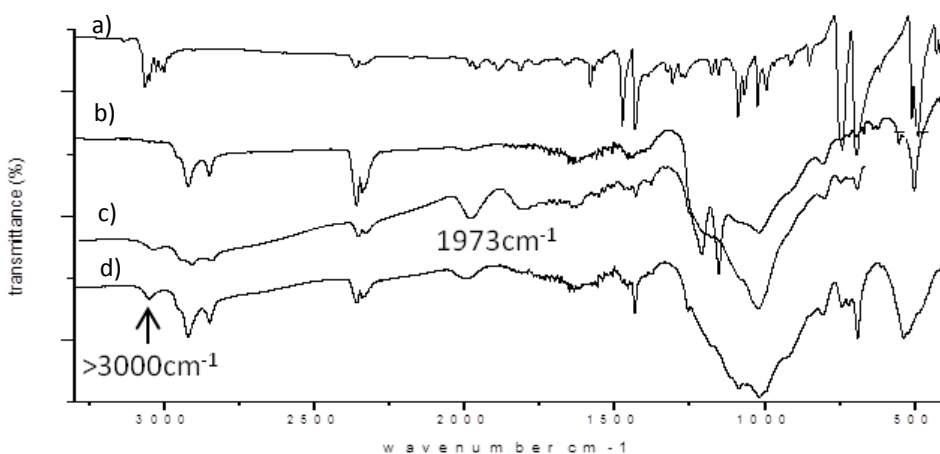
Figure 2.32 IR spectra of: a)PPh$_3$ **1**, b) **Rh1-0.2,** c) **Rh1-0.4,** d) **Rh1-0.6** NPs.

The signals detected in the zone of the stretching vibrations of C-H bonds, at *ca*. 3000 cm^{-1}, were compared to that of the ligand **1** (Figure 2.32). No band corresponding aromatic $\upsilon_{(C-H)}$ was observed in the spectra for the nanoparticles **Rh1-0.2** (spectra b) where only the alkyl $\upsilon_{(C-H)}$ signals were detected. However, for system **Rh1-0.6** (spectra d) signals of both alkylic and aromatic C-H bonds were observed. Comparing these signals to those observed for **Rh1**, the intensity of the band corresponding to aromatic C-H bond stretching increased at higher ligand amount during synthesis, indicating a higher degree of hydrogenation at lower ligand to Rh ratio. These results are therefore in agreement with the results reported for Ru-NPs.[25]

To summarise, when the amount of stabiliser **1** was varied from 0.2 to 0.6 equivalent per rhodium during the synthesis of the nanoparticles, no relevant differences in terms of size, shape, packing, and oxidation state of the metal at the surface were observed. No clear correlation could be deduced between the amount of stabiliser used in synthesis and the organic content of the resulting NPs.

93

IR spectroscopy provided evidence for a higher degree of hydrogenation at lower ligand to Rh ratio and the presence of hydride species at the surface of these nanoparticles.

Liquid NMR experiments at low temperature and under pressure of CO revealed the presence of oxidised and hydrogenated ligands derived from the stabiliser **1**, at the surface of the NPs.

Synthesis of Rh-NPs Rh2-Rh3 stabilised by tricyclohexylphosphine 2 and trimethylphosphine 3

The synthesis of Rh- NPs stabilised by the ligands **2** and **3** was performed (Figure 2.33) under the same conditions than those described for **Rh1**. The Rh precursor was decomposed in the presence of 0.4 equivalent of ligand per Rh under 6 bar of H_2 and at 40 °C. No reports of the stabilisation of Rh-nanoparticles with tricyclohexyl **2** or trimethylphosphine **3** were found in the literature.
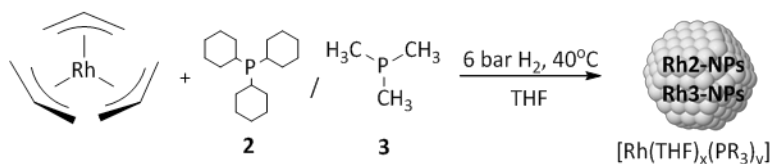
Figure 2.33 Method used for the synthesis of the **Rh2** and **Rh3** NPs.

The formation of the nanoparticles was confirmed by TEM, and the mean diameters for systems **Rh2** and **Rh3** was determined as 1.36 and 1.38 nm**,** respectively. As shown in Figure 2.34, no significant differences in shape and distribution were observed between the systems **Rh2** and **Rh3**. However, these nanoparticles were slightly smaller than the **Rh1** (1.5 nm).
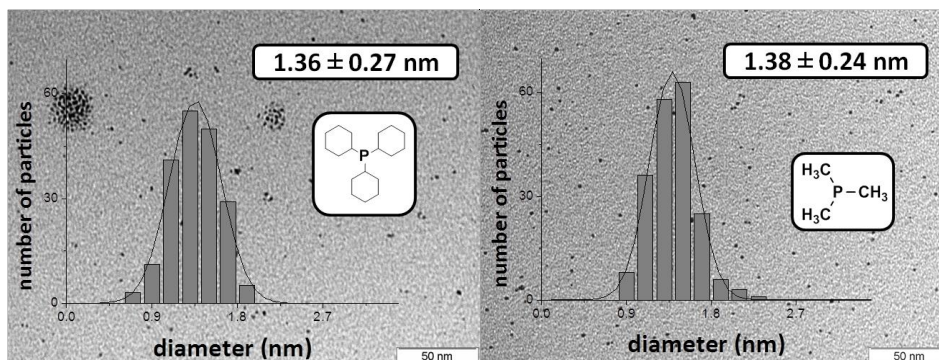
Figure 2.34 TEM micrograph and size distribution of the **Rh2** and **Rh3** NPs.

The samples were also analysed by HRTEM microscopy (Figure 2.35), confirming the good dispersion and spherical shape for both systems. Bond lengths of 0.23 and 0.27 nm were calculated for systems **Rh2** and **Rh3** respectively, which are in agreement with fcc structures.
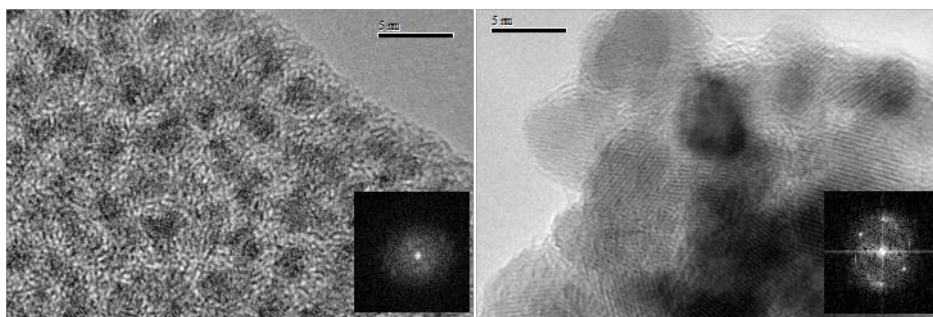
Figure 2.35 HRTEM images of **Rh2** (left) and **Rh3**(right).

The washings of the nanoparticles were analysed by NMR spectroscopy. For systems **Rh2** and **Rh3**, only one signal in the ^{31}P{H} NMR spectrum revealed the presence of the corresponding ligands **2** and **3** in their oxidised form.
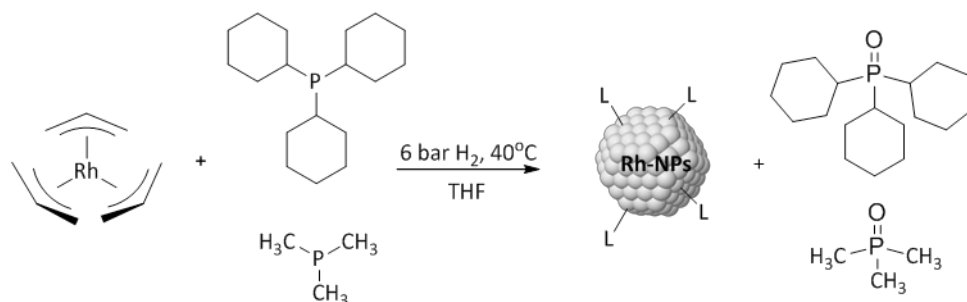
Figure 2.36 Species detected during the synthesis of systems **Rh2** and **Rh3**.

As in the previous systems, crystalline nanoparticles with fcc packing were observed by XRD for **Rh2** and **Rh3** and ca. 40% of $Rh^{\delta+}$ was measured by XPS at the surface of these nanoparticles. This degree of oxidation is comparable to that measured for **Rh1**.

TGA analysis of **Rh2** displayed a larger weight loss for organics (*ca.* 44%) than for the nanoparticles stabilised by trimethylphosphine **Rh3** (26%) and the system **Rh1** (25%).

The number of surface atoms was calculated by the VHH model (Table 2.4). The approximate number of phosphorus per rhodium surface atom was calculated to be between 0.3 and 0.7 for **Rh2** and between 0.5 and 1.1 for **Rh3**.

Table 2.5 Approximate structural features for systems **Rh2** and **Rh3**. Calculations based on the diameter (nm) obtained by TEM and TGA analysis.

	Rh2			Rh3		
	1.09	**1.36**	**1.63**	**1.14**	**1.38**	**1.62**
Nt	49	95	163	56	99	160
Ns	39	66	103	43	68	101
Nt/ Ns	79	69	63	77	69	63
P/Rh$_s$	0.73	0.43	0.28	1.11	0.7	0.47

Although these calculations are only approximate, a higher ligand coverage is indicated for both **Rh2** and **Rh3** compared to **Rh1** ($0.1 < P/Rh_s < 0.3$).

Using the phosphines **2** and **3** as stabilising agents, smaller nanoparticles were obtained compared with those stabilised by triphenylphosphine **1**. The same structure and chemical surface was observed by XRD and XPS analysis than for the model system **Rh1**. TGA analysis and the calculation of the number of atoms of the nanoparticles revealed a more covered surface with these systems than for **Rh1**. The difference between systems **Rh2** and **Rh3** and the model system **Rh1**, could be explained by the absence of aromatic rings in ligands **2** and **3** which could interact with the nanoparticle surface and therefore limit the number of ligand on the **Rh1** NPs.

IR spectra of the nanoparticles **Rh2** and **Rh3** were also recorded. However, little information was obtained. For both systems, the expected stretching vibrations of alkylic C-H bonds were detected 2800-3000 cm^{-1}, together with a band at 1969 and 1991 cm^{-1} for **Rh2** and **Rh3**, respectively which was attributed to Rh-H stretching based on the results obtained with **Rh1** (See supplementary information in the CD attached).

The effect of the steric properties of the ligands was studied for instance Hyeon and co-workers where various phosphines were used to stabilise palladium nanoparticles in order to investigate their coordination at the surface of the nanoparticles by ^{31}P NMR spectrsocopy.[55] The authors explained that small sized phosphine ligands could bind tightly to the systems, which is in agreement with this study, were more P coverage is observed for the less sterical demanding stabilising ligand trimethylphosphine **3**.

Synthesis of the NPs Rh4 stabilised by the diphosphine ligand dppb 4

The effect of the hapticity of the ligands on NPs stabilisation is also of interest and here, the diphosphine ligand dppb **4** was used as stabilising agent. This diphosphine ligand was reported by the group of Chaudret to efficiently stabilise ruthenium nanoparticles[24,56,40] or bimetallic Ru-Pt systems[28] for instance.

In order to maintain the P/Rh ratio using during the synthesis of **Rh1-Rh3**, 0.2 equivalent of the ligand diphenylphosphinobutane **4** was used to synthesise the nanoparticles **Rh4** (Figure 2.37).
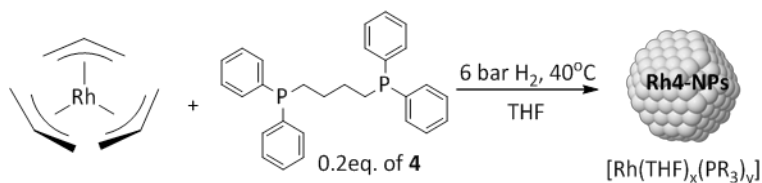
Figure 2.37 Synthesis of **Rh4** NPs.

TEM analysis revealed nanoparticles with a mean size of 1.57± 0.25nm with a narrow distribution, spherical shape and good dispersion. These nanoparticles were therefore slightly larger than **Rh1** (Figure 2.38).
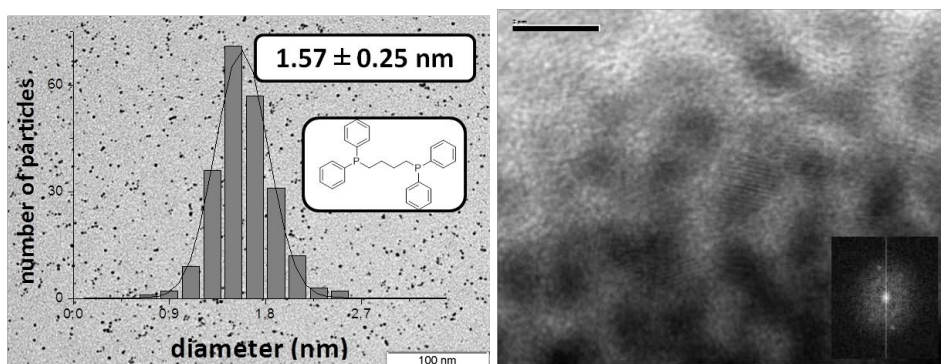
Figure 2.38 TEM micrograph and size distribution (left) and HRTEM image (right) of the **Rh4** NPs.

The observation of this sample by HRTEM confirmed the spherical shape and the good dispersion of these NPs (Figure 2.38, right). Moreover, high resolution images of the single particles revealed highly crystalline faces with a bond length of 0.26 nm, in agreement with a fcc structure.

The washings of the nanoparticles were analyzed by NMR spectroscopy. No signals were observed in the aromatic region of the ^{1}H NMR spectrum indicating that no species containing aromatic rings were present in solution. However, intense signals were detected in the alkyl region of the spectrum (0-3 ppm). Moreover, a unique signal was observed at 51.2 ppm

in the ^{31}P {H} NMR spectrum, that was assigned to compound **14,** a diphosphine oxide derivative bearing cyclohexyl substituents (Figure 2.39), after comparison with literature values.[40]

^{31}P NMR (ppm)	51.2
GC-MS: m/z	326
retention time (min)	26.75
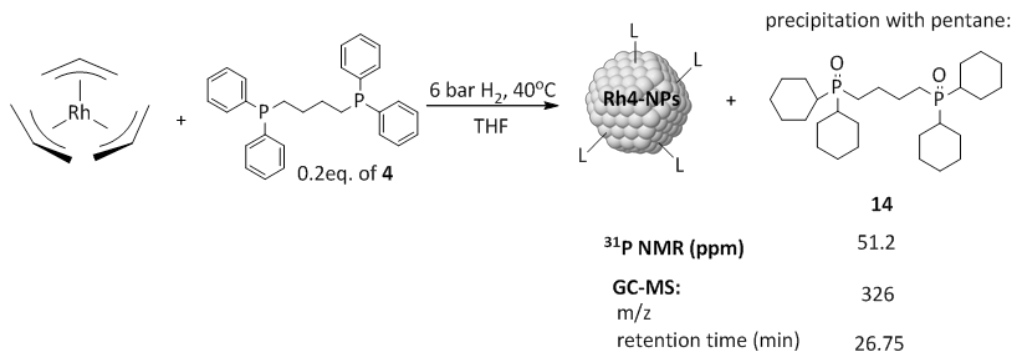
Figure 2.39 Species detected during the synthesis of system **Rh4**.

This observation is in agreement with the results described for the mono phosphine stabilised nanoparticles **Rh1**, for which hydrogenation of the ligands was shown to take place during the synthesis. However, in this case, only the complete hydrogenation product was detected in the washings, which could indicate a stronger interaction between the aryl groups of ligand **4** than those of PPh$_3$ **1** with the nanoparticle surface.

XRD analysis revealed that **Rh4** are crystalline nanoparticles with fcc packing, as in the case of **Rh1**-**Rh3**.

However, XPS analysis of nanoparticles **Rh4** only showed zero valent rhodium at the surface of these NPs. This result is in agreement with a recent report by the group of Chaudret with analogous ruthenium nanoparticles.[56] In this work, CO coordination and oxidation processes were studied using the Ru- dppb nanoparticles. For that purpose, XPS analysis was used to demonstrate that the presence of the diphosphine ligand protect the metal core of the systems from oxidation.

The TGA analysis revealed a content of phosphine derivative and rhodium of 29 and 69%, respectively, which is similar to the results obtained with **Rh1**.

Based on these results and taking into account the size of these NPs, a P/Rh ratio of 0.16 was obtained for system **Rh4**. This value corresponds to *ca*. 1 phosphorus atom for 6 rhodium surface atoms.

Comparing these results with those obtained for our model system **Rh1**, a small variation in size was observed but no differences in packing were observed by XRD and very similar contents in metal and organic stabiliser were obtained by TGA analysis. After calculations, similar P/Rh_s ratios were also obtained for nanoparticles **Rh1** and **Rh4** (Table 2.6).

Table 2.6 Approximate structural features for systems **Rh4.** Calculations based on the diameter (nm) obtained by TEM and TGA analysis.

	1.32	1.57	1.82
Nt	87	146	227
Ns	61	94	135
Nt/ Ns	70	64	59
P/Rh$_s$	0.25	0.16	0.11

The nanoparticles **Rh4** were also analysed by infrared spectroscopy (Figure 2.40). The zone of the stretching vibrations of C-H bonds (*ca*. 3000 cm^{-1}) revealed the presence of aromatic and alkylic $\upsilon_{(C-H)}$. This result is somehow in contrast with the observations by analysis of the washings of these systems where only the completely hydrogenated and oxidised ligand was detected. This thus indicated that the stabiliser at the surface of these NPs contains aromatic ring(s). In this spectrum, a band was observed at 1982 cm^{-1} and again attributed to Rh-H stretching.
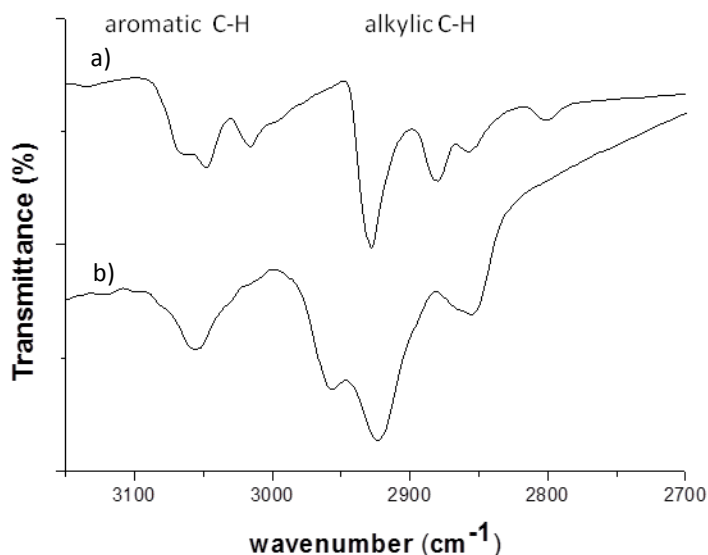
Figure 2.40 Selected region of the IR spectra of: a) dppb ligand **4**, b) **Rh4** NPs.

To summarise, the use of the diphosphine **4** as stabiliser for NPs provides small systems with similar features than their monophosphine counterparts with a diameter of *ca*. 1.5 nm, fcc packing and narrow distribution. Furthermore, a signal for Rh-H was again detected by IR spectroscopy and hydrogenation of the ligand during the NP synthesis was again indicated. Interestingly, XPS analysis of **Rh4** showed that only Rh^0 is present at the surface of these NPs, in contrast with **Rh1-Rh3** which presented some oxidation. This result can be explained by the greater capacity of ligand **4** to protect the NP surface, although the possible oxidation of the samples of **Rh1-Rh3** during their manipulation can be discarded.

*Summary of the characterisation of the phosphine stabilised Rh-NPs **Rh1**-**Rh4***

Various phosphine ligands were used for the stabilisation of Rh-nanoparticles with small size of *ca*. 1.5 nm, spherical shape and good dispersion. In the case of systems **Rh2** and **Rh3**, slightly smaller size was

101

observed (*ca.* 1.4 nm). The same crystalline structure, fcc packing and surface environment was detected by HRTEM, WAXS and XRD analyses. These nanoparticles mainly contain Rh^0, at their surface, as observed by XPS. TGA analysis showed that the systems stabilised with small ligands such as trimethylphosphine **3** leads to higher ligand coverage of the nanoparticles. However, no clear correlation with the resulting NP ligand coverage could be obtained through the variation of the ligand to rhodium ratio during their synthesis.

The titration of hydrides of **Rh1** nanoparticles indicated that *ca.* 0.8 mol of hydride are present per rhodium surface atoms in these materials. The presence of these groups was observed by IR spectroscopy for the phosphine stabilised systems **Rh1**- **Rh4**.

The analysis of the surface by IR revealed that hydrogenation of the stabilising ligands take place during the synthesis of the NPs and occurs in a larger extent when low ligand to Rh ratios are used.

A summary of the characterisation of these NPs is displayed in Table 2.7.

Table 2.7 Summary of P-based nanoparticles **Rh1-Rh4** characterisation.

NPs	Diameter (nm) (TEM)	Diameter (nm) (XRD)	shape (HRTEM)	Structure (XRD)	Oxidation State (%Rh$^{\delta+}$) (XPS)	Rh content (TGA)	L content	M-H (IR)	LH
Rh1-0.2	1.47±0.28	1.39 ± 0.03	Spherical	fcc	48	56	44	1994 cm^{-1}	vv
Rh1	1.52±0.21	1.49±0.03*	hexagonal	fcc	40	70	25	1973cm^{-1}	v
Rh1-0.6	1.46±0.25	1.46 ± 0.03	spherical	fcc	40	70	30	1997 cm^{-1}	v
Rh2	1.36±0.27	1.57 ± 0.03	spherical	fcc	40	54	44	1969 cm^{-1}	-
Rh3	1.38±0.24	1.22 ± 0.02	spherical	fcc	40	72	26	1991cm^{-1}	-
Rh4	1.57±0.25	1.49 ± 0.07	spherical	fcc	0	69	29	1982 cm^{-1}	vv

* WAXS analysis revealed a mean diameter of 2nm/ LH= hydrogenation of the stabilising ligands

2.2.3 *Synthesis and characterisation of Rh-NPs stabilised by phosphite ligands*

Synthesis of Rh- NPs stabilised by triphenylphosphite 5

For this family of ligands, the triphenylphosphite **5** was selected as a model. To the best of our knowledge, the use of monophosphite ligands for the stabilisation of metal nanoparticles has not been reported to date.
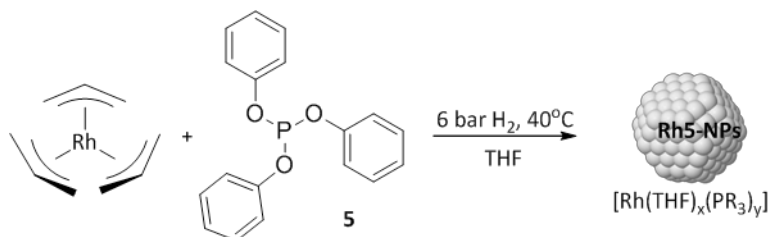
Figure 2.41 Synthesis of **Rh5** NPs.

Initially, 0.4 equivalent of the ligand **5** was used for the synthesis of the Rh-nanoparticles **Rh5** that were analysed by TEM (Figure 2.42, left). Small nanoparticles with a diameter of 1.52± 0.23 nm with narrow distribution, spherical shape and good dispersion were observed. No relevant differences in size were thus observed between this system and **Rh1**.
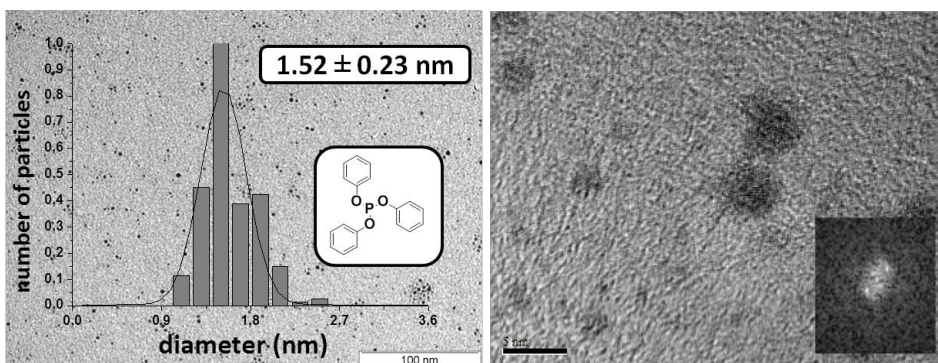
Figure 2.42 TEM micrograph and size distribution (left) and HRTEM image (right) of **Rh5** NPs.

The analysis of these nanoparticles by HRTEM (Figure 2.42, right) confirmed the good dispersion and spherical shape previously observed with a bond length of 0.26 nm, which is in agreement with a fcc structure.

The remaining solution after precipitation of the nanoparticles with pentane and the washings were analysed by ^{1}H and ^{31}P NMR and GC- MS.

In the ^{1}H NMR spectrum, only signals were observed in the aromatic region (6-8ppm) and a single signal was detected by ^{31}P{H} NMR spectroscopy at δ -17.7 ppm, which was assigned to triphenylphosphite oxide.[57] Analysis of the same sample by GC- MS confirmed the identity of this species as triphenylphosphite oxide **15** (Figure 2.43).
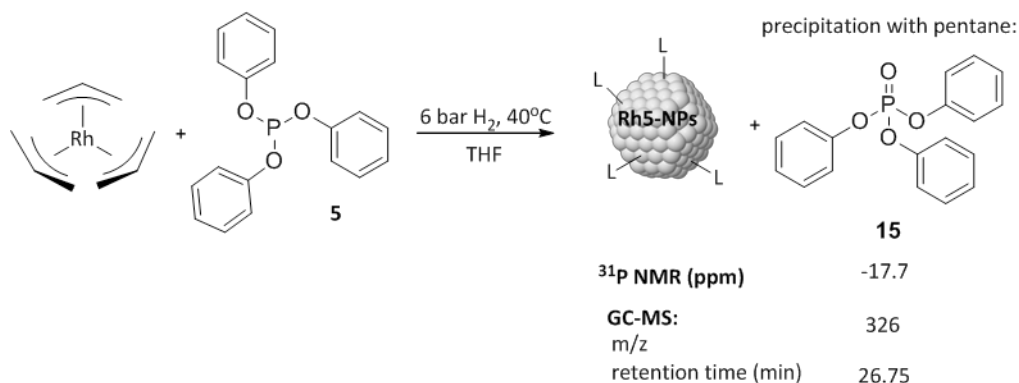
Figure 2.43 Species detected during the synthesis of system **Rh5** NPs.

In contrast with the results described for phosphine stabilised NPs **Rh1** and **Rh4**, no hydrogenation products of this ligand were detected in the washings.

Next, the nanoparticles **Rh5** were characterised by XRD, that showed that these crystalline systems adopt a fcc packing and a mean diameter of 1.53 ± 0.023 nm, in agreement with the size obtained by TEM.

XPS measurements were also performed on this nanoparticles. After the optimisation of the parameters for this sample and the use of the Monte-Carlo approximation, the simulation gave unique bands for the rhodium 3d 5/2 and 3d 3/2 (Figure 2.44).
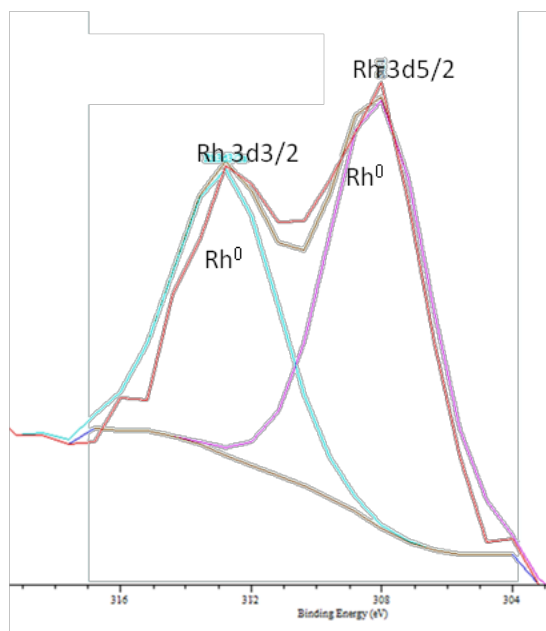
Figure 2.44 XPS spectra of Rh 3d for nanoparticles **Rh5**.

These results indicate that for this catalyst the rhodium atoms at the surface are in a zero valent state, differing with the **Rh1**-NPs that are partially oxidised.

Thermogravimetric analyses were performed to the system **Rh5** and the content of these nanoparticles was evaluated as *ca.* of 2% in weight of solvent, 40% of phosphite ligand and 58% of rhodium (Figure 2.45).
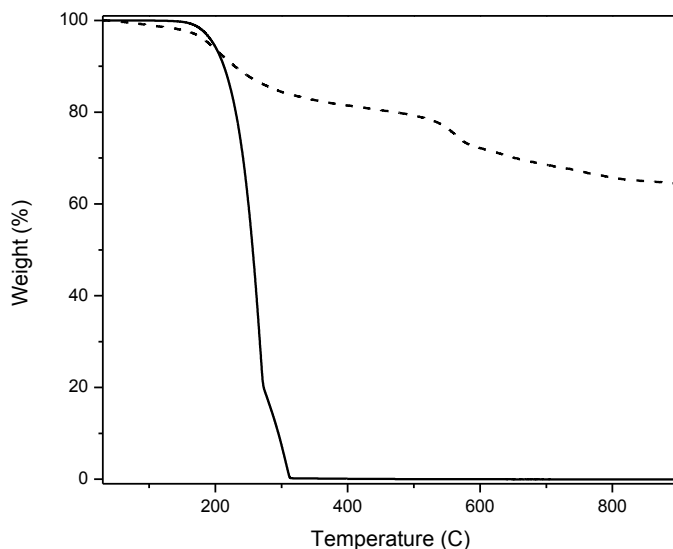
Figure 2.45 TGA curves of free ligand P(OPh)$_3$ **5** (solid line) and the corresponding nanoparticle **Rh5** (dashed line) (10 °C min^{-1} in N$_2$)

All these characterisation techniques revealed no differences in size, shape and packing between the systems **Rh1** and **Rh5**. However differences were observed in terms of oxidation state at the surface, only Rh^0 was detected at the surface for system **Rh5** while Rh$^{\delta+}$ was observed for the system **Rh1**. The TGA analysis revealed higher coverage in stabilising agent for the nanoparticles **Rh5** (42%) than for the **Rh1** (25%).

The smaller cone angle of the phosphite ligand compared to that of ligand **1** and the more coordinative character of phosphites compared to phosphines, could explained this difference in ligand coverage.

An approximation of the numbers of atoms present in **Rh5** were calculated based on the information extracted from the TEM and XRD analysis and using the equations extracted from the Van Hardevel Hartog model.

Table 2.8 Approximate structural features for systems **Rh5**. Calculations based on the diameter (nm) obtained by TEM and TGA analysis.

	1.29	1.52	1.75
Nt	81	132	202
Ns	58	86	122
Nt/ Ns	71	65	60
P/Rh$_s$	0.52	0.35	0.25

As the diameter and structure of the nanoparticles was the same for system **Rh5** than for **Rh1**, the same values, number of total atoms (Nt) of 132, on the surface (Ns) of 86 and 65 of Nt/ Ns ratio were obtained.

However, a ratio of 0.35 atom of phosphorus to rhodium surface atom was obtained for **Rh5**-NPs, which represents *ca.* 1 phosphorus for 3 rhodium surface atoms. Using this phosphite ligand, a higher coverage of the surface is obtained compared to its phosphine analogue (for **Rh1**- NPs 1 phosphorus atom per 4 rhodium surface atoms).

Next, hydride titration and solution NMR were also performed to these nanoparticles **Rh5**.

The titration experiments with system **Rh5** were carried out following the reported procedures.[40] Reaction with norbornene was carried out at room temperature and in d$_8$ THF as the solvent. The conversion obtained, in correlation with the number of atoms at the surface of these nanoparticles, revealed that *ca.* 0.3 mol of hydrides per rhodium surface atoms are present at the surface of these NPs.
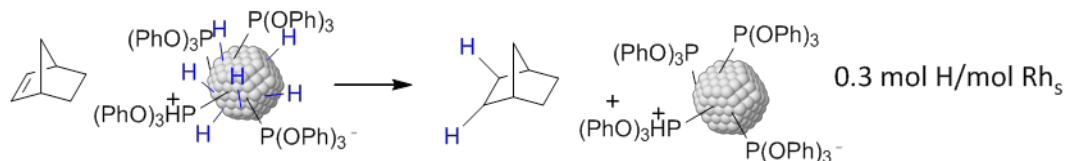
Figure 2.46 Representation of hydrides titration on **Rh5** NPs.

The solution $^{31}P\{1H\}$ spectrum NMR did not contain any signals at room temperature. However, similarly to **Rh1**, the low temperature (-80 °) spectrum showed a signal at -16 ppm readily assigned to triphenylphosphite oxide **15** and indicated the possible interaction of this species with the nanoparticles.
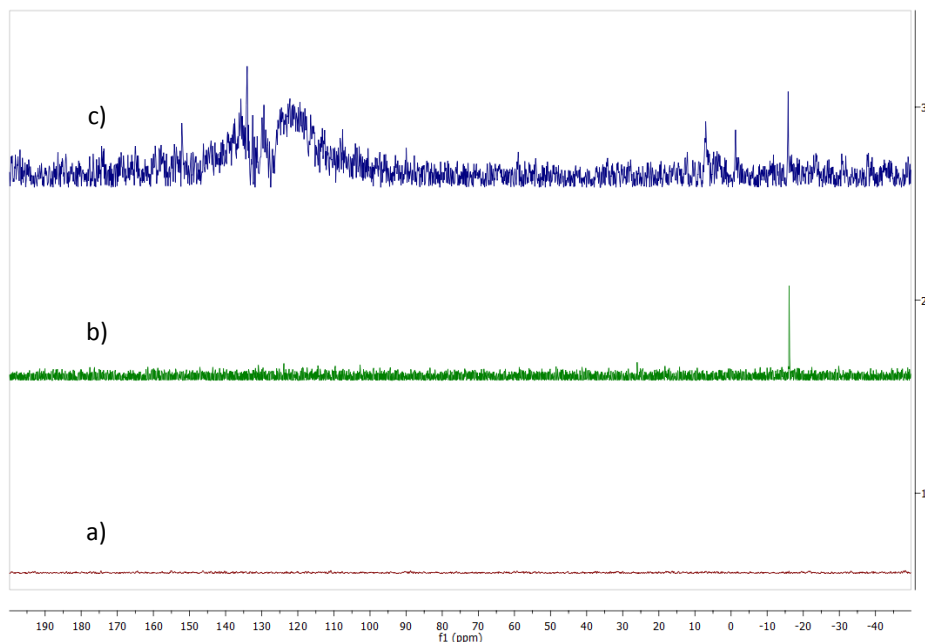
Figure 2.47 Solution $^{31}P\{H\}$ NMR spectra of Rh-NPs **Rh5** in d_8THF at a) room temperature, b) -80°C, c) after 30 bar of CO pressure.

After exposure of the sample to 30 bar of CO pressure, singlet signals at -15.8, -1.15 and 7.02 ppm were observed, and could be attributed to oxidised derivatives of the stabilising ligand **5**. Moreover, two broad resonances centred at *ca*. 120 and 135 ppm were also observed and attributed to phosphite ligands at the surface of the nanoparticles.
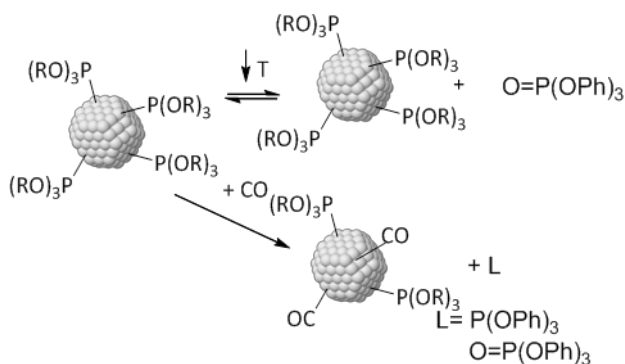
Figure 2.48 Species observed by liquid ^{31}P NMR.

The nanoparticles **Rh5** were also analysed by IR spectroscopy and the corresponding spectrum in shown in Figure 2.49a.
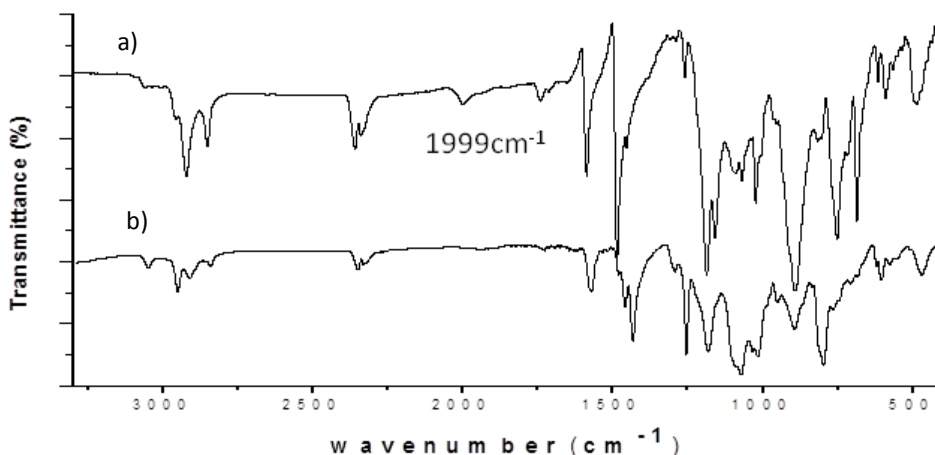
Figure 2.49 IR spectra of a) **Rh5** NPs b) **Rh5** D$_2$ NPs.

The zone concerning the stretching of C- H bonds at *ca.* 3000 cm^{-1} reflected the presence of both alkylic and aromatic $\upsilon_{(C-H)}$ at the surface of these nanoparticles, indicating that some hydrogenation of the ligand had taken place during the synthesis. Interestingly, no hydrogenation products were detected by ^{1}H NMR in the washings of these systems, suggesting that this process could occur at the surface after coordination of the ligand.

Moreover, a small and broad band was observed at 1999 cm^{-1}. To determine the origin of this signal, the NPs **Rh5** were synthesised under D$_2$ and the corresponding spectrum did not exhibit such a band (Figure 2.49b). This band was therefore attributed to a rhodium hydride present at the surface of the nanoparticles. The lower intensity of this signal compared to that of **Rh1** is in agreement of the results obtained by hydride titration (0.3H/Rh$_s$ for **Rh5** vs. 0.8H/Rh$_s$ for **Rh1**).

It should also be noted that several changes were observed in the region 1000-1500 cm^{-1} of the spectra, corresponding to C-C stretching and bending from the ligands that were reduced under D$_2$, thus providing differences in frequency compared to those arising from the ligand reduced under H$_2$.

To summarise, the **Rh5** NPs stabilised by the triphenylphosphite ligand **5** exhibit similar properties than its phosphine counterpart **Rh1** such as size, shape, and structure packing. However, differences in hydride and ligand coverage at their surface were observed. TGA analysis, hydride titration and IR spectroscopy results indicated a higher ligand coverage and a lower hydride coverage for the phosphite system **Rh5** than for **Rh1**.

Synthesis of Rh-NPs at various equivalents of triphenylphosphite 5

As in the case of PPh$_3$ **1**, the number of equivalents of stabilising agent per Rh was varied and the nanoparticles **Rh5-0.1**, **Rh5-0.2** and **Rh5-0.6** were synthesised with 0.1, 0.2 and 0.6 equivalent of ligand **5** per Rh, respectively (Figure 2.50). It is noteworthy that with this ligand, the presence of 0.1 eq of **5** per Rh is a sufficient amount to provide stabilisation of small Rh-NPs while no NPs could be obtained using PPh$_3$ **1** under the same conditions.
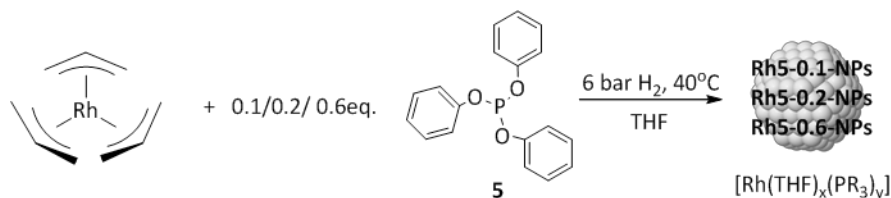
Figure 2.50 Synthetic method used for the preparation of the **Rh5-0.1**, **Rh5-0.2** and **Rh5-0.6** NPs.

The formation of the nanoparticles was confirmed by TEM microscopy and the corresponding micrographs and size distributions are displayed in Figure 2.51. No significant differences in size were observed between the **Rh5-0.2** NPs and the model system **Rh5**. However, in the case of the nanoparticles with higher amount of stabiliser **Rh5-0.6**, a slight increase in size was observed. No clear differences in shape, distribution and dispersion were detected in all the triphenylphosphite **5** stabilised systems **Rh5-0.1-Rh5-0.6**.
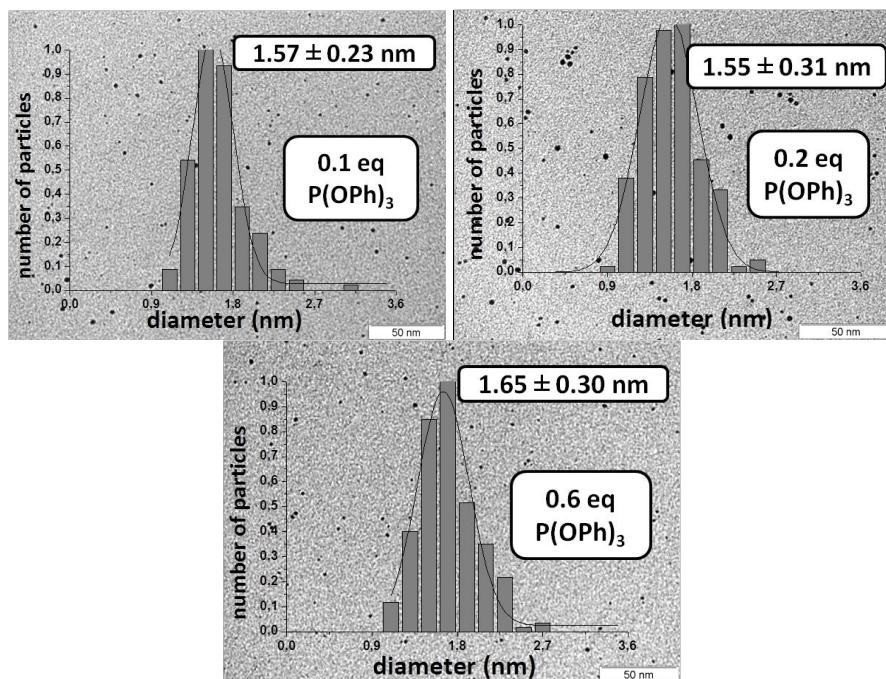
Figure 2.51 TEM micrographs and size distributions of the **Rh5-0.1**, **Rh5-0.2** and **Rh5-0.6** NPs.

The remaining solution of the washings of the nanoparticles was analysed by NMR spectroscopy. The same result was obtained for all the systems stabilised by triphenylphosphite **5**: in all cases, the ^{1}H NMR spectrum revealed the presence of only aromatic signals (6-8 ppm) and in the ^{31}P{H} NMR spectrum, one signal corresponding to the oxidised form of the triphenylphosphite ligand **5** was detected at -17.7ppm.

No difference in crystallinity or packing was observed by XRD between the systems stabilised by triphenylphosphite **5**.

The analysis of the three systems **Rh5-0.1**, **Rh5-0.2** and **Rh5-0.6** by XPS reflected the presence of 40% of Rh$^{\delta+}$ at the surface. These results are in contrast with the previously commented XPS analysis for system **Rh5**, stabilised with 0.4 equivalents of ligand **5**, where only Rh^0 was present at the surface. More amount of ligand should give more protected surface, however, the results are not in coherence with this argument. Maybe the manipulation of the sample before or during the analysis influenced the obtained results.

The systems were also analysed by TGA, revealing a correlation between the amount of ligand used during the synthesis and the ligand coverage on the resulting NPs (Table 2.9). Indeed, when the amount of phosphite 5 was increased from 0.1 to 0.6 equivalent, an increase in ligand content was observed **from** 34% for **Rh5-0.1**, 42% for **Rh5-0.2** and 53% for **Rh5-0.6** NPs. For the model system **Rh5** synthesised with 0.4 equivalents of ligand, 42% of ligand was obtained. Taking into account, for instance the approximate percentage of phosphite derivative obtained by TGA, more amount of ligand was observed increasing the equivalents of triphenylphosphite used for the synthesis.

Table 2.9 TGA analysis of systems stabilised by triphenylphosphite **5**.

NPs	%M	%L
Rh5-0.1	65	34
Rh5-0.2	62	42
Rh5	58	40
Rh5-0.6	45	53

These results are also reflected by the calculations of the approximate number of phosphorus atoms per Rh at the surface of these NPs (Table 2.10).

Table 2.10 Approximate structural features for systems **Rh5-0.1**, **Rh5-0.2** and **Rh5-0.6**. Calculations based on the diameter (nm) obtained by TEM and TGA analysis.

	Rh5-0.1			Rh5-0.2			Rh5-0.6		
	1.24	1.55	1.86	1.34	1.57	1.80	1.35	1.65	1.95
Nt	72	140	242	91	146	220	93	169	279
Ns	52	91	142	63	94	131	65	106	158
Nt/ Ns	73	65	58	70	64	60	69	63	57
P/Rh$_s$	0.4	0.27	0.19	0.66	0.38	0.24	1.02	0.62	0.42

As previously commented, values corresponding to *ca*. 0.3 phosphorus per rhodium surface atom are in agreement with reported data.ref Here, calculations provided P/Rhs ratios comprised between 0.3 and 0.6 (for mean diameter). Such high values of phosphorus coverage at the surface of such small systems seems excessive and indicate that these approximations can only provide qualitative information.

The NPs **Rh5-0.1-Rh5-0.6** were also analysed by IR spectroscopy. No relevant differences were observed between the spectra, except at

frequencies of *ca*. 3000 cm^{-1} (Figure 2.52). Similarly to the results described for PPh3 **1** as stabilisers, complete hydrogenation of the ligand **5** was indicated for **Rh5-0.1** since only aliphatic C-H stretching bands were detected. When higher amount of ligand was used during the synthesis, the detection of both aromatic and aliphatic C-H stretching bands suggested that the reduction of the ligand was only partial.
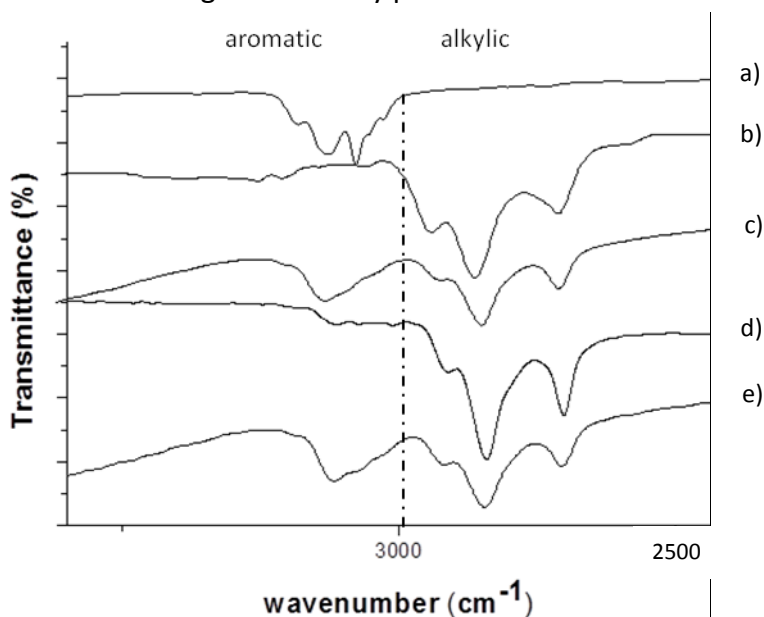
Figure 2.52 Selected region of the IR spectra of a) P(OPh)$_3$ **5**, b) **Rh5-0.1**, c) **Rh5-0.2**, d) **Rh5**, e) **Rh5-0.6**.

To summarise, no significant difference in size was observed between systems **Rh5-0.1**, **Rh5-0.2** and **Rh5**, while **Rh5-0.6** were slightly larger. The same shape, narrow distribution and fcc packing was observed for all these systems. Up to 30% of Rh$^{\delta+}$ was observed by XPS for these systems except for system **Rh5** where only Rh^0 was present at the surface of the nanoparticles. TGA analysis of these samples showed that increasing the equivalents of stabilising ligands during the synthesis is correlated with the ligand coverage on the NPs. Similarly to the **Rh1** NPs, a higher degree of hydrogenation of the stabilising ligand was also observed by IR spectroscopy at low ligand to Rh ratio during the synthesis. Moreover, a

signal attributed to Rh-hydrides at the surface of the nanoparticles was detected. This signal was weaker than that observed for **Rh1**, which is in agreement with results obtained by hydride titration experiments (0.8 for **Rh1** vs. 0.3 for **Rh5**).

Liquid NMR spectroscopy revealed that both phosphite and oxidised phosphite species are interacting with the surface of the nanoparticles in THF solution.

Synthesis of Rh-NPs stabilised by tri-ortho-tertbutyl phenylphosphite 6 and trimethylphosphite 7

The effect of steric properties was also studied in this family of ligands with the use of phosphites **6** and **7** Figure 2.53.

for the synthesis of the Rh NPs **Rh6** and **Rh7**. Similarly to previous systems, the syntheses of **Rh6** and **Rh7** were carried out in the presence of 0.4 equivalent of ligand per Rh by decomposition of $[Rh(\eta^3\text{-}C_3H_5)_3]$ under H_2 atmosphere at 40 °C using THF as the solvent.
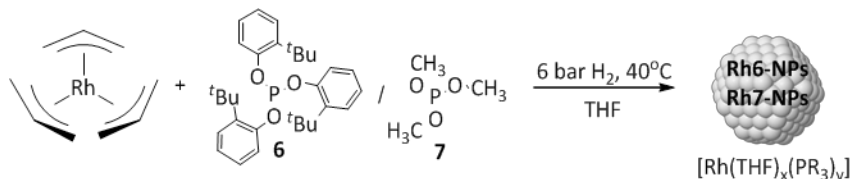
Figure 2.53 Method used for the synthesis of **Rh6** and **Rh7** NPs.

The formation of nanoparticles was confirmed by TEM, and for system **Rh6** a similar size (1.55± 0.23 nm) than in the case of **Rh5**. However, the nanoparticles **Rh7** stabilised by the less hindered $P(OMe)_3$ ligand **7** exhibited a smaller size of *ca*. 1.3 nm (Figure 2.54). Interestingly, similar size was obtained when the analogous PMe_3 **3** ligand was used for the stabilisation of nanoparticles **Rh3** (1.38± 0.24 nm).
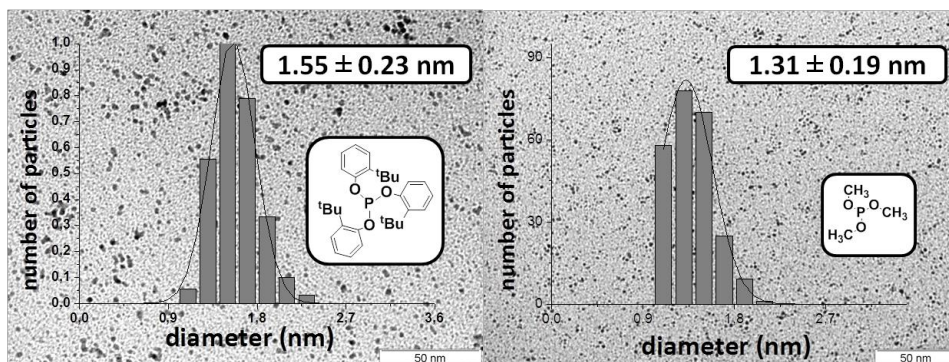
Figure 2.54 TEM micrographs and size distributions of the **Rh6** and **Rh7** NPs.

These systems were analysed by HRTEM confirming the good dispersion and spherical shape of the particles (Figure 2.55) and providing a bond length of 0.21 and 0.26 nm for **Rh6** and **Rh7** respectively, both in agreement with fcc structures.
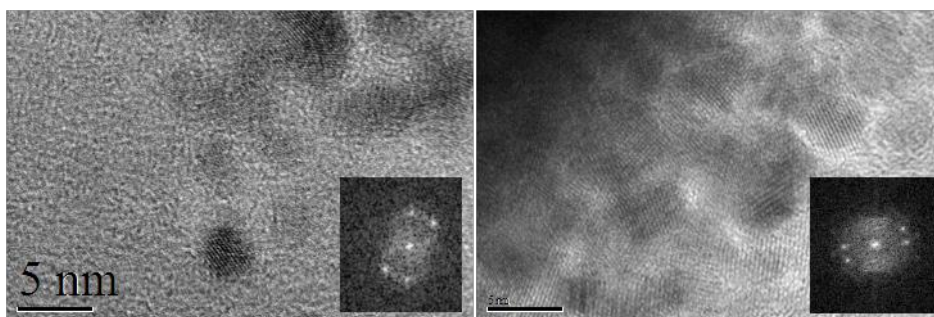
Figure 2.55 HRTEM image of the **Rh6**(left) and **Rh7**(right) NPs.

The analysis of washings of the **Rh6** nanoparticles by ^{1}H NMR spectroscopy revealed the presence of signals in both the aromatic (6-8 ppm) and aliphatic region of the spectra. The large number of signals in the aliphatic region indicated that some hydrogenation of the ligand had taken place. The ^{31}P{H} spectrum showed only a signal at -20.6 ppm, which was attributed to the oxidised form of the ligand used to stabilise the **Rh6** nanoparticles. This result showed that the tert-butyl groups of the ligand could prevent the phenyl rings to approach the surface of the nanoparticles and the consequent hydrogenation.

117

However, for system **Rh7**, stabilised by trimethylphosphite **7** no phosphorus signals were observed by NMR spectroscopy, indicating that most of ligand present during the synthesis ended at the surface of the NPs.

The nanoparticles were analysed by XRD, revealing crystalline structure and fcc packing for both systems. The XPS analysis showed oxidised $Rh^{\delta+}$ zones at the surface of **Rh6**, while only Rh^0 was detected at the surface of **Rh7**.

Regarding the TGA analysis, for nanoparticles **Rh6**, 53% of phosphite was measured, corresponding to an approximate number of phosphorus atom per rhodium surface atom of 1/3. However, for nanoparticles **Rh7,** a value of *ca*. 1 phosphorus atom per rhodium surface atom was calculated. Interestingly, the same ratio was observed using the analogous trimethylphosphine **3** as stabilising agent.

Table 2.11 Approximate structural features for systems **Rh6** and **Rh7**. Calculations based on the diameter (nm) obtained by TEM and TGA analysis.

|	Rh6			Rh7		
	1.32	**1.55**	**1.78**	**1.12**	**1.31**	**1.50**
Nt	87	140	212	53	105	127
Ns	61	91	127	41	72	84
Nt/ Ns	70	65	60	78	68	66
P/Rh$_s$	0.58	0.39	0.28	1.53	0.87	0.75

Again only qualitative information in considered for the systems with such high values of phosphorus coverage at the surface of such small systems as reflected for system **Rh7**. The nanoparticles **Rh6** and **Rh7** stabilised by the monophosphites **6** and **7**, systems were also analysed using infrared spectroscopy. The detection of both stretching vibrations of aromatic and aliphatic C-H bonds at *ca*. 3000 cm^{-1} for system **Rh6** was not very conclusive since both types of bonds are present in the starting ligand. Comparison with the spectrum the ligand revealed similar pattern and it was deduced that no relevant changes had taken place. For both systems a small band

was detected at *ca.* 2000 cm^{-1}, which were again attributed to the presence of Rh-hydride species at the surface of these NPs.
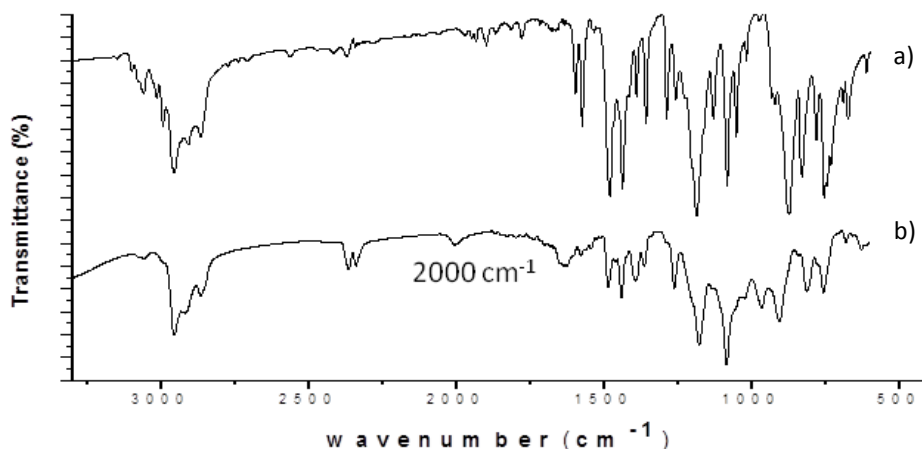
Figure 2.56 IR spectra of: a) ligand **6** and b) nanoparticles **Rh6**.

To summarise, the use of phosphite ligands **6** and **7** provided small Rh-NPs. In terms of size, the **Rh6** system exhibited similar mean diameter than **Rh5** while **Rh7** displayed a smaller diameter, similarly to the results obtained with the PMe$_3$ ligand. It can therefore be concluded that under the synthetic conditions used, the employment of small ligands such as PMe$_3$ or P(OMe)$_3$ provides smaller NPs than when bigger ligands were used.

In contrast, no changes in shape, distribution, dispersion nor packing were observed. XPS measurements showed that Rh$^{\delta+}$ was present at the surface of system **Rh6**, while only Rh^0 was observed for system **Rh5** and **Rh7**. Using the results obtained from the TGA analysis, the calculations of the number of atoms indicated that a similar amount of phosphorus per rhodium surface atoms is present for systems **Rh6** and **Rh5**. However, a more crowded surface was observed for the nanoparticles stabilised with trimethylphosphite **7**, as already observed for the analogous PMe$_3$-stabilised nanoparticles **Rh3**.

Synthesis of Rh- NPs stabilised by the diphosphite ligand 8

Next, the diphosphite ligand **8** derived from 4,4'-dihydroxydiphenyl backbone was used for the synthesis of the **Rh8** NPs. Diphosphite ligands were previously reported as stabilisers for NPs based on palladium[26], platinum[26], iridium[16], ruthenium[16] and rhodium[16,19,] nanoparticles.

As previously for **Rh4**, 0.2 equivalents of **8** were used for the synthesis of **Rh8** to maintain a constant P/Rh ratio (Figure 2.57).

Figure 2.57 Method used for the synthesis of **Rh8** NPs.
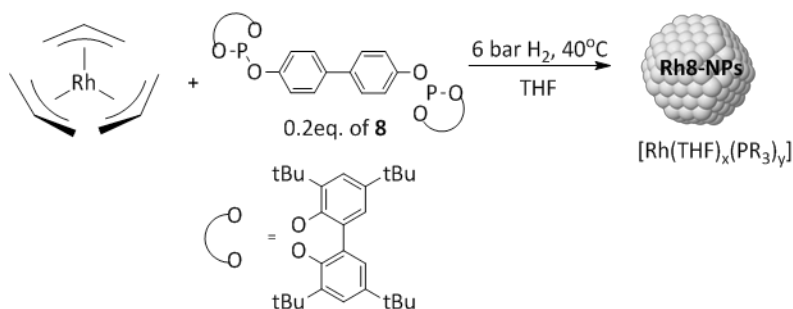
TEM analysis showed that **Rh8** nanoparticles exhibited a diameter of 1.6±0.25 nm with narrow distribution (Figure 2.58), which is slightly larger than for other ligands used in this work. For the first time in this study, some degree of agglomeration was observed in the TEM micrograph and could be attributed to the capacity of the ligand **8** to act as a bridge between NPs.
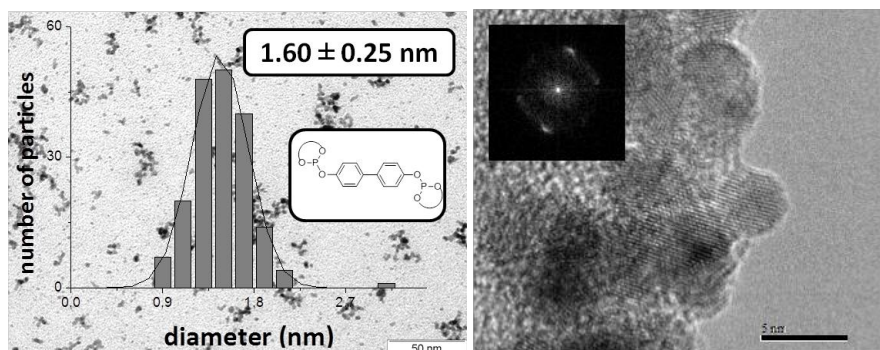
Figure 2.58 TEM micrograph and size distribution (left) and HRTEM image (right) of **Rh8** NPs.

The analysis of system **Rh8** by HRTEM revealed single particles with hexagonal shape (Figure 2.58, right) for this system with a bond length of 0.22 nm that is in agreement with a fcc structure for these nanoparticles. This morphology was also observed for system **Rh1** stabilised with triphenylphosphite **1** .

The analysis of the washings of these nanoparticles showed a signal at -7 ppm in the ^{31}P{H} spectrum which was attributed to the oxidation of the ligand during the synthesis of the nanoparticles.

XRD analysis revealed the crystalline character of these nanoparticles with fcc pagking while XPS analysis revealed 30% of $Rh^{\delta+}$ at the surface of the nanoparticles.

The TGA analysis revealed a content of 66% in phosphite derivative and 35% of rhodium corresponding to *ca.* 1 phosphorus for 4 rhodium surface atoms after calculations using the VDH model.

Table 2.12 Approximate structural features for systems **Rh8.** Calculations based on the diameter (nm) obtained by TEM and TGA analysis.

	1.35	1.60	1.85
Nt	93	154	238
Ns	65	98	140
Nt/ Ns	69	64	59
P/Rh$_s$	0.42	0.28	0.19

The surface of the nanoparticles **Rh8** was also analysed by IR spectroscopy and the corresponding spectrum is displayed in Figure 2.59. Although little information could be extracted, the detection of a very weak Rh-H stretching was obtained in this case.
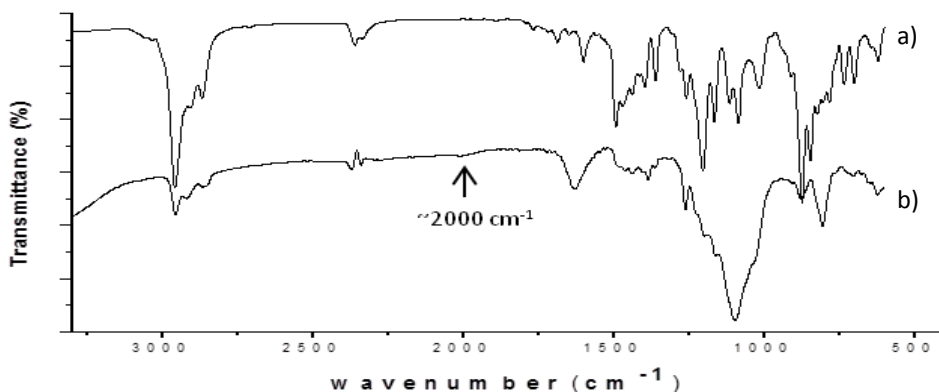
Figure 2.59 IR spectra of: a) ligand **8** and b) nanoparticles **Rh8**.

*Summary of phosphite stabilised Rh-NPs **Rh5**-**Rh8***

The use of phosphite ligands **5-8** provided small Rh nanoparticles of *ca*. 1.5 nm. All the systems presented spherical shape, narrow distribution and good dispersion, except the diphosphite stabilised system **Rh8** that exhibited some degree of agglomeration due to the capacity of this ligand to act as a bridge between NPs. This series of nanoparticles were crystalline with fcc packing as revealed by XRD analysis and HRTEM. Significant amounts of $Rh^{\delta+}$ were detected at their surface by XPS, which might indicate distintc ability of the stabilisers to protect the NPs from oxidation, although the possibility of oxidation of the sample during their manipulation for XPS measurements cannot be discarded.

TGA analysis revealed that these NPs contain between 40-60% in weight of rhodium, and that their surface is significantly more crowded when the small ligand **7** was used as stabiliser. When the series of NPs **Rh5-0.1-Rh5-0.6** was analysed by TGA, a greater ligand coverage was measured when the NPs were synthesised using a higher $P(OPh)_3$ / Rh ratio.

Similarly to the phosphine stabilised systems, hydrogenation of the ligands bearing aromatic rings was shown to take place during the synthesis and for the **Rh0.5 NPs**, higher degree of hydrogenation was observed at low ligand to Rh ratio.

Table 2.13 Summary of phosphite stabilised nanoparticles **Rh5-Rh8** characterisation.

NPs	Diameter (nm)		shape	Structure	Oxidation State (%Rh$^{\delta+}$)	Rh content	L content	M-H	LH
	(TEM)	(XRD)	(HRTEM)	(XRD)	(XPS)	(TGA)	(TGA)	(IR)	
Rh5-0.1	1.57± 0.23	1.53± 0.04	spherical	fcc	40	65	34	-	√√
Rh5-0.2	1.55± 0.31	1.64± 0.05	spherical	fcc	40	62	42	2003 cm^{-1}	√
Rh5	1.52± 0.23	1.53± 0.02	spherical	fcc	0	58	40	1999cm^{-1}	√√
Rh5-0.6	1.65± 0.30	1.53± 0.04	spherical	fcc	40	45	53	2004 cm^{-1}	√
Rh6	1.55± 0.23	1.28 ± 0.08	spherical	fcc	40	45	53	2010 cm^{-1}	n.c.
Rh7	1.31± 0.19	0.83 ± 0.06	spherical	fcc	0	55	39	n.c.	-
Rh8	1.60± 0.25	1.43 ± 0.02	hexagonal	fcc	30	35	65	2009 cm^{-1} (w)	n.c.

LH= hydrogenation of the stabilising ligands

123

2.2.4 *Synthesis and characterisation of ligand-free Rh-NPs*

In the previous section, a series of phosphorus stabilised nanoparticles were synthesised and characterised. To further investigate the effect of these ligands on the properties of rhodium nanoparticles, a series of ligand-free Rh-NPs were synthesised for comparison. For this purpose, two other types of stabiliser were used: the polymer polyvinylpyrrolidone (PVP) **16** and the solvent mixture THF/MeOH.

Rh-NPs stabilised by polyvinylpyrrolidone (PVP) 16

One of the most common compound reported as metal nanoparticle stabiliser is the polymer polyvinylpyrrolidone (PVP) **16**.[5,12,58,59] The use of this stabiliser according to the organometallic approach was previously reported using THF as the solvent.[24,60]

These polymers are characterised by their molecular weight, which is referred as PVP k-n (n= 15, 30 or 90).[61] Since PVP K-90 stabilised ruthenium nanoparticles showed high activity in hydrogenation reactions, this polymer was used in this study.[62]

For this synthesis, 5 equivalents of the PVP k-90 per rhodium **16** was used to stabilise the Rh-NPs, the synthesis was carried out under 6 bars of H_2 and at room temperature.

The formation of the nanoparticles was confirmed by TEM microscopy, obtaining nanoparticles with 1.49± 0.19 nm of mean diameter, with narrow distribution, spherical shape and good dispersion (Figure 2.60).
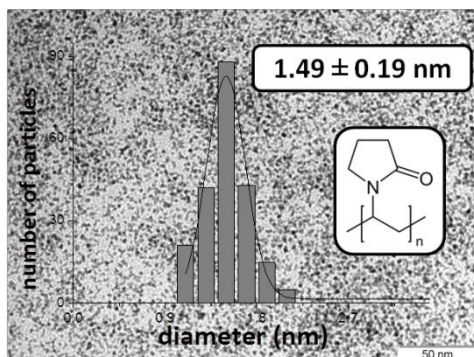
Figure 2.60 TEM micrograph and size distribution of the **Rh16** NPs.

The analysis of the structure of the nanoparticles by XRD revealed again crystalline systems with fcc packing. XPS was also used to analyse the chemical environment at the surface of the nanoparticles and $Rh^{\delta+}$ was detected in 40 % at the surface for this system **Rh16**.

The content of the nanoparticles was also analysed by TGA analysis, revealing 59% in weight of rhodium and 41% in weight of organic part for this system.

The calculation of the number of atoms of these **Rh16** nanoparticles gives values of 125 for Nt, 82 for Ns and a Nt/ Ns ratio of 66.

Table 2.14 Approximate structural features for systems **Rh16.** Calculations based on the diameter (nm) obtained by TEM and TGA analysis.

	1.30	1.49	1.68
Nt	83	125	178
Ns	59	82	110
Nt/ Ns	71	66	62

Using the polymer PVP as stabilising agent no significant differences in terms of size, structure, and surface chemical environment was observed compared to the previous P- based nanoparticles **Rh1**- **Rh8**.

The nanoparticles **Rh16** stabilised by PVP **16** were analysed by IR and the spectrum obtained is shown in Figure 2.61. Initially, the spectrum obtained was compared with that of the corresponding PVP stabiliser.

The bands corresponding to the stretching vibrations of alkylic C-H bonds were observed under 3000 cm^{-1}. Moreover, a band at 1960 cm^{-1} was detected, and attributed to Rh-H species by comparison with previous systems under study. Interestingly, similar signal was also observed by Dyson and co-workers at 1918 cm^{-1}, although no information of the nature of this band was provided by the authors.[35] The signals under *ca*. 1600 cm^{-1} where the bending vibrations of double bonds, methyl and methylene deformations are detected, for instance could not be clearly attributed.

Interestingly, the C=O stretching of the carbonyl of PVP was shifted by 20 cm^{-1} once stabilising the NPs (1673 cm^{-1} for PVP **16** and 1654 cm^{-1} for **Rh16**), indicating that this group interacts with the NP surface, in agreement with previously reported studies.[63,64]
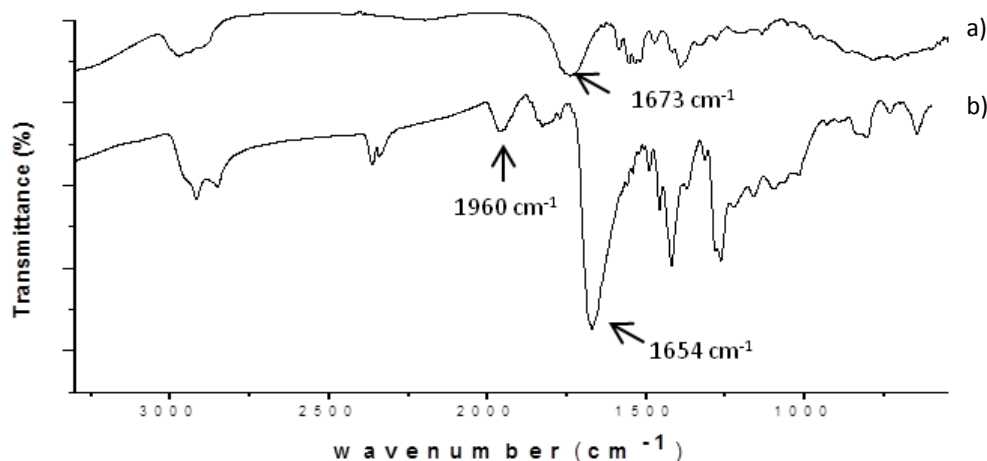
Figure 2.61 IR spectra of a) PVP **16** and b) **Rh16** NPs.

The structural features observed for system **Rh16,** stabilised by the PVP, such as size, shape, morphology and packing were therefore very similar to those of the P-based stabilised systems **Rh1**-**Rh8**. IR spectroscopy revealed

the presence of rhodium hydride species at the surface of these nanoparticles.

Rh-NPs stabilized by THF/MeOH mixture

In 2003, Chaudret and co- workers reported the synthesis of ruthenium nanoparticles stabilised by mixtures of solvents.[65] Different solvent compositions were tested obtaining NPs with different sizes. The composition THF/MeOH 97.5:2.5 % volume ratio provided the smallest (3-6nm) ruthenium nanoparticles, and was selected for the synthesis of Rh-NPs in this work.

The organometallic precursor $[Rh(\eta^3\text{-}C_3H_5)_3]$ was decomposed under H_2 in a Fisher- Porter bottle, at room temperature and in the solvent mixture THF/ MeOH (97.5:2.5 % volume) (Figure 2.62).

6 bar H_2, r.t.

THF/ MeOH (97.5:2.5)

Rh- THF/MeOH NPs

$[Rh(THF)_x(MeOH)_y]$
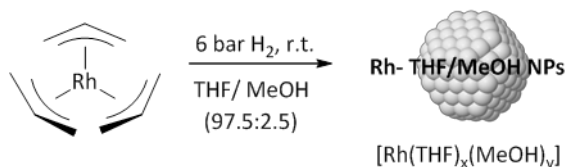
Figure 2.62 Method used for the synthesis of the Rh-THF/MeOH NPs described in this section.

Under these conditions, the solution was observed to rapidly turn black, confirming the decomposition of the complex. Finally, the nanoparticles were isolated as black powders after precipitation and washing with pentane.

The formation of small nanoparticles presenting a "sponge- like" morphology was confirmed by TEM microscopy (Figure 2.63), in agreement with the morphology observed for the analogous ruthenium nanoparticles.[65] The individual particles presented a mean diameter of 1.16± 0.17 nm with a narrow distribution.
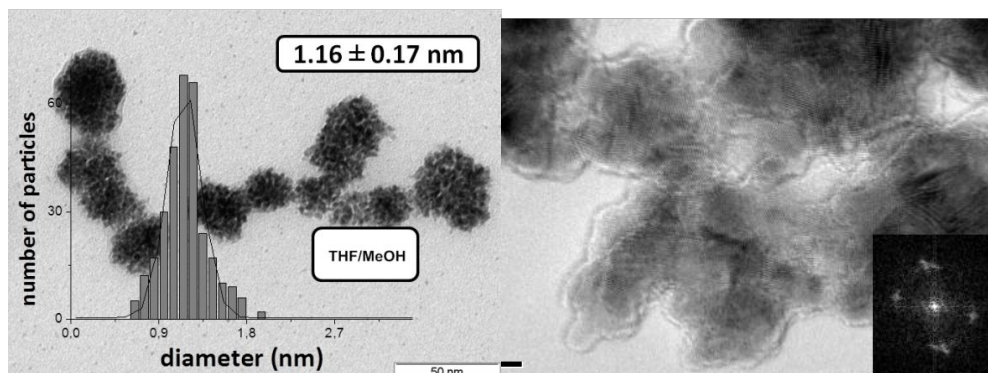
Figure 2.63 TEM micrograph and size distribution (left) and HRTEM image (left) of the **Rh17** NPs.

These nanoparticles were analysed by HRTEM where highly crystalline nanoparticles were observed with a bond length between the rhodium atoms of 0.21 nm, in agreement with a fcc structure, which was confirmed by XRD.

XPS analysis revealed that the surface of these nanoparticles is composed of 40% of $Rh^{\delta+}$ and 60% Rh^0.

The calculation of the number of atoms produced values of 59 for the total atoms (Nt), 45 of surface atoms (Ns) and a Nt/ Ns ratio of 76. The highest surface/ total atoms ratio of this work was obtained with this system due to their small size.

Control of the size of Rh- NPs. The seeded growth method

The solvent stabilised nanoparticles system **Rh17** had a smaller size than the previous P- stabilised nanoparticles. To avoid size effects, new NPs of different sizes were synthesised using the seeded growth method.[59]
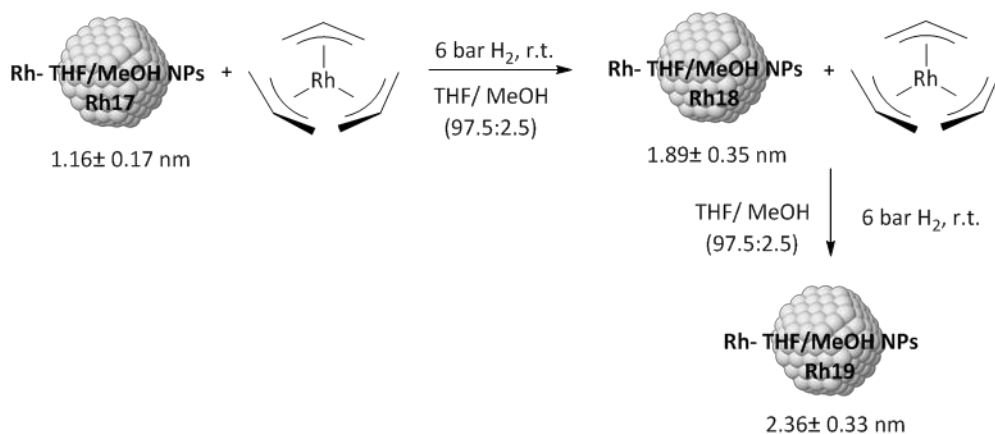
Figure 2.64 Synthetic methodology for **Rh17** NPs.

First, the same standard procedure previously described for **Rh17** was used. A sample was taken for TEM analysis and a new amount of rhodium precursor was added to the suspension and the resulting mixture placed under hydrogen pressure (6 bar) and stirred at 40 °C for 16h.

TEM microscopy confirmed the growth of the Rh-nanoparticles (Figure 2.65) with the same "sponge-like" morphology previously observed for system **Rh17** with a mean diameter of 1.89 ± 0.35 nm.
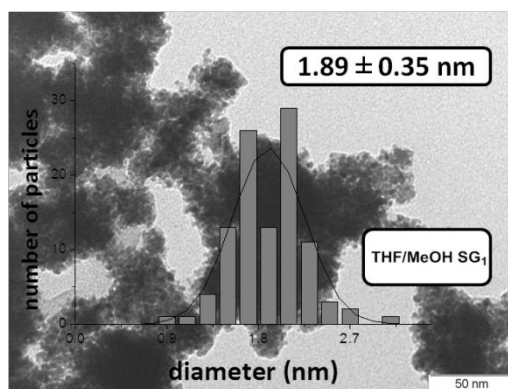
Figure 2.65 TEM micrograph and size distribution of the **Rh18** NPs.

The same procedure was repeated to obtain nanoparticles **Rh19** of bigger size (2.36± 0.33 nm, Figure 2.66). Once more, sponge-like morphology was observed by TEM for these NPs.
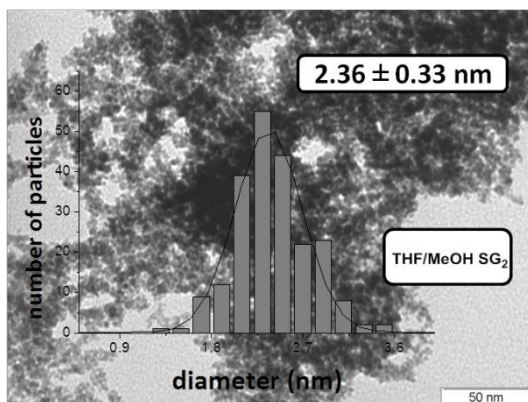
Figure 2.66 TEM micrograph and size distribution of the **Rh19** NPs.

The nanoparticles stabilised by the solvent mixture THF-MeOH exhibited a sponge-like morphology and were smaller (1.16± 0.17 nm) than the P-based and PVP stabilised system (*ca*. 1.5 nm). The seeded growth method was here employed to obtain larger nanoparticles up to *ca*. 2.3 nm that also present a sponge like morphology. These NPs were synthesised in order to corroborate potential size effects in catalysis (see Chapter 3).

2.2.5 *Surface characterisation of NPs Rh1-Rh16 by CO adsorption/Infra-red spectroscopy*

To gain information on the surface of the rhodium nanoparticles previously synthesised, freshly synthesised NPs in the solid state were reacted with 1 atm of CO at room temperature and infra- red (IR) spectra of the sample in KBr pellets were recorded.
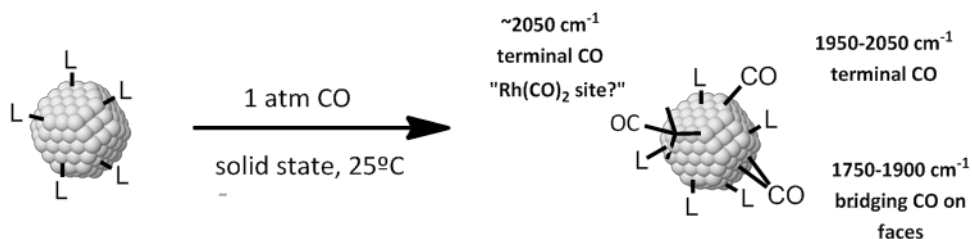
Figure 2.67 Schematic representation of CO adsorption onto metallic nanoparticles.

Two main types of carbonyl groups can be distinguished in the literature.[66,67] Signals of bridging CO are detected at frequencies between 1750 and 1900 cm^{-1}. As these carbonyls are bridged between at least two metallic atoms, the presence of these species is attributed to the faces of the nanoparticles (Figure 2.67) while terminal COs are detected at higher frequencies values, between 1950- 2050 cm^{-1} and are mainly located on low coordination sites, namely edges and apexes. However, terminal COs could also be present on the faces of these species.

Recently, the group of Chaudret and co-workers demonstrated that combined IR and NMR spectroscopic studies could allow the very precise location of carbene ligands at the surface of Ru-NPs.[68,27] They also looked at the dynamics of adsorbed CO molecules by FTIR spectroscopy and observed that the presence of bulky diphosphine as stabiliser could reduce the mobility of these ligands at the surface of Ru-NPs.[24] These results indicated that the use of the appropriate ligands as stabilisers could lead to the modulation of the surface properties of M-NPs, and thus open the way to the rational design of selective nanocatalysts.

Dyson and co-workers also used CO adsorption- IR spectroscopy to show that the addition of phosphines to Rh-PVP NPs of *ca.* 3 nm of diameter improves the selectivity of hydrogenation reactions.[17] They postulated that the selective coordination of these ligands could modify the steric hindrance at specific sites of the NPs and hence generate selectivity.

2.2.6 *Surface characterisation of NPs Rh1 by CO adsorption/Infra- red spectroscopy*

Surface characterisation of NPs Rh1 as a function of CO exposure time

A series of samples of **Rh1** were placed under 1 atm of CO during 2, 4, 6 and 12h and the resulting samples analysed by IR spectroscopy. The carbonyl region of the spectra are displayed in Figure 2.68.
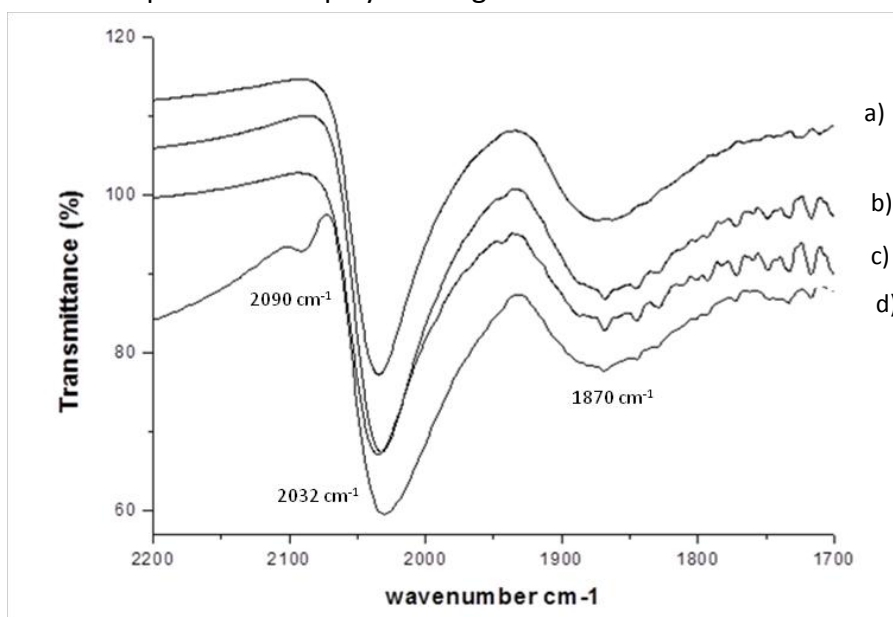
Figure 2.68 Carbonyl region of the IR spectra of **Rh1** NPs after a)2h, b)4h, c) 6h and d) 12h under CO atmosphere.

The spectra of **Rh1** exposed to 1 atm of CO after 2, 4 and 6h were very similar: two large absorptions at 1870 cm^{-1} and 2032 cm^{-1} were observed and attributed to bridging and terminal carbonyl ligands, respectively, in

agreement with previously reported measurements.[72] As no shift to higher frequency was observed as the time of the CO exposure increased, it can be deduced that the CO coverage does not increased during this time.[69] However, after 12h of Co exposure, a new band at 2090 cm^{-1} was also detected. In previously reported studies on Rh surfaces, such a high frequency band was attributed to one component of the signal for geminal Rh$^{\delta+}$-(CO)$_2$, the other component being detected at *ca.* 2020 cm^{-1}.[53,66,70] Here, this latter band could not be detected due to the overlapping with the signal centred at 2032 cm^{-1} and corresponding to terminal CO ligands. In order to investigate the effect of CO pressure, the sample **Rh1** was exposed to 40 bar of CO during 12h, depressurised and analysed by IR. The high frequency band reported for geminal Rh-(CO)$_2$ was slightly more intense and a shoulder at *ca.* 2000 cm^{-1} was revealed under this conditions, confirming the identity of these groups.

These results therefore indicated that CO adsorption on various sites of the NPs **Rh1** had taken place and evolved with time. During the first 6h, coordination of CO in bridging (faces) and in terminal mode (apexes and edges) at the surface of the nanoparticles **Rh1** was observed. At longer reaction times, a geminal Rh(CO)$_2$ stretching was detected, indicating that adsorption of CO to form these groups is slow compared to initial coordination of CO. It was also shown that the formation of these species is favoured when the sample is exposed to higher CO pressure although the small differences between the spectra after exposure to 1 and 40 bar of CO could indicate that the formation of these species is not very sensitive to CO pressure or that it is a reversible process and that in situ experiments are needed to appreciate the corresponding changes.

The detected geminal Rh(CO)$_2$ can be formed at the apexes and edges of the nanoparticles. It is usually assumed that the stabilising P-based ligands are situated on the apexes of metallic nanoparticles, as demonstrated for the well characterised Au$_{55}$Cl$_6$(PPh$_3$)$_{12}$.[71] The Rh atoms in these positions should thus not be able to coordinate to two molecules of CO and based on

this hypothesis, the geminal $Rh(CO)_2$ signals were attributed to Rh sites on the edges of **Rh1**.

Surface characterisation of NPs Rh1-0.2-0.6 by CO adsorption-IR

The nanoparticles **Rh1-0.2** and **Rh1-0.6** were placed under CO pressure under the same previously described conditions for **Rh1** and the results obtained for these systems were compared with those for **Rh1** NPs (Figure 2.69).
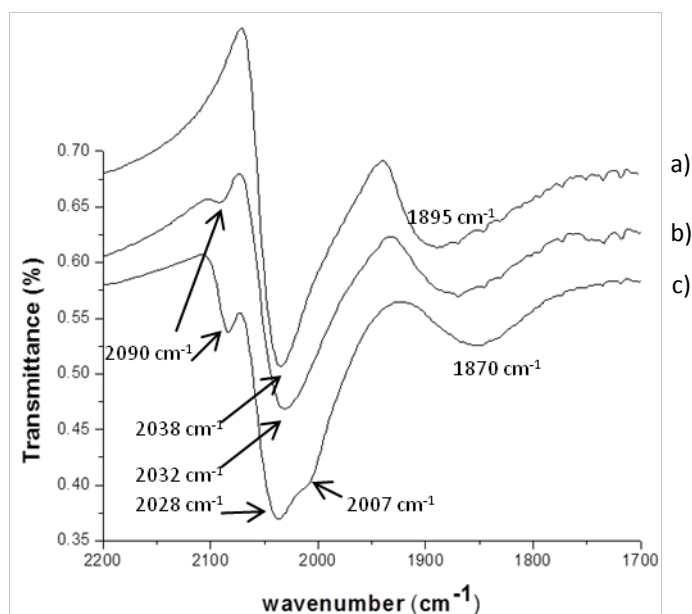
Figure 2.69 Carbonyl region of the IR spectra of a) **Rh1-0.2**, b) **Rh1-0.4** and c) **Rh1-0.6** after 12h under CO atmosphere.

In all these spectra, a broad band at ca. 1800-1900 cm^{-1} was attributed to bridging carbonyl and a more intense band at 2038 cm^{-1} was related to terminal carbonyls. In the spectrum of **Rh1-0.2**, only these two bands were observed. However, at higher ligand/Rh ratio, the bands corresponding to $Rh(CO)_2$ were observed to increase in intensity. For **Rh1-0.6**, the bands for these sites were clearly detected at 2090 and 2007 cm^{-1}. Furthermore, at higher ligand/Rh ratio, the band for the bridging CO ligands was observed to

shift to lower frequency (from 2038 cm^{-1} for **Rh1-0.2** to 2028 cm^{-1} for **Rh1-0.6**) and to decrease in intensity. These observations indicate that at higher ligand concentration during the NPs synthesis, the stabilising ligands coordinate on the faces of the NPs, resulting in an increase in the electron density of the system and a lower CO coverage on these sites, both of which contribute to the lowering of the frequencies for these signals.

Comparing the spectra obtained for the systems **Rh1-0.2**, **Rh1** and **Rh1-0.6**, a clear trend can be deduced: at higher ligand/Rh ratio, the coordination of the ligand **1** on the faces of **Rh1** and the formation of geminal Rh(CO)$_2$ site on edges of the NPs are favoured. The steric hindrance induced by the presence of the phosphine ligands on the faces of the nanoparticles might block the coordination of these ligands on the edges but not that of CO, resulting in larger signals for geminal Rh(CO)$_2$.
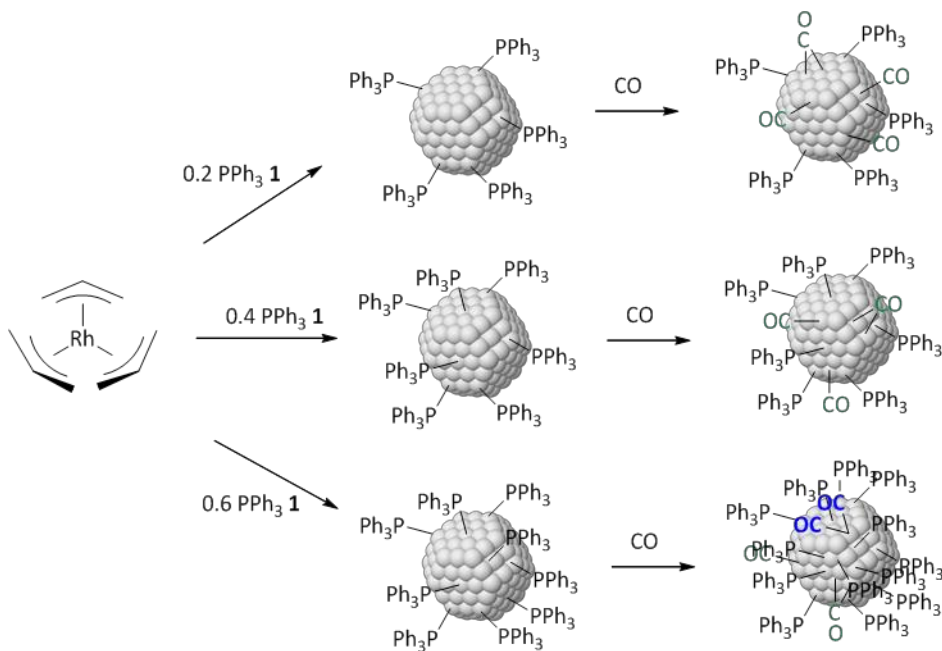
Figure 2.70 Schematic representation of the observations by IR spectroscopy for **Rh1** (0.2, 0.4 and 0.6).

The surface analysis of nanoparticles **Rh1** by CO adsorption-IR spectroscopy as a function of time and with various equivalents of ligand **1** show that

both the CO exposure (time and pressure) and the amount of ligand used during catalysis influence the surface environment of these NPs since the formation of $Rh(CO)_2$ sites was increased at longer exposure, at higher pressure and at higher ligand/Rh ratio.

It should be noted the band previously observed for **Rh1** at *ca.* 2000 cm^{-1} and attributed to Rh-H at the surface of the NPs could not be detected in these samples. This could be due to overlapping of the signal with carbonyl stretches or to the removal of hydride under CO exposure, as previously reported.[24]

2.2.7 *Surface characterisation of NPs Rh2 and Rh3 by CO adsorption/Infra- red spectroscopy*

Following the same procedure, the systems **Rh2-Rh3** were placed under CO atmosphere and their surface analysed by IR spectroscopy. The results obtained were compared with the model system **Rh1** and reflected in Figure 2.71.
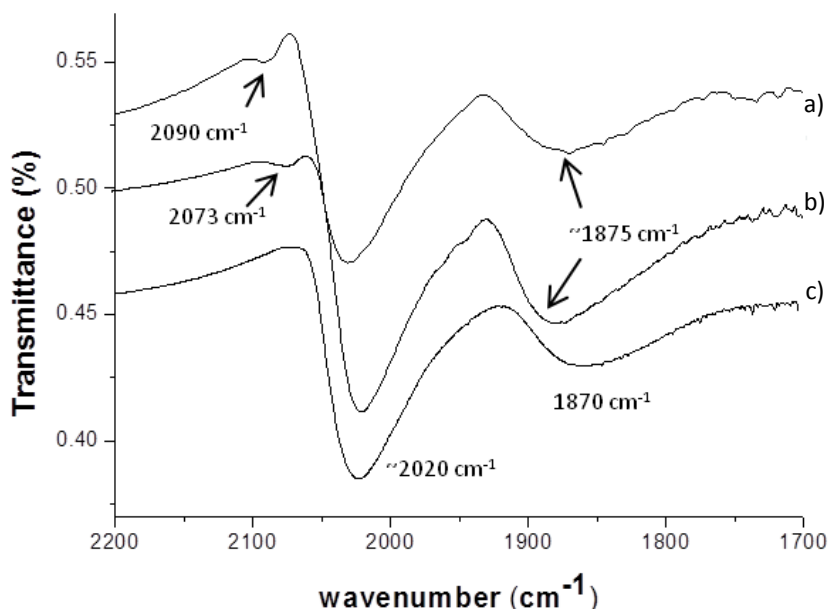
Figure 2.71 Carbonyl region of the IR spectra of a) **Rh1**, b) **Rh2** and c) **Rh3** NPs after CO adsorption.

The IR spectrum of **Rh2** +CO was similar to that of **Rh1** and showed adsorptions corresponding to bridging CO at 1876 cm^{-1} and two terminal CO bands at 2019 and 2073 cm^{-1}. A weak band at *ca*. 2000 cm^{-1} was also detected. For system **Rh3**, only two bands were observed: one at 1870 cm^{-1} corresponding to bridging COs and one at 2022 cm^{-1} attributed to terminal COs.

The bridging carbonyl band appeared at similar frequencies for systems **Rh1** and **Rh2**, stabilised with triphenyl- and tricyclohexylphosphine **1** and **2** respectively. However, this band is more intense in the spectra of system **Rh2** and could indicate that the faces of **Rh2** are less crowded than those of **Rh1**. In the case of **Rh3,** the band of bridging CO appeared at lower frequency values compared to **Rh1** and **Rh2**. This shift indicated a more electron rich surface, which is in agreement with the high phosphine coverage measured by TGA analysis.

Furthermore, for systems **Rh1** and **Rh2,** the signals attributed to geminal Rh(CO)$_2$ was observed while it was not detected for system **Rh3**. This indicated that the use of the small ligand **3** as stabiliser inhibits the formation of geminal carbonyls. In view of the small size of this ligand and the high ligand coverage measured for **Rh3**, it was concluded that this ligand is able to coordinate on the edges of the NPs instead of CO and as such can stop the formation of these groups.

The main terminal CO band is centred at *ca*. 2020 cm^{-1} for systems **Rh2** and **Rh3** while for system **Rh1**, this signal is slightly shifted to higher frequency at *ca*. 2032 cm^{-1}. Similar shift was also observed for the geminal CO (2073 cm^{-1} for **Rh2** and 2090 cm^{-1} for **Rh1)**. These shifts can be related to the electron donating properties of the stabilising ligands and the ligand coverage (higher for **Rh2** and **Rh3** than **Rh1**).

To summarise, the surface of the nanoparticles **Rh1-Rh3** was investigated by CO adsorption-IR spectroscopy. Three main types of CO ligands were detected: bridging COs, terminal COs and geminal Rh(CO)$_2$ Similar spectra were obtained for systems **Rh1** and **Rh2**, stabilised by triphenyl- and

tricyclohexylphosphine **1** and **2** respectively, with the detection of all 3 sites. The presence of geminal $Rh(CO)_2$ signals, attributed to the edges of the nanoparticles, was observed to be favoured by long reaction times with CO and high ligand to metal ratio during synthesis in the case of triphenylphosphine **1** as stabiliser. However, the use of small ligands such as PMe_3 **3** resulted in higher ligand coverage and the blocking of the corresponding sites and no $Rh(CO)_2$ signals could be detected.

2.2.8 *Surface characterisation of NPs Rh4 by CO adsorption/Infra- red spectroscopy*

The IR spectra of nanoparticles **Rh4** after CO adsorption is displayed in Figure 2.72.
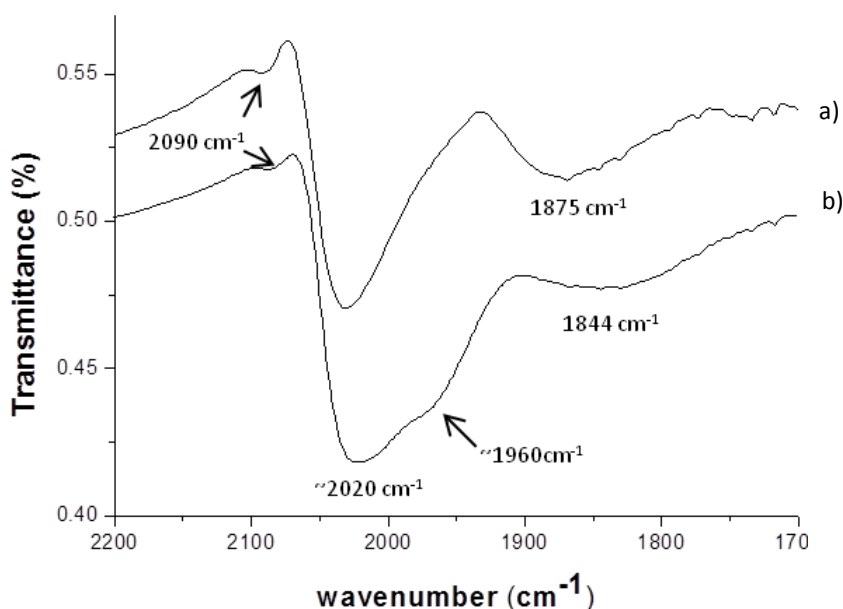
Figure 2.72 Carbonyl region of the IR spectra of a) **Rh1** and b) **Rh4** NPs after CO adsorption.

For this system, a weak band corresponding to bridging carbonyls was detected at 1844 cm^{-1}, while two signals arising from terminal COs could be distinguished at 2020 and 1960 cm^{-1} and a band attributed to geminal CO was observed at 2090 cm^{-1}.

The band for bridging carbonyls was low in intensity and slightly shifted to lower frequency compared to **Rh1** (Figure 2.72). This could be due to the higher ligand coverage at the surface of **Rh4**, as detected by TGA analysis, when compared to the model system **Rh1**. The low intensity of this signal could indicate that this ligand can coordinate on the faces of **Rh4**.

Concerning the terminal carbonyls, the bands previously observed for system **Rh1** were also detected for system **Rh4**. However, an additional terminal band was observed for system **Rh4** at low frequency, indicating that another type of sites is available to CO adsorption for this system. The frequency value indicated an electron rich site.

2.2.9 *Surface characterisation of NPs Rh5 by CO adsorption/Infra- red spectroscopy*

Surface characterisation of NPs Rh5 as a function of CO exposure time

For the **Rh5** system, the effect of the CO exposure time was monitored at 2, 4, 6 and 12h (Figure 2.73).
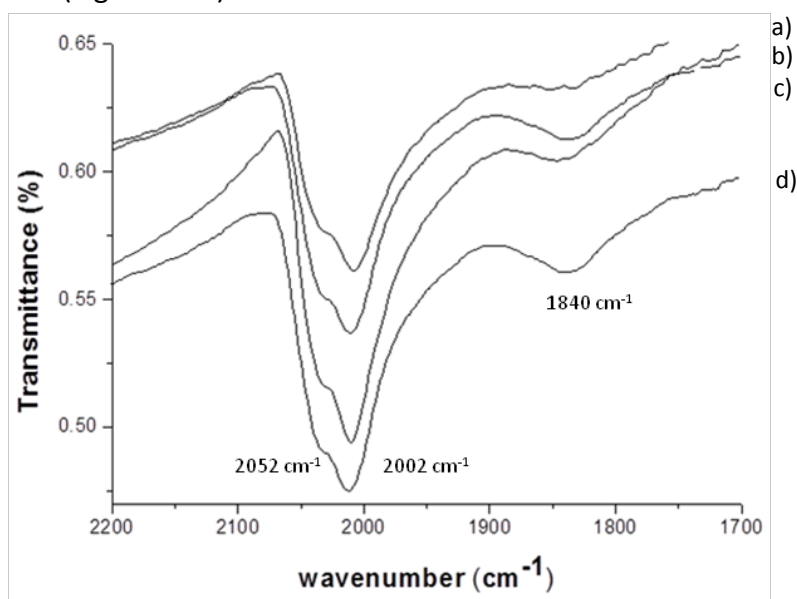
Figure 2.73 Carbonyl region of IR spectra of **Rh5** NPs after CO adsorption during a) 2h, b) 4h, c) 6h and d) 12h.

After 2h of CO exposure, two main signals at 2035 and 2002 cm^{-1} were detected and attributed to terminal carbonyl ligands, together with a very weak band at 1830 cm^{-1} corresponding to bridging COs. Under these conditions, the signals for geminal Rh(CO)$_2$ were not detected.

At longer reaction time, the band for bridging carbonyl was observed to increase in intensity while those for terminal COs remained unchanged. This result indicated that CO could first coordinate to the terminal positions, namely edges and apexes, to later get displaced to bridging positions, which is in contrast with previous IR observations on Ru-NPs.[56]

Surface characterisation of NPs Rh5-0.1-Rh5-0.6 by CO adsorption-IR

The IR spectra of **Rh5-0.1-Rh5-0.6** after CO adsorption are displayed in Figure 2.74.
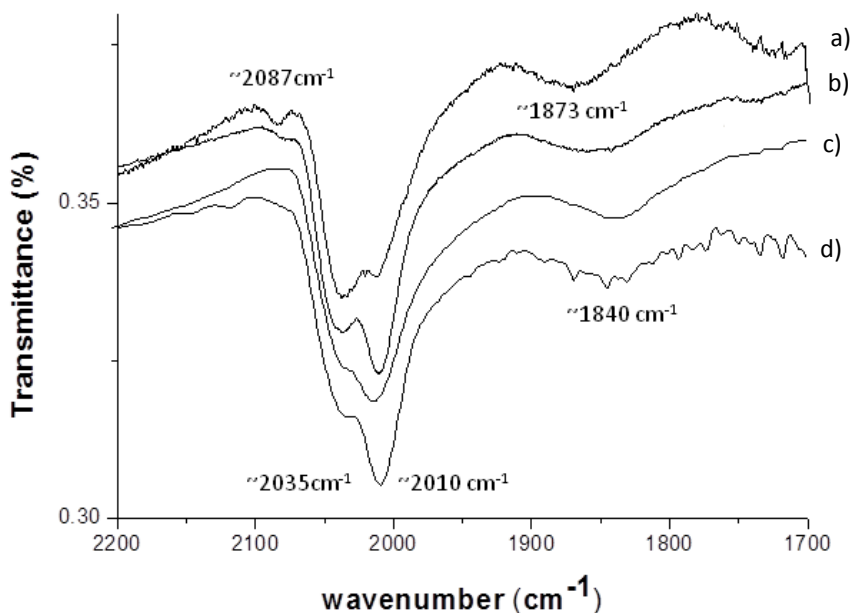
Figure 2.74 Carbonyl region of the IR spectra of sytems a) **Rh5-0.1**, b) **Rh5-0.2,** c) **Rh5** and d) **Rh5-0.6** after CO adsorption.

Interestingly, the CO bridging bands were found to shift to lower frequency when the ligand coverage increased, as expected for an increase in

electronic density of the surface. With this system, the small band at ca. 2090 cm^{-1} previously detected and attributed to a terminal Rh-(CO)$_2$ stretching was only observed at low P-coverage, indicating that the corresponding position is occupied by the ligand at higher P-content. This could thus be explained by the presence of free edge positions on **Rh5-0.1** and to a lesser extent for **Rh5-0.2 NPs**. However, when the amount of ligand is increased, these positions are occupied.

The terminal CO bands at 2035 and 2087 cm^{-1} were more intense for system **Rh5-0.1**, indicating the overlapping of the second component of the geminal CO signal with the main band for terminal COs.

For the systems stabilised by the triphenylphosphite **5**, increasing the amount of stabilising agent during the synthesis of the nanoparticles causes the disappearance of the signal for geminal carbonyls, which are presumably occupied by the additional ligand amount.

2.2.10 *Surface characterisation of NPs Rh6 and Rh7 by CO adsorption/Infra- red spectroscopy*

The same previously procedure was followed for systems **Rh6** and **Rh7** that were placed under CO pressure and IR spectra was recorded. The results obtained are reflected in Figure 2.75 and compared to the model system **Rh5**.
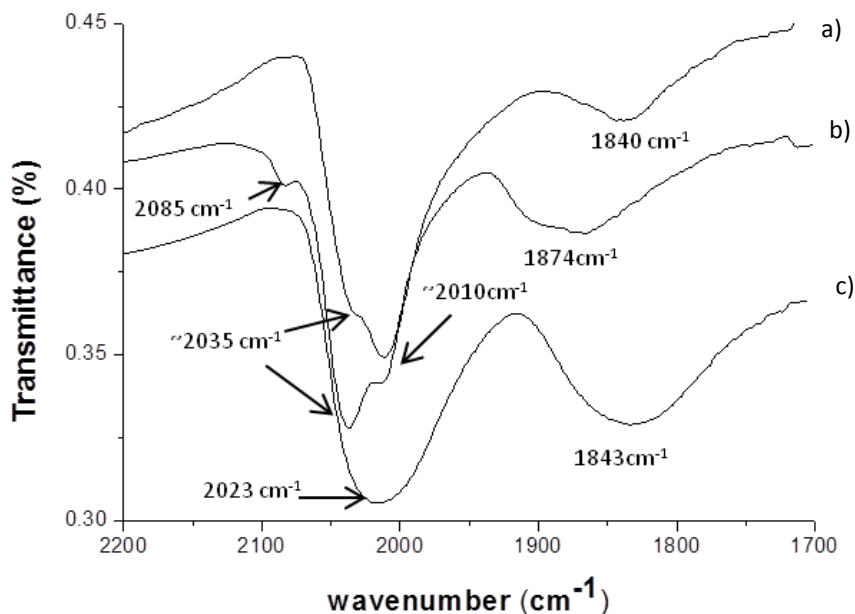
Figure 2.75 Carbonyl region of the IR spectra of a) **Rh5**, b) **Rh6** and **c) Rh7** NPs after CO adsorption.

In both cases, bridging and terminal carbonyl bands were detected, but the number and the broadness of the bands were clearly affected by the ligand properties.

In the case of **Rh6**, 2 bands were detected in the bridging carbonyl region at 1874 and 1909 cm^{-1} while 3 signals at 2013, 2038 and 2085 cm^{-1} were observed for terminal and geminal CO ligands. However, in the case of **Rh7,** only one broad band was detected in each region, at 1833 and 2023 cm^{-1}. In the spectrum of **Rh7,** the broad band at 2023 cm^{-1} was attributed to the high mobility of the CO ligands at the surface of **Rh7** and it can be concluded that the dynamics of the CO molecules are largely influenced by the steric hindrance of the stabilising ligand. Indeed, the bands for CO stretching are better resolved as the cone angle of the ligands increases (**7<5< 6**).

Compared to the results obtained with **Rh5**, the IR spectrum of **Rh6** did not show relevant differences in the terminal CO region of the spectrum, but large variations were observed in the bridging CO region. The detection of

two bridging CO vibrations using the bulky ligand **6** as stabiliser indicates the presence of two bridging CO environments. The frequency of the band at 1870 cm^{-1}, similar to those obtained for the P-ligand stabilised NPs, suggests the presence of bridging CO close to P-ligand(s) while that at 1909 cm^{-1} could arise from CO molecules adsorbed on another type of faces or from COs situated further away from the ligands. It can thus be concluded that either two types of faces are present at the surface or that two CO environments can be differentiated within the same faces.

It is also noteworthy that, similarly to phosphine stabilised systems, the use of small ligands such as P(OMe)$_3$ inhibits the detection of geminal Rh(CO)$_2$, probably due to the coordination of the ligands on these sites. With P(OPh)$_3$ **5**, these sites are only detected at low ligand coverage, indicating that ligand **5** can also coordinate to the Rh sites on the edges of the NPs but that a certain P/Rh ratio is required. However, when larger ligands such as **6** are used, the geminal CO signal was detected.

2.2.11 *Surface characterisation of Rh8 NPs by CO adsorption/Infra- red spectroscopy*

The nanoparticles **Rh8** were placed under CO pressure and the IR spectrum was recorded under the same previously mentioned conditions (Figure 2.76).

Bridging carbonyls were detected at 1870 cm^{-1}, while signals for terminal and geminal carbonyls were observed at 2090, 2030 (shoulder), 2011 cm^{-1}, respectively. A shoulder can also be distinguished at 1985 cm^{-1}.
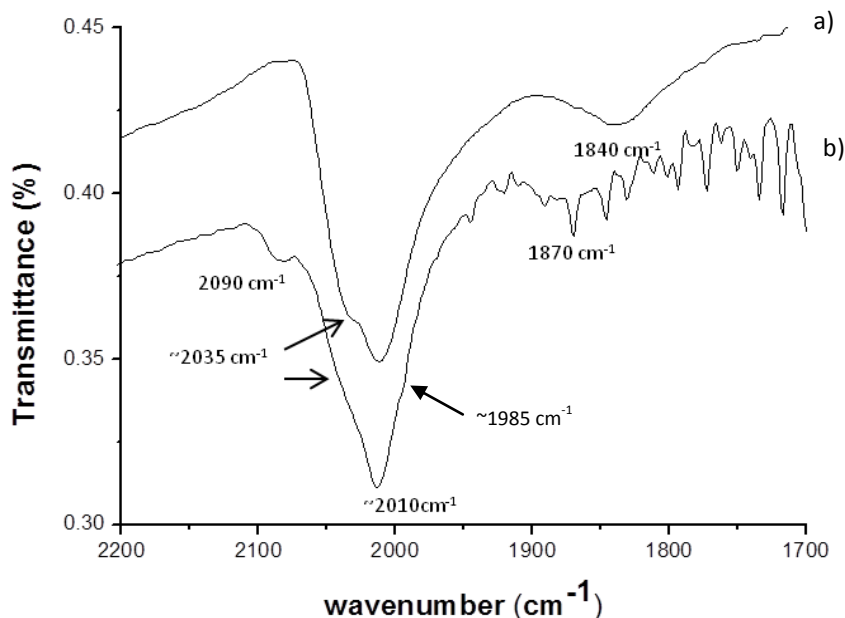
Figure 2.76 Carbonyl region of the IR spectra of a) **Rh5** and b) **Rh8** NPs after CO adsorption.

Using this bulky diphosphite **8** as stabilising agent, the geminal $Rh(CO)_2$ signal was again detected, indicating that these ligands are not coordinated to the edges of the **Rh8** NPs.

2.2.12 *Surface characterisation of Rh16 NPs by CO adsorption/Infra- red spectroscopy*

The NPs **Rh16**, stabilised by PVP, were placed under CO atmosphere during 16h and the IR spectra subsequently recorded in KBr.

The analysis by IR showed two broad absorptions at 1900 cm^{-1} and 2012 cm^{-1} attributed to bridging and terminal carbonyl ligands, respectively (Figure 2.77), in agreement with previous measurements on similar systems.[72,73] Furthermore, a shoulder at 1840 cm^{-1} was also detected and attributed to a new bridging carbonyl site.

However, it should be noted that Dyson and co-workers reported CO adsorption-IR studies for analogous Rh-PVP stabilised nanoparticles, and described the detection of carbonyl bands at 2105, 2072, 2026 and 1997

cm^{-1}. In their study, a distinct synthetic methodology and a different type of PVP (K-30) was employed. Therefore, to determine which of these parameters was responsible for these differences, a sample of K-30 PVP-stabilised Rh-NPs was synthesised by decomposition of $[Rh(\eta^3-C_3H_5)_3]$ under H$_2$ in THF, isolated and placed under CO pressure prior to IR analysis. However, no difference could be observed between the spectra obtained with NPs stabilised PVP K-30 from that of the NPs stabilised with PVP K-90 (Figure 2.77). It was therefore concluded that the synthetic methodology used for the formation of these NPs was responsible for the differences observed by IR after CO adsorption.[35]
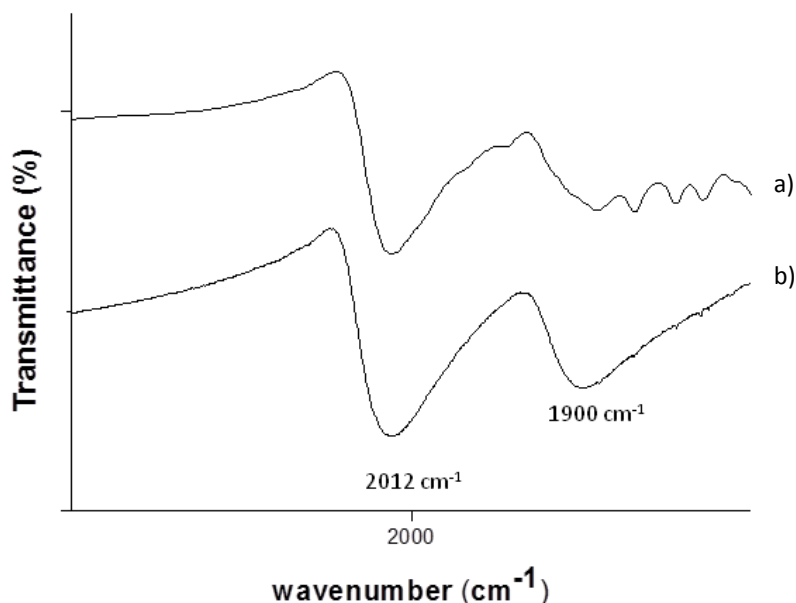
Figure 2.77 Carbonyl region of the IR spectra of a) **Rh16'** (PVP k-30) and b) **Rh16** (PVP k-90) after CO adsorption.

From the results obtained from the CO adsorption-IR study on **Rh16**, it was therefore concluded that both bridging and terminal carbonyls are were coordinated at the surface of these NPs. The geminal Rh(CO)$_2$ signal was not detected in this case, possibly indicating the crowding of edge sites by the polymer.

The spectra obtained for the three model systems, namely the PVP stabilised **Rh16**, the triphenylphosphine **1** system **Rh1** and the triphenylphosphite **5** stabilised NPs **Rh5**, are displayed in Figure 2.78.
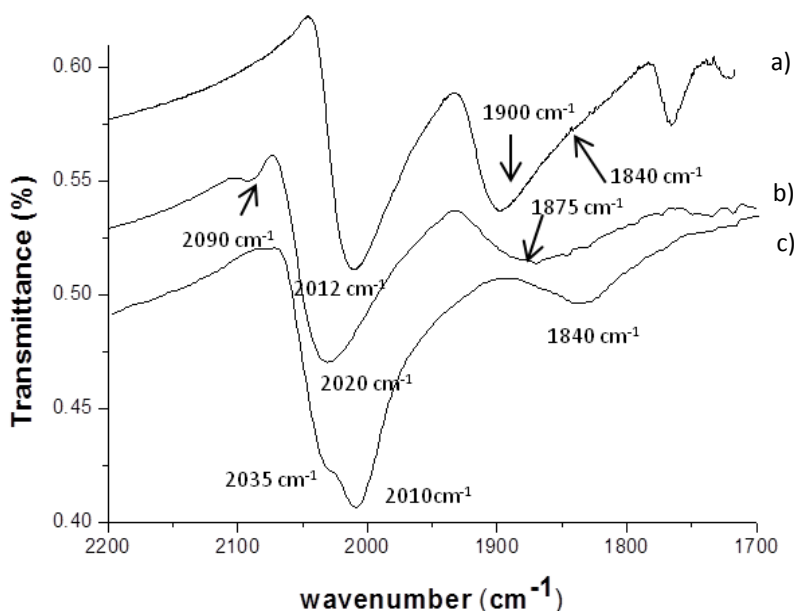
Figure 2.78 Carbonyl region of the IR spectra of a) **Rh16**, b) **Rh1** and c) **Rh5** NPs after CO adsorption.

A striking difference between these spectra was observed in the relative intensities of the bridging and terminal CO bands (Figure 2.78). The **Rh16** spectrum exhibits two strong bands for both types of CO ligands while a much weaker band was observed for bridging COs in the cases of **Rh1** and **Rh5**. The lowest bridging/terminal ratio can be observed for **Rh5**. These data therefore suggest that the presence of P-ligands hinders the faces of the corresponding NPs compared to PVP.

In the bridging CO region, large shifts were observed, which indicate that the presence of these stabilisers mainly influences the organisation and/or the CO coverage at the NPs faces. Indeed, a shift of 60 cm^{-1} was observed between the highest νCO (**Rh16**) and the lowest (**Rh5**). Interestingly, the value of ν_{CO} for bridging carbonyls of **Rh1** was intermediate, indicating that

the frequency shift observed was mainly due to the ligand coverage at the NPs surface rather than the σ-donor properties associated to the nature of the ligands.[74]

2.3 **Conclusions**

The series of Rh-NPs **Rh1-Rh8** synthesised by decomposition of the organometallic precursor [Rh(η^3-C$_3$H$_5$)$_3$] under H$_2$ pressure and in THF as the solvent. These nanoparticles were characterised by several techniques and the information on these species is summarised in Appendix 2.5.

For comparison purposes, the two sets of Rh-NPs **Rh16** and **Rh17-Rh19** stabilized by the polymer PVP and the mixture of solvent THF/MeOH, respectively, were also synthesized and characterized. In the latter case, the seeded growth method was employed to obtain NPs of distinct sizes (1.16, 1.89 and 2.36 nm).

All the nanoparticles synthesized in this work revealed a small diameter (<2 nm) with narrow size distributions, spherical shape and good dispersion. These crystalline materials exhibit a fcc structure and are mainly composed of Rh in the zero valent state. XPS measurements showed some degree of oxidation in some cases, but oxidation of the sample during the manipulation cannot be discarded.

Two families of ligands, namely phosphines and phosphites, were used as stabilizers for these NPs. The ligands triphenylphosphine **1** and triphenylphosphite **5** were used as models for these two series. The amount of model stabilizer was varied during the synthesis between 0.1 to 0.6 equivalent of ligand per Rh. No variation in size nor shape were observed when this parameter was varied. TGA analysis of these samples showed that increasing the equivalents of stabilising ligand **5** during the synthesis increases the ligand coverage on **Rh5**. However, in the case of ligand **1**, no clear correlation could be observed. In both cases, a higher degree of hydrogenation of the stabilising ligand was observed at low ligand to Rh ratio during the synthesis.

Furthermore, solution NMR experiments showed that some ligand oxides are also interacting with the surface of the NPs. In the case of phosphine-stabilised **Rh1**, placing a sample of NPs dispersed in THF under CO pressure resulted in the detection of various ligand phosphine oxide species with

partial or total hydrogenation of their phenyl rings. Oxidation of phosphine ligands under CO atmosphere have been reported by several groups, although the possibility that phosphine oxide species could be the real stabilizers of these NPs cannot be discarded. In the case of the phosphite stabilized NPs **Rh5**, the experiment under CO pressure resulted in the detection of both phosphite and phosphite oxide species.

Hydride titration experiments were performed on **Rh1** and **Rh5**, revealing a higher hydride coverage in the case of the phosphine stabilized **Rh1** (*ca*. 0.8 H/Rh$_s$) than for **Rh5** (*ca*. 0.3H/Rh$_s$). Analysis of the surface of these nanoparticles by infra red spectroscopy revealed the presence of a band at 1950-2000 cm^{-1}, that was attributed to Rh-H stretching based on the analysis of the spectra of the NPs obtained after hydride titration and of these NPs synthesised under D$_2$.

To gain information on the surface environment of these NPs, CO adsorption/Infra-red experiments were performed and several conclusions can be drawn:

- three types of carbonyl signals were observed: bridging (1800-1900 cm^{-1}), terminal (1950-2070 cm^{-1}) and geminal Rh(CO)$_2$ (*ca*. 2100 and 2020 cm^{-1}). The detection of bridging carbonyls was associated with the faces of the NPs and the geminal ones with the edges of the NPs, assuming that the apexes are occupied by the stabilising ligands and therefore cannot coordinates to two CO ligands.

- for the PPh$_3$ system 1, at higher ligand/Rh ratio, the coordination of the ligand **1** on the faces of **Rh1** and the formation of geminal Rh(CO)$_2$ site on edges of the NPs are favored. Using 0.4 eq. of 1 per Rh, the geminal Rh(CO)$_2$ bands were only detected after 12h of exposure to 1 atm of CO. It was also shown that the formation of these species is favoured when the sample is exposed to higher CO pressure (40 bar).

- For the systems stabilised by the triphenylphosphite **5**, increasing the amount of stabilising agent during the synthesis of the nanoparticles causes the disappearance of the signal for geminal carbonyls Rh(CO)$_2$, and it was concluded that at high ligand/Rh ratio, the sites on the edges are

presumably occupied by the additional ligand amount. The smaller cone angle of ligand **5** (128°) compared with that of **1** (145°) could explain these results since it appears that ligand **5** coordinates to the edges of the NPs while ligand **1** cannot and coordinates on the faces of the NPs, resulting in less sterically hindered edges that can thus coordinate CO at higher L/Rh ratio. This hypothesis was confirmed when the NPs Rh_3 and Rh_7, stabilized by the small ligands PMe_3 **3** and $P(OMe)_3$ **7**, were analysed by CO adsorption-IR spectroscopy since no geminal $Rh(CO)_2$ signals were detected in these cases. It was thus concluded that when such small ligands are used, the coordination sites on the edges of the NPs are occupied by the ligands. However, when larger ligands (than 5 in these series) are used, the geminal $Rh(CO)_2$ signals were always detected, indicating that these sites were "free" and could coordinate to two CO ligands.

2.4 **Experimental part**

General methods. All syntheses were performed using standard Schlenk techniques under N_2 or Ar atmosphere. Chemicals were purchased from Aldrich Chemical Co, Fluka and Strem. All solvents were distilled over drying reagents and were deoxygenated before use. Precursor $Rh(\eta^3\text{-}(C_3H_5)_3$ was prepared following previously described methods.[7] Nanoparticle synthesis were performed using 200 ml Fisher Porter and pressurized on a high pressure line.

The deuterated solvents for NMR measurements were dried over molecular sieves. ^1H, ^{13}C {1H}, and ^{31}P {1H} NMR spectra were obtained on a Varian Mercury 400 MHz spectrometer. Chemical shifts were calibrate relative to $SiMe_4$ (^1H and ^{13}C NMR) as internal standard or 85% H_3PO_4 as external standard (^{31}P NMR).

Synthesis of the ligands

- Synthesis of *ortho*- tert- butyltriphenylphosphite **6**

6 was synthesised following standard reported procedures.[75] *Ortho*-tert- butylphenol (4.6g, 0.03mol) was dissolved in 20 ml of dry and degassed toluene. Degassed pyridine (4 ml,) was carefully added to a 0.87 ml (0.01 ml) of distilled PCl_3 at 0°C. The phenol solution was added to the PCl_3/ pyridine solution. The reaction was carried out during 16h at 60°C. The pyridine salts formed during the reaction were removed by filtration under N_2 atmosphere. Purification was carried out by column chromatography under nitrogen with dry and degassed toluene as eluent, yielding **6** as a white solid (yield 3.162g, 55%).
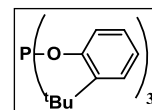
^1H NMR (400MHz, toluene, δ in ppm): 7.48 (d, *J*=1.6Hz, 1H, arom.), 7.47 (d, *J*=1.6Hz, 1H, arom.), 6.94- 6.84 (m, 2H, arom.), 1.43 (s, 9H, CH_3).

^{13}C NMR **(**100MHz, toluene d_8, δ in ppm): δ =151.9 (-C-Ar), 140.0 (-C- Ar), 127.9 (-C- Ar), 123.7 (-C- Ar), 119.8 (-C- Ar), 119.62 (-C- Ar), 34.9 (-C^{IV}-, ^tBu), 30.1 (CH_3-, ^tBu).

^{31}**P** NMR (162MHz, toluene, δ in ppm): δ =132.06.

- *Synthesis of 4,4',6,6'-Tetra-tert-butyl2,2'biphenylphosphorochloridite*

4,4',6,6'-Tetra-*tert*-butyl-2,2'-bisphenol (1.85g,4.5mmol) was dissolved in 55 ml of dry and degassed toluene. Degassed pyridine (4.4ml, 54mmol) was carefully added to a 0.95 ml of distilled PCl$_3$ at 0 °C. A biphenol solution was added to the PCl$_3$/ pyridine solution. The reaction was carried out overnight at 60 °C. The pyridine salts formed during the reaction were removed by filtration under N$_2$ atmosphere. The reaction mixture was concentrated under reduced pressure. The product was used without purification in the following reaction step (estimated yield 90%).
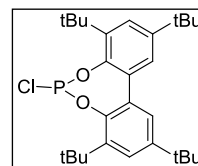
^{1}**H** NMR (400MHz, toluene d$_8$, δ in ppm): 7.46 (d, *J*=2.4Hz, 2H, arom.), 7.17 (d, *J*=2.4Hz, 2H, arom.), 1.47 (s, 18H, *o*-C$_4$H$_9$), 1.35 (s, 3H, *p*-C$_4$H$_9$).

^{31}**P** NMR (162MHz, toluene d$_8$, δ in ppm): δ =167.09.

- *Diphosphite derived from 4-4'-(dihydroxydiphenyl) 8*

4,4',6,6'-Tetra-*tert*-butyl-2,2'-bisphenol (0.9 g, 2.2 mmol) was dissolved in 30ml of dry and degassed toluene. Degassed pyridine (2.13 ml, 27 mmol) was added carefully to 0.46 mL of distilled PCl$_3$ at 0 °C. The bisphenol solution was slowly added to the PCl$_3$/pyridine solution. The reaction was stirred during 16h at 60 °C to form the 4,4',6,6'-tetra-*tert*-butyl-2,2'- biphenylphosphochloridrite. The pyridine salts formed were removed by filtration under argon atmosphere. The reaction mixture was concentrated under reduced pressure and the product was used without purification in the following reaction (yield 97%).
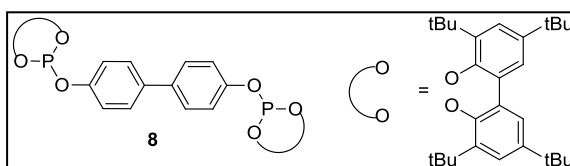
4-4'-dihydroxydiphenyl (0.149 g, 0.8 mmol,1 eq) was dissolved in 4mL of dry and degassed toluene. 4,4',6,6'-tetra- *tert*- butyl- 2,2'- biphenylphosphochloridrite (0.94 g, 1.97 mmol, 2.1 eq) was dissolved in

3.12 mL of degassed pyridine (38.7 mmol). The 4-4'-dihydroxydiphenyl solution was added to the phosphochloridite/pyridine solution and the mixture stirred overnight at room temperature. Purification was carried out by column chromatography under nitrogen with dry and degassed toluene as eluent, yielding **8** as a white solid (yield 400mg, 85%).

^{1}H NMR (400MHz, toluene d$_8$, δ in ppm): δ =7.62 (d, J=2.4Hz, 4H), 7.38 (d, J=2.4Hz, 4H), 7.13 (d, J= 8Hz, 4H), 7.08 (d, J= 8Hz, 4H), 1.61 (s, 36H, ^{t}Bu-*ortho*), 1.28 (s, 36H, ^{t}Bu-*para*).

^{13}C NMR (100MHz, toluene d$_8$, δ in ppm): δ =151.9 (d, J_{PC}= 6 Hz, -C-), 147.1 (-C- Ar), 146.3 (d, J_{PC}= 6Hz, -C-), 140.7 (-C- Ar), 136.45 (-C- Ar), 133.8 (d, J_{PC}= 3Hz, -C-), 128.3 (CH-), 127.15 (CH-), 124.6 (d, J_{PC}= 6Hz, -CH), 122.0 (d, J_{PC}= 8Hz, -CH), 35.7 (-C^{IV}-, ^{t}Bu), 34.7 (-C^{IV}-, ^{t}Bu), 31.5 (CH$_3$-, ^{t}Bu), 31.4 (CH$_3$-, ^{t}Bu).

^{31}P NMR (162MHz, toluene d$_8$, δ in ppm): δ =145.19

Synthesis of the rhodium precursor

The synthesis was carried out according to the procedure described in the literature.[76,77] Allylmagnesium bromide (35 mmol) was added to a cold suspension (-10 °C) of RhCl$_3$ 3H$_2$O (1.1 g, 5.3 mmol) in THF (93 ml). The solution slowly lost its red-brown color to become yellow. The solution was then allowed to warm to room temperature and stirred for an additional 16 hours at 0 °C. The solvent was removed under reduced pressure and the residue extracted with pentane (previously distilled and deoxygenated) (3x20mL). The sublimation was carried out in a water bath at 40 °C and of yellow crystals formed onto the cold finger were collected. (Yield= 520 mg, 55%)

The purity of this complex was checked by ^{1}H and ^{13}C NMR spectroscopy.[78]

Synthesis of the metal nanoparticles

Stabilised by P-based ligands

The synthesis of the Rh nanoparticles was carried out following the organometallic method reported by Chaudret and co-workers.[79] In a typical procedure, the $[Rh(\eta^3-(C_3H_5)_3]$ (64 mg, 0,28 mmol) was placed into a Fischer- Porter reactor and dissolved at -110 °C (acetone/ N_2 bath) in 64 mL of dry and deoxygenated THF (using freeze-pump-thaw techniques) in the presence of the appropriate ligand (0.2 equivalents for bidentate ligands and 0.4 equivalents for monodentate ligands). The Fischer-Porter reactor was then pressurised under 6 bar of H_2 and stirred for 30 minutes at room temperature. The solution was then heated to 40°C and stirred at this temperature during 24 h. The initial colorless solution became black after 1h. A small amount (5 drops approx.) of the solution was deposited under argon atmosphere on a carbon-covered copper grid for transmission electron microscopy analysis. The rest of the solution was concentrated under reduced pressure. Precipitation and washing with pentane (3 x 15ml) was then carried out, obtaining a black precipitate. The solution was dried over vacuum to obtain a crystalline black powder. (Yield= *ca*. 25-30 mg, 30-35%)

- Nanoparticles **Rh1-0.2**, stabilised by PPh$_3$ **1**

TEM: mean size 1.47± 0.28nm

XRD: fcc crystalline Rh nanoparticles, coherence length 1.39 ± 0.026

XPS: Rh^0 3d5/2 (307.137eV) 3d3/2 (311.903eV), 48% of Rh $^{\delta+}$ at the surface of the NPs.

TGA: 55.62% of Rh, 43.79 % of organic pa.

Approximate formula [Rh$_{125}$ (THF)$_2$ (L)$_{39}$]

- Nanoparticles **Rh1-0.4**, stabilised by PPh$_3$ **1**

TEM: mean size 1.52± 0.21nm, <u>HRTEM</u>: bond length: 0.26nm.

XRD: fcc crystalline Rh nanoparticles, coherence length 1.49 ± 0.034

WAXS: well-crystallised Rh NPs, coherence length= 2nm, bond length= 0.269nm.

XPS: Rh^0 3d5/2 (308.32eV) 3d3/2 (313.02eV) 40% of Rh$^{\delta+}$ at the surface of the NPs.

TGA: 72.1% of Rh, 27.2 %of organic part by TGA

Approximate formula [$Rh_{132}THF_2L_{20}$]

- Nanoparticles **Rh1-0.6**, stabilised by PPh_3 **1**

TEM: mean size 1.46± 0.25nm

XRD: fcc crystalline Rh nanoparticles, coherence length 1.46 ± 0.033

XPS: Rh^0 3d5/2 (307.256eV) 3d3/2 (312.129eV)40% of $Rh^{\delta+}$ at the surface of the NPs

TGA: 69.51% of Rh, 29.83 % of organic part

Approximate formula [Rh_{127} THF_2 L_{21}]

- Nanoparticles **Rh2**, stabilised by PCy_3 **2**

TEM: mean size 1.36± 0.27nm, *HRTEM*: bond length: 0.23nm.

XRD: fcc crystalline Rh nanoparticles, coherence length 1.57 ± 0.026

XPS: Rh^0 3d5/2 (308.173eV) 3d3/2 (312.906eV), 40% of $Rh^{\delta+}$ at the surface of the NPs

TGA: 53.7% of Rh, 43.8% of organic part, 2.5% solvent

Approximate formula [$Rh_{95}THF_8L_{28}$]

- Nanoparticles **Rh3**, stabilised by PMe_3 **3**

TEM: mean size 1.38± 0.24nm, *HRTEM*: bond length: 0.27nm.

XRD: fcc crystalline Rh nanoparticles, coherence length 1.22 ± 0.021

XPS: Rh^0 3d5/2 (307.299eV) 3d3/2 (311.379eV) 40% of $Rh^{\delta+}$ at the surface of the NPs

TGA: 72% of Rh, 25.79 % of organic part

Approximate formula [Rh_{99} THF_6 L_{48}]

- Nanoparticles **Rh4**, stabilised by dppb **4**

TEM: mean size 1.57± 0.25nm, *HRTEM*: bond length: 0.26nm.

XRD: fcc crystalline Rh nanoparticles, coherence length 1.49 ± 0.07 nm

XPS: Rh^0 3d5/2 (307.43eV) 3d3/2 (312.13eV), 100% of Rh(0) at the surface of the NPs

TGA: 68.6% of Rh, 29.43% of organic part

Approximate formula [Rh_{146} THF_8 L_{15}]

- Nanoparticles **Rh5-0.1**, stabilised by $P(OPh)_3$ **5**

TEM: mean size 1.57± 0.23nm

XRD: fcc crystalline Rh nanoparticles, coherence length 1.53 ± 0.04 nm

XPS: Rh^0 3d5/2 (307.5eV) 3d3/2 (311.8eV) 40% of $Rh^{\delta+}$ at the surface of the NPs

TGA: 64.5% of Rh, 33.69 % of organic part

Approximate formula [Rh_{146} THF_8 L_{25}]

- Nanoparticles **Rh5-0.2**, stabilised by $P(OPh)_3$ **5**

TEM: mean size 1.55± 0.31nm

XRD: fcc crystalline Rh nanoparticles, coherence length 1.64 ± 0.05 nm

XPS: Rh^0 3d5/2 (307.9eV) 3d3/2 (312.4eV) 40% of $Rh^{\delta+}$ at the surface of the NPs

TGA: 62.3% of Rh, 35.7 % of organic part

Approximate formula [Rh_{140} THF_3 L_{11}]

- Nanoparticles **Rh5-0.4**, stabilised by $P(OPh)_3$ **5**

TEM: mean size 1.52± 0.23nm, *HRTEM*: bond length: 0.26nm.

XRD: fcc crystalline Rh nanoparticles, coherence length 1.53 ± 0.023 nm

XPS: Rh^0 3d5/2 (308.0eV) 3d3/2 (312.77eV) Rh^0 at the surface of the NPs

TGA: 58% of Rh, 40.3 % of organic part

Approximate formula [Rh_{132} THF_6 L_{30}]

- Nanoparticles **Rh5-0.6**, stabilised by $P(OPh)_3$ **5**

TEM: mean size 1.65± 0.30nm

XRD: fcc crystalline Rh nanoparticles, coherence length 1.53 ± 0.04 nm,

XPS: Rh^0 3d5/2 (307.561eV) 3d3/2 (312.546eV) 40% of $Rh^{\delta+}$ at the surface of the NPs

TGA: 45.3% of Rh, 53.42 % of organic part

Approximate formula [Rh_{169} THF_9 L_{66}]

- Nanoparticles **Rh6**, stabilised by P(O(o-^{t}BuPh))$_3$ **6**

TEM: mean size 1.55± 0.23nm, <u>HRTEM</u>: bond length: 0.21nm.

XRD: fcc crystalline Rh nanoparticles, coherence length 1.28 ± 0.08 nm

XPS: Rh^0 3d5/2 (308.27eV) 3d3/2 (312.37eV) 40% of Rh $^{\delta+}$ at the surface of the NPs

TGA: 44.6% of Rh, 52.6% of organic part

Approximate formula [Rh_{140} THF_{15} L_{35}]

- Nanoparticles **Rh7**, stabilised by P(OMe)$_3$ **7**

TEM: mean size 1.31± 0.19nm, <u>HRTEM</u>: bond length: 0.26nm.

XRD: fcc crystalline Rh nanoparticles, coherence length 0.83 ± 0.06 nm

XPS: Rh^0 3d5/2 (306.89eV) 3d3/2 (310.97eV) 100% of Rh ^{0} at the surface of the NPs

TGA: 54.7% of Rh, 39.3 % of organic part

Approximate formula [Rh_{105} THF_{21} L_{62}]

- Nanoparticles **Rh8**, stabilised by diphosphite **8**

TEM: mean size 1.60± 0.25nm, <u>HRTEM</u>: bond length: 0.22nm.

XRD: fcc crystalline Rh nanoparticles, coherence length 1.43 ± 0.019 nm

XPS: Rh^0 3d5/2 (307.57eV) 3d3/2 (312.27eV) 30% of Rh $^{\delta+}$ at the surface of the NPs

TGA: 34.9% of Rh, 65.57 % of organic part

Approximate formula [Rh_{154} THF_{12} L_{27}]

General procedure for synthesis of the nanoparticles stabilised by polyvinylpirrolidone (PVP)

The same procedure was followed for the synthesis of these rhodium nanoparticles with some modifications of the conditions. The amount of ligand used, was 5 mols of monomer of polyvinilpirrolidone per mol of rhodium. In a typical procedure, the [Rh(η^3-(C_3H_5)$_3$] (64 mg, 0,28 mmol) was

placed into a Fischer- Porter reactor, 157 mg of PVP K-90 and 64 ml of THF were added. The Fischer-Porter reactor was then pressurized under 6 bar of H_2 and stirred at room temperature during 16h. The solution became black immediately. A small amount (5 drops approx.) of the solution was deposited under an argon atmosphere onto a carbon-covered copper grid for transmission electron microscopy analysis. The rest of the solution was concentrated under reduced pressure. Precipitation and washing with pentane (3 x 15ml) was then carried out, obtaining a black precipitate. (Yield= *ca*. 10-15 mg, 35-40%)

- Nanoparticles **Rh16**, stabilised by PVP

TEM: mean size 1.49± 0.19nm

XRD: fcc crystalline Rh nanoparticles, coherence length 1.29 ± 0.05

XPS: Rh^0 3d5/2 (308.9eV) 3d3/2 (312.4ºeV) 40% of $Rh^{\delta+}$ at the surface of the NPs.

TGA: 59.2% of Rh, 40.8 % of organic part.

*Stabilised by a THF/MeOH mixture of solvents **Rh17***

The synthesis of the Rh nanoparticles was carried out following the method reported by Chaudret and co-workers.[65] In a typical procedure, the $[Rh(\eta^3-(C_3H_5)_3)]$ (64 mg, 0,28 mmol) was placed into a Fischer- Porter reactor, a mixture of solvents THF/MeOH in a 97.5:2.5 ratio was added. The Fischer-Porter reactor was then pressurized under 4 bar of H_2 and stirred at room temperature during 16h. The solution became black immediately. A small amount (5 drops approx.) of the solution was deposited under an argon atmosphere onto a carbon-covered copper grid for transmission electron microscopy analysis. The rest of the solution was concentrated under reduced pressure. Precipitation and washing with pentane (3 x 15ml) was then carried out, obtaining a black precipitate. (Yield= *ca*. 10-15 mg, 35-40%)

*General procedure for the synthesis of the Rh-NPs using the seeded-growth method **Rh18** and **Rh19***.

In a typical procedure, the corresponding mixture of solvents (THF/MeOH 97.5:2.5) of 32 mL containing $[Rh(\eta^3-(C_3H_5)_3]$ (32 mg, 0.14 mmol) was added to a half THF/MeOH solution of previously prepared Rh-NPs (0.14 mmol of Rh). The reaction mixture was placed in a Fischer-Porter reactor, which was then pressurized under 4 bar of H_2 and stirred at room temperature during 16h. A small amount (5 drops approx.) of the solution was deposited under an argon atmosphere onto a carbon-covered copper grid for transmission electron microscopy analysis (TEM). The rest of the solution was concentrated under reduced pressure. Precipitation and washing with pentane (3 x 15ml) was then carried out, obtaining a black precipitate.

General characterisation techniques

Transmission Electron Microscopy

The TEM experiments were performed at the "Unitat de Microscopia dels Serveis Cientificotècnics de la Universitat Rovira I Virgili" (TEM-SCAN) in Tarragona with a Zeiss 10 CA electron microscope operating at 100 kV with resolution of 3 Å. The particles size distributions were determined by a manual analysis of enlarged images. At least 300 particles on a given grid were measured in order to obtain a statistical size distribution and a mean diameter.

Scanning Electron Microscopy (SEM)

The nanoparticles were characterised by a scanning electron microscope (SEM Jeol SM 6400).
The elemental qualitative analysis of prepared NPs was carried out using energy dispersive X-ray spectroscopy (EDS Oxford Inca- Energy) coupled

with the SEM equipment. The measurements were taken with 15kV and 15mm of work distance.

X- Ray Diffraction (XRD)

XRD measurements were made using a Siemens D5000 difractometer (Bragg- Brentano parafocusing geometry and vertical θ-θ goniometer) fitted with a curved graphite diffracted- beam monochromator, incident and diffracted- beam Soller slits, a 0.06° receiving slit and scintillation counter as a detector. The angular 2θ diffraction range was between 26 and 95°. The data were collected with an angular step of 0.05° at 16s per step and sample rotation. A low background Si(510) wafer was used as sample holder. Cu$_{k\alpha}$ radiation was obtained from a copper X- ray tube operated at 40kV and 30mA.

X-Ray Photoelectron Spectroscopy (XPS)

XPS experiments were performed in a PHI 5500 Multitechnique System (from Physical Electronics) with a monochromatic X-ray source (Aluminium Kalfa line of 1486.6 eV energy and 350 W), placed perpendicular to the analyzer axis and calibrated using the 3d5/2 line of Ag with a full width at half maximum (FWHM) of 0.8 eV. The analysed area was a circle of 0.8 mm diameter, and the selected resolution for the spectra was 187.5eV of Pass Energy and 0.8 eV/ step for the general spectra and 23.5 eV of Pass Energy and 0.1 eV/step for the spectra of the different elements in the depth profile spectra. A low energy electron gun (<10 eV) was used in order to discharge the surface when necessary. All measurements were performed in a ultra high vacuum (UHV) chamber pressure between 5x10^{-9} and 2x10^{-8} torr.

For this analysis, the data processing was carried out with the program CasaXPS. Initially, the general spectrum of the different binding energies observed for this sample was analysed and was used to calibrate the

following calculations. This calibration was performed using the values for the rhodium that is the element of interest for these analyses.

Thermogravimetric analysis (TGA)

The TGA experiments were carried out in the furnace of a Mettler Toledo TGA/SDTA851 instrument.

For a typical TGA experiment, 1-2 mg of nanoparticles were placed in the sample holder in the furnace and the material was heated up at a rate of 10 °C min^{-1} in N$_2$, while the weight was recorded continuously from 30°C to 900°C.

The weight loss of the organic part and metal were used to calculate an approximate number of ligands coordinated to the metal surface. The ligand loss was attributed to the weight loss observed between 100 and 450 °C. For the calculation, the molecular weight of the corresponding ligands and of the metal, and the number of metal atoms at the surface from TEM data were taken into account.

General procedure to perform hydrides titration

Each colloidal solution has been prepared in THF as previously described. On each fresh colloidal solution, five cycles of 1 minute vacuum/1 minute bubbling of argon were performed in order to eliminate the dihydrogen solved into the solvent. Then, 1 equivalent of the olefin (2-norbornene), previously filtered through alumina, were added. Samples were regularly taken from the solutions (after 24, 48 and 60 hours) for GC analyses and estimation of the olefins conversion into alkanes. The method used for the detection of the products consists of 15min. at 40 °C and a 3 ramp of 8 °C/min. until 250 °C.

To remove nanoparticles from the catalytic solutions, filtration of the samples was realised through an Al$_2$O$_3$ pad. For the calculation, the mean sizes and rhodium surface atoms were considered.

Table 2.15 Conversion of norbornene into norbornane and the corresponding values of mols of H for rhodium surface atom

NPs	Conv. (%)	Mols H/ mols Rh
Rh1	26	0.82
Rh5	13	0.3

Conversion obtained by GC-MS

The number of hydrogen atoms per surface rhodium atoms was calculated taking into account the conversion of norbornene into norbornane, according to literature procedures.[40] The same number of atoms of rhodium at the surface of the nanoparticles was assumed due to their similar size. The number of atoms was calculated by the Van Hardevel Hartog that takes into account the structure of the nanoparticles and their diameter.[33]

General procedure for IR analysis of rhodium nanoparticles

IR spectroscopy samples were prepared as KBr pellets. The nanoparticles were used without any preparation step, mixed with dry KBr in the glove-box.

General procedure for infrared analysis of rhodium nanoparticles after CO adsorption

For CO coordination studies, solid Rh nanoparticles were introduced in a Fischer- Porter bottle and were pressurised with 3 bars of H_2 for 12h. After this period of time, the dihydrogen gas was evacuated under vacuum for 10 min. The Fischer- Porter bottle was then pressurised with 1 atm of CO atmosphere for 16h. The gas was evacuated under vacuum for 15 min and IR spectroscopy samples were prepared as KBr pellets in the glove box.

2.5 Appendix: Summary of characterisation for Rh1-Rh8

NPs	Diameter (nm)		shape	Structure	Oxidation State (%Rh^{6+})	Rh content	L content	M-H	HL
	(TEM)	(XRD)	(HRTEM)	(XRD)	(XPS)	(TGA)		(IR)	
Rh1-0.2	1.47±0.28	1.39 ± 0.03	Spherical	fcc	48	56	44	1994 cm^{-1}	νν
Rh1	1.52±0.21	1.49±0.03	hexagonal	fcc	40	70	25	1973cm^{-1}	ν
Rh1-0.6	1.46±0.25	1.46 ± 0.03	spherical	fcc	40	70	30	1997 cm^{-1}	ν
Rh2	1.36±0.27	1.57 ± 0.03	spherical	fcc	40	54	44	1969 cm^{-1}	-
Rh3	1.38±0.24	1.22 ± 0.02	spherical	fcc	40	72	26	1991cm^{-1}	-
Rh4	1.57±0.25	1.49 ± 0.07	spherical	fcc	0	69	29	1982 cm^{-1}	νν
Rh5-0.1	1.57±0.23	1.53±0.04	spherical	fcc	40	65	34	-	νν
Rh5-0.2	1.55±0.31	1.64±0.05	spherical	fcc	40	62	42	2003 cm^{-1}	ν
Rh5	1.52±0.23	1.53±0.02	spherical	fcc	0	58	40	1999cm^{-1}	νν
Rh5-0.6	1.65±0.30	1.53±0.04	spherical	fcc	40	45	53	2004 cm^{-1}	ν
Rh6	1.55±0.23	1.28 ± 0.08	spherical	fcc	40	45	53	2010 cm^{-1}	n.c.
Rh7	1.31±0.19	0.83 ± 0.06	spherical	fcc	0	55	39	n.c.	-
Rh8	1.60±0.25	1.43 ± 0.02	hexagonal	fcc	30	35	65	2009 cm^{-1} (w)	n.c.

HL= hydrogenation of the stabilising ligands

2.6 **References**

[1] D. Astruc (eds), Nanoparticles and Catalysis, Wiley-VCH, Weinheim, **2007**.

[2] A. Roucoux, J. Schulz, H. Patin, *Chem. Rev.* **2002**, *102*, 3757-3778.

[3] B. Léger, A. Denicourt- Nowicki, H. Olivier- Bourbigou, A. Roucoux, *Inorg. Chem*. **2008**, *47*, 9090-9096.

[4] R. R. Dykeman, N. Yan, R. Scopelliti, P. Dyson, *Inorg. Chem*. **2011**, *50*, 717-719.

[5] Y. Borodko, H. Sook Leek, S. Hoon Joo, Y. Zhang, G. Somorjai, *J. Phys. Chem. C*. **2010**, *114*, 1117-1126.

[6] L. A. Aronica, A. M. Capurosso, C. Evangelisti, M. Botavina, G. Alberto, G. Martra, J. *of organomet. Chem.* **2012**, *700*, 20-28.

[7] M. R. Axet, S. Castillón, C. Claver, K. Philippot, P. Lecante, B. Chaudret, *Eur. J. Inorg. Chem.* **2008**, 3460-3466.

[8] D. Astruc, F. Lu, J. Ruiz Aranzaes, *Angew. Chem. Int. Ed*. **2005**, *44*, 7852-7872.

[9] Fine Chemical Synthesis- Homogeneous, J. G. de Vries, *Wiley*, **2002**.

[10] P. Lara, K. Philippot, B. Chaudret, *ChemCatChem*. **2013**, *5*, 28-45.

[11] K. Li, Y. Wang, J. Jiang, Z. Jin, *Catal. Commun.* **2010**, *11*, 542-546.

[12] D. Han, X. Li, H. Zhang, Z. Liu, G. Hu, C. Li, *J. of Mol. Cat. A: Chem.* **2008**, *283*, 15-22.

[13] M. Guerrero, N. T. T. Chau, S. Noël, A. Denicourt- Nowicki, F. Hapiot, A. Roucoux, E. Monflier, K. Philippot, *Curr. Org. Chem.* **2013**, *17*, 364-399.

[14] M. V. Escárcega-Bobadilla, C. Tortosa, E. Teuma, C. Pradel, A. Orejón, M. Gómez, A. M. Masdeu-Bultó, *Catal. Today*, **2009**, *148*, 398-404**.**

[15] S. A. Stratton, K. L. Luska, A. Moores, *Catal. Today*, **2012**, *183*, 96-100.

[16] A. Gual, C. Godard, K. Philippot, B. Chaudret, A. Denicourt-Nowicki, A. Roucoux, S. Castillón, C. Claver, *ChemSusChem*. **2009**, *2*, 769-779.

[17] D.J. Snelders, N. Yan, G. Laurency, P.J. Dyson, *ACS Catal*. **2012**, *2*, 201-207.

[18] J. D. Aiken III, R. G. Finke, *J. Mol. Catal. A: Chem*. **1999**, *145*, 1-44

[19] M. R. Axet, L. Philippot, B. Chaudret, M. Cabié, S. Giorgio, C. R. Henry, *Small*, **2011**, *7*, 235-241.

[20] P. Canton, P. F. Fazzini, C. Meneghini, A. Benedetti, G. Pozzi, Chapter 6 in *Metal Nanoclusters in Catalysis and Materials Science: The issue of size control*. Elsevier, Amsterdam, **2008**, Ed. By B. Corain, G. Schmid, N. Toshima.

[21] J. I. Langford, D. Louer, P. Scardi, *J. Appl. Cryst*. **2000**, *33*, 964-974.

[22] R. J. Matyi, L. H. Schwartz, B. Butt, *Catal. Rev. Sci. Eng*. **1987**, *29*, 41-99.

[23] A. W. Coats, J. P. Redfern, *Analyst*, **1963**, *88*, 906-924.

[24] F. Novio, K. Philippot, B. Chaudret, *Catal. Lett*. **2010**, *140*, 1-7.

[25] D. Gonzalez- Galvez, P. Nolis, K. Philippot, B. Chadret, Piet W. N. M. van Leeuwen, *ACS Catal.* **2012**, *2*, 317-321.

[26] C. Amiens, D. de Caro, B. Chaudret, *J. Am. Chem. Soc*. **1993**, *115*, 11638-11639.

[27] R. Bronger, T. D. Le, S. Bastin, J. García- Antón, C. Citadelle, B. Chaudret, P. Lecante, A. Igau, K. Philippot, *New J. Chem*. **2011**, *35*, 2653-2660.

[28] P. Lara, T. Ayvali, M-J. Casanove, P. Lecante, A. Mayoral, P-F. Fazzini, K. Philippot, B. Chaudret, *Dalton Trans*. **2013**, *42*, 372-382.

[29] I. Cano, A. M. Chapman, A. Urakawa, P. W. N. M. van Leeuwen, *J. Am. Chem. Soc*. **2014**, *136*, 2520-2528.

[30] K. S. Weddle, J. D. Aiken III, R. G. Finke, *J. Am. Chem. Soc*. **1998**, *120*, 5653-5666.

[31] C. Rangheard, C. de J. Fernández, P.- H. Phua, J. Hoorn, L. Lefort, J. G. de Vries, *Dalton Trans*., **2010**, *39*, 8464- 8471.

[32] B. K. Teo, H. Zhang in, D.L. Feldheim, C. A. Foss Jr. (Eds.), *Metal Nanoparticles: Synthesis, Characterization and Applications*, Marcel Dekker, New York, **2002** (Chapter 3); B. K. Teo, N. J. A. Sloane, *Inorg. Chem*. **1985**, *24*, 4545-4558.

[33] V. Hardevel, V. Hartog, *Surf. Sci. **1969**, 15,* 189-230*, A. Borodzinski, M. Bonarowska, Langmuir, **1997**, 13,* 5613-5620*.

[34] R. E. Benfield, *J. Chem. Soc. Faraday Trans*. **1992**, *88*, 1107-1110.

[35] Y. Yuan, N. Yan, P. Dyson, *ACS Catal*. **2012**, *2*, 1057-1069.

[36] Z. L. Wang, *J. Phys. Chem. B.* **2000**, *104*, 1153-1175.

[37] Eds. P. C. J. Kamer, P. W. N. M. van Leeuwen, *Phosphorus (III) Ligands in Homogeneous Catalysis. Design and synthesis*, Wiley, Chichester, **2012**.

[38] B. Chaudret, K. Philippot, *Oil& Gas Science and Technology*, **2007**, 62, 799-817.

[39] a) M. D. Fryzuk, w. E. Piers, in *Organometallic Synthesis*, Elsevier, Amsterdam, **1996**; b) W. A. Herrmann, in *Synthetic Methods of Organometallic and Inorganic Chemistry*, Thieme, Stuttgart, **1996**; c) P. Pertici, G. Vitulli, *Inorg. Synth.* **1983**, *22*, 17; d) J.L. Herde, J.C. Lambert, C.V. Senoff, *Inorg. Synth*. **1979**, *15*, 18; e) M. Green, T.A. Kuc, S. H. Taylor, *J. Chem. Soc. A.* **1971**, 2334-2337.

[40] J. García- Antón, M. Rosa Axet, S. Jansat, K. Philippot, B. Chaudret, T. Pery, G. Buntkowsky, H-H. Limbach, *Angew. Chem. Int. Ed*. **2008**, *47*, 2074-2078.

[41] D. M. Stefanescu, D. S. Glueck, R. Siegel, R. E. Wasylishen, *J. Clust. Sci*. **2008**, *19*, 445-458.

[42] B. P. S. Chauhan, R. Thekkathu, L. Prasanth, M. Mandal, K. Lewis*, Appl. Organometal. Chem*. **2010**, *24*, 222-228.

[43] A. Rodriguez, C. Amiens, B. Chaudret, M-J. Casanove, P. Lecante, J. S. Bradley, *Chem. Mater*. **1996**, *8*, 1978-1986.

[44] T. Gutmann, E. Bonefille, H. Breitzke, P- J. Debouttière, K. Philippot, R. Poteau, G. Buntkowsy, B. Chaudret, *Phys. Chem. Chem. Phys*. **2013**, *15*, 17383-17394.

[45] A) C. R. Hilliard, N. Bhuvanesh, J. A. Gladysz, J. Blümel, *Dalton. Trans*. **2012**, *41*, 1742-1754; b) M. Stankevic, A. Wlodarcyk, *Tetrahedron*, **2013**, *69*, 73-81; c) X. Zhang, H. Liu, G. Tang, J. Zhu, Y. Zhao, *Org. Lett*. **2011**, *13*, 3478-3481.

[46] Library of the ICDD

[47] A. Sánchez, M. Fang, A. Ahmed, R. A. Sánchez-Delgado, *Appl. Catal. A: Gen.* **2014**, *477*, 117-124.

[48] K. Pelzer, B. Laleu, F. Lefebvre, K. Philippot, B. Chaudret, J. P. Candy, J. M. Basset, *Chem. Mater*. **2004**, *16*, 4937-4941.

[49] I. Lopez- Salido, D. C. Lim, R. Dietsche, N. Bertram, Y. D. Kim, *J. Phys. Chem. B.* **2006**, *110*, 1128-1136.

[50] P. Pollow Sarma, D. Kumar Dutta, *Appl. Catal. A: Gen.* **2014**, *470*, 355-360.

[51] B. M. Austin, D. Y. Zubarev, W. A. J. Lester, *Chem. Rev.* **2012**, *112*, 263-288.

[52] T. Pery, K. Pelzer, G. Buntkowsky, K. Philippot, H-H. Limbach, B. Chaudret, *ChemPhysChem*. **2005**, *6*, 605-607.

[53] J. P. Wey, W. C. Neely, S. D. Worley, *J. Phys. Chem*. **1991**, *95*, 8881-8886.

[54] F. Basile, I. Bersani, P. del Gallo, S. Fiorilli, G. Fornasari, D. Gary, R. Mortera, B. Onida, A. Vaccari, *Int. J. Spectr*. **2011**, 1-8.

[55] S. U. Son, Y. Jang, K. Y. Yoon, E. Kang, T. Hyeon, *Nano Letters*, **2004**, *4*, 1147-1151.

[56] F. Novio, D. Monahan, Y. Coppel, G. Antorrena, P. Lecante, K. Philippot, B. Chaudret, *Chem. Eur. J*. **2014**, *20*, 1287-1297.

[57] O. Kühl in Phosphorus-31 NMR spectroscophy, , Ed. Springer, Germany, **2008**, vol 1.

[58] A. Gual, J. A. Delgado, C. Godard, S. Castillón, D. Curulla- Ferré, C. Claver, *Top. Catal*. **2013**, *56*, 1208-1219.

[59] A) C. X. Xiao, Z.P. Cai, T. Wang, Y. Kou, N. Yan, *Angew. Chem. Int. Ed.* **2008**, *47*, 746-749, b) J. D. Hoefelmeyer, K. Niesz, G. Somorjai, T. D. Tilley, *Nano lett*. **2005**, *5*, 435-438.

[60] C. Pan, K. Pelzer, K. Philippot, B. Chaudret, F. Dassenoy, P. Lecante, M-J. Casanove, *J. Am. Chem. Soc*. **2001**, *123*, 17584-7593.

[61] A. Gual, C. Godard, S. Castillón, D. Curulla- Ferré, C. Claver, *Catal. Today*, **2012**, 154-171.

[62] F. Lu , J. Liu, J. Xu*, Mater. Chem. Phys.* **2008***, 108,* 369-374.

[63] S. M. Humphrey, M. E. Grass, S. E. Habas, K. Niesz, G. A. Somorjai, T. D. Tilley, *Nano Letters*, **2007**, *7*, 785-790.

[64] N. Yan, Y. Yuan, P. J. Dyson, *Chem. Commun*. **2011**, *47*, 2529-2531.

[65] K. Pelzer, O. Vidoni, K. Philippot, B. Chaudret, V. Collière, *Adv. Funct. Mater*. **2003**, *13*, 118-126.

[66] A. C Yang, C. W. Garland, *J. Am. Chem. Soc.* **1957**, *61*, 1504.

[67] B. L. Mojet, S. D. Ebbesen, L. Lefferts, *Chem. Soc. Rev*. **2010**, *39*, 4643-4655.

[68] a) P. Lara, O. Rivada-Wheelaghan, S. Conejero, R.Poteau, K. Philippot, B. Chaudret *Angew. Chem. Int. Ed*. **2011**, *50*, 12080-12084.

[69] J. T. Yates Jr., T. M. Duncan, S. D. Worley, R. W. Vaughan, *J. Chem. Phys*. **1979**, *70*, 1219-1224.

[70] A. J. Bruss, M. A. Gelesky, G. Machado, J. Dupont, *J. Mol. Catal. A: Chem*. **2006**, *252*, 212-218.

[71] G. Schmid (ed.), *Nanoparticles*, Wiley-VCH, Weinheim, **2004**.

[72] N. Yan, Z.-G. Zhang, Y. Tong, S. Yao, C. Xiao, Z. Li, Y. Kou, *Chem. Commun*. **2009,** 4423-4425.

[73] M. E. Grass, S. H. Joo, Y. Zhang, G. A. Somorjai, *J. Phys. Chem. C*, **2009**, *113*, 8616- 8623.

[74] Mucalo, M. R.; Cooney, R. P. *Chem. Mater*. **1991**, *3*, 1081-1087.

[75] A. Van. Rooy, E. N. Orij, P. C. J. Kamer, P. W. N. M. van Leeuwen, *Organometallics*, **1995**, *14*, 34-43.

[76] M. D. Fryzuk, W. E. Piers in *Organometallic Syntheses* (Eds.:R. B. King, J. J. Eisch), Elsevier, Amsterdam, **1986**, vol. 3, p.128.

[77] W. A. Herrmann in *Synthetic Methods of Organometallic and Inorganic Chemistry* (Ed.: W. A. Herrmann), Thieme, Stuttgart, **1996**, p. 38.

[78] K. D. John, K. V. Salazar, B. L. Scott, R. T. Baker, A. P. Sattelberger, *Organometallics*, **2001**, *20*, 296-304.

[79] B. Chaudret, *C. R. Physique*, **2005**, *6*, 117-131.

Chapter 3.

Catalytic hydrogenation of arenes using phosphorus-stabilised Rh nanoparticles
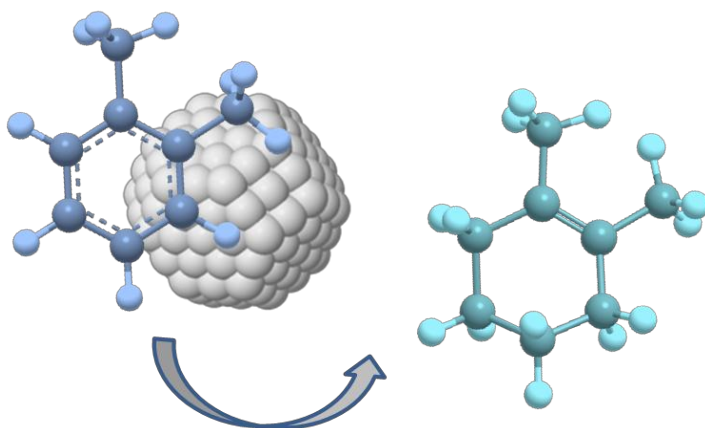
3.1 Introduction

3.1.1 Background

As previously mentioned in Chapter 1, the hydrogenation of monocyclic arenes is an active area of research due to the high industrial interest in the production of cyclohexanes from the corresponding arenes.[1]
In this introduction section, a general overview of the topic will be presented and the recent advances in this field will be particularly detailed. The nanocatalysts are classified according to the stabilising agents used in their synthesis and their corresponding catalytic performances ordered as: activity, chemoselectivity and *cis/trans* selectivity.

3.1.2 Mechanism of arene hydrogenation

The generally accepted mechanism for the hydrogenation of arenes was first proposed in 1974 and was based on the observation that labile arene exchange takes place in a number of metal–arene complexes.[2]
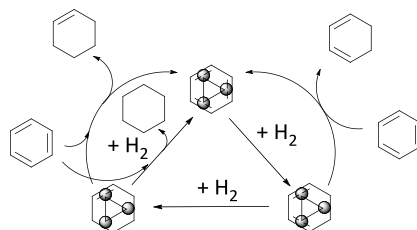
Figure 3.1 Proposed arene-exchange mechanism for homogeneous cluster or heterogeneous catalysts.

The mechanism may be applied for any arenes which interact with more than one metal centre, which is possible at a cluster, nanoparticle, or bulk metal surface. The coordination modes of arenes to several metallic centres have been previously reviewed.[3] A common coordination mode in cluster chemistry is the μ_3-η^2: η^2: η^2 mode that is illustrated in Figure 3.1, which has

also been reported on metal surfaces.[4] The addition of hydrogen across one double bond would result in a μ_3-η^2: η^2-diene and further hydrogenation would lead to a monoene. The release of the diene and monoene products can therefore take place during the reaction by replacement of the partially hydrogenated product by a new arene substrate. The μ^2-η^3: η^3 coordination mode of arene between two metal centres has also been reported[5] and a hydrogenation mechanism involving such a bonding mode cannot be discarded.

The most intriguing question in elucidating the mechanism of this reaction is the influence of substituents on reaction rate and the origin of the formation of *cis*- and *trans*-disubstituted cyclohexanes, since only the formation of the *cis* product is expected if the aromatic molecule is adsorbed in a flat fashion on the surface. Several studies were devoted to catalytic hydrogenation of substituted aromatic compounds such as toluene and dialkylbenzenes to form dialkyl-cyclohexene and *cis*- and *trans*-dialkylcyclohexanes. The *cis* stereoisomer is the kinetically favoured product, while the *trans* isomer is thermodynamically favoured.
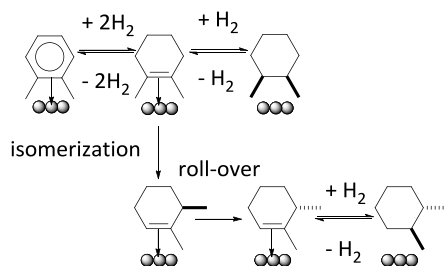
Figure 3.2 Proposed mechanism for the hydrogenation of *ortho*-xylene on metal surfaces.

In a disubstituted substrate such as *o*-xylene, the aromatic ring adsorbs parallel to the surface although to relieve the steric repulsion, the two methyl groups should be oriented away from the surface. According to the rollover mechanism (Figure 3.2), 1,2-dimethylcyclohexene isomerises to 2,3-dimethylcyclohexene, and the latter rolls over and hydrogenation of the double bond can thus yield the *trans* isomer.[6] According to this scheme, a

desorption and re-adsorption of the 2,3-dimethylcyclohexene from the other side of the plane, in addition to rollover, are also possible.

In 2005, Dupont and co-workers studied the influence of substituents in monoalkylbenzenes on the hydrogenation rate constants using M-NPs and classical heterogeneous catalysts.[7] The initial rate constants were obtained in various competitive hydrogenation experiments catalysed by M-NPs stabilised by imidazolium ionic liquids (ILs) or by surfactants using toluene/benzene and toluene/monoalkylbenzene mixtures as substrates. From these results, it was suggested that for these substrates, the reaction constants for the alkyl-substituents can be expressed by steric factors and are independent of any other non-steric factors under these conditions. Therefore, bulky substituents on the substrate lower the overall hydrogenation rate for both M-NPs and classical heterogeneous hydrogenation reactions.

In summary, the rate of aromatic hydrogenation at metallic surfaces is strongly affected by steric factors as the hydrogenation rate decreases by substitution of alkyl groups to the aromatic ring.[8] The reaction rate: (a) decreases with increasing length of substituent (benzene > toluene > ethylbenzene > cumene), (b) decreases with increasing number of substituents (benzene >> toluene ~ xylenes > mesitylene), and (c) is significantly affected by the relative positions of the substituent, the *para*-position being the most reactive and the *ortho*-position the least reactive (*p*-xylene > *m*-xylene > *o*-xylene).

The electronic properties of the substituents at the arene ring also influence the rate of hydrogenation at metallic surfaces.[9] Indeed, the presence of electron-donating groups was shown to accelerate the reduction of the aromatic ring whereas electron-withdrawing groups decrease the rate of hydrogenation.

3.1.3 Modern metal nanoparticles catalysed hydrogenation of arenes

Nowadays, the use of metallic nanoparticles as catalysts provides excellent opportunities to improve the catalytic outcome of hydrogenation reactions and to explore new potential activity/selectivity due to the chemical and physical properties of these systems.

Catalytic activity

Although new metal nanocatalysts based on Co, Pd, Ni and Fe have recently shown promising results in hydrogenation reactions, Ru, Rh, Pt and Ir are still currently the metals of choice for arene hydrogenation nanocatalysts.[10] As the M-NPs require stabilisation because they are unstable with respect to agglomeration towards the bulk, the nature and properties of the stabilising agent used is of crucial importance in terms of stability/activity of these catalysts.

In the following section, the activity of soluble M-NPs in the hydrogenation of arenes is discussed according to the type of stabilisers present at their metallic surface.

Catalyst activity is defined as the number of moles of reactants consumed per mol of soluble metal catalyst and corresponds to the turn over numbers (TON). It should be noted that in the literature, TON is reported in two different ways, either per total mol of metal or per mol of metal exposed at the NP surface.[11] The number of metallic atoms present at the surface of these systems can be calculated by the methods explained in Chapter2. Moreover, the turnover frequency (TOF) should be estimated for low substrate conversions, due to the possible change in size and shape of these catalysts during reaction that could affect the real value.

Polymer stabilised Metal-NPs

The stabilisation of metal-NPs by polymers, and in particular polyvinylpyrrolidone (PVP), has been largely described since this stabilising

agent is non-toxic and soluble in many polar solvents.[12] These polymers are characterised by their molecular weight, which is referred to as PVP K-n (n= 15, 30 or 90) in this study (Figure 3.3).

PVP
PVP K-15 (Mw = 10000)
PVP K-30 (Mw = 40000)
PVP K-90 (Mw = 360000)

PVP modified with 1-vinyl-3-alkyl imidazolium salts

Cn-PVP

R= C_2H_5, C_4H_9, C_6H_{13}, C_8H_{17}

PVP grafted onto silica
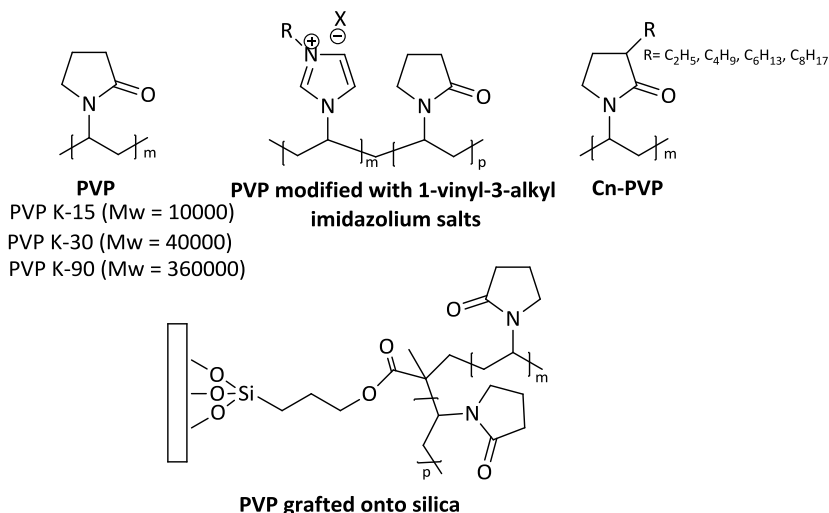
Figure 3.3 Structure of PVP and derivatives used in the stabilization of NPs catalysts for arene hydrogenation.

In 1997, a colloidal system obtained by reduction of $RhCl_3.3H_2O$ with ethanol in the presence of PVP was reported by James and co-workers and applied in the monophasic hydrogenation of various substrates such as benzyl acetone, 4-propylphenol and benzene derivatives under mild conditions (25°C and 1 bar H_2).[13] However, these nanoparticles were poorly characterised and their activity when benzyl acetone was the substrate, was low (50 Total Turn Over number (TTO) in 43 h).

In 2001, Chaudret and co-workers described the synthesis and characterisation of Rh-NPs stabilised by PVP K-30 using the organometallic approach, starting from $[Rh(\mu-Cl)(C_2H_4)_2]_2$.[14] They later reported the application of these nanocatalysts in the hydrogenation of benzene, toluene and phenylacetylene.[15] When the reaction was performed in pure

benzene with a substrate/Rh ratio of 34000, 60% conversion to cyclohexanes was obtained at 80 °C under 20 bar H_2. However, when the reaction was performed in a biphasic media (water/benzene), complete conversion (Turn Over Frequency (TOF) up to 675h^{-1}) was obtained with a substrate/Rh ratio of 2000 at 30 °C under 7 bar of H_2. As could be expected, the hydrogenation of substituted arenes such as toluene and phenylacetylene required the use of more drastic conditions (*ca.* 80°C under 40 bar H_2).

In 2006, Xu and co-workers reported the synthesis of Ru-NPs stabilised by water-soluble amphiphilic PVP K-90.[9] These nanocatalysts were described as microreactors in the aqueous/organic hydrogenation of arenes since in this system, PVP provides a hydrophobic microenvironment that prevents the nanoparticles from aggregation in water. The high activity of these Ru-NPs catalysts for the hydrogenation of arenes was explained by the fact that catalyst and substrates are confined in the hydrophobic pocket, which enhances the contact between them. With this protocol, fast aqueous/organic hydrogenation of arenes, olefins and carbonyl compounds were achieved using this Ru/PVP-NPs system.

R= H, Me, Et, OMe, CO_2Me, C(O)Me
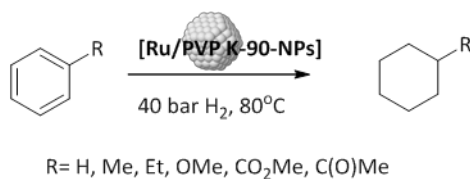
Figure 3.4 System used by Xu and co-workers.[16]

As expected, the highest TOF value (45000h^{-1}) was obtained with benzene as substrate. Interestingly, when the substrates contained electron-donating substituents, all the TOFs exceeded 10000h^{-1}. However, with arenes bearing electron-withdrawing substituents, lower TOF values were measured (*ca.* 1000h^{-1}). These results were attributed to the decrease of electron density in the aromatic ring.

Surfactants stabilised Metal-NPs

Januskiewciz and Alper described the first colloidal metal-NPs stabilised by tetraalkylamonium salts.[16] The organometallic approach was used for their synthesis in biphasic conditions using [RhCl(1,5-hexadiene)]$_2$ as the precursor and tetraalkylammonium bromide as protective agent. These systems were used in the hydrogenation of several benzene derivatives with TTO up to 100. Later, James reported the synthesis of Rh- and Ru-NPs stabilised by tetrabutylammonium (TBA) salts and their use in the hydrogenation of 2-methoxy-4-propylphenol.[17] The best results were obtained using the Ru nanocatalysts, achieving TTO up to 300. An other example was reported by Lemaire and co-workers who used Rh-NPs stabilised by methyltrioctylammonium chloride in the hydrogenation of dibenzo-18-crown-6-ether into *syn*, *anti*-dicyclohexane-18-crown-6-ether.[18]
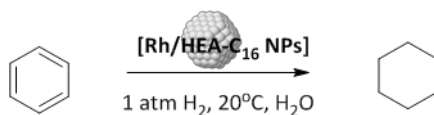
Figure 3.5 System used by Roucoux and co-workers.[19]

Moreover, Roucoux and co-workers reported the first example of efficient nanocatalysts under biphasic conditions for this reaction, with recycling at room temperature and using 1 atm of hydrogen pressure.[19,20] They compared the results obtained with colloidal Rh-NPs stabilized by N,N-dimethyl-N-cetyl-N-(2-hydroxyethyl)ammonium bromide (HEA-16-Br) with those obtained with the standard Rh/C heterogeneous catalyst and with the classical water-soluble Rh/PVP and Rh/PVA systems synthesised in hydroalcoholic media by Hirai.[12b,21] In the hydrogenation of anisole and toluene, their Rh/HEA-16-Br-NPs were shown to be the most active.

The lifetime of Rh/HEA-16-Cl and Ir/HEA-16-Cl-NPs catalysts was studied reusing the aqueous phase for successive hydrogenation runs.[22] They observed that the NPs efficiently remained in the aqueous phase and the

total turnover numbers (TTO) obtained with the Rh and Ir-NPs catalysts in the hydrogenation of benzene were 400 and 100, respectively. In the case of anisole, these values were 2000 and 3000, respectively.

Ionic Liquids stabilised Metal-NPs

As already mentioned, Dupont and co-workers reported the first synthesis of stable and re-dispersible M-NPs obtained by simple reduction of transition-metal compounds dissolved in 1-n-butyl-3-methylimidazolium hexafluorophosphate (BMI·PF_6) with molecular hydrogen as the reducing agent.[23]

[Ir/BMI·PF$_6$ NPs]

4 atm H$_2$, 75°C, CH$_2$Cl$_2$
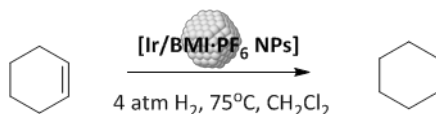
Figure 3.6 Hydrogenation of cyclohexene reported by Dupont and co-workers.[23]

Later, the same group described the application of Rh, Ir, Ru and Pt-NPs stabilised by BMI·PF_6 in the hydrogenation of benzene.[24,25,26] These nanocatalysts could be used in biphasic, homogeneous and heterogeneous hydrogenation of arenes under mild reaction conditions (75°C and 4 bar). The reactions performed under solventless conditions were found to be faster than those performed with the NPs dispersed in IL (biphasic system) which was explained by the influence of typical mass transfer processes of a multiphase system.[27] However, Finke and co-workers reported that imidazolium ILs produce the poisoning of Ir-NPs via the formation of Ir N-heterocyclic carbene complexes.[28] Under the same reaction conditions, the Ir-NPs and Ru-NPs stabilised by ILs are much more active in the hydrogenation of benzene than their Pt and Rh analogues. The Rh/BMI·PF_6, Ir/ BMI·PF_6 and Pt/ BMI·PF_6-NPs catalyst lifetimes were studied in successive runs in the hydrogenation of benzene. For the Rh-NPs, a decrease of the catalytic activity associated to the agglomeration of NPs was observed. In contrast, the recovered Ir-NPs and Pt-NPs could be reused several times without any significant loss in catalytic activity. These Ir-NPs

provided total turnover numbers (TTO) of 3509 in 32h. However, they produced the simultaneous hydrogenolysis of the C-O bonds during the hydrogenation of functionalised arenes such as anisole and acetophenone.

Recently, Rossi and co-workers described the synthesis of Ru-NPs through reduction of commercially available RuO_2 using ionic liquids as stabilising agents (BMI·PF_6, BMI·BF_4, BMI·CF_3SO_3).[29] Other Ru-precursors such as $RuCl_3$ were not reduced under mild reaction conditions (75 °C and 4 bar H_2) and required the use of other reducing agents, such as $NaBH_4$. These catalysts were applied in the hydrogenation of benzene and toluene the use of NPs under solventless conditions produced higher activities than when ILs were employed. Interestingly, the obtained activities in the hydrogenation of benzene and toluene (TOFs up to 953h^{-1} and 556h^{-1}) were much higher than those observed for Ru-NPs prepared from [Ru(COD)(COT)] in similar conditions.[26] The catalyst lifetime under solventless and BMI·PF_6 biphasic conditions were also investigated and TTOs up to 2700 and 1200 were achieved.

Other stabilisers

N-donor stabilisers

Amines and aromatic imines are the most commonly used N-donor ligands used as NP stabilisers (see Chapter 1).[30]

Pertici and co-workers reported the synthesis of Ru-NPs by decomposition of [Ru(COD)(COT)] using trioctylamine (TOA) as stabilizing agent.[31] These NPs were isolated and characterised by TEM microscopy with a mean diameter of *ca*. 2.9 nm. These NPs were later supported onto alumina and revealed to be efficient catalysts for the hydrogenation of deactivated aromatic compounds such as 4-methyl benzoate and 2-(4-carbomethoxyphenyl)-1,3-dioxane.
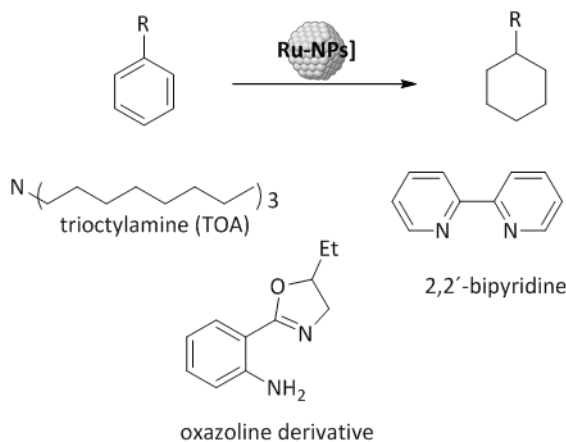
Figure 3.7 Examples of N-donor molecules used as M-NPs stabilisers.

In 2006, Chaudret and co-workers reported the synthesis of Ru-NPs through decomposition of [Ru(COD)(COT)] using oxazolines as stabilisers.[32] These NPs were active in the hydrogenation of arenes although upon addition of extra oxazolines during catalysis rendered the system completely inactive.

- P-donor stabilisers

Recently, several examples of NPs stabilised by P-donor molecules were reported to be active in the hydrogenation of arenes.
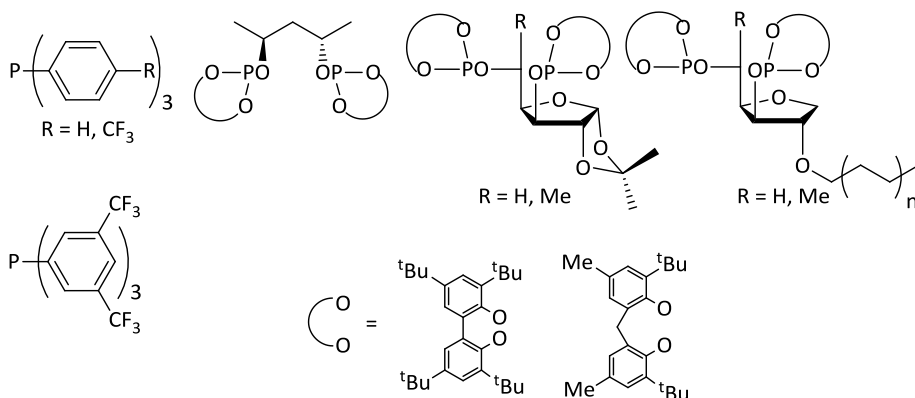
Figure 3.8 P-donor molecules used as stabilisers for soluble nanocatalysts in the hydrogenation of arenes.

Masdeu-Bultó, Gómez and co-workers reported the synthesis of Rh and Ru-NPs stabilised by triphenylphosphine and its fluorinated derivatives.[33] These NPs were found to be active in the hydrogenation of styrene, *p*-methylanisole and isopropen-2-yl benzyl ether in scCO$_2$ and in THF with interesting selectivities that will be described in details in the next section. Our group, in collaboration with that of Chaudret, reported the use of chiral diphosphites derived from carbohydrates as stabilisers for Rh-, Ru- and Ir-NPs and their application in the hydrogenation of *ortho*- and *meta*-methyl anisoles.[34] The Rh-NPs were found to be the most active of the series and significant effect of the diphosphite structures were observed on the catalytic activity of these catalysts.

Wang and co-workers reported the use of phosphine ligands bearing polyethyleneglycol (PEG) chains that combined both polymeric and phosphine moieties for the stabilisation of rhodium nanoparticles.[35] TOFs up to *ca.* 3000 cm^{-1} were obtained in the hydrogenation of benzene and the NPs could be reused five times without loss in activity.

Interestingly, Dyson and co-workers recently showed that the addition of phosphines to Rh-NPs of *ca.* 3 nm in diameter previously synthesised in the presence of PVP improves the selectivity of Rh-NPs in hydrogenation reactions.[36] The authors postulated that the selective coordination of these ligands could modify the steric hindrance at specific sites of the NPs and hence generate selectivity.
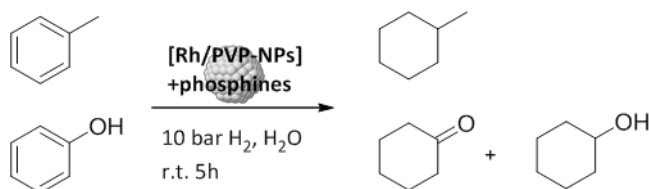
Figure 3.9 Hydrogenation of toluene or phenol by PVP- stabilised Rh-NPs in the presence of phosphine ligands.[36]

Van Leeuwen, Chaudret and co-workers also recently reported the use of carbene and large bite angle diphosphine ligands as stabilisers for Ru-NPs and their application in the hydrogenation of aromatics, with interesting ligand effects.[37,38] Moreover, the same group reported the use of secondary phosphine oxides as pre-ligands for Ru-NPs active in the hydrogenation of aromatic substrates.[39] This methodology provides the possibility to employ these catalysts without solvent and at very low loading.

Selective partial hydrogenation of arenes

Several soluble nanoparticles have been reported as catalysts for the partial hydrogenation of arenes to cyclohexene derivatives, and usually, ruthenium and rhodium are used as metals. In this reaction, the degree of substitution at the aromatic ring largely influences the selectivity towards the corresponding cyclohexene products. To avoid misleading comparisons, the results reported in the partial hydrogenation of benzene will first be described.

Only a few examples of production of cyclohexene by selective hydrogenation of benzene are described in the literature using soluble nanocatalyst systems.

Dupont and co-workers reported the use of imidazolium ionic liquids (Figure 3.10) to stabilise Ru nanoparticles of *ca*. 2.6 nm able to perform the catalytic reactions under solventless conditions or in ILs medium.[40] The best results were obtained with the system using BMI·PF$_6$ with a selectivity of 39% to cyclohexene. However, this result was obtained at 1% conversion, and the selectivity dropped to 11% at 15% conversion.

$X= BF_4 \cdot BMI \cdot BF_4$
$X= PF_6 \cdot BMI \cdot PF_6$
$X= CF_3SO_3 \cdot BMI \cdot CF_3SO_3$

ILs-Ru NPs

6 atm H_2, 75°C, ILs medium

39% selectivity
1% conversion
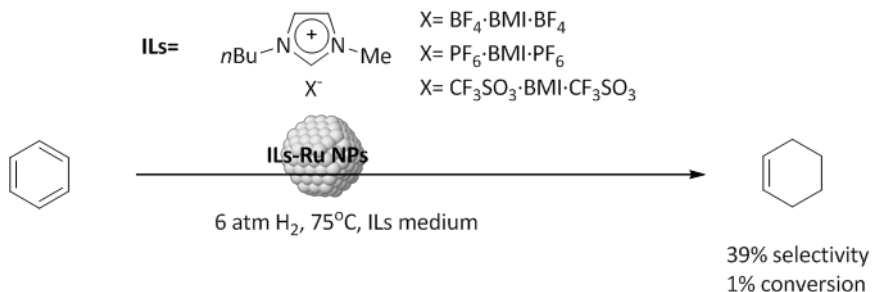
Figure 3.10 Catalyst systems used for the selective hydrogenation of benzene in a ILs medium.[40]

The authors concluded that the selectivity towards cyclohexene products is due to the different cyclohexene/benzene solubility in the ILs and that this moiety is acting as a reaction modifier. The same ionic liquid stabiliser for ruthenium nanoparticles was used by Rossi and Machado a few years later.[41] In this case, the precursor used was $RuO_2 \cdot 3H_2O$ and the turnover frequency of the catalyst obtained was *ca.* twice higher than that measured for the Ru-NPs synthesised from the organometallic precursor [Ru(COD)(COT)]. Different parameters were evaluated such as the ionic liquid counterion or the temperature and the optimised conditions were obtained using the BMI·BF_4 ionic liquid at 120°C with a maximum selectivity of 65% for the cyclohexene product at 0.3% of benzene conversion.

Partial hydrogenation of substituted arenes

In this reaction, the degree of substitution and the steric hindrance induced by the substituents strongly affect the selectivity since bulky groups favour the dissociation of the partially hydrogenated substrate from the catalyst surface and disfavour its re-adsorption.
In 1987, Blum et al. observed the formation of cyclohexenes derivatives (2,3,5,6-tetramethylcyclohexene and 1,2,4,5-tetramethylcyclohexene) using the solvated ion pair $[(C_8H_{17})_3NCH_3]^+[RhCl_4]^-$.[42] The partially hydrogenated

183

products were only observed when very sterically hindered substrates like durene (1,2,4,5-tetramethylbenzene) were used. Importantly, even if the system was a priori a homogeneous catalyst, Finke and co-workers demonstrated later the nanocluster nature of the real catalyst in this transformation.[43] The same research group reported a few years later the use of polyoxoanion- and tetrabutylammonium-stabilised Rh(0) nanoclusters.[44] These systems were used as catalysts in the hydrogenation of anisole and a maximum selectivity of 8% of the 1- methoxycyclohexene product at 41% of conversion was achieved at 78 °C. They postulated that the adsorbed polyoxoanions at the surface of the nanocatalysts are predominantly responsible for the selectivity and that this adsorption affects the desorption equilibrium constant of the monoene intermediate, which is represented in Figure 3.11.
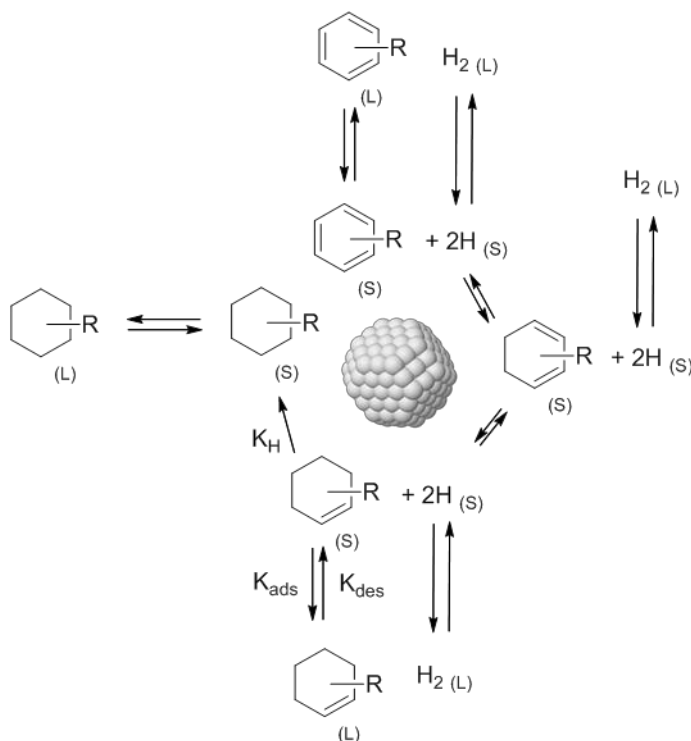
Figure 3.11 Proposed mechanism for the catalytic hydrogenation of arenes by group VIII metals ((L) indicates that the compound is dissolved in the liquid phase, while species adsorbed on the catalyst surface are indicated with (S)).[44]

Some years later, the groups of Dyson and Kou reported the use of ionic liquid like copolymer to stabilise rhodium nanoparticles.[45] The nanoparticles were prepared in 1-butyl-3-methylimidazolium tetrafluoroborate ([BMIM][BF$_4$]) containing a polyvinylpyrrolidone derivative (Figure 3.12), using RhCl$_3$ as precursor, and H$_2$ as the reducing agent.
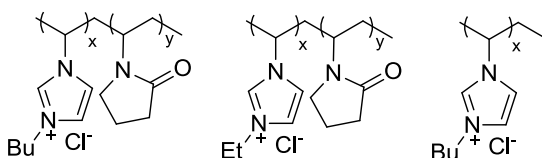
Figure 3.12 Structure of the polyvinyl pyrrolidinone derivatives reported by Dyson and Kou as stabilisers for Rh- NPs.[45]

One of the advantages of this stabilisation method is the facile separation of the products by decantation from the IL phase containing the catalyst. Using these NPs in the hydrogenation of arenes (benzene, mono and disubstituted), significant quantities of partially hydrogenated products were obtained. Up to 32% of the cyclohexene derivative was obtained at 33% of conversion using *o*-xylene as substrate, for instance.

The group of Gómez and co-workers used ruthenium nanoparticles bearing the 4-(3-phenylpropyl)-pyridine ligand as stabiliser (Figure 3.13) and as catalyst in the hydrogenation of various substrates.[46] For *p*-methylanisole, this catalyst was less active than for acetophenone or toluene, for example. However, 25% selectivity for the partially hydrogenated product was measured for *p*-methylanisole while the analogous products were not formed with the other substrates.
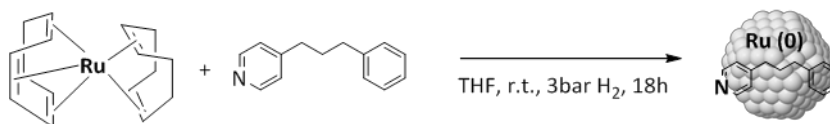
Figure 3.13 Synthetic methodology used by Gomez and co-workers.[46]

More recently, Chaudret and van Leeuwen reported the use of NHC carbenes to stabilise ruthenium nanoparticles and their application in the hydrogenation of aromatics (Figure 3.14).[47]
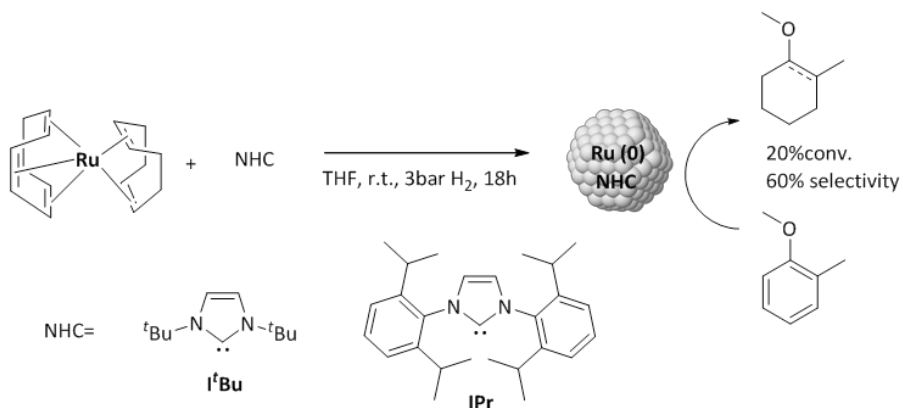
Figure 3.14 NHC ligands and reaction conditions reported for the synthesis of Ru NPs by Chaudret and co-workers.[47]

These systems were applied in the hydrogenation of mono and disubstituted arenes. Various parameters were evaluated such as the amount of ligand used for the synthesis of these catalysts, the solvent or the temperature of the catalytic reactions. As in the previous examples, higher temperatures shifted the selectivity towards the partial hydrogenated products. At 393 K and 20% conversion, *ca.* 60% of the cyclohexene derivative was obtained using *o*-methylanisole as substrate and the NP stabilised with the IPr-substituted NHC-carbene.

Chemoselectivity

Chemoselectivity refers to the selective formation of products of interest by reduction of one type of functional groups in the presence of other reducible functions in the substrates. In this context, the aromatic ring will therefore be considered as a reducible group in the presence of other reactive functions such nitro groups, as previously described for heterogeneous catalysts by Corma and co-workers.[48]

Several examples of chemoselective hydrogenation of arenes using soluble metal NPs are described in this section.

Styrene

The main results reported in the literature for the selective hydrogenation of styrene are detailed in this section.

In 2006, Roucoux and co- workers reported the synthesis of ruthenium nanoparticles synthesised by chemical reduction of $RuCl_3$ with $NaBH_4$ and stabilised by methylated cyclodextrins (CDs).[49] The cavity of these molecules can be modulated by the substitution degree (SD) that is defined as the average number of hydroxyl groups substituted per glucopuranose unit. Moreover, the use of CDs allows the reactions to be performed under biphasic conditions due to their solubility in water. In this study, the hydrogenation of several aromatic substrates such as benzene, toluene, styrene or ethylbenzene are reported in water and under mild conditions (1 bar H_2 and 20 °C).
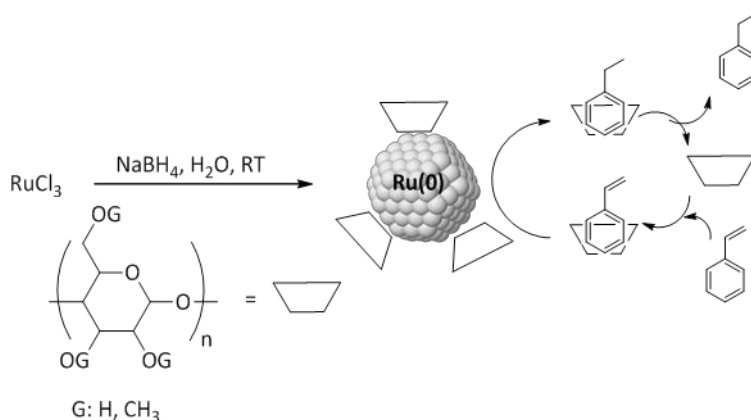
Figure 3.15 Selective hydrogenation of styrene with Ru NPs stabilised by cyclodextrin as catalysts.[49]

In the hydrogenation of styrene, the selectivity towards ethylbenzene or ethylcyclohexane was shown to be influenced by the substitution degree of the CDs. Ethylbenzene was selectively obtained when the systems Me-α–CD and Me-β-CD with a substitution degree of 1.8 while the NPs bearing Me-γ-CD and Me-β-CD with a low substitution degree (0.7) only provided ethylcyclohexane as the product. In this study, the important role of the protective agent was highlighted since in this case, the CD was acting as a stabiliser, a phase transfer agent and a suitable host molecule for the substrate.

More recently, Philippot and co-workers reported the synthesis of water soluble ruthenium NPs and their application in the hydrogenation of styrene.[50] The organometallic precursor [Ru(COD)(COT)] was reduced under H_2 in THF in the presence of various alkyl sulphonated diphosphines (Figure 3.16). Several ligand/metal ratios were tested, and small differences in the size of the resulting nanoparticles were observed (1.2-1.5 nm). These NPs were active in the hydrogenation of styrene but mixtures of ethylbenzene and ethylcyclohexane were obtained in most cases. However, the authors showed that the use of high L/Ru ratio provides more sterically hindered surface, which in turn increase the selectivity to ethylbenzene by restricting the access of the aromatic ring.
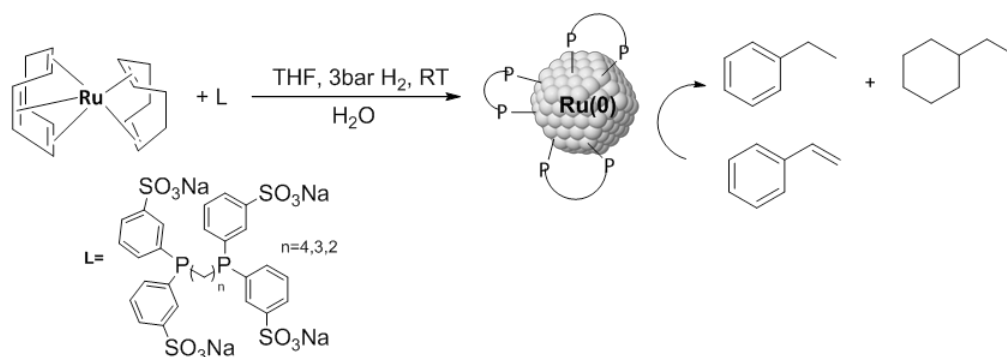
Figure 3.16 Sulphonated diphosphines used by Philippot and co-workers as stabilisers for Ru NPs for the hydrogenation of styrene.[49]

Within this series, the best results in terms of selectivity towards ethylbenzene (100%) were obtained using the Ru-NPs stabilised by the sulphonated diphenylphosphinobutane derivative at 50 °C under 1 bar of H_2 pressure and in water as solvent. The same research group also reported the use of bimetallic ruthenium/platinum nanoparticles stabilised by the diphosphine ligand dppb for this transformation (Figure 3.16).[51] The organometallic approach was also used in this case for the synthesis of the NPs, which presented a very disordered structure. The ruthenium core was evidenced by HRTEM and EXAFS and the shell of Pt-Ru by WAXS and several spectroscopic methods.
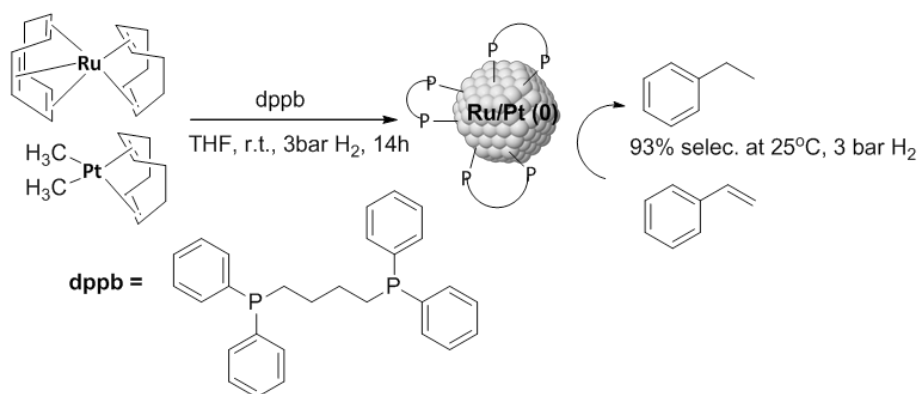
Figure 3.17 Synthesis of RuPt/ dppb NPs and their application in styrene hydrogenation.[51]

The reactivity of these bimetallic systems was studied in the hydrogenation of styrene under mild conditions (25 °C and 3 bar of H_2). The two steps of the reaction were observed: first, the reduction of the vinyl group to form ethylbenzene and in a second step, ethylbenzene is converted into ethylcyclohexane. As the two pathways of the formation of the products diverge sufficiently, ethylbenzene could be isolated with 93% selectivity.

Another example of ruthenium nanocatalyst used for this transformation is reported by the group of Montserrat Gomez (Figure 3.18).[46] Full conversion of styrene was obtained after 6h under 40 bar of hydrogen and at 50 °C.

Under these conditions, 25% of ethylbenzene was obtained together with 75% ethylcyclohexane.
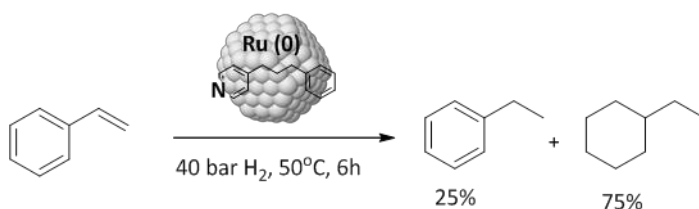
Figure 3.18 Hydrogenation of styrene catalysed by Ru-NPs reported by Gómez and co-workers.[46]

Roucoux and co- workers reported the synthesis of rhodium nanoparticles by chemical reduction of rhodium chloride.[52] Sodium borohydride was used as reducing agent and the ionic liquid N,N-dimethyl-N-dodecyl-N-(2-hydroxyethyl) ammonium trifluoromethanesulfonimide salt (HEA 12N (Tf)$_2$) as stabiliser. These surfactant-stabilized Rh (0) hydrosol nanoparticles were treated with LiN(Tf)$_2$ to form the ionic liquid phase, as shown in Figure 3.19. In preliminary tests using these catalysts in the hydrogenation of styrene at room temperature and atmospheric hydrogen pressure, the exocyclic double bond was selectively reduced to form ethylbenzene.
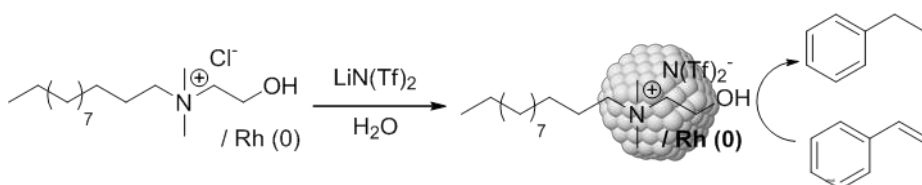
Figure 3.19 Selective hydrogenation of styrene to ethylbenzene by ILs stabilised Rh NPs.[52]

The same group reported a few years later a similar procedure but using in this case a mixture of bipyridine and ionic liquids as stabilising agents (Figure 3.19).[53] Their characterisation by TEM and XPS revealed that these systems presented narrow size distribution and an average diameter of 2.0-2.5 nm, and contained rhodium, fluorine (from ionic liquid residue), sodium, carbon and nitrogen.
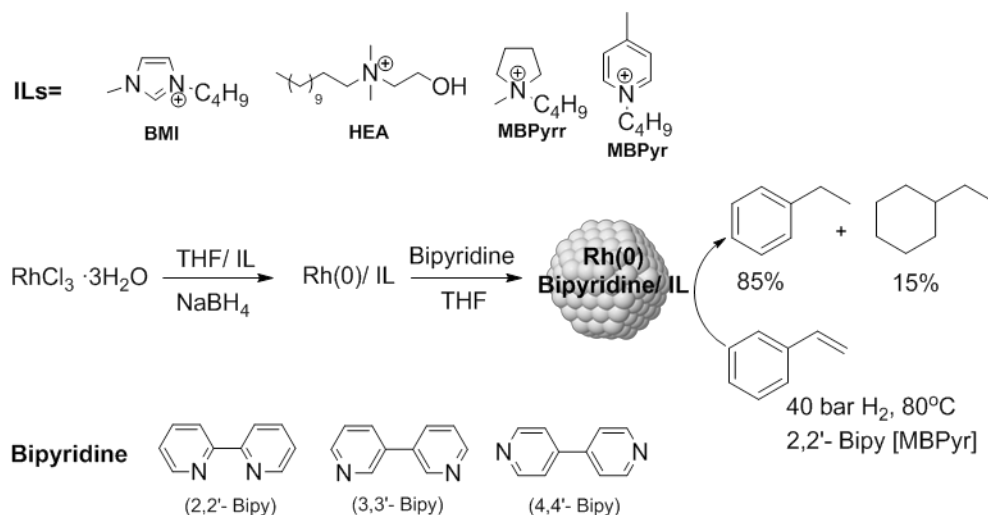
Figure 3.20 System used by Roucoux and co-workers for the selective hydrogenation of styrene.[53]

These systems were tested in the hydrogenation of styrene at 80 °C and 40 bar of hydrogen pressure. Different combinations of the bipyridine ligand and ionic liquid were tested, obtaining high activity and high selectivity towards the totally hydrogenated product ethylcyclohexane. However, up to 85% of selectivity for ethylbenzene was obtained in some cases.

Dyson and co-workers reported a similar procedure for the synthesis of Rh nanoparticles stabilised by a combination of PVP and hydroxyl-functionalised ILs.[54] PVP-protected Rh nanoparticles were first synthesised from the rhodium chloride precursor refluxed in a mixture ethanol, water and in presence of the stabiliser, and dispersed in a range of ionic liquids (Figure 3.21).
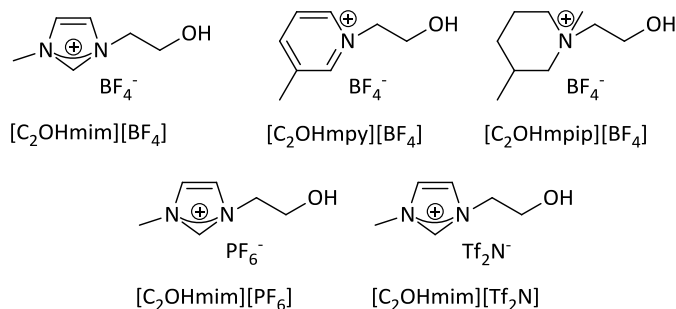
Figure 3.21 Hydroxyl- functionalised ionic liquids used in the study of Dyson and co-workers.[54]

The influence of the hydroxyl cation was evaluated in the hydrogenation of styrene using tetrafluoroborate ILs with imidazolium, pyridinium, and tetraalkyl ammonium cations. High conversions and selectivities towards ethylbenzene were obtained in almost all the cases at 40°C and 50 bar of hydrogen pressure.

The use of palladium nanoparticles for this transformation was also reported.[55] Stearic and isostearic Pd precursors were synthesised and further reduced under CO_2 and H_2 pressure in the presence of oleylamine as stabilising agent (Figure 3.22). Slightly smaller sizes were obtained with the isostearic palladium precursor *ca*. 2.4 nm vs. 3 nm for the nanoparticles obtained by the reduction of the stearic palladium precursor. Interestingly, different shapes were observed depending on the precursor used, due to the different steric hindrance of the acids.
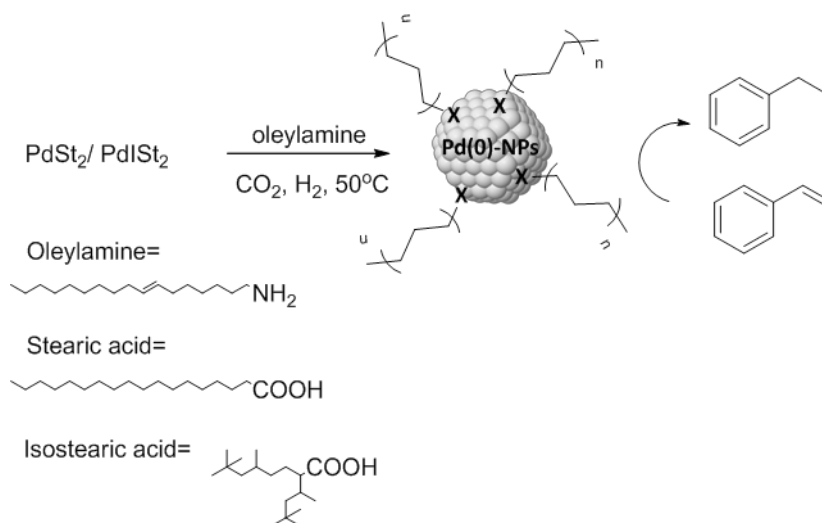
Figure 3.22 Pd NPs used in the hydrogenation of styrene.[55]

When these systems were applied to the hydrogenation of styrene, only ethylbenzene was observed in all the cases. Conversion up to 99 % was obtained at relatively short times (30min) at 50 °C and under 20 bar of hydrogen pressure.

Cis / trans selectivity

The reduction of disubstituted benzene derivatives using heterogeneous or/and nanoparticles catalysts preferentially produce *cis* cyclohexanes.[56] The *cis* selectivity is affected by the substitution pattern of the arene, the nature of the substituents, the nature of the catalyst, solvent, temperature and pressure.

The formation of the *cis* products is rationalised by addition of hydrogen to each carbon atom of the aromatic compound during a single period of adsorption onto the catalyst surface while the formation of the *trans* products can be explained by desorption of any partially reduced species

that is later re-adsorbed and hydrogenated (see mechanism in section 3.1.2).[57]

The effect of the temperature and hydrogen pressure on the stereoselectivity was investigated by Schuetz and Siegel.[58] They observed that high *cis* selectivities were achieved in the hydrogenation of a series of xylenes with increasing pressure and decreasing temperature. Such conditions favour the fast hydrogenation of the substrate and disfavour its desorption during catalysis.

In 1995, Lemaire and co-workers described a promising method for the hydrogenation of arenes using a Ru nanocatalyst stabilised by TOA under mild conditions (50 bar H_2 and room temperature).[59] This method produced excellent *cis* selectivity in the hydrogenation of a variety of *ortho*-substituted arenes. These examples also illustrated how the stereoselectivity is dependent on the nature of the substituents on the arene. It should to be noted that higher *cis* selectivities were obtained for arenes bearing electron-withdrawing substituents.

Roucoux and co- workers applied Rh, Ir and Ru-NPs stabilised by HEA-16-Cl in the hydrogenation of disubstituted arenes.[60] Their results suggested that Rh-NPs and Ru-NPs produced higher *cis* selectivities than those obtained using Ir-NPs. As previously reported, the *cis* selectivity decreases in the order *ortho> meta> para*.

The nature of the stabiliser was also shown to have an effect on the stereoselectivity of the reaction. Roucoux and co-workers also reported the application of Rh-NPs stabilised by THEA-16-Cl in the hydrogenation of *o,m,p*-xylenes obtaining lower *cis/trans* selectivities than with Rh-NPs stabilised by HEA-16-Cl (92/8, 80/20 and 66/34, respectively).[61]

Chaudret and co-workers described the application of Ru-NPs stabilised by a chiral oxazoline in the hydrogenation of *o,p*-methylanisole in MeOH as a solvent under 40 bar H_2 and 50 °C.[62] Interestingly, the *trans* product was the major stereoisomer, with a ratio *cis/trans* of 5/95 and 34/66 for *o*- and *p*-methylanisole, respectively.

The application of Rh, Ru and Ir-NPs stabilised by carbohydrate derived chiral diphosphites in the hydrogenation of *o*- and *m*-methylanisole was also reported.[63] Interestingly, all these metal-NPs only produced *cis*-1-methoxy-2-methylcyclohexane from the hydrogenation of *o*-methylanisole. For the *m*-methylanisole, Ru and Ir-NPs produced higher *cis* selectivity than the Rh-NPs. It should to be noted that slightly higher *cis/trans* selectivities were obtained when the reaction was carried out at higher pressures. No clear effect of the diphosphite structure on the *cis/trans* selectivity of the reactions was observed during this study.
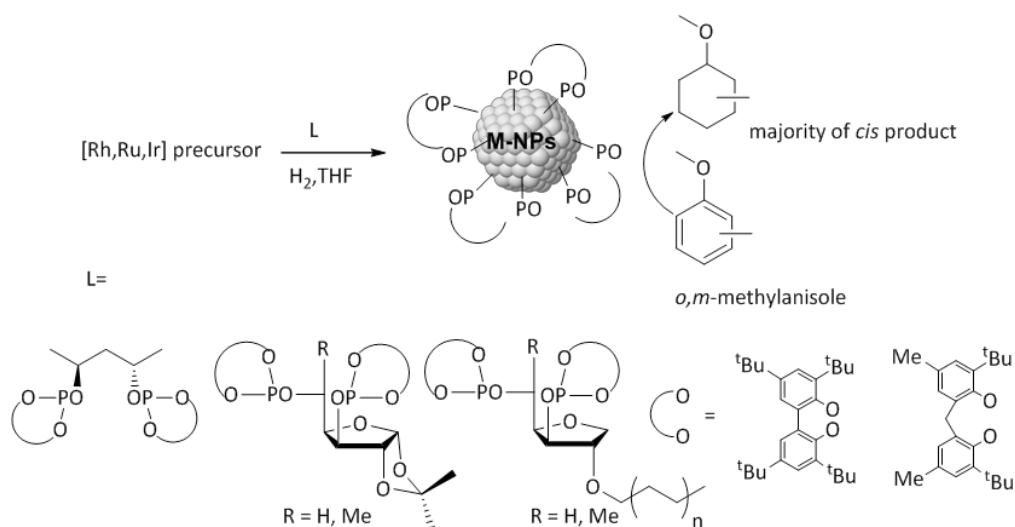
Figure 3.23 System used in our group for the hydrogenation of disubstituted arenes.[63]

3.2 Results and discussion

As previously detailed in the introduction section of this chapter, interesting results were reported a few years ago by our group using carbohydrate derived diphosphite stabilised rhodium nanoparticles in the hydrogenation of *ortho-* and *meta*-methylanisoles.[63] The structure of the ligands was shown to affect the size of the resulting nanoparticles and in turn the activity of these catalysts. In this study, no conversion was observed in THF nor in CH_3CN, whereas relevant activity was observed in pentane. This difference was explained by a competitive adsorption between the substrate and the solvent at the NPs surface, preventing the reaction.

Based on these results, heptane was used as solvent for the catalytic experiments presented here, since this solvent presents similar coordinating properties to pentane but with a higher boiling point.

3.2.1 Hydrogenation of disubstituted arenes

The main objective of this study was therefore the exploration of the catalytic activity of the rhodium nanoparticles stabilised by phosphine and phosphite ligands in the hydrogenation of disubstituted arenes. The effect of the nature of the substituent was analysed using xylenes and methylanisoles. The effect of the relative position of these substituents was also looked at through the use of the *ortho*, *meta* and *para* substituted substrates (Figure 3.24).
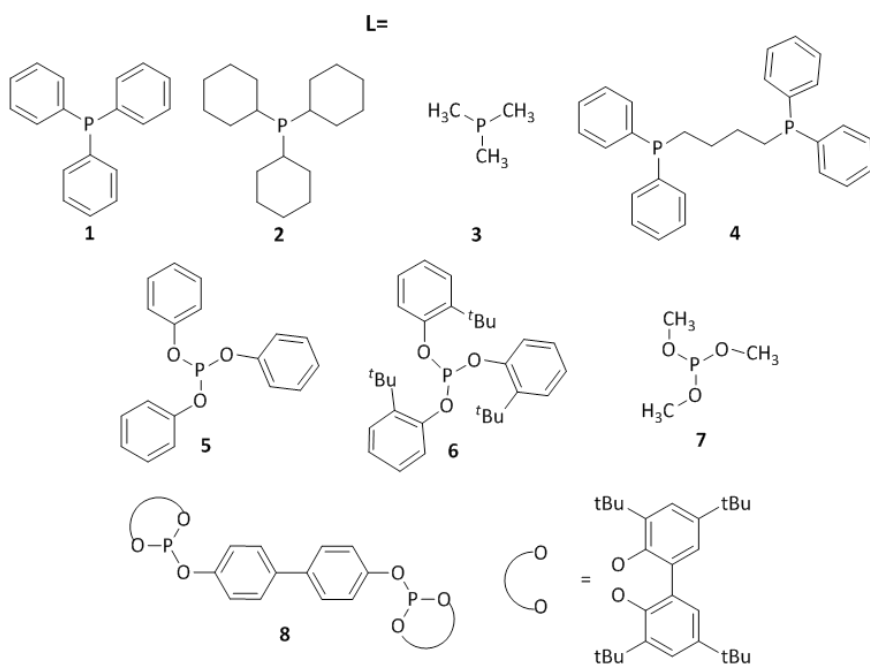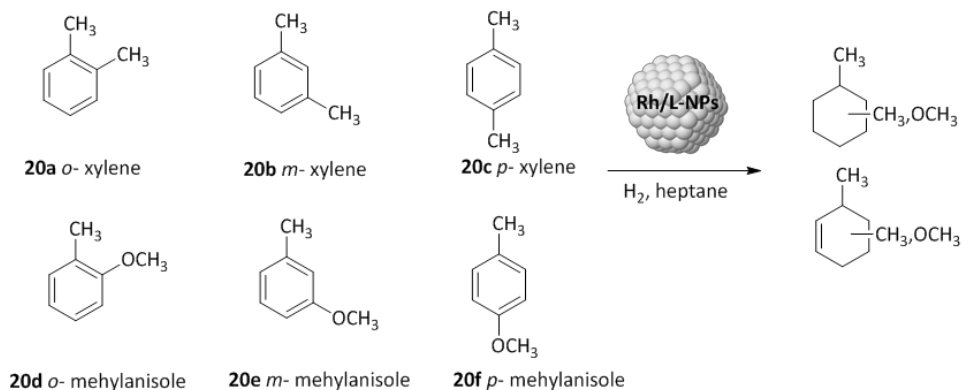
Figure 3.24 Arene substrates and P-stabilisers used in this chapter.

In the following sections, the results obtained in the hydrogenation of these substrates using the Rh-NPs **Rh1**-**Rh8** are described. Note that the catalytic experiments were performed using 2 mol% catalyst (based on the Rh surface atoms), except in the case of **Rh8** where 1 mol% catalyst was used.

197

Hydrogenation of ortho-xylene 20a and ortho-methylanisole 20d

First, the hydrogenation of *o*-xylene **20a** was performed in heptane under 40 bar of H_2 during 16h at 80 °C. The results are summarised in Table 3.1.

Table 3.1 Hydrogenation of *o*-xylene **20a** using **Rh1**-**Rh8** as catalysts.
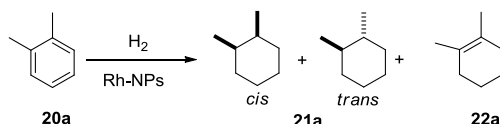
Entry	Cat.	%Conv.[b]	Cis/trans[b]	% Sel.22a[b]	TON[c]
1	**Rh1**	75	78/22	17	56
2	**Rh2**	76	72/28	4	53
3	**Rh3**	>99	76/24	-	69
4	**Rh4**	40	83/17	23	30
5	**Rh5**	0	-	-	-
6	**Rh6**	56	75/25	2	40
7	**Rh7**	50	79/21	5	36
8[b]	**Rh8**	>99	75/25	8	152

[a] General conditions: 1.24 mmol of substrate, 2 mol% of Rh-NPs, 10 mL of heptane, T = 80 °C, P= 40 bar H_2, t= 16h; [b] Determined by GC; [c]TON was defined as the number of mols of substrate converted per mol of surface Rh. The substrate/Rh ratio was calculated based on TGA data of each NP. [b] [cat]= 1 mol%

Using the phosphine stabilised nanoparticles **Rh1-Rh4** as catalysts, from moderate to excellent conversions were obtained (Entries 1-4). In all cases, the *cis/trans* selectivities were very similar (*ca*. 75/25), indicating that the properties of the stabilising ligands do not influence the *cis/trans* selectivity of this process. The highest activity was obtained using the trimethyl phosphine stabilised catalyst **Rh3** (>99%, Table 3.1, Entry 3) while the

lowest activity was observed for the catalyst **Rh4**, bearing the bidentate phosphine dppb **4** (40%, Table 3.1, Entry 4). Interestingly, in the latter case, the partially hydrogenated product dimethylcyclohexene **22a** was detected with 20% selectivity. Similar selectivity to this product was also obtained with **Rh1** (17%, Table 3.1, Entry 1) at 75% conversion. It is noteworthy that the tricyclohexylphosphine stabilised NP **Rh2** provided identical conversion than **Rh1**, but the selectivity to **22a** was very low (4%, Table 3.1, Entry2).

The activities observed can be correlated with the steric hindrance of the phosphine stabilisers since the catalyst **Rh3,** bearing by the smallest ligand of the series PMe$_3$ **3**, provided the highest conversion, followed by **Rh2** (PCy$_3$) and **Rh1** (PPh$_3$) and the lowest activity was provided by **Rh4**. It was therefore concluded that the steric hindrance induced by these ligands could restrict the coordination of the substrates at the surface of the catalysts. The low activity of the dppb **4** stabilised catalysts **Rh4** could also be due to the bidentate nature of this ligand, blocking a larger surface than the monodentate ligands and minimising the decoordination of this ligand from the Rh surface. Such a difference in activity between mono- and bidentate ligands was reported by Chaudret, van Leeuwen and co-workers for Ru-NPs in the hydrogenation of *o-* methylanisole.[37]

As could be expected, the highest selectivity to the partially hydrogenated product **22a** was obtained with the less active catalyst **Rh4**. However, the difference in selectivity observed between the catalysts **Rh1** and **Rh2**, at the same conversion is striking. As shown in Chapter 2, the catalyst **Rh1** bears mainly PCy$_2$Ph ligands (and/or the corresponding oxides) at its surface since two phenyl rings of PPh$_3$ were hydrogenated during the synthesis of the NPs and therefore only differs from the PCy$_3$ **2**-stabilised **Rh2** by the presence of a phenyl ring at P. It is therefore interesting to note that the presence of this phenyl ring provides higher selectivity to **22a**, which indicates the possible interaction of this phenyl substituent with the surface of the NP.

Next, the Rh-nanoparticles **Rh5-Rh8** stabilised by phosphite ligands were used as catalysts in this reaction (Table 3.1, Entries 5-8). Surprisingly, when **Rh5** was used as catalyst, no conversion was obtained with this substrate (Table 3.1, Entry 5). When **Rh6** and **Rh7** were probed, *ca.* 50% conversion and *ca.* 75/25 *cis/trans* selectivities were obtained (Table 3.1, Entries 6-7). In both cases, traces of product **22a** were detected. When **Rh8**, stabilised by the large diphosphite ligand **8**, was used as substrate, total conversion was measured with 80% *cis* selectivity and 8% selectivity to **22a**.

From these results, no clear conclusions could be drawn on the effect of the stabilising ligands on the activity and *cis/ trans* selectivity of the nanocatalysts in this reaction. The lack of activity observed in the case the P(OPh)$_3$-**5**-stabilised Rh-NPs **Rh5** could be due the crowding of the surface of these NPs by the ligands (Chapter 2, section 2.2.2).

Additionally, in contrast with the results obtained with **Rh4** stabilised by dppb **4** which provided lower activity in this reaction than the catalysts stabilised by monophosphine ligands, the NPs **Rh8** stabilised by the diphosphite ligand **8** provided the highest activity of the series **Rh5-Rh8** stabilised by phosphites. This could indicate that ligand **8** is coordinated in a monodentate manner while dppb **4** is forming a chelate at the NPs surface.

When *ortho*-methylanisole **20d** was used as a substrate under the same conditions, similar results were obtained although in this case, higher activities were obtained for the catalysts stabilised by phosphine ligands (Table 3.2). When the monophosphine stabilised NPs **Rh1-Rh3** were used, total conversion was obtained in all cases. In contrast, 40% conversion was obtained when **Rh4** was tested, which again indicated that the coordination of the arene substrate onto this catalyst is disfavoured compared to that on catalysts bearing monodentate stabilisers.

Table 3.2 Hydrogenation of *o*-methylanisole **20d** using **Rh1**-**Rh8** as catalysts.
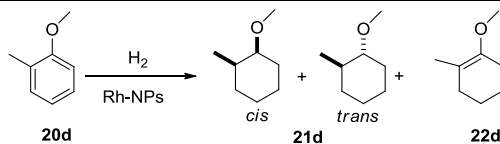
Entry	Cat.	%Conv.[b]	Cis/trans[b]	% Sel.22d[b]	TON[c]
1	**Rh1**	>99	98/2	-	74
2	**Rh2**	>99	80/20	-	69
3	**Rh3**	>99	90/10	-	69
4	**Rh4**	40	>99	-	30
5	**Rh5**	0	-	-	-
6	**Rh6**	33	91/9	8	23
7	**Rh7**	15	90/10	-	11
8[b]	**Rh8**	35	>99	36	54

[a] General conditions: 1.24 mmol of substrate, 2 mol% of Rh-NPs, 10 mL of heptane, T = 80 °C, P= 40 bar H_2, t= 16h; [b] Determined by GC; [c]TON was defined as the number of mols of substrate (**1a-f**) converted per mol of surface Rh. The substrate/Rh ratio was calculated based on TGA data of each NP. [b] [cat]= 1 mol%

Using this substrate, higher *cis* selectivities were obtained (>90%, Table 3.2) than for *ortho*-xylene (*ca*. 70-80%, Table 3.2). With *o*-methylanisole **20d** as substrate, **Rh1** and **Rh4** provided total selectivity to the *cis* product (Table 3.2, Entries 1 and 4,) while the lowest value (80%) was obtained with **Rh2**. Again, a significant difference was observed between systems **Rh1** and **Rh2** that only differ by the presence of a phenyl group at P for the system stabilised with triphenylphosphine **1**.

In this reaction, no conversion of the substrate **20d** was observed when **Rh5** was used as catalyst (Table 3.2, Entry 5) while low to moderate activities were obtained with **Rh6**-**Rh8** (Table 3.2, Entries 6-8). The lowest conversion was obtained with **Rh7** as catalyst (15%). In terms of *cis* selectivity, excellent results (>90%) were obtained using the phosphite stabilised NPs **Rh6-Rh8**. However, no clear correlation between the steric hindrance of the ligands and the activity / selectivity could be deduced from these experiments.

The lower activities observed using **Rh5-Rh8** compared to the phosphine stabilised catalysts **Rh1-Rh4** could be explained by the stronger coordination of phosphite ligands at the surface of **Rh5-Rh8**, which would limit the decoordination of these stabilising agents, and as such disfavour the coordination of the substrate. In the case of phosphines, which present less electron withdrawing properties, the decoordination from a low oxidation state metal atom(s) could be expected to be favoured compared to phosphite ligands.

To summarise, the general trends observed in the hydrogenation of the ortho-substituted substrates **20a** and **20d** are:

- In the hydrogenation of **20d**, the phosphine stabilised catalysts **Rh1**-**Rh4** were more active than their phosphite counterparts **Rh5**-**Rh8** (Table 3.2) while no relevant differences were observed when **20a** was the substrate (Table 3.1). This could be attributed to the higher steric hindrance induced by **20d**, which makes it coordination more sensitive to the surrounding ligands at the surface of the NP.

- The dppb **4** stabilised NPs **Rh4** was the less active of the NP stabilised by phosphine ligands, which was attributed to the bidentate coordination and/or the steric hindrance induced by the ligand.

- The partially hydrogenated products **22a** and **22d** were detected in both sets of experiments. The highest selectivities to these products were achieved with **Rh4** in the case of *o*-xylene (23%) while 38% was achieved using the catalyst **Rh8** when *o*-methylanisole **20d** was the substrate.

- In terms of *cis* selectivity, no relevant variations were observed when these catalysts were used, indicating that the properties of the stabilising ligands do not influence the *cis* selectivity of this reaction. However, higher selectivity was obtained for the *o*-methylanisole **20d** than for *o*-xylene **20a**, indicating that the nature of the substituent on the substrate is the parameter that mainly affects the *cis* selectivity under these conditions.

Hydrogenation of meta-xylene 20b and meta-methylanisole 20e

The results obtained in the hydrogenation of *meta*-xylene **20b** are summarised in Table 3.3.

When the phosphine stabilised catalysts **Rh1**-**Rh4** were tested in the hydrogenation of this substrate (Table 3.3, Entries 1-4), high conversions were obtained in all cases. The **Rh1** catalyst provided excellent *cis* selectivity (95%) and 11% of partially hydrogenated product **22b** while **Rh2**-**Rh4** afforded *ca*. 70% *cis* product.

Using the phosphite stabilised catalysts **Rh5**-**Rh8**, lower activities were observed than for **Rh1-Rh4** and *ca*. 70% *cis* selectivity was obtained in all cases (Table 3.3, Entries 5-8). It should be noted that no conversion was again observed for the reaction catalysed by **Rh5**. In the reaction catalysed by **Rh8**, 15 % of partially hydrogenated **22b** was obtained.

The lower activities of the phosphite stabilised NPs Rh-NPs were again related to the stronger coordinating character of these ligands compared to phosphine, yielding a more crowded surface in solution.

Table 3.3 Hydrogenation of *m*-xylene **20b** using **Rh1**-**Rh8** as catalysts.
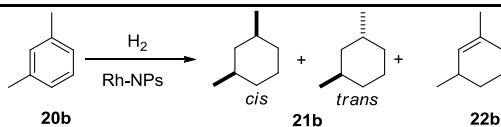
Entry	Cat.	%Conv.[b]	Cis/trans[b]	% Sel.22b[b]	TON[c]
1	**Rh1**	78	95/5	11	58
2	**Rh2**	85	69/31	-	60
3	**Rh3**	>99	70/30	-	69
4	**Rh4**	74	67/33	6	71
5	**Rh5**	0	-	-	-
6	**Rh6**	14	67/33	-	10
7	**Rh7**	48	70/30	-	34
8[b]	**Rh8**	51	75/25	15	78

[a] General conditions: 1.24 mmol of substrate, 2 mol% of Rh-NPs, 10 mL of heptane, T = 80 °C, P= 40 bar H_2, t= 16h; [b] Determined by GC; [c]TON was defined as the number of mol of substrate (**1a-f**) converted per mol of surface Rh. The substrate/Rh ratio was calculated based on TGA data of each NP. [b] [cat]= 1 mol%

When *meta*-methylanisole **20e** was used as substrate (Table 3.4), the same trends were observed. The phosphine stabilised Rh-NP **Rh1-Rh4** (Table 3.4, Entries 1-4) provided higher activities than their phosphite counterparts **Rh5-Rh8** (Table 3.4, Entries 5-8) and within the series **Rh1-Rh4**, the **Rh4** catalyst stabilised by dppb **4** was the less active (Table 3.4, Entry 4 vs Entries1-3). The triphenylphosphite stabilised NP **Rh5** was inactive in this reaction (Table 3.4, Entry 5) while **Rh6** stabilised by P(OMe)$_3$ **6** and **Rh8** bearing the diphosphite **8** provided *ca*. 40% conversion. With this latter catalyst, 39% selectivity to the partially hydrogenated product **22e** was obtained with this substrate.

Interestingly, the *cis* selectivity in these experiments revealed lower (*ca.* 50-70%) than that obtained for *meta*-xylene **20b** as substrate (*ca.* 70-95%). This is in contrast with the results obtained in the hydrogenation of the ortho-substituted substrates **20a** and **20d** where higher *cis* selectivity was observed for the methylanisole substrate **20d**.

Table 3.4 Hydrogenation of *m*-methylanisole **20e** using **Rh1**-**Rh8** as catalysts.

Entry	Cat.	%Conv.[b]	Cis/trans[b]	% Sel.22e[b]	TON[c]
1	**Rh1**	>99	58/42	-	74
2	**Rh2**	>99	56/44	-	69
3	**Rh3**	>99	55/45	-	69
4	**Rh4**	19	63/37	-	14
5	**Rh5**	0	-	-	-
6	**Rh6**	37	51/49	4	26
7	**Rh7**	19	50/50	-	14
8[b]	**Rh8**	38	68/32	39	58

[a] General conditions: 1.24 mmol of substrate, 2 mol% of Rh-NPs, 10 mL of heptane, T = 80 °C, P= 40 bar H_2, t= 16h; [b] Determined by GC; [c]TON was defined as the number of mol of substrate converted per mol of surface Rh. The substrate/Rh ratio was calculated based on TGA data of each NP. [b] [cat]= 1 mol%

To summarise, the general trends observed in the hydrogenation of meta-substituted substrates **20b** and **20e** are:

- The phosphine stabilised catalysts **Rh1**-**Rh4** were more active than their phosphite counterparts **Rh5**-**Rh8**. This was attributed to the stronger coordination of the phosphite ligands thus disfavouring the decoordination of the stabilisers under catalytic conditions and consequently blocking the active sites at the surface of the NPs.
- The dppb stabilised NPs **Rh4** was the less active of the NP stabilised by phosphine ligands, which was attributed to the bidentate coordination and/or steric hindrance induced by the ligand.
- The catalyst **Rh8** provided the highest selectivity to the partially hydrogenated products **22b** and **22d** (15% and 39%, respectively).
- In terms of *cis* selectivity, no relevant variations were observed when these catalysts were used, indicating that the properties of the stabilising ligands do not influence the *cis* selectivity of this reaction. However, higher selectivity was obtained for *meta*-xylene than for *meta*-methylanisole, indicating that the nature of the substituent on the substrate is the parameter that mainly affects the *cis* selectivity under these conditions.

Hydrogenation of para-xylene 20c and para-methylanisole 20f

Next, the hydrogenation of *p*-xylene **20c** was performed under the same conditions (in heptane under 40 bar of H_2 during 16h at 80°C). The results are summarised in Table 3.5.

With this substrate, low to moderate activities were obtained in all cases, except for **Rh5** which was again inactive (Table 3.5). In these experiments, no relevant differences in activity were observed using the catalysts bearing phosphines (Table 3.5, Entries 1-4) and those stabilised by phosphites (Table 3.5, Entries 6-8). However, it is noteworthy that within these series of catalysts, slightly higher activities were observed with the NPs bearing the less sterically hindered ligands of the series **Rh3** (PMe_3) (Table 3.5, Entry 3) and **Rh6** ($P(OMe)_3$) (Table 3.5, Entry 6). Once again, the NPs stabilised by the bidentate ligand dppb **4** provided the lowest activity of the series **Rh1**-

Rh4 while the highest selectivity to the hydrogenated product **22c** (22%, Table 3.5, Entry 8) was obtained with those stabilised by the diphosphite **8**. No significant differences in terms of *cis/trans* selectivity were observed across these series with values of *ca*. 60/40 obtained with all catalysts.

Table 3.5 Hydrogenation of *p*-xylene **20c** using **Rh1**-**Rh8** as catalysts.

Entry	Cat.	%Conv.[b]	Cis/trans[b]	% Sel.22c[b]	TON[c]
1	**Rh1**	37	55/45	8	27
2	**Rh2**	47	57/43	-	46
3	**Rh3**	50	58/42	3	35
4	**Rh4**	25	65/35	-	19
5	**Rh5**	0	-	-	-
6	**Rh6**	52	58/42	-	37
7	**Rh7**	25	62/38	2	18
8[b]	**Rh8**	36	67/33	22	55

[a]General conditions: 1.24 mmol of substrate, 2 mol% of Rh-NPs, 10 mL of heptane, T = 80 °C, P= 40 bar H_2, t= 16h; [b] Determined by GC; [c]TON was defined as the number of mols of substrate converted per mol of surface Rh. The substrate/Rh ratio was calculated based on TGA data of each NP. [b] [cat]= 1 mol%

Similar trend was observed in the hydrogenation of *p*-methylanisole **20f** (Table 3.6), although slightly higher *cis* selectivities (*ca*. 70/30) were measured with this substrate. In contrast with the results with *p*-xylene **20c**,

in this case, the NPs stabilised with phosphine ligands (Table 3.6, Entries 1-4) were more active than their phosphite counterparts (Table 3.6, Entries 6-8). However, several trends remained unchanged: the catalyst **Rh4** provided the lowest activity of the series **Rh1-Rh4** (Table 3.6, Entry 4 vs entries 1-3), **Rh5** was inactive in this reaction (Table 3.6, Entry 5) and **Rh8** provided the highest selectivity to the partially hydrogenated **22f** (21%, Table 3.6, Entry 8).

Table 3.6 Hydrogenation of *p*-metylanisole **20f** using **Rh1-Rh8** as catalysts.

Entry	Cat.	%Conv.[b]	Cis/trans[b]	% Sel.22f[b]	TON[c]
1	**Rh1**	>99	66/34	-	74
2	**Rh2**	>99	69/31	-	69
3	**Rh3**	>99	65/35	-	69
4	**Rh4**	32	71/29	-	24
5	**Rh5**	0	-	-	-
6	**Rh6**	33	70/30	5	23
7	**Rh7**	38	70/30	-	19
8[b]	**Rh8**	49	71/29	21	75

[a]General conditions: 1.24 mmol of substrate, 2 mol% of Rh-NPs, 10 mL of heptane, T = 80 °C, P= 40 bar H_2, t= 16h; [b] Determined by GC; [c]TON was defined as the number of mols of substrate converted per mol of surface Rh. The substrate/Rh ratio was calculated based on elemental analysis data of each NP. [b] [cat]= 1 mol%

To summarise, the general trends observed in the hydrogenation of the *para*-substituted substrates **20c** and **20f** are:

- In the hydrogenation of **20f**, the phosphine stabilised catalysts **Rh1**-**Rh4** were more active than their phosphite counterparts **Rh5**-**Rh8** (Table 3.5) while no relevant differences were observed when **20c** was the substrate (Table 3.5). This could be attributed to the higher steric hindrance induced by **20d**, which makes its coordination more sensitive to the surrounding ligands at the surface of the NP.

- The dppb **4** stabilised NPs **Rh4** was the less active catalyst of the NP stabilised by phosphines, which was attributed to the bidentate coordination and/or steric hindrance induced by the ligand.

- Partially hydrogenated products **22c** and **22f** were detected in both sets of experiments and the highest selectivities were achieved with the catalyst **Rh8** with similar values for both substrates (*ca.* 20%).

- In terms of *cis* selectivity, no relevant variations were observed when these catalysts were used, indicating that the properties of the stabilising ligands do not influence the *cis* selectivity of this reaction. However, higher selectivity was obtained for the *o*-methylanisole than for *o*-xylene, indicating that the nature of the substituent on the substrate is the parameter that mainly affects the *cis* selectivity under these conditions.

Hydrogenation of xylenes and methylanisoles: conclusions

From the results obtained in the hydrogenation of the disubstituted substrates **20a**-**20f** using the nanocatalysts **Rh1**-**Rh8**, the following conclusions can be drawn:

- The phosphine stabilised catalysts **Rh1**-**Rh4** were in general more active than their phosphite counterparts **Rh5**-**Rh8**. This was attributed to the stronger coordination of the phosphite ligands thus disfavouring the

decoordination of the stabilisers under catalytic conditions and consequently blocking the active sites at the surface of the NPs.

• Within these series of phosphine and phosphite stabilised Rh-NPs, the highest activities were obtained in most cases using the less sterically hindered stabilisers PMe_3 and $P(OMe)_3$. This might be attributed to more accessible active sites at the surface of the catalysts due to lower steric hindrance at the surface or to the weaker coordination of the ligands, thus favouring their decoordination/substitution by the substrate.

•The dppb stabilised NPs **Rh4** was the less active of the NP stabilised by phosphine ligands, which was attributed to the bidentate coordination of the ligand. Such a trend was not observed in the case of the diphosphite **8**, which could indicate that this ligand does not coordinate in a bidentate manner at the surface of the NP.

•The catalyst **Rh8** provided in most cases (except for *o*-xylene **20a**) the highest selectivity to the partially hydrogenated products **22**.

• In terms of *cis* selectivity, no relevant variations were observed when these catalysts were used, indicating that the properties of the stabilising ligands do not influence the *cis* selectivity of this reaction. However, differences were observed depending on the nature and situation of the substituents on the substrates. For xylenes **20a-c**, the formation of *cis* products followed the trend *ortho> meta> para*. However, for methylanisoles **20d-f**, the lowest selectivity was observed for the *meta* substrate.

Comparing the results obtained with xylenes **20a-c** and methylanisoles **20d-f**:

• Using the phosphine stabilised catalysts **Rh1**-**Rh4**, higher activities were obtained when methylanisoles were the substrates than when xylenes were hydrogenated. However, this trend was not observed with the phosphite stabilised catalysts. Therefore, no clear conclusions could be drawn.

•In terms of selectivity to the partially hydrogenated products **3a-f**, comparing the results obtained with **Rh8** as catalyst, higher values were obtained using the methylanisole substrates, probably due to the higher steric hindrance induced by the methoxy group. In the case of *para*-substituted substrates, however, similar values were obtained (*ca*. 20%)

Optimisation of reaction conditions for the partial hydrogenation of disubstituted arenes using Rh8 NPs as catalyst.

In view of the results obtained with the catalyst **Rh8** in terms of selectivity to the partially hydrogenated products **22**, the optimisation of several parameters (Temperature, pressure, etc..) was performed using *p*-xylene **20c** as model substrate.

a) Temperature optimisation

The reaction was carried out under 40 bar of hydrogen pressure during 16h and heptane as solvent. When the temperature was increased from 60°C to 120°C, a decrease in conversion from 51% to 15% was observed whereas the selectivity towards the partially hydrogenated product increased from 6% to 32% (Figure 3.25).

These results indicated that the adsorption of both the substrate and the cyclohexene derivative product from the NP surface is not favoured by increased temperature, thus lowering the conversion and increasing the selectivity to the partial hydrogenation product, as previously reported for heterogeneous catalyst.[64]
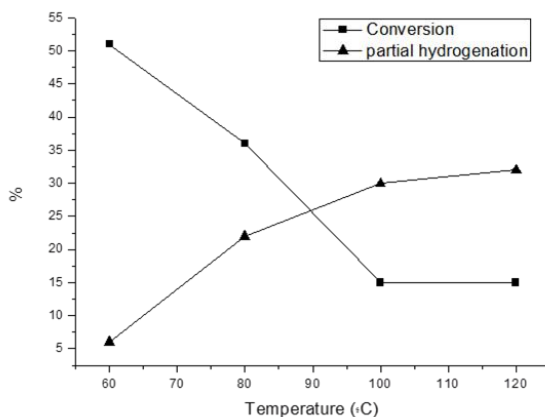
Figure 3.25 Effect of temperature in the partial hydrogenation of *p*-xylene **20c** using **Rh8** as catalyst (General conditions: 1.24 mmol of substrate, 3.5 mg of Rh-NPs, 10 mL of heptane, t=16h; P= 40 bar H_2).

After these tests, the reaction temperature was maintained to 80°C since it corresponded to the best correlation between conversion and amount of partial hydrogenated product.

b) Pressure optimisation

At 80°C, when the pressure was increased from 3 to 40 bar of H_2, the conversion increased from 7% to 36%. Interestingly, the selectivity for the partially hydrogenated product was also improved and reached a maximum of 27% at 20 bar H_2, but decreased again when 40 bar of H_2 pressure was used.

It is accepted that hydrogenation of aromatics occurs in a consecutive manner and hydrogen pressure affects the different steps of aromatic ring hydrogenation in different ways (Figure 3.26). Odenbrand and Lundin reported that the hydrogenation of cyclohexenes to cyclohexanes is less dependent on H_2 pressure than the hydrogenation of aromatics to cyclohexenes.[65] Here, increasing the hydrogen pressure might increase more the rate for aromatic ring hydrogenation to cyclohexene than that for

cyclohexene hydrogenation to cyclohexane, resulting in the higher selectivity for cyclohexene. However, when the pressure is further increased, both rates are higher, which results in a higher yield of total hydrogenation.
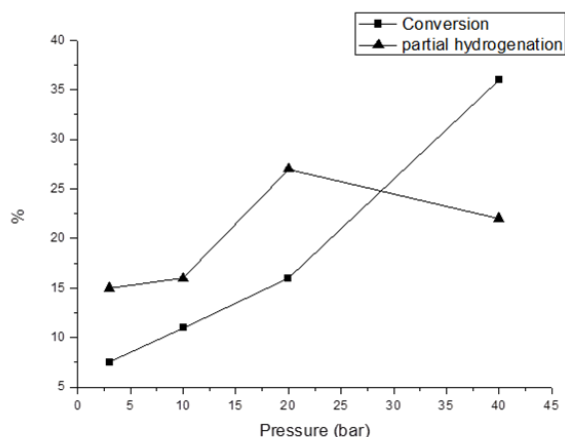
Figure 3.26 Effect of the pressure in the partial hydrogenation of *p*-xylene **20c** using **Rh8** as catalyst (General conditions: 1.24 mmol of substrate, 3.5 mg of Rh-NPs, 10 mL of heptane, t=16h, T= 80 °C).

c) Other experiments: use of water and addition of ligand

Addition of water

Various strategies were reported to favour the formation of partially hydrogenated products, such as the use of additives or the modification of the solvent systems.[66]

In this work, experiments involving the addition of water to the reaction medium, and the use of water as solvent were carried out and the results are summarised in Table 3.7.

First, the reaction was performed after the addition of 1ml of water to the catalytic mixture (Table 3.7, entry2). Under these biphasic conditions, a decrease in conversion and in selectivity for the partial hydrogenated

product **22c** was observed. However, the *cis/ trans* selectivity remained unchanged.

When the reaction was performed with water as solvent, almost full conversion for the hydrogenation of *p*-xylene **20c** was obtained (Table 3.7, entry 3). However, the partial hydrogenated product **22c** was not detected under these conditions and no significant changes in the *cis/ trans* selectivity (70/30) was observed.

Table 3.7 Rh-NPs (**Rh8**) catalysed the hydrogenation of *p*-xylene (**20c**)

Entry	Solvent	L	%Conv.[b]	Cis/trans[b]	% Sel.22c[b]
1	Heptane	-	36	67/33	22
2	Heptane/H$_2$O*	-	26	67/33	16
3	H$_2$O	-	97	70/30	-
4	Heptane	0.1eq	12	61/39	12
5	Heptane	0.2eq	0	-	-

[a] General conditions: 1.24 mmol of *p*- xylene, 1 mol% of Rh-NPs, 10 mL of heptane, T = 80 °C, P= 40 bar H$_2$, t= 16h; [b] Determined by GC; * 9ml heptane/ 1ml H$_2$O.

As the use of water did not produce the expected results of increasing the amount of partial hydrogenated product, this strategy was not followed for further experiments.

Next, the addition of free ligand to the reaction medium was explored. In Table 3.7 the results corresponding to the reaction without addition of free ligand, compared to the addition of 0.1 and 0.2 equivalents are presented. The addition of free diphosphite ligand leads to a decrease in activity, conversion of 12% was obtained adding 0.1 equivalent of the ligand (entry 4) and no activity (entry 5) was obtained when 0.2 equivalent was added. This could be explained by a competition between the free ligand and the

substrate, thus blocking the active sites of the catalyst. No improvement of the selectivity to partial hydrogenated product was observed during these experiments.

To summarise, increasing the reaction temperature led to an improvement in the selectivity for partially hydrogenated product although a drop in activity was observed under these conditions. A hydrogen pressure of 20 bar during the reaction provided the highest selectivity to the cyclohexene derivative. However, the addition of water or ligand as additives did not improve their selectivity for this product.

Catalytic hydrogenation of p-xylene using Rh-nanoparticles stabilised by THF/MeOH mixtures (Rh17, Rh18 and Rh19)

To study the effect of the P- based stabilisers for the hydrogenation of disubstituted arenes, the nanoparticles stabilised by solvent mixture THF/MeOH **Rh17** were used as catalyst under the same conditions of solvent, pressure and temperature than for the previous studies.

Surprisingly, when the system **Rh17** was used as catalyst, no activity was obtained using the disubstituted arenes **20a**- **20f** as substrates. As explained in Chapter2, these nanoparticles showed a smaller size, 1.21nm than the P-based **Rh1**-**Rh8** nanoparticles (*ca.* 1.5nm). These catalytic results indicated that either the substitution of P-donor stabilisers at the surface of these NPs by THF/MeOH or their smaller size was inhibiting the hydrogenation reaction.

To distinguish between these two possibilities, the seeded growth method (see chapter2) was applied to synthesise the nanoparticles of larger size **Rh18** and **Rh19** (1.89±0.35 and 2.5±0.33 nm of diameter, respectively). When these systems were applied in the hydrogenation of *p*-xylene **20c** under the same conditions, no catalytic activity was observed. It was therefore concluded that the presence of the P-donor stabilising agents **1-8**

in the systems **Rh1-Rh8** somehow provides activity in this reaction and/or that substitution of these by the mixture of THF and MeOH molecules has an inhibiting effect on their catalytic performance.

Catalytic test using the heterogeneous catalyst Rh/C

For comparative purposes, the heterogeneous rhodium on carbon Rh/C was used as catalyst in the hydrogenation of disubstituted arenes **20a**- **20f**, under the same conditions than for the Rh-NPs.

From high to excellent conversions were obtained in all the cases using substrates **20a-20f**. The same *cis*/ *trans* selectivity (76/24) was detected using *ortho* and *meta* substituted xylenes **20a** and **20b** (Table 3.8, entries 1,2). However, a slight decrease in *cis* selectivity was observed when *p*-xylene **20c** was used as substrate (Table 3.8, entry3).

Moreover, methylanisoles were also employed as substrates. When the reaction was carried out with *o*-methylanisole **20d**, high selectivity to the *cis* product was obtained (Table 3.8, entry4), while this selectivity decrease (66%) using *m*-methylanisole **20e** as substrate, and again a decrease in selectivity was observed using *p*-methylanisole **20f** (51%) (Table 3.8, entry6).

Using Rh/C as catalyst, full conversion was obtained in all the cases, except for *o*-xylene **20a** (80%, Entry 1). No clear effect of the position or nature of the substrates substituents was detected, however, the highest selectivity was observed using *o*-methylanisole **20d** in agreement with previous observations using Rh- NPs systems **Rh1**-**Rh8**. No partial hydrogenation product was detected using Rh/C as catalyst, although reaction should be performed with lower catalyst loading and/or reaction time, to observed the possible formation of this product at low conversion values.

Table 3.8 Rh/C catalysed the hydrogenation of *o*-,*m*- ,*p*-xylene (**20a-c**) and *o*-,*m*- ,*p*-methylanisole (**20d-f**).

R= CH$_3$: *ortho*- (**20a**), *meta*- (**20b**) and *para*-xylene (**20c**)

R= OCH$_3$: *ortho*- (**20d**), *meta*- (**20e**) and *para*-methylanisole (**20f**).
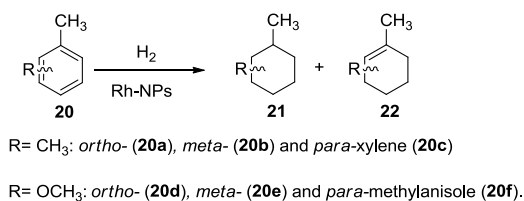
Entry	Substrate	%Conv.[b]	Cis/trans[b]	% Sel.22[b]	TON[c]
1	**20a**	80	76/24	-	82
2	**20b**	100	76/24	-	102
3	**20c**	100	68/32	-	102
4	**20d**	100	95/5	-	102
5	**20e**	100	66/34	-	102
6	**20f**	100	51/49	-	102

[a]General conditions: 1.24 mmol of substrate, 1mol% of Rh/C, 10 mL of heptane, T = 80 °C, P= 40 bar H2, t= 16h; [b] Determined by GC; [c]TON was defined as the number of mol of substrate (**20a-f**) converted per mol of surface Rh. The substrate/Rh ratio was calculated based on elemental analysis data of each NP.

3.2.2 Hydrogenation of monosubstituted arenes

Hydrogenation of styrene

In this study, 3.5mg of nanoparticles (**Rh1, Rh4, Rh5, Rh8** and **Rh17)** was used, which correspond to approximately 2mol% for the systems **Rh1**, **Rh4**, **Rh5** and **Rh17** and 1 mol% for system **Rh8**.

When the catalytic reactions were performed at 80 °C (Table 3.9), full conversions were obtained with all the systems after 1h. In most cases, the selectivity for the total hydrogenation product **24** increased once the vinylic group was reduced. Interestingly, under these conditions, the aromatic ring of styrene was hydrogenated even using the **Rh17** system, which was totally inactive in the hydrogenation of *p*-xylene at 80 °C (Table 3.9, Entries 9 and 10).

Table 3.9 Rh-NPs catalysed the hydrogenation of styrene **23** at 80 °C

entry	t (h)	NPs	%Conv.[b]	%24 [b]	%25[b]	%26 [b]	TON[c]
1	1	**Rh1**	100	27	0	73	74
2	16	**Rh1**	100	65	18	17	74
3	1	**Rh4**	100	29	0	71	76
4	16	**Rh4**	100	100	0	0	76
5	1	**Rh5**	100	2	0	98	94
6	16	**Rh5**	100	3	0	97	94
7	1	**Rh8**	100	67	9	24	157
8	16	**Rh8**	100	76	16	8	157
9	1	**Rh17**	100	14	8	78	99
10	16	**Rh17**	100	91	3	5	99

[a]General conditions: 3.5 mg of Rh-NPs, 1.24 mmol of styrene, 10 mL of heptane, T = 80 °C, P= 40 bar H_2; [b]Determined by GC; [c]TON was defined as the number of mols of substrate (**23**) converted per mol of surface Rh .

This result suggests that increased steric hindrance in the case of the xylene substrate was inhibiting the reaction. In contrast, total selectivity for ethylbenzene **26** was achieved using **Rh5** as catalyst (Table 3.9, Entries 3

and 4), even after 16h of reaction time, suggesting that the monophosphite ligand **5** efficiently blocks the coordination sites of the Rh-NPs required for the hydrogenation of the aromatic ring of styrene. Under these conditions, yields of up to 18% of partial hydrogenation products were detected when **Rh1** or **Rh8** were employed. It is noteworthy that these values were obtained at complete conversion of the substrate. The higher activities obtained with styrene can be explained by the lower steric hindrance associated with the presence of only one substituent on the aromatic ring.

To obtain selectivity data at lower conversions, the reaction was performed at ambient temperature using a much larger ratio of substrate to Rh (54 mmol of styrene, 1:1 volume ratio with heptane) (Table 3.10). In all cases, ethylbenzene **26** was the major reaction product. No partial hydrogenation products were detected when the reaction was performed at this temperature, in agreement with the results presented in the previous sections where the temperature was optimised with the disubstituted arenes **20a**-**20f** as substrates. After 15 minutes of reaction time, conversions between 5 and 65% were obtained with total selectivity for ethylbenzene **26**, corresponding to TOFs up to *ca.* 13039 h^{-1} using **Rh8** (Table 3.10, entry 10). **Rh5**, stabilised by P(OPh)$_3$ **5**, was once again the least active catalyst: after 16h at this temperature, the totally hydrogenated product **24** was detected in all cases except for this catalyst (Table 3.10, entry 9). These results clearly show that the properties of the stabilising ligand affects the catalytic performance of these highly active nanocatalysts.

Table 3.10 Rh-NPs (**Rh1**-**Rh4**) catalysed the hydrogenation of styrene **23** at RT.

entry	t (h)	NPs	%Conv.[b]	%24[b]	%26[b]	TON[c]	TOF[c] (h^{-1})
1	0.25	**Rh1**	27	0	100	904	3618
2	1	**Rh1**	100	8	92	3350	-
3	16	**Rh1**	100	15	85	3350	-
4	0.25	**Rh4**	23	0	100	782	3130
5	1	**Rh4**	54	0	100	1837	1837
6	16	**Rh4**	100	2	98	3402	-
7	0.25	**Rh5**	5	0	100	211	842
8	1	**Rh5**	24	0	100	1011	1011
9	16	**Rh5**	84	0	100	3538	-
10	0.25	**Rh8**	46	0	100	3260	13039
11	1	**Rh8**	100	0	100	7087	-
12	16	**Rh8**	100	11	89	7087	-
13	0.25	**Rh17**	65	0	100	2886	11546
14	1	**Rh17**	100	0	100	4440	-
15	16	**Rh17**	100	21	79	4440	-

[a]General conditions: 3.5 mg of Rh-NPs, 54 mmol of styrene (5 mL), 5mL of heptane, T = RT, P= 40 bar H_2; [b]Determined by GC; [c]TON was defined as the mol substrate (**23**) converted per mol of surface Rh. TOF was calculated at styrene conversions lower than 65% and it is defined as the mol substrate (**23**) converted per mol of surface Rh per hour. The substrate/Rh ratio was calculated based on TGA analysis data of each NP.

To investigate further the triphenylphosphite system **Rh5**, which provided interesting selectivity to ethylbenzene and was inactive in the hydrogenation of disubstituted arenes, the series of NPs **Rh5-0.1-Rh5-0.6**,

which present distinct ligand coverage, were tested as catalysts in the hydrogenation of styrene at 80 °C during 16h. The results are summarised in Table 3.11. The partially hydrogenated product **25** was not detected in any of these experiments.

In all experiments, full conversion of the substrate was observed. However, the selectivity for ethylbenzene **26** or for the fully hydrogenated product ethylcyclohexane 24 revealed to be strongly affected by the ligand coverage on these catalysts. Indeed, the selectivity to ethylbenzene **26** was observed to steadily increase when the ligand coverage on the catalyst was increased and reach 100% selectivity when **Rh5-0.6** was used. It was therefore concluded that at high ligand coverage, the sites responsible for the hydrogenation of arenes are occupied by the stabilizer and thus, only the vinyl unit of the substrate can be hydrogenated.

Table 3.11 Catalytic hydrogenation of styrene **23** using **Rh5-0.1-Rh5-0.6**

entry	NPs	%Conv.	%24	%26
1	**Rh5-0.1**	100	73	26
2	**Rh5-0.2**	100	13	87
3	**Rh5-0.4**	100	3	97
4	**Rh5-0.6**	100	0	100

[a] General conditions: 1.24 mmol of substrate, 2 mol% of Rh-NPs, 10 mL of heptane, T = 80 °C, P= 40 bar H_2, t= 16h; [b] Determined by GC.

As described in Chapter 2 (see Section 2.2.8, p. 142), CO adsorption-Infra-red spectroscopy experiments showed that the edges of these NPs were occupied by the ligands at high phosphite coverage while these sites were available for CO adsorption at low ligand coverage, such as in **Rh5-0.1** and to a lesser extent **Rh5-0.2**. A correlation could therefore be deduced between the availability of the edge sites of the NPs and their ability to hydrogenate the aromatic ring of the substrate. However, it was deduced from CO adsorption – IR analysis of the systems **Rh3** and **Rh7**, bearing the ligands PMe$_3$ and P(OMe)$_3$ respectively, that the edge sites of these NPs are occupied by these small stabilizers and both systems were observed to be highly active in the hydrogenation of disubstituted arenes. No clear correlation could therefore be deduced from these results.
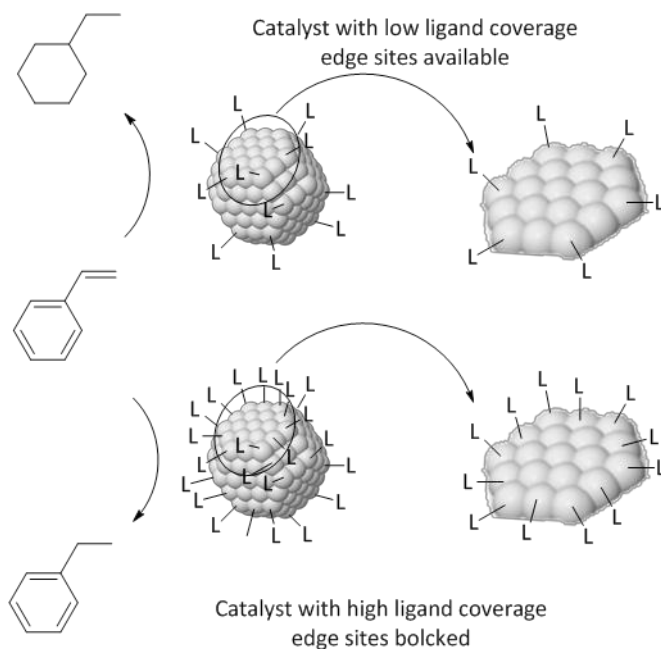
Figure 3.27 Schematic representation of the effect of the ligand coverage in the hydrogenation of styrene.

Hydrogenation of toluene

Since the system **Rh5** was not active in the hydrogenation of substrates **20a-f,** this catalyst was not used here.

Moderate to excellent conversions were obtained using all the rhodium systems (Table 3.12). As for disubstituted substrates, the systems stabilised by the phosphite ligands **Rh6**-**Rh8** were less active than the phosphine stabilised catalysts **Rh1**-**Rh4**, which was attributed to the stronger coordination of these ligands to the NP surface. The heterogeneous Rh/C also showed full conversion using toluene as substrate.

Table 3.12 Rh-systems catalysed the hydrogenation of toluene **27**.
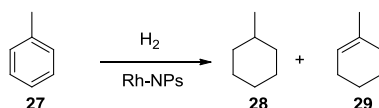
Entries	NPs	%Conv.[b]	%28[b]	%29[b]	TON[c]
1	**Rh1**	100	100		78
2	**Rh2**	100	100		102
3	**Rh3**	71	>99	<1	53
4	**Rh4**	100	100		82
6	**Rh6**	64	97	3	57
7	**Rh7**	58	100		53
8	**Rh8**	98	99	1	107
9	**Rh17**	100	100		155
10	**Rh/C**	100	100		102

[a]General conditions: 2mol% of Rh-NPs, 1.24 mmol of toluene, 10 mL of heptane, T = 80 °C, P= 40 bar H_2, 16h; [b]Determined by GC; [c]TON was defined as the number of mol of substrate (**27**) converted per mol of surface Rh .

Only in few cases and with small amount, the product of the partial hydrogenation of toluene was obtained. However, as explained in the introduction section these values are in agreement with the literature values.[67]

Hydrogenation of benzene

As explained in the introduction of this chapter, to obtain significant selectivity to cycloxene in the hydrogenation of benzene remains a challenge. In view of the detection of cyclohexene derivatives in the hydrogenation of xylenes and methylanisoles using the nanoparticles systems **Rh1**-**Rh8**, these catalysts were used with benzene as substrate.

Table 3.13 Rh-systems catalysed the hydrogenation of benzene **30**.

entries	NPs	%Conv.[b]	%31 [b]	TON[c]
1	**Rh1**	100	100	78
2	**Rh2**	78	100	80
3	**Rh3**	100	100	74
4	**Rh4**	100	100	82
6	**Rh6**	56	100	50
7	**Rh7**	10	100	9
8	**Rh8**	90	100	98
9	**Rh17**	100	100	155
10	**Rh/C**	100	100	102

[a]General conditions: 2 mol% of Rh-NPs, 1.24 mmol of benzene, 10 mL of heptane, T = 80 °C, P= 40 bar H_2, 16h; [b]Determined by GC; [c]TON was defined as the number of mol of substrate (**30**) converted per mol of surface Rh .

The results obtained at 80 °C, 40 bar of H_2 during 16h are shown in Table 3.13. High to full conversion were obtained using phosphine stabilised

systems **Rh1**- **Rh4**. However, as in the previous studies with disubstituted arenes as substrates, less activity was detected using the phosphite stabilised systems **Rh5**- **Rh8**. This was again attributed to the stronger coordination of these ligands at the surface of these RhNPs.

With this substrate, the **Rh17** and Rh/C systems provided the highest TON for this transformation. In the case of the solvent stabilised system **Rh17** that was not active in the hydrogenation of disubstituted arenes, perhaps the lower steric hindrance induced by benzene could explain this difference.

3.3 Conclusions

- The hydrogenation of disubstituted arenes **20a-f** was investigated using soluble Rh- NPs as catalysts. Only the triphenylphosphite **5** stabilised nanoparticles **Rh5** were inactive for this reaction.

Phosphine stabilised nanoparticles **Rh1**- **Rh4** were shown to be more active than phosphite stabilised **Rh6**- **Rh8** for these substrates, however **Rh4** was the less active of the series maybe due to the bidentate coordination of dppb **4** stabiliser. This fact could be explained by the stronger coordination of the phosphite ligands that could compete with the substrate, blocking the active sites at the surface of the NPs.

No clear effect on the *cis*/*trans* selectivity was observed neither by the nature or position of the substituents of the substrates nor by the stabilising agent of the nanoparticles.

Partially hydrogenated products were detected using systems **Rh1**-**Rh8**. The catalyst **Rh8** stabilised by the diphosphite **8** provided the highest selectivity to this product, up to 39% for *m*- methylanisole **20e**. Different parameters were studied in order to increase this selectivity. Temperature, pressure, solvent were modified and additives (water and ligand) were used, without improvement of the selectivity.

The presence of the P-ligand was shown to be critical: THF- MeOH stabilised **Rh17, 18,19** were inactive in the hydrogenation of disubstituted arenes **20a-f**.

- Rh/C was used for comparative purposes obtaining higher activities than the soluble nanoparticles, while lower selectivities were observed and no partially hydrogenated products were detected.
- Styrene was used as substrate, detecting high TOFs up to 13039h^{-1} at room temperature with system **Rh8**.
- Toluene and benzene were successfully hydrogenated using the soluble nanoparticles as catalysts, however no significant amounts of partially hydrogenated products were detected using these substrates.

3.4 Experimental part

General methods

All syntheses were performed using standard Schlenk techniques under N_2 or Ar atmosphere. Chemicals were purchased from Aldrich Chemical Co, Fluka and Strem. All solvents were distilled over drying reagents and were deoxygenated before use. Precursor $Rh(\eta^3\text{-}(C_3H_5)_3$ was prepared following previously described methods. Nanoparticles synthesis were performed using 200ml Fisher Porter and pressurized on a high pressure line.

The deuterated solvents for NMR measurements were dried over molecular sieves. ^1H, ^{13}C {^1H}, and ^{31}P {^1H} NMR spectra were obtained on a Varian Mercury 400 MHz spectrometer. Chemical shifts were calibrate relative to $SiMe_4$ (^1H and ^{13}C NMR) as internal standard or 85% H_3PO_4 as external standard (^{31}P NMR).

Hydrogenation experiments

A 5 entries autoclave for the optimisation studies, an autoclave Par 477 equipped with PID control temperature and reservoir for kinetic measurements and HEL 24 Cat reactor for substrate scope were used as reactors for the hydrogenation reactions. In all experiments, the autoclave was charged in the glove-box with 3.5 mg of Rh nanoparticles and 1.24 mmol of the substrate in 10 ml of heptane. When using the HEL 24 Cat reactor, a stock solution of Rh nanoparticles in heptane was prepared. Molecular hydrogen was then introduced until the desired pressure was reached. At the end of the reaction, the autoclave was depressurized and the solution was filtered over celite and analyzed by Gas Chromatography. The identification of the reaction products were performed by GC-MS and the quantification by GC-FID on a HP 6890A spectrometer with an HP-5 column (0.25mm x 30m x 0.25um), T°= 205°C injector, flow 1.5ml/min.

3.5 References

[1] (a) J. A. Widegren, R. G. Finke, *J. Mol. Catal. A: Chem.* **2003**, *191*, 187-207; (b) A. Roucoux *Top. Organomet. Chem*. **2005**, *16*, 261-279; (c) A. Roucoux, J. Schultz, H. Patin *Chem. Rev*. **2002**, *102*, 3757-3778; (d) A. Stanislaus, B. H. Cooper *Catal. Rev. Sci. Eng.* **1994**, *36*, 75-123.

[2] M. A. Bennett and A. K. Smith, *J. Chem. Soc., Dalton Trans*. **1974**, 233-241.

[3] T. J. Geldbach, P. J. Dyson, *J. Organomet. Chem*. **2005**, *690*, 3552- 3557.

[4] M. A. VanHove and G. A. Somorjai, *J. Am. Chem. Soc.* **1986**, *108*, 2532-2537.

[5] (a) J. Muller, P.E. Gaede, K. Qiao, *Angew. Chem. Int. Ed. Engl*. **1993**, *32*, 1697-1699; (b) A. J. Blake, P.J. Dyson, B.F.G. Johnson, C.M. Martin, *J. Chem. Soc., Chem. Commun*. **1994**, 1471-1472.

[6] (a) M. Viniegra, G. Córdoba, R. Gómez, *J. Mol. Catal*. **1990**, *58*, 107-114; (b) G. Cordoba, J.L.G. Fierro, A. López-Goana, N. Martin, M. Viniegra, *J. Mol. Catal. A: Chem*. **1995**, *96*, 155-161; (c) N. Martin, G. Córdoba, A. López-Gaona, M. Viniegra, *React. Kinet. Catal. Lett*. **1991**, *44*, 381-385; (d) S. Smeds, T. Salmi, D. Murzin, *Appl. Catal. A: Gen.* **1996**, *145*, 253-265; (e) S. Smeds, D. Murzin, T. Salmi, *Appl. Catal. A: Gen.* **1996**, *141*, 207-228; (f) S. Smeds, T. Salmi, D. Murzin, *Appl. Catal. A: Gen.* **1997**, *150*, 115-129; (g) M. Viniegra, N. Martin, A. López-Gaona, G. Córdoba, React. *Kinet. Catal. Lett.* **1993***, 49,* 353-360; (h) M.A. Aramendía, V. Borau, C. Jiménez, J.M. Marinas, F. Rodero, M. E. Sempre, *React. Kinet. Catal. Lett*. **1992**, *46*, 305-312; (i) R.A. Saymeh, H. M. Asfour, *Orient. J. Chem.* **2000**, *16*, 67-72; (j) R.A. Saymeh, H.M. Asfour, W.A. Tuaimen, *Asian J. Chem*. **1997**, *9*, 350-358; (k) A.K. Neyestanaki, P. Mäki-Arvela, H. Backman, H. Karhu, T. Salmi, J. Väyrynen, D. Murzin J. Catal. **2003**, *218,* 267-279.

[7] G. S. Fonseca, E. T. Silveira, M. A. Gelesky, J. Dupont, *Adv. Synth. Catal.* **2005**, *347*, 847-853.

[8] S. Toppinen, T.K. Rantakyla, T. Salmi, J. Aittamaa, *Ind. Eng. Chem. Res*. **1996**, *35*, 4424-4433.

[9] (a) F. Lu, J. Liu, J. Xu, *Adv. Synth. Catal.* **2006**, *348*, 857-861; (b) F. Lu, J. Liu, J. Xu, *J. Mol. Catal. A: Gen.* **2007**, *271*, 6-13.

[10] N. Yan, C. Xiao, Y. Kou *Coord. Chem. Rev*. **2010**, *254*, 1179-1218.

[11] A. P. Umpierre, E. de Jesús, J. Dupont, *Chem. Cat. Chem*. **2011**, *3*, 1413-1418.

[12] B. He, Y. Ha, H. Liu, K. Wang, K. Y. Liew, *J. Coll. Inter. Sci.* **2007**, *308*, 105-111.

[13] T.Q. Hu, D.R. James, C.L. Lee *J. Pulp Paper Sci*. **1997**, *23*, J200-J205.

[14] R. Choukroun, D. De Caro, B. Chaudret, P. Lecante, E. Snoeck, *New. J. Chem.* **2001**, *25*, 525-527.

[15] J.-L. Pellegatta, C. Blandy, V. Collière, V. Choukroun, B. Chaudret, P. Cheng, K. Philippot, *J. Mol. Catal. A: Gen.* **2002**, *178*, 55-61.

[16] (a) K.R. Januszkiewicz, H. Alper, *Organometal.* 1983, **2**, 1055-1057; (b) K.R. Januszkiewicz, H. Alper, *Can. J. Chem.* **1984**, *62*, 1031-1033.

[17] a) T.Q. Hu, D.R. James, J.S. Retting, C. Lee, *Can. J. Chem.* **1997**, *75,* 1234-1239; b) T.Q. Hu, D.R. James, C. Lee, *J. Pulp. Paper Sci.* **1997**, *23*, J153-J156; c) D.R. James, Y. Wang, C.S. Alexander, T.Q. Hu, *Chem. Ind.* **1998**, *75*, 233-242.

[18] (a) P. Drognat-Landré, M. Lemaire, D. Richard, P. Gallezot, *J. Mol. Catal.* **1993**, *78*, 257-261; (b) P. Drognat-Landré, D. Richard, M. Draye, P. Gallezot, M. Lemaire, *J. Catal.* **1994**, *147*, 214-222.

[19] J. Schulz, A. Roucoux, H. Patin, *Chem. Eur. J.* **2000**, *6*, 618-624.

[20] J. Schulz, S. Levigne, A. Roucoux, H. Patin, *Adv. Synth. Catal.* **2002**, *344*, 266-269.

[21] (a) H. Hirai, Y. Nayao, N. Toshima, *J. Macromol. Sci. Chem.* **1978**, *A12*, 1117-1141; (b) H. Hirai, Y. Nakao, N. Toshima, *J. Macromol. Chem.* **1979**, *A13*, 727-750.

[22] V. Mévellec, A. Roucoux, E. Ramirez, K. Phillipot, B. Chaudret, *Adv. Synth. Catal.* **2004**, *346*, 72-76.

[23] J. Dupont, G. S. Fonseca, A. P. Umpierre, P. F. P. Fichtner, S. R. Teixeira, *J. Am. Chem. Soc.* **2002**, *124*, 4228-4229.

[24] G. S. Fonseca, A. P. Umpierre, P. F. P. Fichtner, S. R. Teixeira, J. Dupont, *Chem. Eur. J.* **2003**, *9*, 3263-3269.

[25] C. W. Scheeren, G. Machado, J. Dupont, P. F. P. Fichtner, S. R. Texeira, *Inorg. Chem.* **2003**, *42*, 4738-4742.

[26] (a) E. T. Silveira, A. P. Umpierre, L. M. Rossi, G. Machado, J. Morais, G. V. Soares, I. J. R. Baumvol, S. R. Teixeira, P. F. P. Fichtner, J. Dupont, *Chem. Eur. J.* **2004**, *10*, 3734-3740; (b) L. M. Rossi, J. Dupont, G. Machado, P. F. P. Fichtner, C. Radtke, I. J. R. Baumvol, S. R. Teixeira, *J. Braz. Chem. Soc.* **2004**, *15*, 904-910.

[27] S. S. Divekar, B. M. Bhanage, R. M. Deshpande, R. V. Gholap, R. V. Chaudari, *J. Mol. Catal.* **1994**, *91*, L1-L5.

[28] (a) L. S. Ott, M. L. Cline, M. Deetlefs, K. R. Seddon, R. G. Finke, *J. Am. Chem. Soc.* **2005**, *127*, 5758-5759; (b) L. S. Ott, S. Carmpbell, K. R. Seddon, R. G. Finke, *Inorg. Chem.* **2007**, *46*, 10335-10344.

[29] L. M. Rossi, G. Machado, *J. Mol. Catal. A: Gen.* **2009**, *298*, 69-73.

[30] (a) F. Fache, S. Lehuede, M. Lemaire, *Tetrahedron Lett.* **1995**, *36*, 885-888; (b) K. Nasar, F. Fache, M. Lemaire, J.C. Béziat, M. Besson, P. Gallezot *J. Molec. Catal.* **1994**, *87*, 107-115.

[31] G. Marconi, P. Pertici, C. Evangelisti, A. M. Caporusso, G. Vitulli, G. Capannelli, M. Hoang, T. W. Turney, *J. Organometal. Chem.* **2004**, *689*, 639-646.

[32] S. Jansat, D. Picurelli, K. Pelzer, K. Philippot, M. Gómez, G. Muller, P. Lecante, B. Chaudret, *New J. Chem.* **2006**, *30,* 115-122.

[33] M. V. Escárcega-Bobadilla, C. Tortosa, E. Teuma, C. Pradel, A. Orejón, M. Gómez, A. M. Masdeu-Bultó, *Catal. Today* **2009***, 148*, 398-404.

[34] (a) A. Gual, M. R. Axet, K. Philippot, B. Chaudret, A. Denicourt-Nowicki, A. Roucoux, S. Castillón, C. Claver, *Chem. Commun.* **2008**, 2759-2761; (b) A. Gual, C. Godard, K. Philippot, B. Chaudret, A. Denicourt-Nowicki, A. Roucoux, S. Castillón, C. Claver, *ChemSusChem* **2009**, *2*, 769-779.

[35] Y. D. Lu, Y. H. Wang, Z. L. Jin, *Chinese Chem. Lett*. **2010**, *21*, 1067-1070.

[36] D.J. Snelders, N. Yan, G. Laurency, P.J. Dyson, *ACS Catal*. **2012**, *2*, 201-207.

[37] D. Gonález- Gálvez, P. Nolis, K. Philippot, B. Chaudret, P. W. N. M. van Leeuwen, *ACS Catal*. **2012**, *2*, 317-321.

[38] D. Gonzalez-Galvez, P. Lara, O. Rivada-Wheelaghan, S. Conejero, B. Chaudret, K. Philippot and P. W. N. M. van Leeuwen, *Catal. Sci. Technol.* **2013**, 3, 99-105.

[39] E. Rafter, T. Gurman, F. Low, G. Buntkowsky, K. Philippot, B. Chaudret, P. W. N. M. van Leeuwen, *Catal. Sci. Technol*. **2013**, *3*, 595-599.

[40] E. T.Silveira, A. P.Umpierre, L. M.Rossi, G. Machado, J. Morais, G. V.Soares, I. J.R. Baumvol, S.R.Teixeira, P.F.P. Fichtner, J. Dupont, *Chem. Eur. J*. **2004**, *10*, 3734- 3740.

[41] L.M. Rossi, G. Machado, *J. Mol. Catal. A: Gen.* **2009**, *298*, 69–73.

[42] J. Blum, I. Amer, K. P. C. Vollhart, H. Schwarz, G. Hoehne, *J. Org. Chem*. **1987**, *52*, 2804-2813.

[43] K. S. Weddle, J. D. Aiken III, R. G. Finke, *J. Am. Chem. Soc*. **1998**, *120*, 5653-5666.

[44] J. A. Widegren, R. G. Finke, *Inorg. Chem.* **2002**, *41*, 1558-1572.

[45] C. Zhao, H.Z. Wang, N. Yan, C.X. Xiao, X.D. Mu, P.J. Dyson, Y. Kou, *J. Catal.* **2007**, *250*, 33-40.

[46] M. Jahjah, Y. Kihn, E. Teuma, M. Gomez, *J. Mol. Catal. A: Chem.* **2010**, *332*, 106-112.

[47] D. Gonzalez-Galvez, P. Lara, O. Rivada-Wheelaghan, S. Conejero, B. Chaudret, K. Philippot, P.W.N.M. van Leeuwen, *Catal. Sci. Technol*. **2013**, *3*, 99-105.

[48] A. Corma, P. Serna, *Science* 2006, **313**, 332-334.

[49] A. Nowicki, Y. Zhang, B. Léger, J-P. Rolland, H. Bricout, E. Monflier, A. Roucoux, *Chem. Commun*. **2006**, 296-298.

[50] M. Guerrero, A. Roucoux, A. Denicourt- Novicki, H. Bricout, E. Monflier, V. Collière, K. Fajerwerg, K. Philippot, *Catal. Today* **2012**, *183*, 34-41.

[51] P. Lara, T. Ayvali, M.-J. Casanove, P. Lecante, A. Mayoral, P.- F. Fazzini, K. Philippot, B. Chaudret, *Dalton Trans.* **2013**, *42*, 372-382.

[52] V. Mervellec, B. Leger, M. Mauduit, A. Roucoux, *Chem. Commun*., **2005**, 2838-2839.

[53] B. Leger, A. Denicourt- Nowicki, H. Olivier- Bourbigou, A. Roucoux, *Inorg. Chem*. **2008**, *47*, 9090-9096.

[54] X. Yang, N. Yan, Z. Fei, R. M. Crespo- Quesada, G. Laurency, L. Kiwi- Misker, Y. Kou, Y. Li, P. Dyson, *J. Inorg. Chem*. **2008**, *47*, 7444-7446.

[55] C.H. Yen, H- H. Wei, H- W. Lin, C- S. Tan, *Appl. Organometal. Chem*. **2012**, *26*, 736-742.

[56] T.J. Donohoe, R. Garg, C. A. Stevenson, *Tetrahedron: Asymmetr.* **1996**, *7*, 317-344.

[57] P. R. Linstead, W. E. Doering, S. B. Davis, P. Levine, R. R. Whetstone, *J. Am. Chem. Soc.* **1942**, *64*, 1985-1991.

[58] (a) R. D. Schuetz, L. R. Caswell, *J. Org. Chem.* **1962**, *27*, 486 -489; (b) S. Siegel, G. V. Smith, B. Dmuchovsky, D. Dubbel, W. Halpern, *J. Am. Chem. Soc.* **1962**, *84*, 3132-3136.

[59] (a) F. Fache, S. Lehuede, M. Lemaire *Tetrahedron Lett.* **1995**, *36*, 885-888; (b) K. Nasar, F. Fache, M. Lemaire, J.C. Béziat, M. Besson, P. Gallezot, *J. Mol. Catal.* **1994**, *87*, 107-115.

[60] (a) J. Schulz, A. Roucoux, H. Patin, *Chem. Eur. J.* **2000**, *6*, 618-624. (b) J. Schulz, S. Levigne, A. Roucoux, H. Patin, *Adv. Synth. Catal.* **2002**, *344*, 266-269. (c) A. Roucoux, J. Schulz, H. Patin, *Adv. Synth. Catal.* **2003**, *345*, 222-229.

[61] C. Hubert, A. Denicourt-Nowicki, J. P. Guégan, A. Roucoux, *Dalton Trans.* **2009**, 7356-7358.

[62] S. Jansat, D. Picurelli, K. Pelzer, K. Philippot, M. Gómez, G. Muller, P. Lecante, B. Chaudret, *New J. Chem.* **2006**, *30*, 115-122.

[63] (a) A. Gual, M. R. Axet, K. Philippot, B. Chaudret, A. Denicourt- Nowicki, A. Roucoux, S. Castillón, C. Claver, *Chem. Commun*. **2008**, 2759-2761; (b) A. Gual, C. Godard, K. Philippot, B. Chaudret, A. Denicourt-Nowicki, A. Roucoux, S. Castillón, C. Claver, *ChemSusChem* **2009**, *2*, 769-779.

[64] P. Zhang, T. Wu, T. Jiang, W. Wang, H. Liu, H. Fan, Z. Zhang, B. Han, *Green Chem.* **2013**, *15*, 152-159 and references therein.

[65] C.U.I. Odenbrand, S.T. Lundin, *J. Chem. Technol. Biothechnol*. **1980**, *30*, 677-687.

[66] J. A. Widegren, R. G. Finke, *Inorg. Chem.* **2002**, *41*, 1558-1572.

[67] Y. Yuan, N. Yan, P. J. Dyson, *ACS Catal*. **2012**, *2*, 1057-1069.

Chapter 4.

Catalytic hydrogenation of aromatic ketones using phosphorus-stabilised Ru and Rh nanoparticles
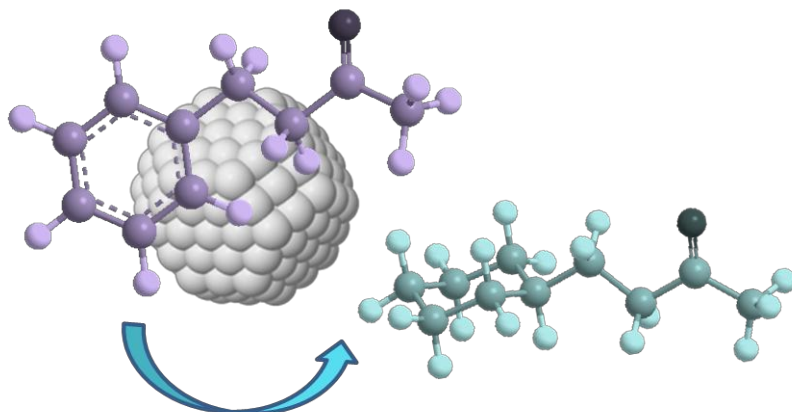
4.1 Introduction

As mentioned in the introduction of this thesis, soluble nanoparticles are nowadays applied as catalysts in a wide range of transformations such as the catalytic hydrogenation of aromatic substrates.[1,2,3]

In the hydrogenation of aromatic ketones (Figure 4.1), the use of Ru and Rh-NPs was mainly reported, although a few examples of Pd- and Ir-NPs were also described.[4]
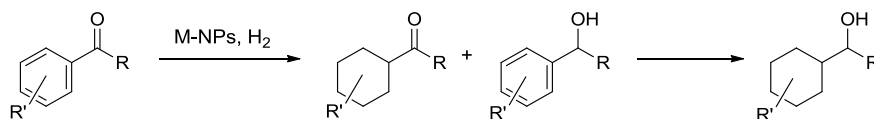
Figure 4.1 Hydrogenation of aromatic ketones.

The chemoselective hydrogenation of aromatic rings in such substrates is extremely challenging and acetophenone is usually employed as model substrate.

In 2010, Gómez and co-workers reported a comparative catalytic study between unsupported Ru-NPs stabilised by a pyridine derivative and supported nanoparticles on multi-wall carbon nanotubes in terms of activity, selectivity and recycling.[5] The ruthenium nanoparticles were prepared by decomposition of [Ru(COD)(COT)] in the presence of 4-(3-phenylpropyl)pyridine ligand and under hydrogen atmosphere, providing small (mean size: 1.31 ± 0.43 nm) and homogenously dispersed nanoparticles, as previously described.[6]
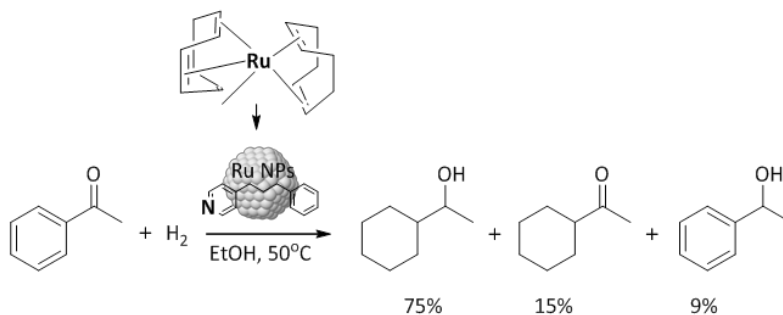
Figure 4.2 Results obtained by Gómez and co-workers in the hydrogenation of acetophenone catalysed by Ru NPs.[5]

These NPs were applied in the hydrogenation of acetophenone, obtaining up to 99% of conversion and 75% of selectivity to the totally hydrogenated product after 16h of reaction time using the supported system. The non-supported catalysts were less active than those onto CNTs for all the substrates. However, 100% selectivity towards the totally hydrogenated product was obtained in this case.

Recently, Chaudret, van Leeuwen and co-workers demonstrate the influence of the nature of the ligands attached to the surface of the nanoparticles on their catalytic activity in the hydrogenation of several substrates such as acetophenone and other aromatic compounds containing ketones.[7]

The nanoparticles were prepared following the reported procedure, using the organometallic complex [Ru(COD)(COT)] (1,5-cyclooctadiene)(1,3,5-cyclooctadiene)ruthenium(0) as the metal source and the carbenes I^{t}Bu and IPr as stabilisers (Figure 4.3). Small and monodisperse nanoparticles were formed, with mean size of 1.7± 0.2 nm for the particles prepared using 0.5 molar equiv. of I^{t}Bu per ruthenium (RuI^{t}Bu$^{0.5}$) and 1.7± 0.2 nm and 1.5± 0.2 nm for the particles prepared using 0.2 and 0.5 molar equivalents of IPr (RuIPr$^{0.2}$ and RuIPr$^{0.5}$) respectively.
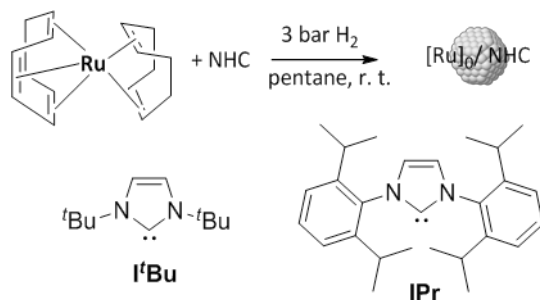
Figure 4.3 Synthetic strategy used by Chaudret and co-workers for the preparation of NHC-stabilised Ru-NPs.[7]

RuIPr$^{0.2}$ applied in the hydrogenation of acetophenone and provided selectivities up to 80% towards the hydrogenation of the arene, cyclohexylmethylketone product with conversions under 50% using only 0.03% of total Ru.

Subsequently RuIPr$^{0.2}$ was tested as a catalyst in the hydrogenation of other aromatic compounds containing ketones in THF (Figure 4.4). Interestingly, they observed that as the length of the alkyl chain between the aryl and keto group of the substrate increases, the selectivity towards the hydrogenation of the arene fragment is enhanced. Over 98% selectivity to the ring hydrogenated product was achieved at full conversion using 4-phenyl-2-butanone and 5-phenyl-2-pentanone as substrates. These remarkable results show that nanoparticles may hydrogenate very selectively the arene groups of arylketones as a probable consequence of the thermodynamic preference for arene coordination over ketone coordination on ruthenium surfaces. In the case of acetophenone, the approach through the phenyl ring is also preferred as deduced from the faster production of cyclohexylmethylketone than phenylethanol, as observed by kinetic analysis of the hydrogenation reaction.

3-Acetylpyridine reacted more slowly than the benzene derivative at 353 K and 40 bar of hydrogen. In this case, a complex mixture of compounds was obtained, in which at 26% conversion, the major compounds were the ones produced by ketone hydrogenation (15%) and α,β-saturated ketones (8%). Only 3% of the products contained fully hydrogenated pyridine ring were detected, in agreement with previous reports.[8,9]

X = CH, n= 0	36%	-	64%	-
X = CH, n= 1	92%	5%	3%	-
X = CH, n= 2	98%	-	2%	-
X = CH, n= 3	99%	-	1%	-
X = N, n= 0	2%	15%	1%	8%
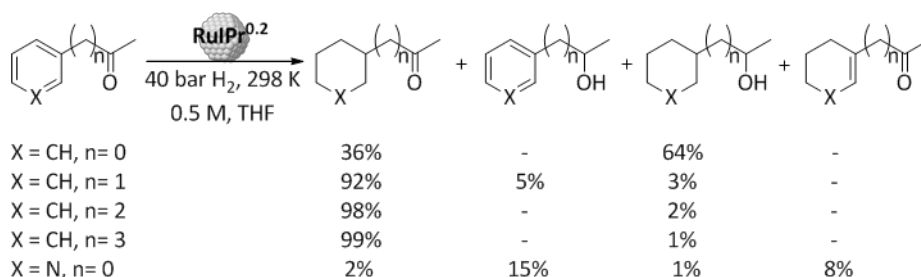
Figure 4.4 Products formed in the hydrogenation of aromatic ketones as reported by Chaudret, van Leeuwen and co-workers using Ru NPs stabilized by NHC ligands.[7]

Philippot and co-workers reported the use of water-soluble ruthenium nanoparticles using alkyl sulfonated diphosphines as stabilisers.[10] These systems were active in the hydrogenation of unsaturated substrates under

aqueous/organic biphasic catalysis conditions. The nanoparticles were synthesised by decomposition of [Ru(COD)(COT)] under hydrogen using various [L]/[metal] molar ratios (0.1, 0.2 or 0.5) of the sulfonated diphosphine. TEM/HRTEM analysis revealed the presence of small and well-dispersed particles displaying a mean diameter between 1.2 and 1.5 nm depending on the [L]/[metal] ratio.
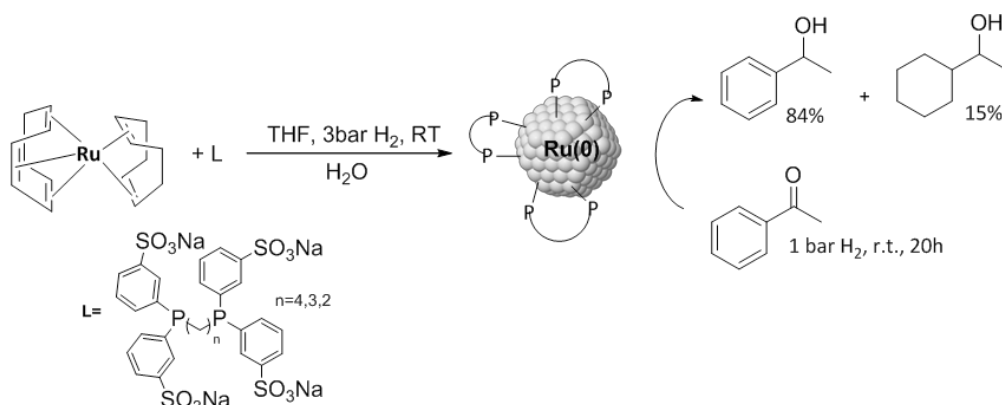
Figure 4.5 Catalytic system used by Philippot and co-workers for the hydrogenation of acetophenone.[10]

When acetophenone was used as substrate with these systems, 100% conversion was achieved in 20h with interesting selectivities into phenylethanol (84%) and cyclohexylethanol (15%) at only 1 bar of hydrogen pressure (Figure 4.5). Moreover, to obtain full hydrogenated product, the pressure was increased to 10 bar of H_2.

Later, the same group reported a similar system, the authors attempted to modify the coordination properties of the sulfonated diphosphine via the addition of cyclodextrin (CD).[11] In this purpose, a combination of 1,4-bis[(di-m-sulfonatophenyl)phosphine]butane (L) and RAME-β-CD (0.2, 1.0 and 5.0 equiv.) were used for the synthesis of the RuNPs. The formation of supramolecular inclusion complexes between the sulfonated diphosphine and cyclodextrin molecules and the dispersion of these systems in water was determined by DLS.
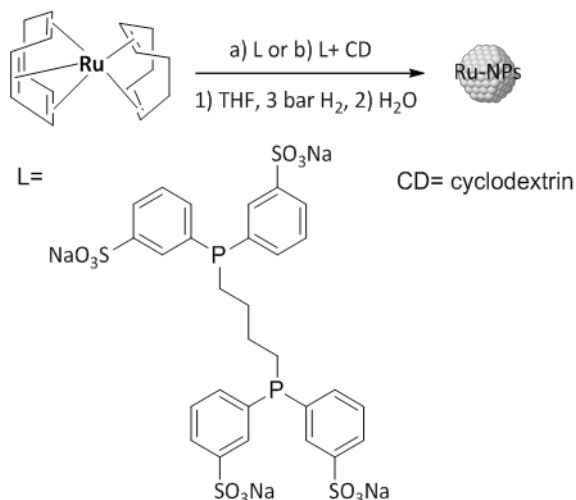
Figure 4.6 Synthetic strategy reported by Philippot and co-workers for the preparation of water soluble Ru nanoparticles.[11]

The catalytic properties of the sulfonated diphosphine-stabilised RuNPs and sulfonated-diphosphine-cyclodextrin-stabilised Ru-NPs were compared in the hydrogenation reaction of acetophenone in biphasic liquid-liquid conditions and relevant differences in terms of activity and selectivity were observed.

Under 1 bar of H_2, an increase in turnover number (TON) and TOF values was observed for the systems bearing CD. In terms of selectivities, the 1-phenylethanol (B, 82–86%) was the major product but 1-cyclohexylethanone (A, 3%–9%) and 1-cyclohexylethanol (C, 11–16%) were also produced, indicating that the hydrogenation of the aromatic cycle could take place. The increase in reaction pressure from 1 to 10 bar H_2 provided strong acceleration of the reaction for all catalytic systems and TON and TOF values were further increased with high quantities of CD. Concerning the selectivity, the total hydrogenated product (1-cyclohexylethanol; C) was obtained with 100% selectivity with **Ru/L** and **Ru/L/0.2CD** nanocatalysts after 2h of reaction, whereas the systems more rich in CD (**Ru/L/1.0CD** and **Ru/L/5.0CD**) presented only 34 and 26% selectivity to product C after the same time, indicating an influence of the

CD on the outcome of the reaction. This study therefore demonstrated that the presence of the cyclodextrin during the synthesis of the nanoparticles has an influence on the catalytic performances of the sulfonated-diphosphine-stabilised RuNPs in the hydrogenation of acetophenone in terms of activity and selectivity.

Dupont and co-workers reported the synthesis of Ir(0) nanoparticles with 2.3 ± 0.4 nm in diameter prepared by simple reduction of $[Ir(COD)Cl]_2$ in 1-n-butyl-3-methylimidazolium hexafluorophosphate as stabiliser constituting a simple, efficient and recyclable catalytic system for the solventless or biphasic hydrogenation of ketones under mild condition reactions.[12] They observed that the hydrogenation of cyclohexanone with the iridium nanoparticles dispersed in BMI·PF$_6$ required longer reaction times than when the reaction was performed under solventless conditions. This difference was attributed to the characteristic biphasic nature of the reaction in the ionic liquid. However, the recovered ionic liquid catalytic dispersion could be reused at least 15 times without significant loss in catalytic performance, in contrast with the solventless system, which started to lose activity after the third recycle. The reduction of acetophenone catalysed by these Ir(0) nanoparticles was carried out at 75°C and under 4 atm of hydrogen. Modest selectivity (35%) was observed for the hydrogenation of the aromatic ring over that of the carbonyl function at 50% conversion. It was concluded that in the hydrogenation of acetophenone, there is no preferential coordination mode (arene vs. carbonyl group) to the metal surface. However, the hydrogenation of phenylacetone revealed to mainly produce the reduction of the aromatic ring under the same reaction conditions with 92% selectivity to the cyclohexylketone at 97% conversion.
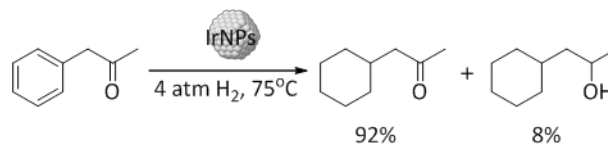
Figure 4.7 Results reported in the hydrogenation of phenylacetone using Ir-NPs stabilised by ILs.[12]

Dyson and co-workers study the hydrogenation of phenylacetone to cyclohexylacetone.[13] This transformation was achieved with chemoselectivities exceeding 90% using a nanocatalyst comprising PVP-stabilised Rh nanoparticles dispersed in water and water soluble phosphine ligands as additives. A series of phosphine ligands with different steric and electronic properties and polarities were investigated and several trends were observed, showing the potential of well-defined phosphine ligands as modifiers in nanocatalysis.
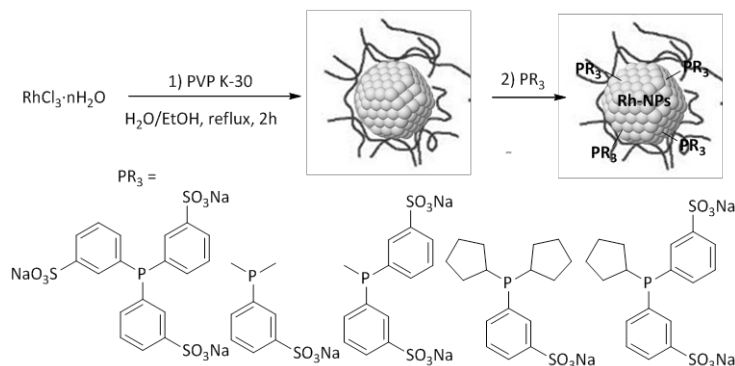
Figure 4.8 Sulfonated phosphines used as additive by Dyson and co- workers.[13]

The authors did not observed a significant influence of the phosphine ligands on the morphology of the nanoparticles, indicating that the differences in catalytic performance could be attributed to the modification of the nanoparticle surface (site blocking) by coordination of the phosphine ligands.

In the hydrogenation of phenylacetone, the PVP-Rh nanoparticles afford 1-cyclohexylpropan-2-one with 70% selectivity in the absence of a phosphine

ligand but the chemoselectivity of the reaction could be increased up to 92% upon addition of one of the phosphines under optimised conditions.

In absense of phosphine: 5%   70%   19%
In presence of phosphine: 6%   92%   2%
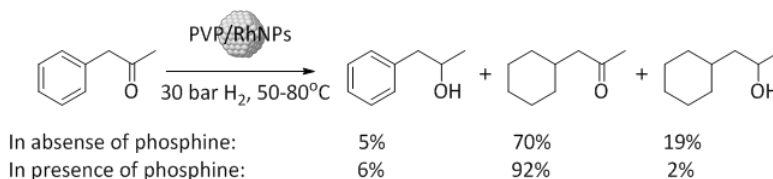
Figure 4.9 Results reported by Dyson and co-workers in the hydrogenation of phenyl acetone using Rh-PVP and Rh-PVP-PR$_3$ as catalyst.[13]

In 2000, this transformation was studied using Rh colloids in biphasic aqueous/supercritical ethane reaction media, and the hydrogenation of 4-phenylbutanone was essentially complete and highly selective (97%) for hydrogenation at the arene ring using these colloids.[14]

F. Jutz and co-workers reported the use of ionic liquids and supercritical carbon dioxide to facilitate a green pathway for the solventless noble metal-catalysed hydrogenation of acetophenone.[15] The catalytic system consisted of in situ-synthesized palladium and rhodium nanoparticles stabilised by various ionic liquids ([BMIm][PF$_6$], [BMIm][OTf] and (N(C$_6$H$_{13}$)$_4$Br). Supercritical CO$_2$ extraction was employed for the removal of the metal precursor in the catalysts synthesis step as well as for the separation of the hydrogenation products. All steps, including the catalysts synthesis, reaction and product separation, were followed by in situ infrared spectroscopy. Among the tested catalysts, Pd-[BMIm][PF$_6$] showed the best performance. Catalyst deactivation was not observed after six reaction cycles and the slight loss in activity in the first reaction cycle could be eliminated by subsequent supercritical CO$_2$ extraction and caused by the hydrogenolysis of the PF$_6^-$ anions. These nanoparticles showed good activity with a selectivity of nearly 90% towards 1-phenylethanol. In the case of Rh nanoparticles, the selectivity towards the hydrogenation of the carbonyl group was significantly lower, obtaining in all cases significant aromatic ring hydrogenation while the hydrogenolysis byproduct ethylbenzene was observed as traces.

In the following sections, the synthesis and characterisation of a series of Ru and Rh-NPs stabilised by P-donor ligands and their application in the hydrogenation of aromatic ketones are described. The objective of this work was the comparison of the catalytic behaviour of Ru and Rh-NPs stabilised by the same ligands under identical catalytic conditions. The selectivity of the reaction, namely the hydrogenation of the arene *vs*. that of the ketone function, has been particularly looked at using several series of aromatic ketones as substrates.

The study described in this chapter has been carried out in collaboration with the groups of Prof. Sergio Castillón and B. Chaudret and the work on the ruthenium systems was entirely carried out by Ms. Emma Bressó-Femenia in the context of her PhD work. Since the interest of the study was based on the comparison between Ru and Rh systems, the results obtained with both sets of NPs will be discussed here.

4.2 Results and discussion

The soluble Ru-NPs stabilised by the phosphorus donor ligands **1** and **4** (P:Ru/Rh= 0.4) (Figure 4.10) were synthesised by decomposition of the organometallic precursor [Ru(COD)(COT)] in THF under H_2 pressure. The NPs were isolated as black powders after precipitation with pentane and characterised by transmission electron microscopy (TEM), X-ray diffraction (XRD), X-ray photoelectron spectroscopy (XPS) and thermogravimetric analysis (TGA).
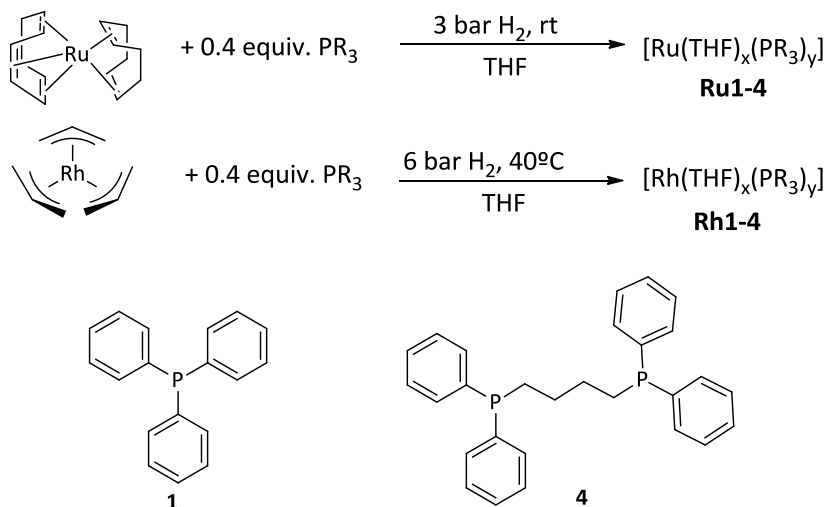
Figure 4.10 P-donor ligands used in this study to stabilise the Ru-NPs and Rh-NPs.

The TEM micrographs of these NPs revealed in all cases the formation of small nanoparticles with spherical shape, narrow size distribution and similar diameter (*ca*. 1.5 nm diameter, Figure 4.11). The ruthenium nanoparticles stabilised by triphenylphosphine **Ru1** showed the smallest size of the series (*ca.* 1.3 nm of diameter). The mean diameter and size distribution of the **Ru1,4** NPs are in agreement with the size of Ru-NPs stabilised with these ligands previously reported at lower L/M ratios (0.1 equivalent of triphenylphosphine[16] and dppb[17]). It was therefore concluded that for these systems, the amount of ligand used to stabilise the nanoparticles does not affect significantly their size.

Diffuse peaks were observed in the XRD pattern of these NPs, as expected for an homogeneous distribution of very small particles with a hexagonal close-packing (hcp) lattice structure. No reflections due to ruthenium oxide were observed, and coherence lengths in agreement with TEM analysis were obtained. Thermogravimetric analysis of **Ru1, Ru4** systems showed that these NPs contained *ca*. 2% of solvent, 25% of phosphine ligands and 70% of Ru, in agreement with previous reports.[16] Similar results were obtained with the Rh systems (see details Chapter 2).
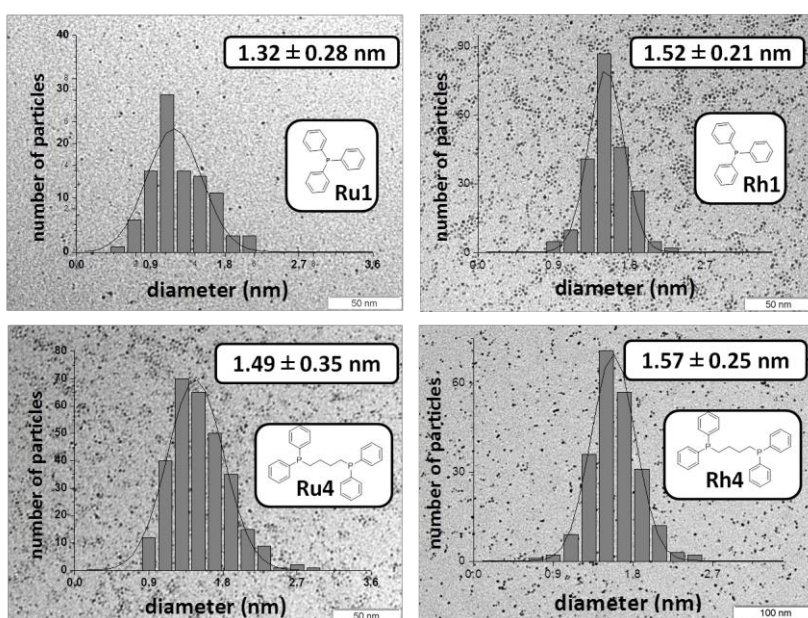
Figure 4.11 TEM micrographs and the corresponding size histograms of nanoparticles **Ru1,Ru4** and **Rh1**,**Rh4**.

4.2.1   Acetophenone reduction

Acetophenone **31** was first used to evaluate the selectivity of the hydrogenation (aryl group *vs.* ketone group) using these catalysts. As described in Figure 4.12, three main products were expected in this process: cyclohexylmethylketone **31a** resulting from the selective reduction of the aromatic ring, phenylethanol **31b** resulting from selective reduction

of the ketone group and cyclohexylethanol **31c,** formed by complete hydrogenation of the substrate.
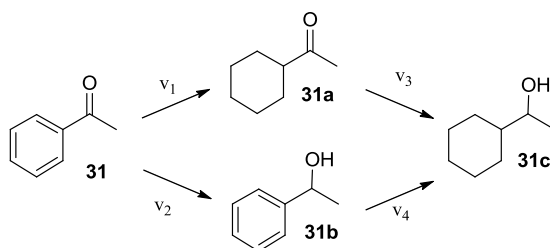
Figure 4.12 Expected products for acetophenone hydrogenation.

Ruthenium-rhodium comparative study

Initially, the ruthenium nanoparticles **Ru1** stabilised by triphenylphosphine **1**, were tested in the hydrogenation of acetophenone **31** in various solvents at 30°C and under 20 bar H_2. In THF, full conversion (TON=77) was obtained when the reaction was carried out during 5h (Table 4.1, entry 1). Under these conditions, 87% of the total hydrogenated product **31c** was obtained. When the reaction was repeated during 2.5h under the same conditions, 90% conversion (TON=69) was reached with up to 57% selectivity for product **31a** (Table 4.1, entry 2), and 39% for the fully hydrogenated **31c**. In this experiment, only 4% of phenylethanol **31b** was obtained. When the reaction was conducted in pentane (Table 4.1, entry 3), the reaction was slower than in THF and in contrast with the previous experiment, the major product was **31b** (53%). This result was rather surprising since the coordinating properties of the solvent usually control the activity of such heterogeneous catalysts via competitive coordination with the substrate and was attributed to the poor solubility of the NPs in this solvent. In acetonitrile, the reaction did not proceed (Table 4.1, entry 4), and no conversion was obtained. This result was in agreement with previous reports[18] and indicated that competitive coordination of acetonitrile at the surface blocks the active sites of the catalyst. From this screening, it was deduced that the best results in terms of activity and selectivity were

obtained using THF as solvent and subsequent experiments were carried out in this solvent.

When the reaction was performed for 5h using the catalytic system **Ru4** (Table 4.1, entry 5), a TON of 59 was obtained with selectivities of 43% and 41% for **31a** and **31b**, respectively**.** The **Ru4** nanoparticles were therefore apparently less active than **Ru1**, which could be attributed to the more facile dissociation of the monodentate PPh$_3$ **1** from the surface of **Ru1**. The variations observed when **Ru1** and **Ru4** were used as catalysts indicated that the ligand used to stabilise the nanoparticles has an effect on both their activity and selectivity. It is noteworthy that bidentate phosphine stabilised Ru-NPs are usually more active than their monodentate counterparts.[19]

Next, the rhodium nanoparticles **Rh1,4** were used as catalysts in the hydrogenation of acetophenone **31** under the same reaction conditions. When **Rh1** was used as catalyst in this reaction during 5h (entries 8-10), THF again provided high conversion and selectivities (entry 8). However, with this catalyst, in addition to the expected products **31a-c** obtained in 15, 23 and 33%, respectively, the hydrogenolysis products ethylbenzene **31d** and ethylcyclohexane **31e** were also detected (13% and 17%, respectively). In previous reports on hydrogenation of acetophenone by soluble Rh-NPs, these products were at most formed as traces.[4b,20]

Table 4.1 Ru-NPs (**Ru$_{1,4}$**) and Rh-NPs (**Rh$_{1,4}$**) catalysed hydrogenation of acetophenone **31**.[a]

	S	NPs	Solvent	Time (h)	Conv. (%)[b]	31a (%)[b]	31b (%[b])	31c (%[b])	31d (%)[b]	31e (%)[b]
1	**31**	**Ru1**	THF	5	100	13	-	87	-	-
2	**31**	**Ru1**	THF	2.5	90	57	4	39	-	-
3	**31**	**Ru1**	Pentane	5	24	23	53	24	-	
4	**31**	**Ru1**	Acetonitrile	5	0	-	-	-	-	-
5	**31**	**Ru4**	THF	5	70	43	41	16	-	-
6	**31a**	**Ru1**	THF	16	100	-	-	100	-	-
7	**31b**	**Ru1**	THF	16	5	-	95	5	-	-
8	**31**	**Rh1**	THF	5	90	15	23	33	13	17
9	**31**	**Rh1**	Pentane	5	100	6	1	8	57	27
10	**31**	**Rh1**	Acetonitrile	5	0	-	-	-	-	-
11	**31**	**Rh1**	THF[*]	24	100	22	-	73	-	5
12	**31**	**Rh1**	THF[**]	5	100	12	-	21	35	32
13	**31a**	**Rh1**	THF	16	0	-	-	-	-	-
14	**31a**	**Rh1**	pentane	5	0	-	-	-	-	-
15	**31b**	**Rh1**	THF	16	100	1	26	-	-	63
16	**31c**	**Rh1**	THF	16	0	-	-	-	-	-
17	**31**	**Rh4**	THF	5	100	28	46	26		

[a]General conditions: 2mol% M (M=Ru-NPs,Rh-NPs),1.24 mmol of substrate, T = 30°C, P= 20 bar H_2. [*]addition of molecular sieves [**]addition of 1ml of H_2O

The formation of these products could involve the protonation and dehydratation of product **31b** with subsequent elimination of water to form **31d** as shown in Figure 4.13. In this case, styrene should be formed as reaction intermediate but was not detected in these reactions. However the system **Rh1** is very active as catalyst for the hydrogenation of styrene and the reaction could take place too rapidly to allow its detection in the catalytic mixture.
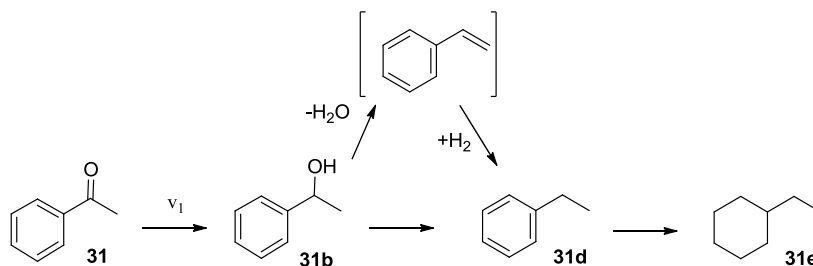
Figure 4.13 Possible reaction pathway for the formation of the hydrogenolysis products **31d** and **31e**.

In order to favor the hydrogenolysis process, the reaction was repeated in the presence of activated molecular sieves. However, under these conditions, the hydrogenation of acetophenone **31** was completed but only provided 5% of ethylcyclohexane **31e** even after 24h (Table 4.1, entry 11).

Next, the reaction was carried out under the same conditions of pressure and temperature but 1ml of water was added to the reaction mixture. Surprisingly, after 5h, the amount of hydrogenolysis product already increased to 35% and 32% for ethylbenzene **31d** and ethylcyclohexane **31e**, respectively (Table 4.1, entry 12). These results therefore indicated that the presence of water enhance the rate of hydrogenolysis, which disagree with the mechanism described earlier.

Furthermore, the reaction conditions were optimised for this system and the results are displayed in Table 4.2.

When the hydrogen pressure was decreased to 10 bar, a significant decrease in conversion was observed with up to 52% selectivity to the cyclohexylmethylketone **31a** (Entry 2 vs 1). When the pressure was increased to 40 bar, full conversion was obtained (Table 4.2, entry3) and only 9% (6% of **31d** and 3% of **31e**) of hydrogenolysis products were detected. Under these conditions, the hydrogenation of the ketone is therefore favoured over hydrogenolysis.

The temperature was also varied and when the reaction was carried out at 10 °C, a decrease in conversion was observed (Table 4.2, entry4) but the selectivity to cyclohexylmethylketone **31a** remained unchanged (17%).

However, only traces of hydrogenolysis products were detected. Finally, when the temperature was raised to 50 °C, a decrease in conversion to 23% was observed (Table 4.2, entry4), possibly due to deactivation of the catalyst under these conditions.

Table 4.2 Optimisation of pressure and temperature for **Rh1** catalysed hydrogenation of acetophenone **31**.[a]
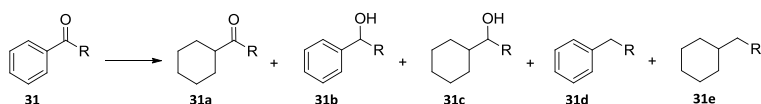
Entry	S	P	T	Time (h)	Conv. (%)[b]	31a (%)[b]	31b (%[b])	31c (%[b])	31d (%)[b]	31e (%)[b]
1	**31**	20	30	5	90	15	23	33	13	17
2	**31**	10	30	5	12	52	-	30	18	T
3	**31**	40	30	5	100	17	52	22	6	3
4	**31**	20	10	5	38	17	72	11	T	T
5	**31**	20	50	5	23	12	66	8	12	2

[a]General conditions: 2mol% Rh, 1.24 mmol of substrate, 2 mL of THF, T = 30 °C, P= 20 bar H_2.

After the optimisation of the reaction conditions, the subsequent reactions were completed at 30 °C and under 20 bar of H_2 pressure.

Finally, the system **Rh4** bearing dppb **4** as stabilising ligand was used under the optimised conditions, and full conversion (TON=83) was obtained after 5h (Table 4.1, entry17). Interestingly, in terms of selectivity, relevant differences between the two rhodium systems were observed. Indeed, using **Rh4** as catalyst, the hydrogenolysis products **31d** and **31e** were not detected while 1-phenylethanol **31b** (46%) was the main product, and **31a** and **31c** were obtained with similar selectivity (28% and 26%, respectively). These results therefore indicated strong differences depending on the metal and stabilising agents used. In terms of activity, no important changes were observed, although the system **Ru4** was slightly less active than the

other NPs. However, large differences were observed in terms of selectivity. With the ruthenium systems, the selectivity towards the cyclohexylmethylketone **31a** varied from 13% with **Ru1** (57% at shorter reaction times) to 43% using **Ru4**. With the rhodium systems, the same trend was observed, although in this case the main difference in selectivity was the formation or not of hydrogenolysis products since products **31e** and **31f** were only detected using the system **Rh1**, and not with **Rh4**. This therefore suggests that the stabilising dppb ligand **4** blocks the active sites of the NPs **Rh4** responsible for the hydrogenolysis process.

To further investigate this reaction, the hydrogenation of acetophenone **31** catalysed by **Ru1** and **Rh1** were repeated and monitored by GC-MS.

Using the **Ru1** system, full conversion was obtained after *ca.* 4h. During the first 30 min, the conversion reached *ca.* 20% and rapid formation of all 3 products **31a**, **31b** and **31c** was observed, with **31a** as the major product (*ca.* 60%). Comparing the initial rates of formation of **31a** and **31b**, the hydrogenation of the arene ring revealed to be 3 times faster than that of the ketone function. The concentration of **31a** remained constant for *ca.* 1h before decreasing to 15% after 5h of reaction. At 20% conversion, the product **31b** reached a maximum of *ca.* 20% selectivity, progressively decreasing at longer reaction times, until full disappearance after 5 h. During the reaction, 2-cyclohexylethanol **31c** became the main product via the hydrogenation of **31a** and **31b**.
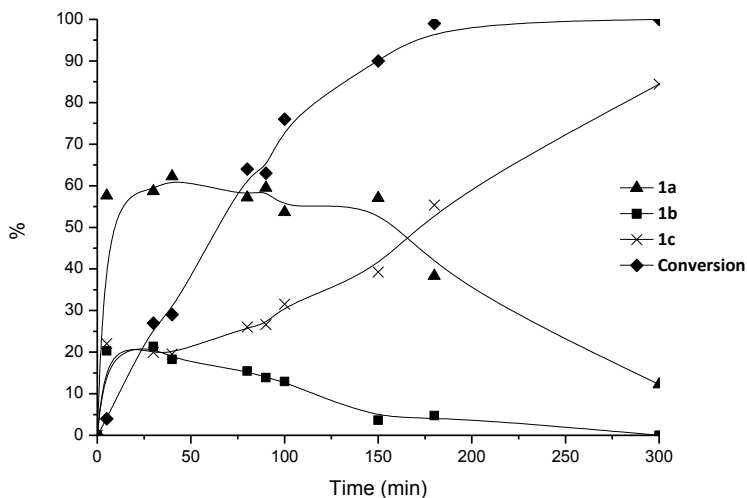
Figure 4.14 Monitoring of the catalytic hydrogenation of acetophenone **31** using **Ru1** as catalyst. (Conditions: 1.24 mmol of substrate, 2mol% **Ru1**, solvent= THF, T = 30°C, P= 20 bar H_2)

To compare the reactivity of the intermediates **31a** and **31b** under hydrogenation conditions, these compounds were used as substrates under the same reaction conditions than **31** (Table 4.1, entry 6-7). Surprisingly, when the reaction was performed with 1-phenylethanol **31b** as substrate, only 5% conversion (TON=4) into the total hydrogenated product **31c** was obtained, even after 16h. This result is in contrast with the kinetic study where **31b** fully disappeared after 5h, although in this case, conversion in **31b** was very low. It was deduced that the relative concentration of phenylethanol **31b** in solution could explain the difference observed. Kühn and co-workers[21] have recently reported that alcohols like **31b** can deactivate the catalyst by forming stable adducts with the active species. However, when cyclohexylmethylketone **31a** was used, total conversion (TON=77) was observed (Table 4.1, entry 6). This thus indicated that **31c** is mainly formed through **31a**.

The same study was carried out using the rhodium system **Rh1** and at early stages of the reaction, the product **31b** is rapidly formed and reached a

252

maximum selectivity of *ca*. 60%. Comparing the initial rates of formation of **31a** and **31b**, the hydrogenation of the arene ring revealed to be 4 times slower than that of the ketone function. At longer reaction times, the concentration of **31b** was observed to steadily decrease. The selectivity in **31a** reached 20% after 40 min and practically remained unchanged at higher conversion. As expected, the formation of the product **31c** progressively increased until the end of the reaction. The hydrogenolysis product **31d** followed a similar pattern than **31a**, with rapid formation at the very start of the reaction and constant concentration during the rest of the hydrogenation process. The concentration in product **31d** was also practically constant throughout the experiment, suggesting that this product is formed at a similar rate than that at which it is converted into **31e**.
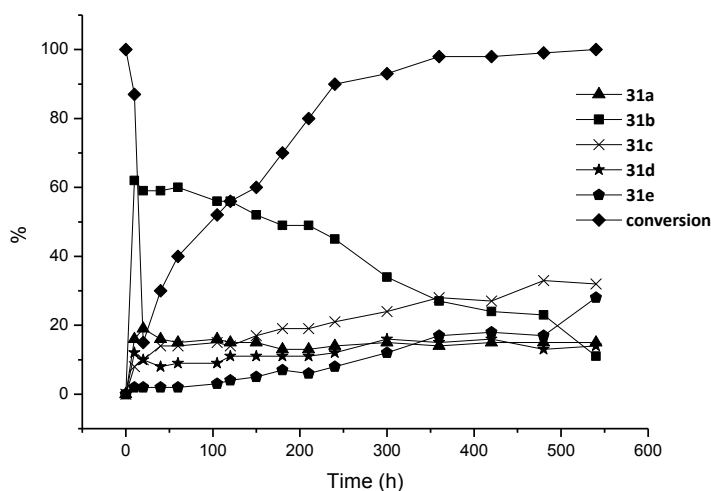

Figure 4.15 Monitoring of the catalytic hydrogenation of acetophenone **1** using **Rh1** as catalyst. (Conditions: 1.24 mmol of substrate, 2mol% **Rh1,** solvent= THF, T = 30°C, P= 20 bar H_2)

Next, the products **31a-31c** were used as substrates in the hydrogenation reaction using **Rh1** as catalyst. Interestingly, when cyclohexylketone **31a** or

253

cyclohexylethanol **31c** were reacted, no conversion was achieved even at 80°C. In contrast, when 1-phenylethanol **31b** was used as substrate, complete conversion (TON=78) was achieved with up to 66% selectivity for the hydrogenolysed product **31d**, and 26% of **31c**.
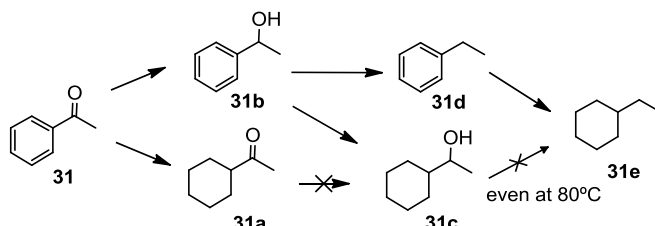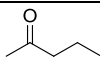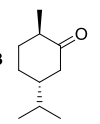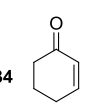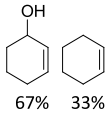
Figure 4.16 Reaction pathway for the hydrogenation of acetophenone **31** using the **Rh1** system.

In order to study the origin of the inactivity when product **31c** was used as substrate with this system, additional experiments were performed. To check whether the reaction could be inhibited by a competition between the substrate and the solvent, THF was replaced by pentane under the same conditions. However, as shown in Table 4.1, entry 14, no reaction was obtained, which was attributed to the low solubility of the NPs in this solvent.

Moreover, penten-2-one **32**, S-isopropyl-2-methylcyclohexanone **33** and cyclohex-2-enone **34** were also used as substrates under the previously described conditions (Table 4.3).

When the linear **32** and the cyclic **33** ketone were used as substrates, no reaction was observed. However, the use of the α,β insaturated ketone **34**, revealed complete hydrogenation of this substrate with 67% selectivity for the corresponding alcohol and 33% of the hydrogenolysed product. These results evidenced that the presence of at least one insaturation conjugated to the ketone is required for the hydrogenation of the carbonyl function to take place.

Table 4.3 Rh1 catalysed non-aromatic ketones (**32,33,34**).[a]

Entries	NPs	Substrate	Solvent	Conv. (%)[b]	Products	
1	Rh1	**32**	THF	0	-	-
2	Rh1	**33**	THF	0	-	-
3	Rh1	**34**	THF	100	67%	33%

[a] General conditions: 1.24 mmol of substrate, 2 mol% of Rh-NPs, 10 mL of THF, t= 5h; T = 30°C, P= 20 bar H_2. [b] Determined by GC;

The study of the hydrogenation of the cyclohexylketone **31a** showed that during the hydrogenation of **31**, the formation of product **31c** only arises from the hydrogenation of the aryl group of **31b**, and not from the hydrogenation of the ketone group of **31a** (Figure 4.16). Furthermore, the formation of the hydrogenolysis product **31e** necessarily involves the product **31b** as intermediate while the transformations of **31a** and **31c** into **31e** were shown not to proceed under these conditions.

To summarise, the results obtained in the hydrogenation of acetophenone **31** show that, very surprisingly, distinct reaction pathways are employed depending on the metal and ligand used:

- Ru NPs favour the reduction of the aromatic ring over that of the keto group, and are able to reduce **31a** to produce **31c**. However, with these catalysts, **31b** is reduced very slowly. Selectivity is influenced by the stabilising ligand.

- Rh NPs favour the reduction of the keto group over that of the aromatic ring to produce 1-phenylethanol **31b**, which is then further hydrogenated to form **31c** or hydrogenolysed to **31d** exclusively when **Rh1** is used as catalyst. Interestingly, the Rh-NPs do not reduce the cyclohexylketone **31a**.

The selectivity trends observed for the hydrogenation of acetophenone **31** are summarised in Figure 4.17.
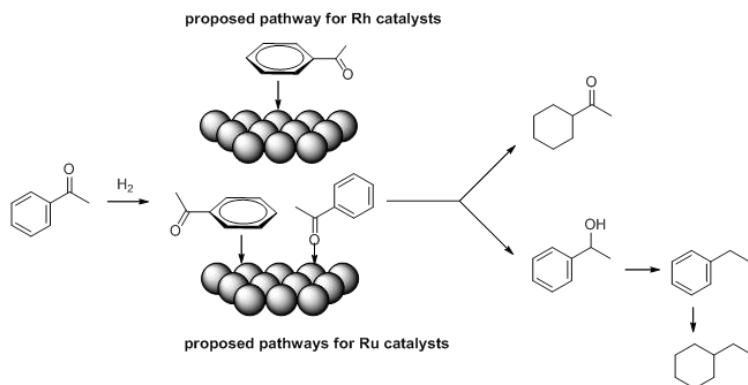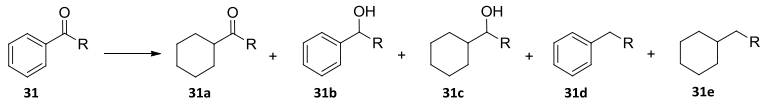
Figure 4.17 Schematic representation of the selectivity trends observed in the hydrogenation of acetophenone **31**.

Based on these results, the **Ru1** nanoparticles appeared more active than **Ru4** and **Rh1,4**. Therefore, in order to obtain similar conversions and to facilitate the comparisons in terms of selectivity, the hydrogenation of the other substrates **35-42** was carried out during 2.5h using **Ru1** as catalyst and 5h when **Ru4** and **Rh1,4** were employed.

The behaviour of Ru and Rh NPs in the reduction of acetophenone seems to be complementary: Ru-NPs mainly reduce the arene ring while Rh-NPs reduce first the keto group. On the other hand, Ru-NPs reduce the keto group of cyclohexyl methyl ketone **31a**, while Rh-NPs do not. These results prompted us to explore the behaviour of these nanocatalysts in the hydrogenation of non-conjugated aryl ketones.

Rhodium systems as catalysts

The hydrogenation of acetophenone **31** was explored using the P-ligand stabilised nanoparticles **Rh1- Rh8** synthesised in chapter 2 and Rh/C for comparative purposes as catalysts. The results are summarised in Table 4.4. The already commented results obtained with system **Rh1** and **Rh4** are also shown to facilitate the comparison.

Table 4.4 Hydrogenation of acetophenone **31** using Rh catalysts.[a]

entries	NPs	Conv. (%)[b]	31a (%)[b]	31b (%[b])	31c (%)[b]	31d (%)[b]	31e (%)[b]
1	**Rh1**	90	15	23	33	13	17
2	**Rh2**	100	14	74	11	T	-
3	**Rh3**	100	8	73	12	6	T
4	**Rh4**	100	28	46	26	-	-
5	**Rh5**	0	-	-	-	-	-
6	**Rh6**	86	24	55	18	-	-
7	**Rh7**	2	63	-	37		
8	**Rh8**	9	65	-	35		
11	**-**	0	-	-	-	-	-

[a] General conditions: 1.24 mmol of substrate, 2 mol% of Rh-NPs, 10 mL of THF, t= 5h; T = 30°C, P= 20 bar H_2. [b] Determined by GC; (T=traces)

When system **Rh2** bearing tricyclohexylphosphine **2** as stabilising agent was used as catalyst, full conversion was obtained for this substrate **31** (Table 4.4, entry 2). The same amount of cyclohexylketone **31a** than with the model system **Rh1** was detected. However, no significant formation of hydrogenolysis products was observed using **Rh2** as catalyst. Consequently, the highest selectivity was towards phenylethanol **31b**. The difference between system **Rh1** and **Rh2** could indicate that even if these systems differed only in the presence of some aromatic rings in the case of **Rh1**, the active sites responsible of the hydrogenolysis reaction are somehow occupied in the case of system **Rh2**. Moreover, as detailed in chapter 2, more crowded surface was observed by TGA using ligand **2** as stabiliser, which is in agreement with this observation.

When the system **Rh3,** bearing PMe$_3$ as stabiliser, was applied as catalyst in this reaction, full conversion was obtained (Table 4.4, entry 3). Moreover, lower selectivity to cyclohexylketone **31a** (8%) was detected than in the previous systems **Rh1** and **Rh2** and up to 6% of ethylbenzene **31d** was observed.

The systems **Rh5-Rh8** stabilised with phosphite ligands were also tested as catalysts. No activity was observed when the system **Rh5** bearing the triphenylphosphite **5** as stabiliser was used. In Chapter 3, this catalyst revealed to be inactive in the hydrogenation of substituted arenes but converted styrene into ethylbenzene selectively.

System **Rh6** bearing the bulky phosphite **6** as stabilising agent was also used as catalyst with substrate **31** (Table 4.4, entry 6). High conversion was observed (86%) with the highest selectivity (55%) towards the phenylethanol **31b**. No hydrogenolysis products were detected with this system.

Finally, system **Rh7** and **Rh8** bearing the trimethylphosphite **7** and the diphosphite **8** as stabilising agents, respectively, were used as catalysts under the same conditions. In both cases, very low activity with selectivity of *ca*. 65% for **31a** and 35% for **31c** were obtained (Table 4.4, entries 7 and 8).

This study revealed that phosphine stabilised systems **Rh1**-**Rh4** were much more active than the phosphite stabilised systems, except for system **Rh6** that also showed high activity (86%). This could indicate that the bulky ligand **6** is more weakly coordinated to the surface of the Rh-NPs than the other phosphites under study, thus favouring its decoordination/substitution by this substrate. The stronger coordination of phosphites **5**, **7** and **8** would therefore explain the low activities observed for **Rh5**, **Rh7** and **Rh8** under these conditions. The highest selectivity for the hydrogenolysed products was obtained using system **Rh1**, whereas the systems **Rh2** and **Rh3** only provided traces of these products.

Comparison with Rh/C

For comparative purposes, the heterogeneous Rh/C catalyst was used for the hydrogenation of acetophenone **31**. The reaction was monitored under the same previous employed conditions, 30°C and 20 bar of hydrogen pressure (Figure 4.18).
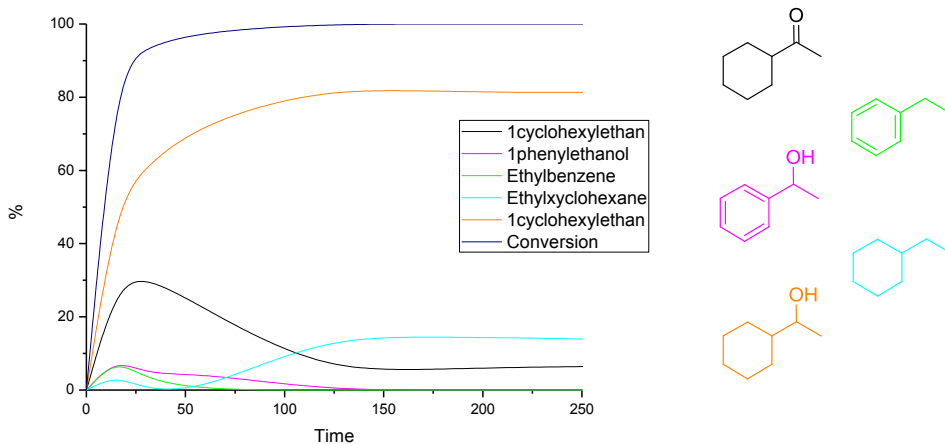
Figure 4.18 Monitoring of the catalytic hydrogenation of acetophenone **31** using Rh/C as catalyst. (Conditions: 1.24 mmol of substrate, 1mol% Rh/C, solvent= THF, T = 30°C, P= 20 bar H$_2$)

Full conversion was obtained after 90 min, and at this reaction time, 80% of the substrate had been converted into 1-cyclohexylethanol **31c**. Using this catalyst, the hydrogenation of the arene ring is preferred over that of the ketone group since phenylethanol **31b** and ethylbenzene **31e** were only detected in low quantity.

Using Rh/C as catalyst, faster hydrogenation than with the rhodium nanoparticles **Rh1-Rh8** was therefore obtained with the formation of the totally hydrogenated product **31c**. Hydrogenolysis products were also observed but in low amount. Upon addition of PPh$_3$ **1** to the reaction mixture (0.4eq phosphine ligand per rhodium), only 7% conversion was obtained after 5h, and it was concluded that the phosphine was acting as a poison for this system.

4.2.2   Reduction of non-conjugated aryl ketones

The reduction of non-conjugated aryl ketones and the influence of the alkyl chain length between the phenyl and the ketone groups (substrates **35** and **36**) was studied using **Ru1-4** and **Rh1-4** as catalysts. Using the ruthenium systems **Ru1-4**, *ca*. 67% conversion was obtained for both substrates (Table 4.5, entries 1-2 and 4-5). For substrate **35**, 58% selectivity for the arene-hydrogenated product **35a** was obtained (entry 1) using **Ru1** while only 30% was achieved using **Ru4** system (entry 2). For substrate **36**, the selectivity to **36a** is higher than for **35a**, similarly to the trend observed in the hydrogenation of **35**, **Ru1** provided higher selectivity to **36a** than **Ru4**.

When the reaction was performed with the rhodium nanoparticles **Rh1-4** as catalysts, high conversions (*ca.* 70%) were obtained in all the cases. In these reactions, high to excellent selectivity for the arene hydrogenated products were achieved, obtaining up to *ca*. 75% of the cyclohexylketone derivative **35a** and up to 94% of product **36a**. The selectivities obtained for both substrates were similar using both systems **Rh1** and **Rh4**. High selectivity towards arene reduction in the presence of distant carbonyl groups has been already observed.[4a,7,13] It should be noted that low selectivity for the fully hydrogenated products was obtained in these experiments.

For substrates **35** and **36**, the nature of the metal affects significantly the catalytic results. Indeed, with rhodium NPs, the selectivity for arene reduction increases when the separation between arene and carbonyl group increases until reaching practically total selectivity for arene reduction. Moreover, the ligand stabiliser shows neither influence on the conversion nor on the selectivity. Thus the selectivities obtained with **Rh1** and **Rh4** are identical. This suggests that substrate coordination takes place through the aromatic ring while the carbonyl group is progressively pushed away from the nanoparticle. The fact that the ligand does not affect conversion and selectivity indicates that both ligands leave enough space at the surface of these nanoparticles for the arene coordination.

Table 4.5 Hydrogenation of ketones **35**, **36** catalysed by Ru- (**Ru₁₋₄**) and Rh-NPs (**Rh₁₋₄**).[a]

35: n= 1   35a: n= 1   35b: n= 1   35c: n= 1
36: n= 2   36a: n= 2   36b: n= 2   36c: n= 2
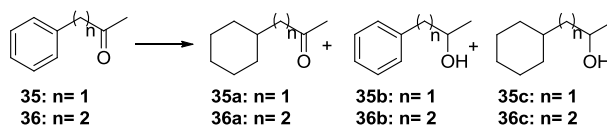
	Substrate	NPs	Conv. (%)[c]	a (%)[c]	b (%)[c]	c(%)[c]
1[b]	**35**	**Ru1**	67	58	39	3
2	**35**	**Ru4**	66	30	70	-
3[b]	**36**	**Ru1**	66	74	17	9
4	**36**	**Ru4**	67	47	37	16
5	**35**	**Rh1**	78	76	24	-
6	**35**	**Rh4**	64	74	26	0
7	**36**	**Rh1**	73	93	3	4
8	**36**	**Rh4**	80	94	2	4

[a]General conditions: 2mol% M (M=Ru,Rh), 1.24 mmol of substrate, 10 mL of THF, T = 30 ºC, P= 20 bar H_2, t=5h. [b]t=2.5h. [c] 3 mg of Ru-NPs, 1.24 mmol of substrate, 10 mL of THF, T = 30 ºC, P= 20 bar H_2, t=5h.[c]Determined by GC.

In the case of the Ru catalysts, the stabilising ligand does not influence the conversion but affects the selectivity, increasing the percentage of ketone reduction when dppb **4** is the stabiliser **Ru4**. It is relevant that even for compound **36**, 37% of ketone reduction was obtained. However, this is not suprising since we observed earlier that ruthenium is able to reduce alkyl ketones like **31a** (See Table 4.1). These results suggest that the stronger coordination and higher steric hindrance of the dppb **4** ligand limits more efficiently the coordination of the arene than the coordination of ketone. This may be due to a higher bonding energy of phosphines towards ruthenium than towards rhodium and/or to the different geometries of these small polyhedral NPs as a result of their different crystal structure, namely hcp and fcc.
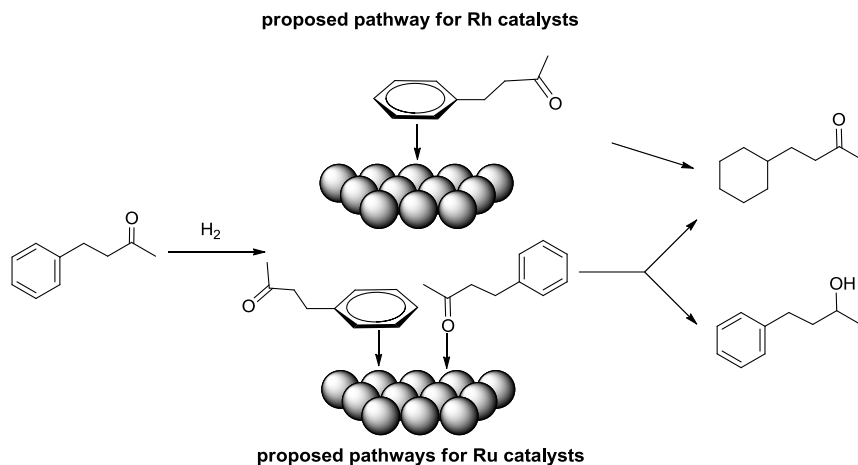
Figure 4.19 Schematic representation of the selectivity trends observed in the hydrogenation of aryl ketones **31**, **35**.

Comparing the results of Table 4.1 and Table 4.5, it can be observed that the rhodium NPs reduce selectively the arene in compounds **35** and **36**, which can be related to the fact that they do no reduce alkyl ketones such as **31a**. However, in the case of acetophenone **31** the reduction of the ketone group is preferred. Concerning, ruthenium NPs the situation is different since reduction of arene and carbonyl groups are competitive for all substrates, including for non-conjugated aryl ketones. Although the selectivity towards arene reduction also increases when aryl and keto groups become more and more separated.

These results therefore suggest that acetophenone **31**, which is often selected for testing the competition between reduction of arene and carbonyl group, is in fact a particular case that deserves additional attention. In this context, we decided to enlarge the study to the reduction of the acetophenone derivatives **37-42** containing different substituents in the alkyl and phenyl moieties, compounds, in search of information about the particular behaviour of acetophenone **31**.

Table 4.6 Rh-NPs (**Rh1,4**) catalysed hydrogenation of ketones **37**-**42**.[a]
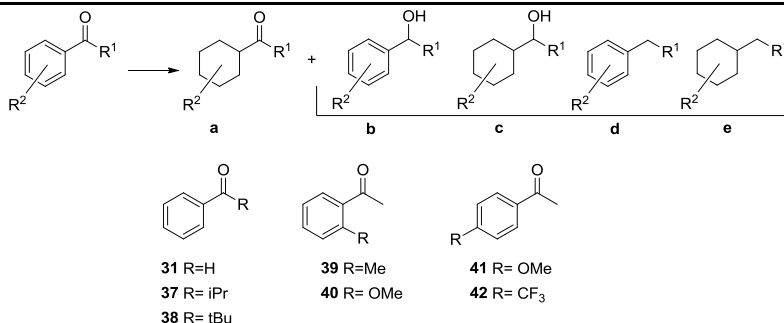
Entry	Substrate	NPs	Conv. (%)[b]	a (%)[b]	(b+c+d+e) (%)[b]
1	31	Rh1	90	15	85[c] (23, 33, 13, 17)
2	31	Rh4	100	28	72[c] (46, 26, ---, ---)
3	37	Rh1	90	13	87[c] (69, 18, ---,---)
4	37	Rh4	91	21	79[c] (63, 16, ---,---)
5	38	Rh1	50	18	82[c] (71, 11, ---,---)
6	38	Rh4	54	27	73[c] (66, 7, ---, ---)
7	39	Rh1	85	23	77[c] (59, ---, 14, 3)
8	39	Rh4	81	32	68[c] (59, 9, ---, ---)
9	40	Rh1	100	20	80[c] (50, ---, 26, 4)
10	40	Rh4	75	6	94[c] (73, 16, ---, ---)
11	41	Rh1	96	10	90[c] (43, 9, 24, 7)
12	41	Rh4	98	16	84[c] (48, 36, ---, ---)
13	42	Rh1	100	5	95[c] (57, ---, 23, 12)
14	42	Rh4	100	0	100[c] (87, 13, ---, ---)

[a] General conditions: 2mol% M (M=Ru,Rh), 1.24 mmol of substrate, 10 mL of THF, T = 30 °C, P= 20 bar H_2, t=5h. [b] Determined by GC [c] Addition of percentage of compounds **b-e.**

The results of the reduction of compounds **37-42** in the presence of **Rh1,4** are collected in Table 4.6 (Results obtained in the reduction of acetophenone **31**, under the same reaction conditions are also included for comparison). Moreover, since it was demonstrated in Table 4.1 that **Rh1,4** do not reduce cyclohexyl alkyl ketones it can be considered that compounds **c**, **d**, **e**, are generated from **b**, and a new value resulting from the addition of the percentages of all these compounds was included in the table.

From these results (Table 4.6), the following conclusions can be drawn:

a) Conversions are significantly affected by the steric hindrance of the alkyl substituent of the ketone (compounds **37, 38**, entries 3 and 6) but the ratio of products a : b+c+d+e remains practically unchanged, which indicates that the hydrogenation of these substrates follows a similar mechanism. Which implies that the reactions of 1, 4 and 5 adopt a similar mechanism.

Interestingly, the presence of substituents on the aromatic ring has little influence and high conversions were obtained in all cases. It is worth noting that conversion of compounds with substituents in *para* position (**41**, **42**), and more generally when **Rh1** were used, was not affected by the substitution. In contrast with previous studies which determined that substrates with electron donating groups are hydrogenated faster than substrates with electron-withdrawing groups,[22] no clear effect of the substituents on the aromatic ring on the activity was observed in this study (entries 11-14).

b) Concerning the selectivity, products obtained from reduction of the ketone group were preferably obtained in all cases (>70%), and the phenylethanol derivatives **39b**-**42b** were the major products (entries 7-14), in agreement with the results observed for compound **1**.

In general, ketone reduction slightly decreases when **Rh4** (dppb stabiliser) is used. The selectivity is not influenced by the modification of the alkyl moiety, but is more significantly affected when substituents are present on the arene moiety. This is particularly true when the substituent is located in *para* position, since arene reduction decreases notably. Interestingly, using **Rh4** nanoparticles as catalysts, exclusive reduction of the carbonyl group with full conversion was obtained in the reduction of compound **42**, which incorporates the electron withdrawing group CF_3. However, a general trend concerning the influence of the stabilizing ligand on the selectivity cannot be established. c) Hydrogenolysis of 1-phenylethanol, produced by the reduction of the carbonyl group of these substrates to give ethyl benzene and then ethylcyclohexane was also observed. As for substrate **31**, this process was only observed with the Rh nanoparticles stabilised with PPh_3 **1**.

The hydrogenolysis process was stopped when the steric hindrance of the alkyl side chain increases, but not when the substituents are present in *ortho* or *para* position of the aromatic ring.

These results can be related with the lability of the monophosphine in contrast with the stronger coordinating diphosphine. Indeed, PPh_3 **1** can dissociate from the particle and therefore liberate the sites responsible for the hydrogenolysis reaction. These sites are therefore expected to be the apex and edge sites which are left undercoordinated.

In the case of rhodium nanoparticles, the coordination of the arene group seems to dominate the interaction of the substrate with the catalyst surface, while the coordination of carbonyl group with the nanoparticle is not evidenced by the results of this study since alkyl ketones and aromatic compounds containing a carbonyl group far from the ring, only the aromatic ring is reduced. The case of acetophenone derivatives is singular, since despite coordination to the nanoparticle takes place through the aromatic ring, the carbonyl group remains in a position very favorable for its reduction, in such a way that it takes place faster than the arene reduction. The selectivity of this process is scarcely affected by substitution in the alkyl or arene sides, and only the substitution in *para* completely drives the reaction towards the reduction of ketone. No significant electronic effect was observed (Entries 11, 12 vs. 13, 14).

Once the carbonyl group is reduced, further aromatic ring reduction can take place and when the reaction is catalysed by **Rh1** (PPh_3 stabiliser), hydrogenolysis is also observed.

The results obtained in the hydrogenation of the acetophenone derivatives **37-42** using **Ru1,4** as catalysts are summarised in Table 4.7.

Table 4.7 Ru-NPs (**Ru1,4**) catalysed hydrogenation of ketones **37-42**.[a]
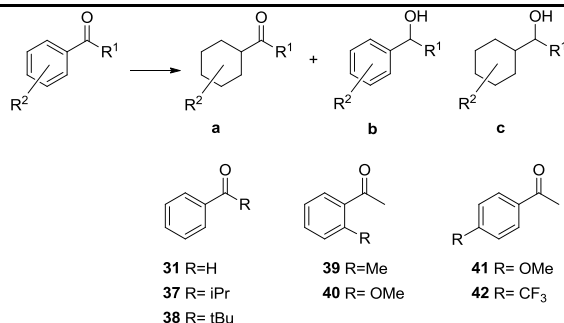
Entry	Substrate	NPs	Conv. (%)	a (%)[b]	b (%)[b]	c (%)[b]
1	31	Ru1	90	57 (96)[c]	4	39
2	31	Ru4	70	43(59)[c]	41	16
3[d]	37	Ru1	39	54 (67)[c]	33	13
4	37	Ru4	35	47 (59)[c]	41	12
5[d]	38	Ru1	35	38 (46)[c]	54	8
6	38	Ru4	36	35 (41)[c]	59	6
7[d]	39	Ru1	44	64	36	--
8	39	Ru4	25	36	64	--
9[d]	40	Ru1	39	--	100	--
10	40	Ru4	20	22	78	--
11[d]	41	Ru1	60	32 (50)[c]	50	18
12	41	Ru4	42	20(39)[c]	61	19
13[d]	42	Ru1	62	16	84	--
14	42	Ru4	49	14	86	--

[a] General conditions: 2mol% M (M=Ru,Rh), 1.24 mmol of substrate, 10 mL of THF, T = 30 °C, P= 20 bar H_2, t=5h. [b] Determined by GC. [c] Selectivity in arene reduction considering that compound **c** it has been generated from **a**. [d] t= 2.5 h.

The general trends that can be deduced from the results contained in Table 4.7 are:

Reduction of aromatic ring is preferred to the reduction of the keto group, especially with **Ru1** nanoparticles. Taking into account that 1-phenylethanol is reduced very slowly by these catalysts, it can be considered that compound **31c** is formed from **31a**, which suppose that the initial selectivity towards the reduction of the aromatic ring is very high.

In general, conversions with **Ru1,4** NPs were lower than when **Rh1,4** were used, and the increase of substitution in the alkyl chain (entries 3-6) or in the aromatic ring (entries 7-14), particularly when the substituents are located in *ortho* position (entries 7-10). For substrates **37**, **38** and **39**, the products resulting from the total reduction were not observed. The stabilising ligand also affects significantly the conversion and, in general, when **Ru1** NPs (entries 3, 5, 7, 9, 11, 13) were used, conversions were higher or similar than with **Ru4** NPs (entries 4, 6, 8, 10, 12, 14). This indicates that in this case, the coordination of both aromatic ring and keto groups are strongly affected by steric factors in the substrate or in the ligand. Consequently, only 25 and 20% of reduction was achieved for substrates **39** and **40** in respectively (entries 8 and 10).

The selectivity is also affected by the same factors. Thus, the increase of steric hindrance in the substrate or the use of dppb **4** as stabiliser shifts the selectivity towards ketone reduction, which indicates that the rate of arene reduction is more affected than that of ketone reduction. Furthermore, in this case, substrate **40** has a particular behavior, since the reaction affords high percentages of carbonyl group reduction. This fact probably confirms the slow arene reduction in the 1-arylethanol derivative, since in this case, product **42c** was not observed.

A particular case is the reduction of compound **40** with **Ru1** where exclusively product **40b** was detected in the selected reaction time. Although the origin of this behavior is unknown, the possibility of this substrate to act as a bidentate ligand may initially orientate the reaction towards ketone reduction and thus impedes further arene reduction.

Comparing the results obtained with substrates **31** and **37-42**, the reduction of the arene group is largely preferred in compound **31** as a consequence of the affinity of the arene for the NPs. However, the results obtained with compounds **37-42**indicate that small variations in the steric properties of the substituents of the aromatic ring and of the alkyl keto group cause important shifts in selectivity.

4.3 Conclusions

A series of Ru and Rh nanoparticles stabilised by P-based molecules were successfully synthesised and characterised. Comparable results in terms of size and stabiliser content were obtained. A comparative study of aryl ketones reduction using these nanoparticles was carried out which provided some general clues about this process.

For the selective reduction of aryl ketones, acetophenone **31**, which is often selected for testing the competition between reduction of arene and carbonyl group, adopts a singular behaviour and two types of substrates have to be distinguished:

When the aryl ketones are not conjugated (**35-36**), a general preference for arene reduction is observed, this selectivity being higher for rhodium than for ruthenium NPs. The selectivity for arene reduction also increases when the number of methylene groups between the arene ring and the keto group increases. In the case of Ru NPs the selectivity for arene reduction decreased when **Ru4** NPs were used. These results suggest that the higher coordination ability and bulkiness of dppb ligand limits more strongly the coordination of the arene than the coordination of ketone. This may be due to a higher bonding energy of phosphines towards ruthenium than towards rhodium and/or to the different geometries of these small polyhedral NPs as a result of their different crystal structure, namely hcp and fcc.

For acetophenone derivatives **37-42**, the selectivity trends observed were distinct, but were general independently of the substituents present on the phenyl ring. These trends observed for ruthenium and rhodium nanoparticles are distinct and can be summarized as follows: a) Ru NPs reduce preferentially the arene group, but also reduce cyclohexylmethylketone and forms the fully reduced compound. b) Rh NPs mainly reduce the keto group. The reaction further proceeds providing hydrogenolysis products in most cases, and arene reduction to a lower extent. c) Rh NPs reduce dialkyl ketones very slowly and the reaction is even inhibited when the substrate does not contain insaturations. This

general selectivity trend is not affected by the substitution on the arene ring or in the alkyl chain of acetophenone. d) Substitution in the alkyl chain strongly affects the conversion with all NPs used but does not influence the selectivity. e) Substitution on the arene ring affects negatively the conversion when Ru NPs were used, but not with Rh NPs. f) The stabilizing ligand has an influence on both the conversion and the selectivity with Ru NPs while in the case of Rh NPs, the selectivity "arene versus ketone reduction" is practically not affected by the phosphine ligand. g) however, the selectivity towards hydrogenolysis is strongly affected since this process mainly takes place with **Rh1** as catalysts. It is noteworthy that this hydrogenolysis process is stopped when the steric hindrance of the alkyl moiety of the substrate increases, but not when substituents are present at *ortho* or *para* positions in the aromatic ring. h) changing the phosphine stabilizers for phosphite ligands caused in most cases a strong decrease in activity, except in the case of the catalyst bearing the bulky monophosphite **6**.

In general, it can be considered that in the case of rhodium NPs, the coordination of arene dominates the interaction of the substrate with the nanoparticle, while the coordination of the ketone group with the nanoparticle was not evidenced, and for alkyl ketones and aromatic compounds containing a carbonyl group far from the ring, the carbonyl remains unaltered and only the aromatic ring is reduced.

The case of acetophenone derivatives is singular, since despite coordination to the nanoparticle takes place through the aromatic ring, the carbonyl group remains at a position very favorable for its reduction, in such a way that it is hydrogenated faster than the arene moiety. The selectivity of this process is scarcely affected by substitution in the alkyl or arene groups, and only the substitution in *para* position of the aromatic ring completely drives the reaction towards the reduction of ketone.

For Ru NPs, however, the results show that both arene and ketone coordinate to the NPs surface in a competitive way. The selectivity is

strongly affected by the steric hindrance in the ligand and in the substrate, which in both cases increases the ketone reduction.

As a whole, this study using two similar platinum metal nanoparticles of similar sizes and bearing two ligands of very similar electronic and steric effects but with different dissociation abilities, leads to different results in terms of activities and selectivities. This therefore demonstrates the interest for tayloring the composition and surface of these organometallic nanoparticles in order to modify their reactivity, in a way comparable to what is nowadays commonly achieved for molecular complexes.

4.4 Experimental part

Reagents and general procedures

All syntheses were performed using standard Schlenk techniques under N_2 or Ar atmosphere. Chemicals were purchased from Aldrich Chemical Co, Fluka and Strem. All solvents were distilled over drying reagents and were deoxygenated before use. The precursor [Ru(COD)(COT)] was purchased from Nanomeps. The precursor $Rh(\eta^3\text{-}(C_3H_5)_3$, was prepared following previously described methods.[1][2] The synthesis of the nanoparticles were performed using 1L Fisher Porter and pressurized on a high pressure line.

Characterization techniques (See Experimental part of Chapter 2)

General procedure for the synthesis of the Ru-NPs.

In a typical procedure, the [Ru(COD)(COT)] (400 mg, 1,268 mmol) was placed into a Fischer-Porter reactor in 400 mL of dry and deoxygenated THF by freeze-pump-thaw cycles in the presence of the ligand (0.2 equiv. for dppb and 0.4 equiv. for PPh_3). The Fischer-Porter reactor was then pressurised under 3 bar of H_2 and stirred for 24 h at room temperature. The initial yellow solution became black after 20 minutes. After elimination of excess dihydrogen, a small amount (5 drops approx.) of the solution was deposited under an argon atmosphere on a carbon-covered copper grid for transmission electron microscopy analysis (TEM). The rest of the solution was concentrated under reduced pressure to 40 ml. Precipitation and washing with pentane (3x15 ml) was then carried out, obtaining a black precipitate.

General procedure for the synthesis of the Rh-NPs (See Experimental part of Chapter 2).

General procedure for the hydrogenation reactions.

Autoclave Par 477 equipped with PID control temperature and reservoir for kinetic measurements and HEL 24 Cat reactor for substrate scope were used as reactors for the hydrogenation reactions. In a typical experiment, the autoclave was charged in the glove-box with Ru or Rh nanoparticles (3 mg for Ru-NPs, 1.6mol%; 3.5 mg of Rh-NPs, 2 mol%; the catalyst concentration was calculated based on the total number of metallic atoms in the NPs) and the substrate (1.24 mmol, approx. substrate to Metal ratio=55) in 10 mL of THF. Molecular hydrogen was then introduced until the desired pressure was reached. The reaction was stirred for 5h at 30°C. The autoclave was then depressurised. The solution was filtered over silica and analysed by gas chromatography. The conversion and the selectivities of the product were determined using a Fisons instrument (GC 9000 series) equipped with a HP-5MS column.

GS-MS spectroscopy was carried out on a HP 6890A spectrometer, with an achiral HP-5 column (0.25mm x 30m x 0.25um). The method used consist in an initial isotherm period at 40 °C for 3 min followed by a 3 °C min^{-1} temperature ramp to 120 °C and a hold time of 12 min, flow 1.3 ml/min.

4.5 References

[1] J. A. Widegren, R. G. Finke, *J. Mol. Cat. A: Chem.* **2003**, 191, 187-207.

[2] A. Roucoux, *Top. Organomet. Chem.* **2005**, 16, 261-279.

[3] A. Gual, C. Godard, S. Castillon, C. Claver, *Dalton Trans.* **2010**, 39, 11499-11512.

[4] a) G.S. Fonseca, J.D Scholten, J. Dupont, *Synlett* **2004**, *9*, 1525-1528; b) F. Jutz, J.-M Andanson, A.Baiker, *J. Catal*. **2009**, *268*, 256-266.

[5] M. Jahjah, Y. Kihn, E. Teuma, M. Gómez, *J. Mol. Catal. A: Chem.* 332, **2010**, 106–112.

[6] I. Favier, S. Massou, E. Teuma, K. Philippot, B. Chaudret, M. Gómez, *Chem. Commun*. **2008**, 3296–3298.

[7] D. Gonzalez-Galvez, P. Lara, O. Rivada-Wheelaghan, S. Conejero, B. Chaudret, K. Philippot, P. W. N. M. van Leeuwen, *Catal. Sci. Technol.* **2013**, 3, 99-105.

[8] M. Freifelder, *J. Org. Chem.* **1964**, 29, 2895–2898.

[9] E. Wenkert, K. G. Dave, F. Haglid, R. G. Lewis, T. Oshi, R. V. Stevens, M. Terashim, *J. Org. Chem.* **1968**, 33, 747–753.

[10] M. Guerrero, A. Roucoux, A. Denicourt-Nowicki, H. Bricout, E. Monflier, V. Collière, K. Fajerwerg, K. Philippot, *Catal. Today,* **2012**, 183, 34–41.

[11] M. Guerrero, Y. Coppel, N. T. T. Chau, A. Roucoux, A. Denicourt- Nowicki, E. Monflier, H. Bricout, P. Lecante, K. Philippot, *Chem. Cat. Chem*, **2013**, *5,* 1 – 11.

[12] G. S. Fonseca, J. D. Scholten, J. Dupont, *Synlett* **2004**, 9, 1525-1528.

[13] D. J. M. Snelders, N. Yan, W. Gan, G. Laurenczy, P. J. Dyson, *ACS Catal.* **2012**, 2, 201–207.

[14] R. J. Bonilla, B. R. James, P. G. Jessop, *Chem. Commun.* **2000**, 941-942.

[15] F. Jutz, J. M. Andanson, A. Baiker, *J. Catal.* 268, **2009**, 356–366.

[16] M.V. Escárcega-Bobadilla, C. Tortosa, E. Teuma, C. Pradel, A. Orejón, M. Gómez, A.M Masdeu-Bultó, *Catalysis Today*, **2009**, *148*, 398–404.

[17] J. García-Antón, M.R. Axet, S. Jansat, K. Philippot, B. Chaudret, T. Pery, G. Buntkowsky, H.-H. Limbach, *Angew. Chem. Int. Ed.* **2008**, *47*, 2074 –2078.

[18] A. Gual, C. Godard, K. Philippot, B. Chaudret, A. Denicourt-Nowicki, A. Roucoux, S. Castillón, C. Claver, *ChemSusChem*, **2009***, 2*, 769–779.

[19] P. Lara, K. Philippot, B. Chaudret, *ChemCatChem*, **2013**, *5*, 28-45.

[20] G.S. Fonseca, A.P. Umpierre, P.F.P Fichtner, S.R.Teixeira, J. Dupont, *Chem.Eur.J.* **2003**, *9*, 3263-3269.

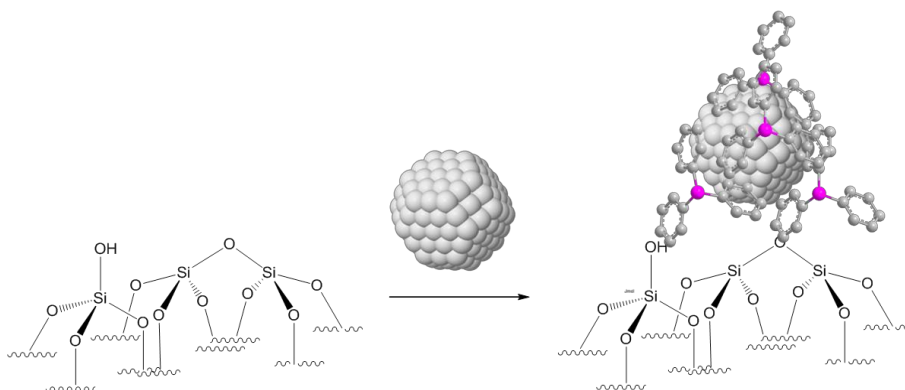[21] D. Jantke, M. Cokoja, M. Drees, W.A. Herrmann, F.E Kühn, *ChemCatChem*. **2013**, *5*, 3241-3248.

[22] P. Lara, O. Rivada-Wheelaghan, S., R. Poteau, K. Philippot and B. Chaudret, *Angew. Chem., Int. Ed.* **2011**, 50, 12080-12084.

Chapter 5.

Anchoring of organometallic RhNPs onto modified silica: a preliminary study

5.1 Introduction

Catalysis is a key technology in today's world economy since over 70% of industrial chemical processes involve catalysts. In most cases, the use of supported catalysts is required to ensure the sustainability of these processes, due to benefits offered by these catalysts in terms of recovery and reuse, and consequently in terms of energy and chemical costs.[1]

In this context, the last chapter of this thesis deals with the anchoring of Rh-nanoparticles stabilised by PPh_3 derivatives onto modified silica. This work was carried out in the context of a collaboration with Prof. Catherine Santini during a short stay under the supervision of Dr. Mostafa Taoufik in the École Supérieure de Chimie Physique Électronique in Lyon, France. The aim of this project was to explore several approaches for the anchoring of Rh-NPs and the characterisation of the resulting species using the techniques employed in surface organometallic chemistry that will be detailed in the following sections.

A catalyst support can be defined as a material, usually a solid with a high surface area, to which a catalyst is attached.[2] The reactivity of the catalysts occurs at the surface atoms; therefore, efforts are made to maximise the surface area of the catalyst through a good distribution over the support. Understanding the chemical and physical factors involved such as the interaction between the catalyst and the support is therefore key to design more efficient catalysts.

Several approaches have been reported for supporting metal nanoparticles (see Chapter1, Section 1.4).[3] These catalysts are usually supported onto materials such as alumina, silica, titania or carbon nanotubes and the most common methodologies are impregnation or deposition.[4]

For their characterisation, the techniques used for unsupported metal nanoparticles are usually employed for supported materials providing valuable information about the properties of the supported catalysts. However, information on the nature and strength of the interaction

between the catalysts and the support are difficult to obtain by these characterisation techniques.

In this project, surface organometallic chemistry (SOMC) approach was used to support metal NPs stabilised by P-based ligands as it provides accurate synthetic strategies to obtain well defined supported catalysts.[5] SOMC can be defined as the study at a very fundamental level of the synthesis, structure, stoichiometry and reactivity of organometallic fragments grafted onto inorganic supports. The main objective of this approach is the transfer of concepts and tools from molecular chemistry to surface science, affording heterogeneous catalysts able to perform selective chemical transformations. For instance, surface organometallic chemistry provides relevant information for supported catalytic systems with the formation of well defined species, which allows a better understanding of their reactivity/selectivity.[6]

5.1.1 *Support modification using surface organometallic chemistry (SOMC)*

The use of SOMC for the anchoring of nanoparticles has proved to be very difficult from an experimental point of view due to the low percentage of metal particle grafted on a support and the low surface area of the metal particles in comparison with the high surface area of the supports.[7]
However, a collaboration between the groups of Chaudret and Basset, following this approach reported the successfully synthesis of ruthenium nanoparticles stabilised by octylsilane ligands.[8]

The strategy followed in this project is represented in Figure 5.1. The modification of the silica support consists in a two-step synthesis where different elements are added onto the silica. First, a linker is anchored to the silica surface that provides the possibility to incorporate the spacer between the support and the catalyst. These modifications are expected to

strengthen the interaction between the catalyst and the support, and the robustness of the system.
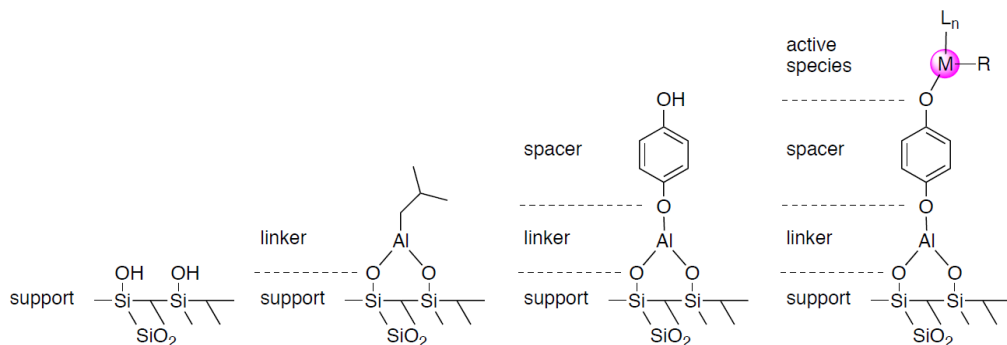
Figure 5.1 Strategy followed for the modification of the silica support.

5.1.2 Silica as a catalyst support

Silica is the most thoroughly studied support due to its high surface area and porosity compared to other materials. Furthermore, it exhibits no phase transition on heating, allowing the use of this support for reactions at high temperatures.[9] However, it is not an inert solid and can react with water vapour to form a volatile hydrosilicate at high temperatures. The nature and quantity of the reactive surface groups are well studied and can be modulated and controlled.[10] Over the last few decades, advances in spectroscopic and theoretical methods have led to an improvement in the understanding of the silica surface[11] which is composed by different types of surface silanol groups (Figure 5.2). If a distance of ca. 50Å exists between these groups, they are defined as isolated silanols. However, if this distance is close enough to form hydrogen bonding, they are called vicinal. Germinal silanols containing two hydroxyls attached to one silicon atom are also present at the surface of silica, together with perturbed isolated silanols, containing a hydroxyl group that is interacting with other functional group at the surface.[12]
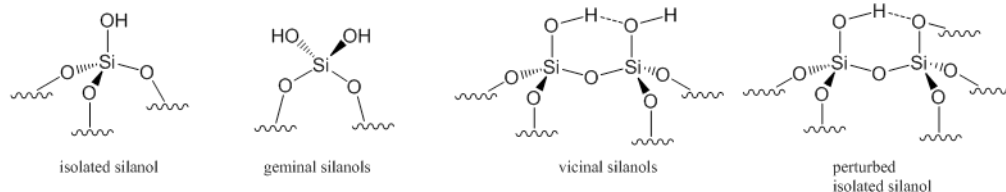
Figure 5.2 The different types of hydroxyl groups present on silica surface.

Among the different types of materials, SBA-15 was selected for this study as this type of silica presents an ordered mesoporous network formed by regular spheres of an average diameter of 150 Å and a large surface area of *ca.* 200 m^2/g.[13]

Thermal treatment is required to control the reactivity of this surface. This process is called partial dehydroxylation, leading to a support referred to as SiO$_{2-(t)}$, for which T is dehydroxylation temperature. This process occurs via condensation of two adjacent silanols ($\equiv$SiOH) into a siloxane bridge and H$_2$O. Moreover, after thermal treatment, the overall structural features of SBA-15 and its characteristic properties previously mentioned are retained.

When silica is treated under mild conditions (typically 200-500 °C), both non-interacting and interacting (vicinal) silanol species are present, with the latter being the most abundant, with a hydroxyl concentration of 3.5 OH/nm^2 (SiO$_{2-200}$). However, highly dehydroxylated silica such as SiO$_{2-700}$ (0.7 OH/nm^2), can be obtained by heating at 700 °C under high vacuum. This material mostly features non-interacting silanol species. This transformation can be monitored by IR spectroscopy via the decrease in intensity of the characteristic sharp peak at 3747 cm^{-1} (υ_{Si-OH}).

After this treatment, the silica obtained contains a known concentration of an unique type of hydroxyl groups. This latter treatment was utilised in the work presented here.

5.1.3 Modification of the silica support to anchor organometallic complexes

The direct grafting of organometallic complexes onto silica surfaces has been studied extensively.[5] More specifically, the anchoring of tungsten, rhenium and tantalum complexes, was reported onto this type of surfaces.[14] In these studies, the interactions between the metallic centre with the silanol groups of the silica surface were studied. The tantalum complex immobilised onto a partially dehydroxylated silica described in this report is represented in Figure 5.3.[14c]
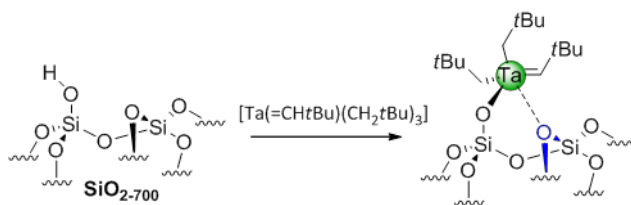

Figure 5.3 Tantalum complex anchored onto SiO_{2-700}.

The characterisation of the system by EXAFS, IR, mass balance analysis and NMR revealed the presence of stabilising interactions at the Ta- centre that exhibited a pseudo- octahedral geometry through interaction with an adjacent silanol surface bridge (Figure 5.3). This catalytic system was applied in alkane metathesis and the stabilisation of the complex on the silica surface was shown to influence the initiation step of the reaction and the product selectivity.

In order to avoid these surface interactions, the introduction of a spacer between the complex and the surface was envisaged. Due to their rigidity, large size and stability, most of the spacers used for this purpose were molecules containing aromatic moieties.[15]
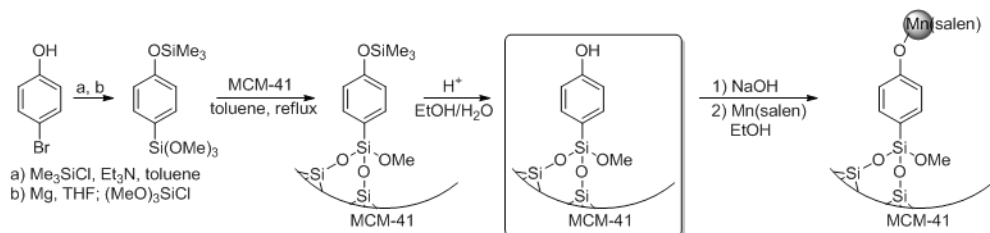
Figure 5.4 Modification of a mesoporous silica with an aromatic group as spacer.

Li and co-workers reported the modification of a mesoporous silica with the phenyl derivative used as spacer and the subsequent anchoring of a salen complex (Figure 5.4).[16] The system was used in the asymetric epoxidation of unfunctionalized olefins. In this study, the functionalisation of the surface was not complete and the residual silanols were shown to hinder the selective grafting of the complexes and result in a multiplicity of sites. A passivation of this unreactive silanols is necessary for instance to minimise these side reactions.

Face to this fact, a different approach was required to improve the synthesis of a single-site catalyst, leading to the strategy shown in Figure 5.1. So, in addition of the use of a spacer, a linker is required to improve the anchoring to the silica surface.

Triisobutylaluminium as a linker

One way to overcome these drawbacks is the treatment of the surface silanols with a compound reactive enough to quantitatively consume them and also able to further react selectively with other chemicals. The modification of silica surface by aluminium alkyls is one of the most versatile approaches to surface functionalisation.[17] Over the last decades, an impressive number of academic and industrial studies have been dedicated to the study of the reactivity of AlR_3 with silica. The choice of this alkyl group is crucial, since many aluminium derivatives have the tendency to dimerise or trimerise by formation of Al-C-Al bridges. The group of Taoufik and co-workers reported the generation of a well-defined

supported aluminium mono-isobutyl species using the commercially available triisobutyl aluminium as precursor (Figure 5.5).[18]
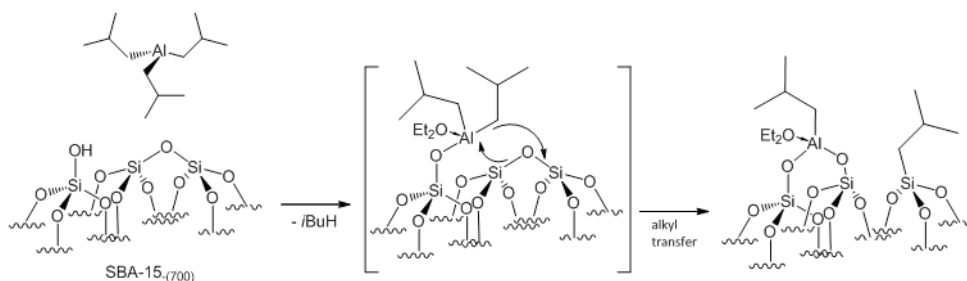

Figure 5.5 Formation of silica supported linker, grafting of Al*i*Bu$_3$ on SiO$_{2-700}$.

This aluminium species is more prone to dissociation to mononuclear complex than the extensively studied, methyl and ethyl analogues,[19] and more reactive than bulkier derivatives.[20]

The choice of the solvent to perform this transformation, revealed to be important as well.[21] The authors showed that diethyl ether saturates the metal coordination sphere during grafting, thus preventing the formation of Al-C-Al bridges, and chemisorption through surface Si-O-Si ligation on the metal centre. Furthermore, using triisobutylaluminium as a linker, complete passivation of the silica surface was achieved with only bipodal surface.

Hydroquinone as a spacer

As previously mentioned the synthetic strategy followed requires the use of a spacer inserted between the organometallic fragment and the surface in order to prevent undesired interactions (Figure 5.6).
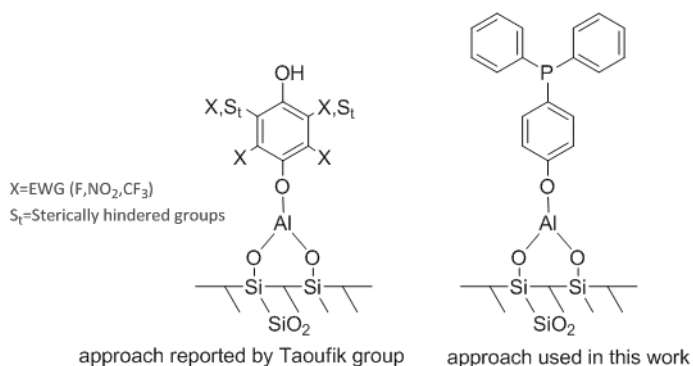
Figure 5.6 Silica modified with an aromatic compound as spacer.

Aromatic compounds are usually used, for their characteristics (rigidity, etc..) and for the versatility that they provide to tune their electronic and steric properties. Taoufik and co- workers have developed the use of hydroquinone as spacer, which fulfils the mentioned requirements, is an aromatic compound, rigid and inert toward the metals that can be anchored to it.[22]

In this project, the selected spacer was a phosphine derivative bearing a *para*-phenol substituent that is also a stabiliser similar to those used for the synthesis of rhodium nanoparticles in this thesis (Figure 5.6).

The active species will be grafted to the modified surface by the spacer. In the case of the hydroquinone spacer, the species are grafted by the hydroxyl group that remains free after the anchoring of this moiety to the silica surface modified with triisobutylaluminium. In the case developed in this study, the phosphine group will be used as anchoring point to subsequently coordinate to the metallic species.

5.1.4 Objective: Application of the SOMC approach for the anchoring of rhodium nanoparticles

The objective of this project was to investigate the use of an approach derived from surface organometallic chemistry to support the P- based stabilised nanoparticles developed in this thesis.

This study was carried out as follow:

First, a silica partially dehydroxylated was synthesised and modified with triisobutylaluminium groups, following the reported procedure by Taoufik and co- workers.[11] The modification of the support was completed by the anchoring of a phosphine ligand containing a phenol substituent.

In a second stage, the molecular rhodium $[Rh(\eta^3\text{-}C_3H_5)_3]$ was anchored to the silica surface. For comparison purposes, the reactivity of this rhodium precursor with the silica obtained prior to phosphine introduction was also performed. The reactivity towards hydrogen pressure of both immobilised complexes was also looked at.

In a third stage, two methodologies to anchor rhodium nanoparticles onto silica surfaces were studied. The first one, synthesising in situ P- based stabilised nanoparticles in the presence of the phosphine modified silica and the second immobilising previous synthesised nanoparticles onto the silica modified with triisobutylaluminium.
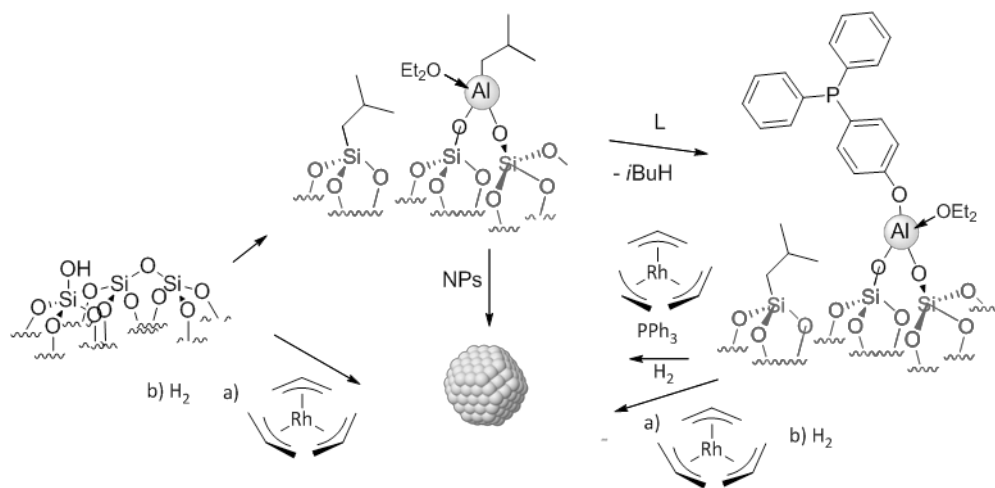
Figure 5.7 Schematic representation of the strategy followed in this work.

In this chapter, the materials synthesised were characterised by classical techniques such as IR, elemental analysis and solid state NMR to obtain information of the structure and chemical composition of the groups presents at the surface and the reactions were monitored by gas chromatography to analyse the volatiles formed during the different steps.

5.2 Results and discussion

5.2.1 Synthetic modifications of the silica support

In this section the modification of the silica following the procedures reported in the group of Lyon will be described in a first stage. Furthermore, a phosphine will be anchored to this modified silica to adapt this approach to the work developed in this thesis.

### Synthesis of the silica 700 (SiO$_{2\text{-}700}$) 43

The first modification of the silica was carried out following a procedure adapted from the literature.[23] Silica with a specific area of 200 m^2/g was calcined at 500° C for 4h and then dehydroxylated at 700°C under high vacuum (10^{-5} mmHg) during 16h to generate **SiO$_{2\text{-}700}$ 43** as a white solid. Using DRIFT analysis, the characteristic peak at 3747 cm^{-1} corresponding to isolated silanols on the silica was observed and confirmed the formation of **SiO$_{2\text{-}700}$ 43** (Figure 5.8). After this thermal treatment, the specific area of the silica is maintained and a hydroxyl concentration of 0.7 OH/nm^2 is obtained.[13]
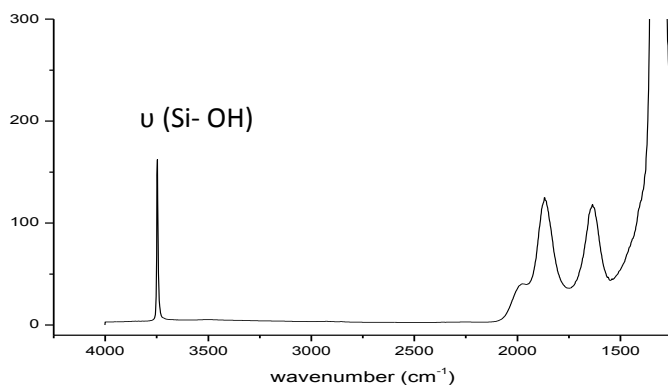
**Figure 5.8** DRIFT spectrum of SiO$_{2\text{-}700}$ **43**.

Synthesis of SiO$_{2\text{-}700}$ modified with triisobutyl aluminium 44

Next, the introduction of the alkyl aluminium derivative that will act as a linker for subsequent modifications was performed. Following a reported procedure, the thermally treated silica SiO$_{2\text{-}700}$ **43** was reacted with an excess of triisobutylaluminium in diethyl ether ([(Al*i*Bu$_3$)(Et$_2$O)]) for 2h at room temperature (Figure 5.9).[24] Subsequently, repeated washings with diethyl ether were carried out, followed by evacuation of the volatiles under high vacuum (10^{-5} mmHg) and the resulting modified silica **44** was obtained as a white solid.
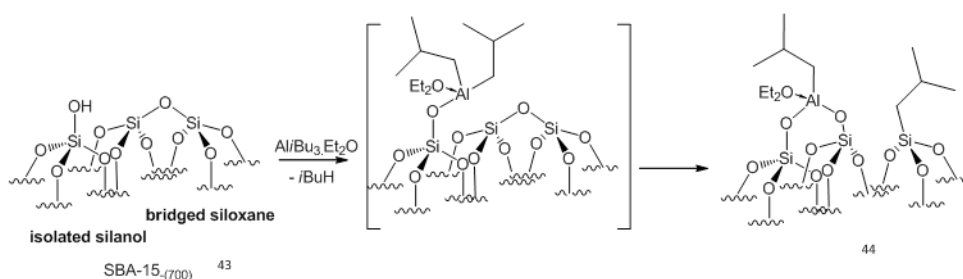
Figure 5.9 Synthetic route used to prepare ([(≡SiO)$_2$Al*i*Bu.(Et$_2$O)]) **44.**

At this stage, the 3747 cm^{-1} band could not be detected by DRIFT spectroscopy (Figure 5.10), demonstrating the complete transformation of the isolated silanols during the reaction with Al*i*Bu$_3$. However, two series of bands at 2800-3000 cm^{-1} and at 1300-1500 cm^{-1} corresponding respectively to the stretching υ$_{(C\text{-}H)}$ and bending δ $_{(C\text{-}H)}$ vibrations of the alkyl moieties, were detected.
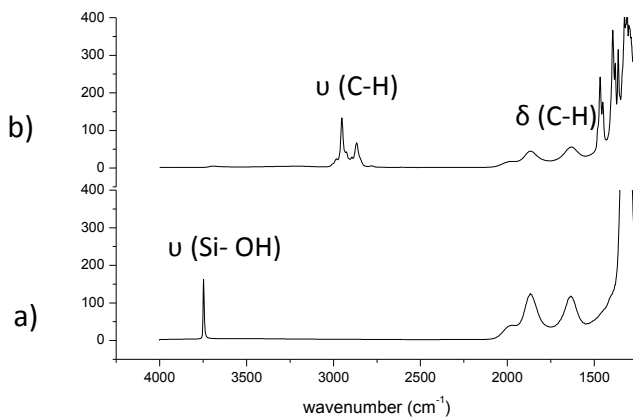
Figure 5.10 IR spectra of a) Si-(700) **43**, b) Si-(700) + AliBu$_3$·Et$_2$O **44**.

The presence of aluminium alkyl species was further supported by elemental analysis, which indicated the presence of aluminium (1.6 %wt, 0.593 mmol g^{-1} of SiO$_{2-700}$) and carbon (7.83% wt, 6.53 mmol g^{-1} of SiO$_{2-700}$) within the modified silica, giving a relation of C/Al of 11 (theoretical ratio= 12).

Gas chromatography analysis of the reaction gas phase showed the formation of isobutane, quantified as 0.87 iBuH per aluminium by the use of an external standard. These results evidenced the transfer of an isobutyl group onto the silica surface, as previously demonstrated by the group of Taoufik.[18]

The material was also characterised by CPMAS NMR (Figure 5.11).
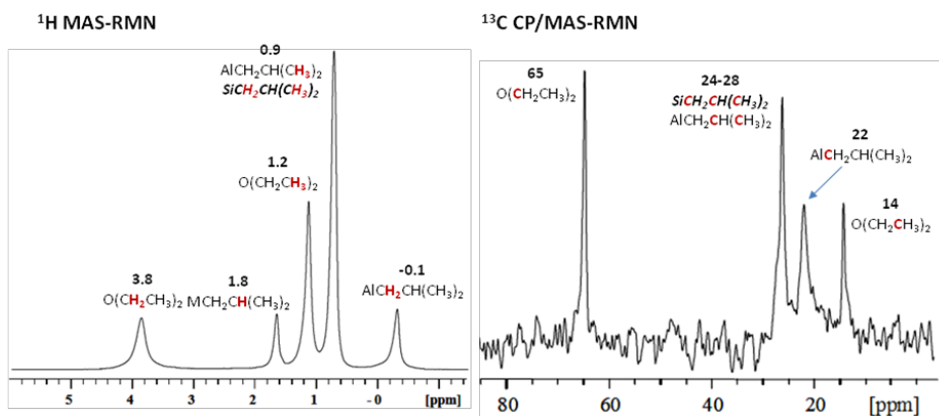
Figure 5.11 ^{1}H and ^{13}C{^{1}H} NMR spectra of ([(≡SiO)$_2$Al*i*Bu.(Et$_2$O)]) **44**.

In the ^{1}H MAS-NMR spectrum of the material, five broad singlet signals were observed. The signals at 3.8 and 1.2 ppm corresponded to the protons of the ether group coordinated to the aluminium atom. The signals at 1.8 and 0.9 ppm were attributed to the CH and CH$_3$ protons of isobutyl moieties coordinated to the aluminium centre, and the residual isobutyl bonded to the silicon atom. Finally, the peak detected at lower chemical shift was attributed to the methylenic protons of the isobutyl bonded to the aluminium atom.

In the ^{13}C{^{1}H} spectrum, signals at 65 and 14 ppm were observed as broad singlets and attributed to the ether group. The signal at 22 ppm that appeared as a broad singlet corresponds to the carbon of the isobutyl group that is bonded to the aluminium atom. The signals observed as a broad singlet between 24 and 28 ppm were attributed to the carbons of methyls and methylene fragments of the isobutyls groups bonded to silicon and aluminium atoms.

From these results, it was therefore concluded that the support had been successfully modified with triisobutylaluminium, obtaining a material without free silanols on the surface, with an isobutyl group linked to the aluminium and another at the silicon atoms and with diethyl ether blocking the coordination to the aluminium (Figure 5.10). The strong bond formed

between silicon and carbon in this process was expected to be stable and remain untouched during the subsequent modifications.

Anchoring of the 4- (diphenylphosphino)phenol in the modified silica 44

Once the linker was introduced onto the modified silica **44**, the subsequent step was the anchoring of the spacer group. As previously mentioned, this was the first variation to the procedure reported by Taoufik and co-workers in order to adapt the synthetic strategy to the project of this thesis.[11]

The following modification was performed according to a procedure reported for the anchoring of hydroquinone onto the SiO_{2-700} modified with triisobutyl aluminium ($[(\equiv SiO)_2AliBu.(Et_2O)]$).[22] To the best of our knowledge, the anchoring of phosphines through this method onto this **44** modified silica has not been reported so far, although several other approaches were used to anchor phosphines onto silica.[25,26,27]

The product **44** was treated with 1.2% of excess of 4-(diphenylphosphino)phenol **45** in diethylether at room temperature during 16h.
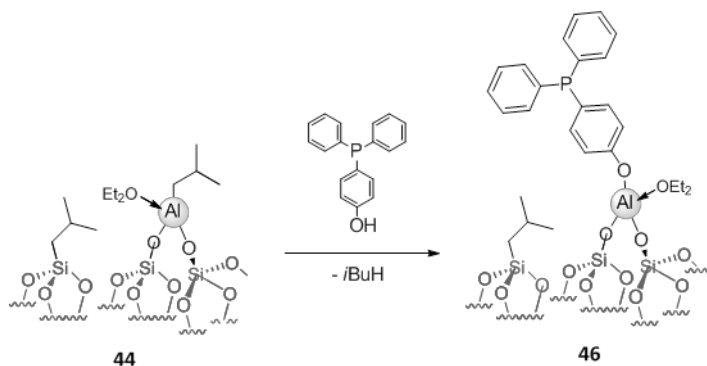
**Figure 5.12** Synthesis of the phosphine modified $[(\equiv SiO)_2AliBu.(Et_2O)]$ **46**.

Repeated washings with the Et_2O were performed, followed by removal of the volatiles under high vacuum. The phosphine-modified silica **46** was obtained as a white solid.

DRIFT spectroscopy revealed the apparition of a set of bands at frequencies higher than 3000 cm^{-1}, and in the 1700-1800 cm^{-1} region, corresponding to the $\upsilon(C_{sp2}$-H) and the υ(C=C) of the aromatic rings of the phosphine respectively. Several bands in the 2700- 3000 cm^{-1} and 1300-1500 cm^{-1} regions were also observed in the spectra and correspond to the $\upsilon_{(C-H)}$ and $\delta_{(C-H)}$ vibrations of the alkyls groups of isobutane grafted on the silicon atom, respectively (Figure 5.13).
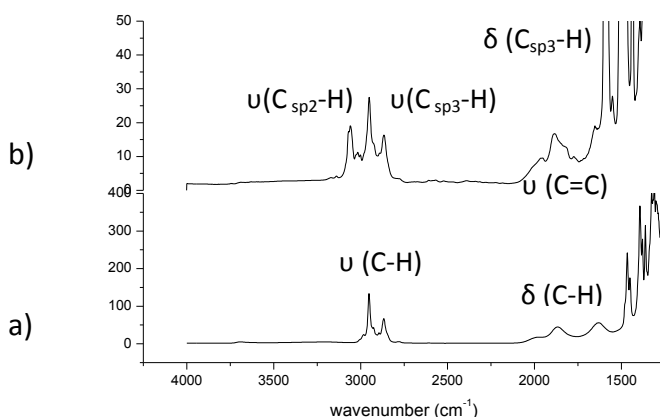
Figure 5.13 A) Si-(700) + AliBu3·Et$_2$O **44**, b) Si-(700) + AliBu3·Et$_2$O + P(Ph$_2$)(PhOH) **46**.

Gas chromatography analysis of the reaction gas phase showed the formation of isobutane, which was quantified by external standard as 0.87 isobutane per aluminum. This result indicated that elimination of the isobutyl group attached to the aluminium atom had taken place, and consequently confirmed the anchoring of the phosphine on the support.

Solid state MAS NMR was also used to characterise this material. The ^{1}H NMR showed three broad singlets at 7.1, 4.1 and 0.8 ppm. The first resonance was attributed to the aromatic rings of the phosphine, the second signal to protons of ether molecules while that at *ca*. 0.8ppm was attributed to the alkyl groups of the isobutane remaining on the surface. The disappearance of the characteristic peak previously detected at -

0.1ppm corroborated the successful grafting of the phosphine onto the aluminium moiety.

The ^{13}C {H} NMR spectrum of the sample displayed 12.69 and 25.89 ppm were also detected and assigned to the isobutane moiety attached to silicon. Furthermore, aromatic signals corresponding to the phosphine moiety were also detected between 126 and 133 ppm. However, the baseline of the spectrum was very distorted and a detailed analysis of these signals could not be performed.

The $^{31}P\{^1H\}$ NMR spectrum displayed a main signal at -6.18 ppm that was attributed to the anchored ligand (Figure 5.14).
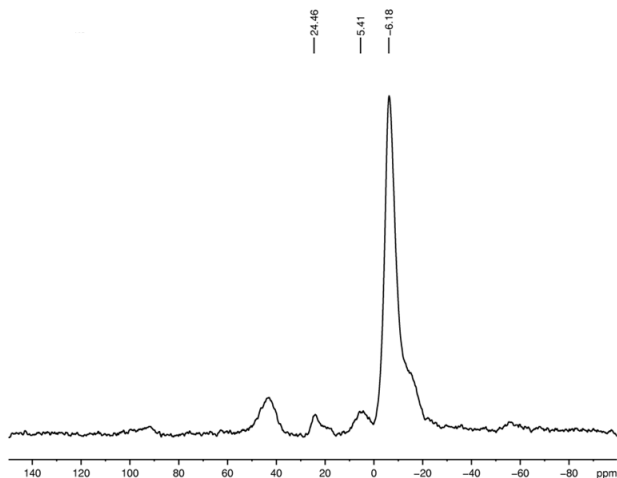
Figure 5.14 $^{31}P\{^1H\}$ CP-MAS NMR spectrum for the phosphine modified silica **46**.

Interestingly, the chemical shift of this species remained almost unchanged after its grafting onto SiO_{2-700} **44**. This behaviour was also observed in other studies of supported phosphines onto silica.[25] Two broad phosphorus resonances at 5.41 and 24.46 ppm were also detected in the spectra. The chemical shift of the signal at 24.46 ppm could match the oxidised form of the phosphine formed during the reaction, although it is usually observed at *ca.* 30 ppm.[28] The identity of the species giving rise to the signal at 5.41 ppm could not be determined unambiguously.

This results therefore showed that 4-(diphenylphosphino)phenol **45** was successfully grafted onto modified silica **46**.

5.2.2   Anchoring of [Rh(η^3-C$_3$H$_5$)$_3$] onto silica

This section describes the anchoring of the rhodium complex onto two different surfaces. First of all, the direct anchor to the silica surface without modification will be evaluated. Secondly, to the phosphine modified silica **46** previously synthesised. The reactivity under hydrogen of both materials will be also studied.

### Direct anchoring of the rhodium complex onto the SiO$_{2\text{-}700}$ 43 surface

First, the direct grafting of [Rh(η^3-C$_3$H$_5$)$_3$] onto the **SiO$_{2\text{-}700}$ 43** surface was tested as a model experiment, following reported procedures.[29] SiO$_{2\text{-}700}$ **43** was treated with 1.5% of excess of [Rh(η^3-C$_3$H$_5$)$_3$], in pentane, for 2h at room temperature. A change in colour of the material was observed from white to yellow-orange. Washings with pentane and subsequent evacuation of the volatiles under vacuum were then carried out in order to isolate the material **47**.
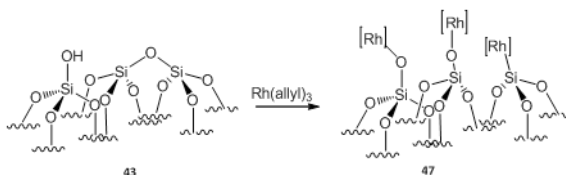
Figure 5.15 Schematic representation of the anchoring of Rh(η^3-C$_3$H$_5$)$_3$ in SiO$_{2\text{-}700}$ **43**.

When a sample of **47** was analysed by DRIFT spectroscopy and the spectrum compared to that of the starting silica, a decrease in intensity of the peak corresponding to the silanol bonds was observed. Furthermore, a new set of bands in the 2700-3000 cm^{-1} region was detected, corresponding to the υ(C-H) vibrations of unsaturated C=C bonds and were attributed to allyl ligands coordinated to rhodium. Since remaining silanols were detected at the surface after the reaction, a larger excess (2%) of the rhodium complex was employed. However, no differences were observed,

and complete conversion of the silanols groups could not be reached even with higher amounts of rhodium complex.
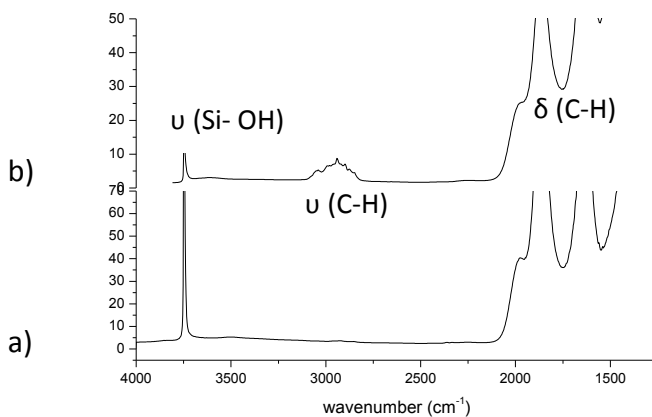
Figure 5.16 Infra-red spectra of a) Si-(700) **43** ; b) Si-(700) + Rh (allyl)$_3$ **47**.

Surprisingly, no volatiles were detected in the gas phase.

In view of these results, no conclusions could be drawn since no clear evidence for the reaction between the Rh complex and the silanol groups of the surface were obtained. Further experiments are needed to provide more information on the structure of the immobilised complex.

Reactivity of the rhodium allyl complex grafted onto the SiO$_{2-700}$ 41 towards hydrogen

The hydrogen reduction of metal complexes previously immobilised onto a solid support is a common strategy for the synthesis of supported metal nanoparticles.[29]

It was therefore thought that for comparison purposes, the study of the reactivity of the rhodium complex grafted onto the silica surface towards hydrogen would be of interest.
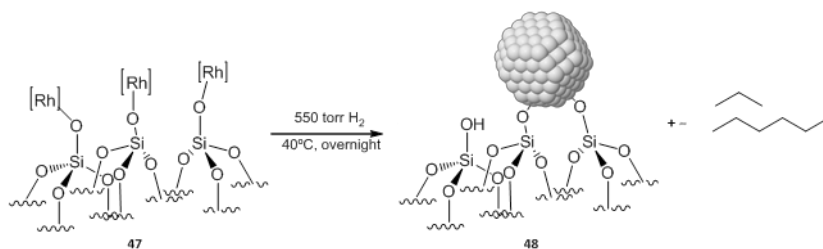
Figure 5.17 Scheme of the treatment under hydrogen of the Rh (allyl)$_3$ modified silica.

The material previously synthesised **47** was placed under 550 torr of hydrogen pressure, during 16h at 40°C of temperature (Figure 5.17).[14] The colour of the modified silica turned black immediately. The material **48** was characterised by TEM microscopy to distinguish between the formation of nanoparticles or bulk metal (Figure 5.18). The micrograph showed a non homogeneous distribution of Rh-NPs at the surface of the silica support. The diameter of these nanoparticles was determined to be 1.43± 0.26 nm, although it should be noted that this measurement could only be performed on a few NPs (*ca.* 50). Importantly, nanoparticles detached from the support were also observed, indicating that some of the species formed under these conditions were not well anchored onto the silica surface.
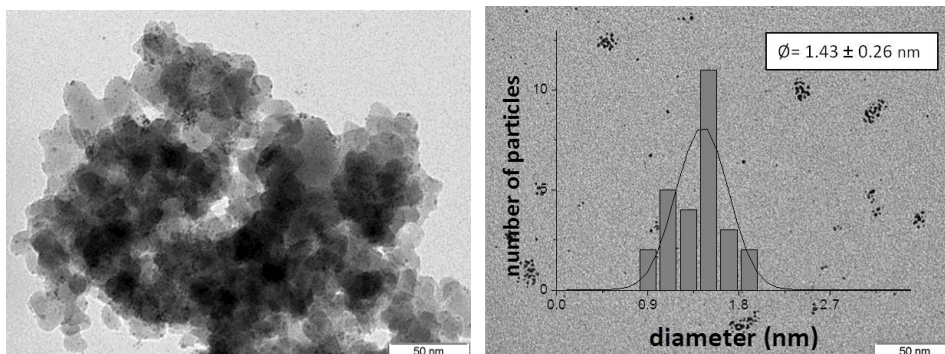
Figure 5.18 TEM analysis of the Rh complex grafted in SiO_{2-700}, (**48**) after the reaction with H_2.

DRIFT spectroscopy was also used to characterise this material for which an increase in intensity of the signal at 3747 cm^{-1} corresponding to silanols

groups was observed, revealing the regeneration of the Si-OH groups at the silica surface (Figure 5.19). The migration of rhodium atoms initially anchored to the Si-O groups to form the nanoparticles under hydrogen, could explain this observation.
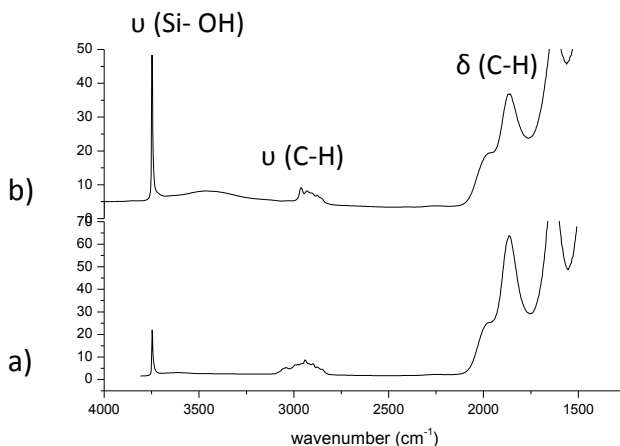
Figure 5.19 Infra-red spectra of a) Si-(700) + Rh (allyl)$_3$ **47**, b) Si-(700) + Rh (allyl)$_3$ + H$_2$ **48**.

The analysis of the gas phase by GC analysis indicated the formation of C3 and C6 compounds during the reaction in the presence of H$_2$, suggesting that under the reaction conditions, the allyl ligands coordinated to the rhodium centres were hydrogenated and undergo C-C coupling to form C6-species (Figure 5.20). Such reaction was previously reported for analogous experiments of the allyl complex with the silica support.[30]

$$(\equiv SiO)(\equiv SiOH)Rh(\eta^3-C_3H_5)_2 + 3H_2 \longrightarrow C_3H_8 + 1/_2 C_6H_{11} + Rh^0 + 2 \equiv SiOH$$
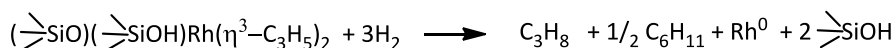
Figure 5.20 Reaction reported for the rhodium complex anchored on silica under H$_2$ pressure.

To summarise this part, the rhodium complex was anchored onto the silica surface, but not completely in all de silanol groups even with an excess of the metallic precursor. An optimisation of the reactions conditions is needed to improve this anchoring.

After reaction with molecular hydrogen, the formation of nanoparticles was observed; however the anchoring on the surface is not well controlled using this methodology as unsupported NPs were observed.

Anchoring of the rhodium complex to the phosphine modified silica surface 46

Next, another approach consists on the anchoring of the rhodium complex [Rh(η^3-C$_3$H$_5$)$_3$] onto previously synthesised phosphine modified silica **46** was performed.

The material **46** was treated with [Rh(η^3-C$_3$H$_5$)$_3$] complex in 1.5% excess, in pentane, for 2h at room temperature. During the reaction, the colour of the modified silica changed from white to yellowish. Washings with pentane were carried out followed by the elimination of the volatiles under high vacuum.
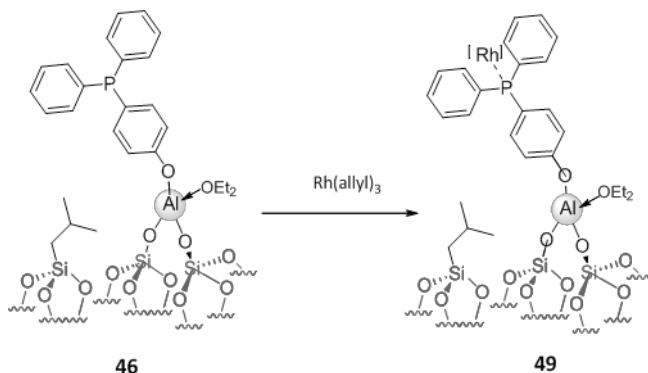
Figure 5.21 Scheme of the anchoring of Rh(η^3-C$_3$H$_5$)$_3$ onto the phosphine modified SiO$_{2\text{-}700}$.

Using DRIFT spectroscopy, no significant changes with the starting material **46** were observed (Figure 5.22).
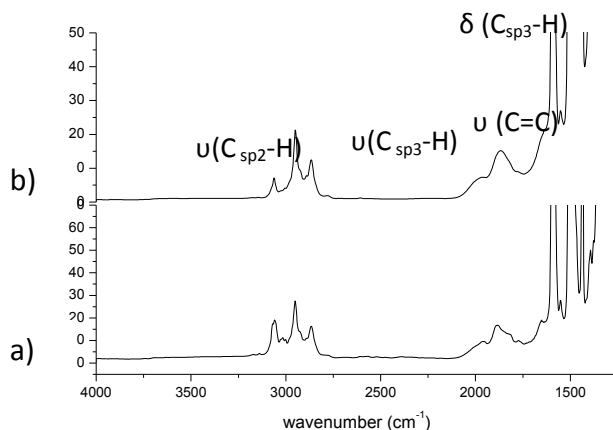
Figure 5.22 Infra-red spectra of a)Si-(700) + AliBu3·Et$_2$O + P(Ph$_2$)(PhOH) **46**, b) Si-(700) + AliBu3·Et$_2$O + P(Ph$_2$)(PhOH) + Rh(allyl)$_3$ **49**.

In the CPMAS ^{1}H NMR spectra, a broad band was detected at 7.1 ppm corresponding to aromatic protons of the phosphine ligand. Furthermore, in addition to the signals corresponding to the isobutyl fragment, broad resonances were detected between 1.5 and 4.8 ppm, chemical shifts that could correspond to allyl moieties as reported in the literature.[31]

In the corresponding ^{31}P{^{1}H} NMR spectrum, three main resonances at 40.16, 19.05 and -6.18 ppm were detected, together with a small broad peak at 24.46 ppm (Figure 5.23). It should be noted that the width of the signals detected did not permit the observation of their multiplicity in terms of Rh-P coupling ([1]J$_{Rh-P}$= *ca*. 100-250 Hz).
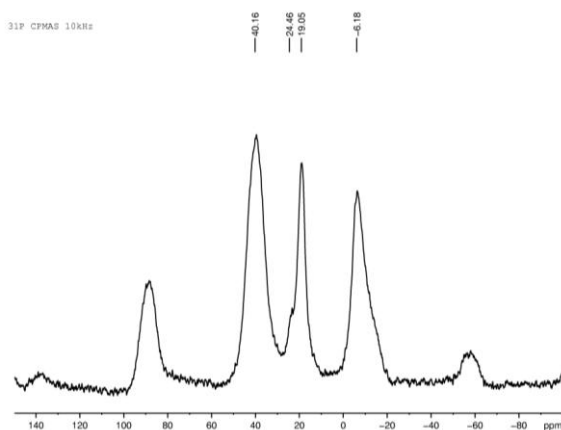
Figure 5.23 ^{31}P{^{1}H} CP-MAS NMR spectrum for **49**.

The previously detected resonances at -6.18 and 24.46 ppm were readily assigned to the grafted phosphine and the corresponding oxidised ligand. The detection of uncoordinated ligand indicated that the reaction was not complete.

The detection of two new signals at such chemical shifts indicated that reaction of the ligands with the rhodium complex took place. According to literature values, the resonance at 19.05 ppm could correspond to a phosphorus ligand coordinated to Rh.[25]

Concerning the peak at 40.16 ppm, similar chemical shifts were found in the literature in the reaction media for bistriphenylphosphineallyl rhodium complex.[32]

From these results, two main conclusions were extracted. On one hand, the anchoring of the rhodium complex in the phosphine modified silica took place but full conversion was not reached, since uncoordinated phosphine was observed by ^{31}P NMR after the reaction. On the other hand, the anchoring of this allylrhodium complex was indicated but not clearly demonstrated by NMR spectroscopy.

Reactivity of the rhodium allyl complex grafted onto the modified silica 49 towards hydrogen

In this case, the reactivity of the rhodium species **49** under H_2 was looked at using the so-called "dynamic experiment", which was carried out in an *in situ* infrared spectrometer coupled to a GC-MS, in a chamber where flows of gases could be introduced and the temperature adjusted.

49
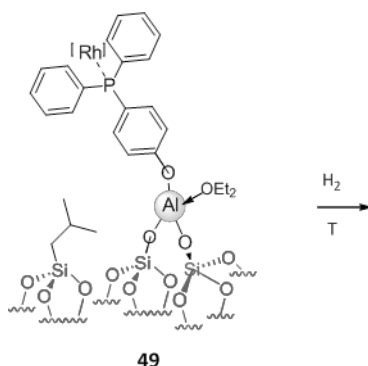
Figure 5.24 Scheme of the treatment under hydrogen of the **49**.

The previously synthesised material **49** was introduced in a DRIFT chamber under a flow of hydrogen. The temperature was increased from 30 °C to 150°C and IR measurement was performed every minute while the volatiles were analysed by GC- MS. During this experiment, changes in two regions, namely 3300-2700 cm^{-1} (Figure 5.25a) and 2200-1700 cm^{-1} (Figure 5.25b), corresponding to vibrations of alkyls groups and $\upsilon(C_{sp2}-H)$ and the $\upsilon(C=C)$ of the aromatic rings of the phosphine , respectively, were mainly analysed.
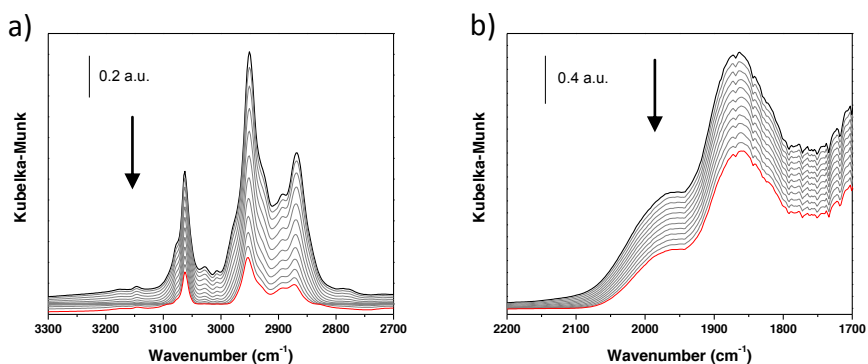
Figure 5.25 IR spectra of the material **49** under H_2 and increasing the temperature from 30 to 150 °C a) 3300- 2700 cm^{-1} zone. B) 2200- 1700 cm^{-1}.

When the temperature was increased, a decrease in the intensity of the bands in both regions was observed, reflecting that products were being volatised from the surface while heating. This was confirmed by analysis of the gas phase by GC- MS with the detection of several compounds as shown in Figure 5.26. The main species observed was isobutane and ether although traces of propane, cyclohexane and hexane were also detected. These latter products were previously detected by gas chromatography analysis after hydrogenation of the complex directly anchored onto the silica surface. Hexane and cyclohexane should come from a coupling between the allyl groups of the rhodium complex.
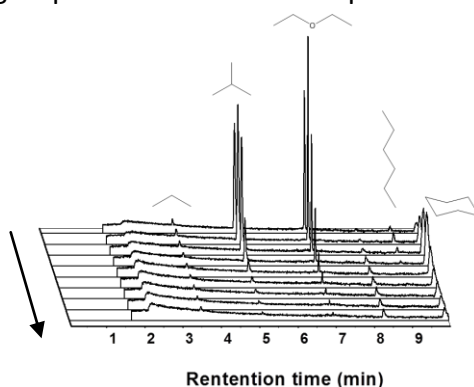
Figure 5.26 GC-MS chromatogram during the reaction of **49** with hydrogen, increasing the temperature from 30 °C to 150 °C.

Next, the sample was heated for 5 minutes at 150 °C. Under these conditions, a shoulder appeared at 1990 cm^{-1} and after background subtraction, the formation of this peak was evident (Figure 5.27). According to literature values, this frequency value could correspond to rhodium hydrides, although such species are usually not easily detected by infrared spectroscopy.[33]

a)   b)
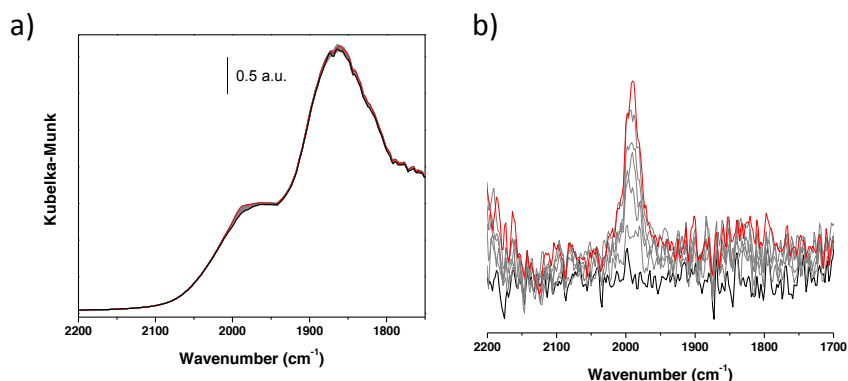
Figure 5.27 a) IR spectra of **49** after 5 min at 150 °C, b) with background subtraction.

To corroborate this hypothesis, the material containing the rhodium allyl complex anchored in the phosphine modified silica **49** was treated under 550 torr of hydrogen gas and the temperature was set to 80 °C. The colour of the material turned immediately from yellowish to black. After two hours under these conditions, the sample was analysed by ^{1}H CPMAS solid state NMR. However, no hydride signals could be detected.

Therefore, the shoulder observed at 1990 cm^{-1} by IR spectroscopy was not unambiguously assigned. A dynamic experiment under flow a D_2 is planned to confirm the identity of the corresponding species as a Rh-hydride.

5.2.3   Supporting of Rh-NPs onto the prepared silica

This section will contained two approaches. The first one is the formation of P-stabilised nanoparticles in situ in presence of the phosphine modified silica **46**. The second one explored the immobilisation of previously synthesised nanoparticles onto the triisobutylaluminium modified silica **44**.

Nanoparticles stabilised by triphenylphosphine 1 formed insitu in presence of the phosphine modified silica 46

In the previous sections, the modification of the silica support by triisobutyl moieties and the anchoring of phosphines and rhodium complexes to this material were studied. In the last part of this chapter, the anchoring of rhodium nanoparticles stabilised by P- based ligands was explored.

The first approximation used was to synthesise the colloids by decomposition of $[Rh(\eta^3\text{-}C_3H_5)_3]$ under H_2 in the presence of both PPh_3 and the phosphine modified silica **46** (Figure 5.28).
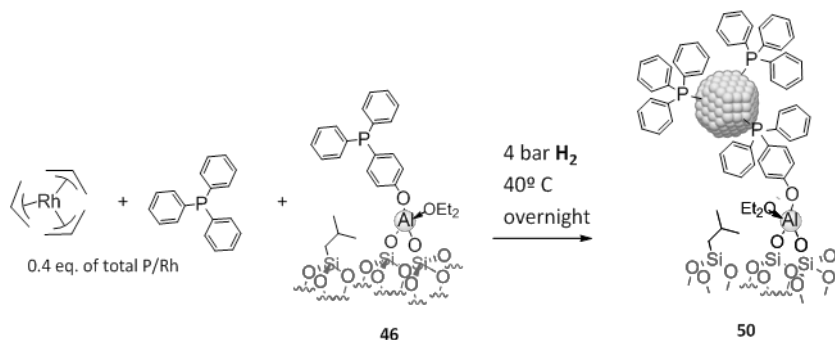
Figure 5.28 Scheme of the synthesis of PPh_3 stabilized NPs in presence of the phosphine modified silica (**50**).

The amount of triphenylphosphine used in this synthesis was calculated taking into account the presence of the phosphine in the modified silica and the TGA results previously detailed in chapter2 in order to maintain the

ratio P/Rh used to synthesised nanoparticles **Rh1**, that are the corresponding analogous.

The phosphine modified silica support **46**, triphenylphosphine and [Rh(η^3-C$_3$H$_5$)$_3$] were placed in THF and treated overnight under 4 bar of hydrogen at 40 °C. The solution turns black after a few hours.
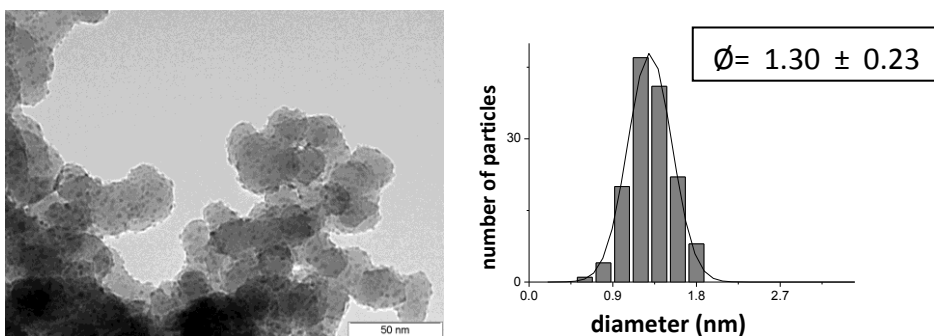
Figure 5.29 TEM micrograph and size histogram distribution of the supported Rh-NPs **50**.

The material **50** was characterised by TEM (Figure 5.29) and a homogeneous distribution of the nanoparticles on the support was observed. It is noteworthy that for this sample, all the NPs detected in the micrograph were onto the support. NPs with spherical shape, a mean diameter of 1.3±0.23 nm and narrow size distribution were obtained. Interestingly, the supported NPs were found to be slightly smaller than the **Rh1** system previously studied (1.5 nm), indicating the potential stabilising role of the silica surface. This result is in agreement with previous reports that described that supported nanoparticles are usually smaller than the corresponding unsupported systems.[7]

By CPMAS ^{1}H NMR, apart from the peaks at *ca*. 0.1-0.7 ppm corresponding to the support (isobutane that remains bonded to Si), broad resonances in the alkylic region around 2 ppm and in the aromatic region at 7 ppm, were observed. In the corresponding ^{31}P NMR spectrum, three broad resonances at 22, 41 and 60 ppm with spinning side bands were observed.
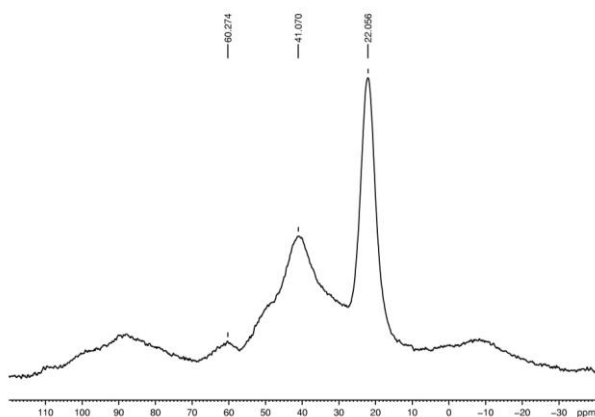
Figure 5.30 ^{31}P{^{1}H} CP-MAS NMR spectrum of **50**.

The two signals at lower chemical shift were already detected in the sample of the phosphine modified silica after reaction with the allyl rhodium precursor and were attributed to molecular Rh complexes bearing one of two phosphine ligands. The broad signal at 60 ppm was not previously detected and could arise from P-ligands at the surface of the NPs.

To summarise this section, when the Rh precursor was decomposed under H_2 in the presence of both PPh$_3$ ligand and the supported analogue, TEM spectroscopy revealed the formation of nanoparticles homogeneously dispersed on the support and well distributed in size. Under these conditions, no nanoparticles detached from the support were detected, revealing a stronger interaction of the metallic catalysts with the phosphine modified silica than with the phosphine-free silica.

Analysis by solid state NMR showed that no uncoordinated phosphine remained on the support after reaction, and that the detection of the previously observed signals at 22 and 41ppm could indicate that molecular rhodium phosphine and rhodium bisphosphine complexes are also formed under these conditions. A new signal at 60 ppm was also observed and is tentatively assigned to the stabilising ligands of the rhodium nanoparticles formed.

305

It was therefore concluded that using this methodology, well defined Rh-nanoparticles can be successfully synthesised and anchored onto the phosphine modified silica.

Anchoring of the Rh-NPs stabilised with 4- (diphenylphosphino)phenol 45 in the modified silica 44.

Next, another synthetic approach was evaluated: Rh-nanoparticles stabilised by the triphenylphosphine derivative containing a hydroxyl group in *para* position **45** were synthesised in a first step and then reacted with the aluminium modified silica ([($\equiv$SiO)$_2$AliBu.(Et$_2$O)]) **44** (Figure 5.31).

In this latter step, the potential reaction between the phenolic groups contained in the ligands and the isobutylaluminium linker should be indicated by the detection of isobutane in the gas phase during the anchoring of the nanoparticles onto the support.
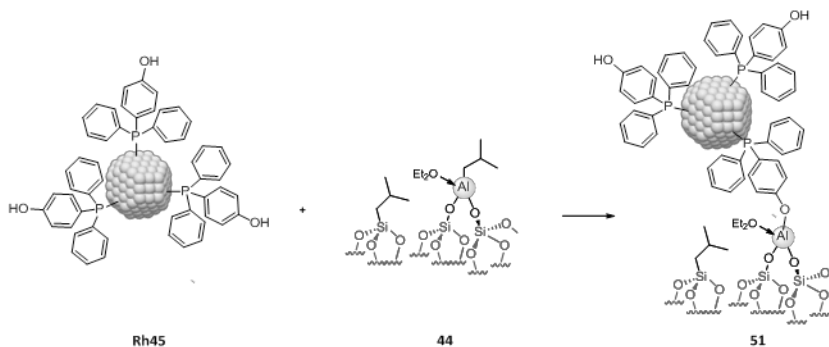
Figure 5.31 Synthetic strategy followed for the anchoring of the **Rh45** NPs onto the ([($\equiv$SiO)$_2$AliBu.(Et$_2$O)]) surface **44**.

Synthesis of the Rh-NPs Rh45 stabilised by 4- (diphenylphosphino)phenol 45

Rh45-NPs stabilised by 4- (diphenylphosphino)phenol **45** were synthesised according to the procedure described in Chapter 2 for Rh-NPs stabilised by PR$_3$ ligands. The rhodium precursor [Rh(η^3-C$_3$H$_5$)$_3$] was decomposed under hydrogen atmosphere at 60 °C in the presence 0.4 equivalent of 4-

(diphenylphosphino)phenol using THF as the solvent. During the course of the synthesis, the initial yellow solution was observed to slowly turn black, confirming the decomposition of the complex. The NPs were isolated as black powder after precipitation with pentane and characterised by transmission electron microscopy (TEM).
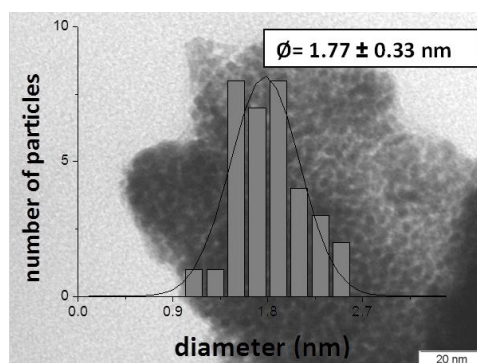
Figure 5.32 TEM micrograpfh and size distribution of nanoparticles **Rh45**.

As shown in Figure 5.32, sponge- like Rh-nanoparticles with a mean diameter of 1.77± 0.33 nm were obtained. This morphology was previously observed for the solvent stabilised nanoparticles **Rh45** and for reported nanoparticles in alcoholic media where polar interactions promote the formation of these structures.[34]

In the corresponding solid state ^{1}H NMR spectrum, the peaks corresponding to the solvent at 1, 1.5 and 3.4 ppm, to aryl moieties between 6.4- 7.4 ppm and the acidic proton of the ligand at 8.8ppm were observed. The latter signal was assigned to the hydroxyl group of the stabilising ligand. The CPMAS ^{31}P{^{1}H} NMR spectra of these nanoparticles showed two signals, the more intense at 29.1 ppm and a smaller signal at 37.6 ppm (Figure 5.33).
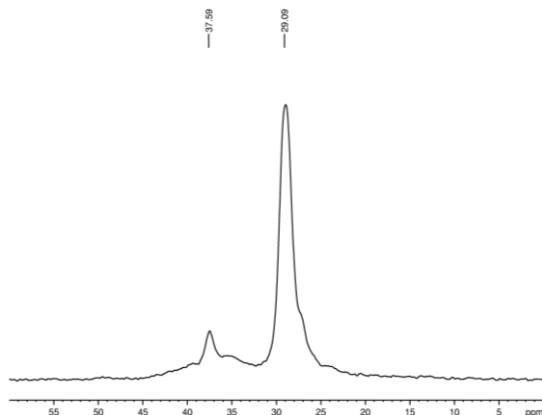
Figure 5.33 ^{31}P{^{1}H} CP-MAS NMR spectrum of the nanoparticles **Rh45**.

These signals could not be unambiguously assigned. Interestingly, ^{31}P signals with similar chemical shifts were attributed to phosphine ligands bonded to the metallic atoms of ruthenium nanoparticles stabilised with these ligands.[35] The signal detected in this work could therefore arise from the stabilising P-ligands at the surface of the Rh-nanoparticles. However, the chemical shift of the signal at 29.1 ppm is also close to that of the oxidised ligand.[36] More experiments will thus be required to determine the identity of the corresponding species.
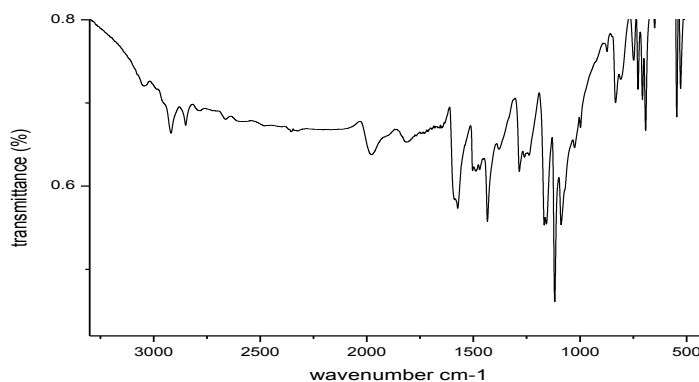
Figure 5.34 IR spectrum of the **Rh45** NPs.

When the nanoparticles **Rh45** were analysed by IR spectroscopy, the bands corresponding to the stretching vibrations of C-H bonds were observed (Figure 5.34). The presence of alkylic $\upsilon_{(C-H)}$ below 3000 cm^{-1} for these nanoparticles indicated that hydrogenation of the ligands could take place during the synthesis, as previously described in this thesis (Chapter 2). Moreover, a broad band was detected at 1977 cm^{-1} as in the case of nanoparticles **Rh1**.

Therefore, Rh-nanoparticles stabilised by 4- (diphenylphosphino)phenol **45** were successfully synthesised and exhibited a sponge-like morphology and a mean diameter of 1.77 nm, slightly larger than their analogous triphenylphosphine **Rh1** nanoparticles (1.5 nm). The acidic proton of the ligand detected by ^{1}H NMR and the signals observed by ^{31}P NMR could indicate the coordination of phosphorus ligands at the nanoparticles surface. Moreover, hydrogenation of the ligands was evidenced during the synthesis of the NPs, as previously described in Chapter 2 for other phosphine stabilised nanoparticles.

Anchoring of the NPs Rh45 onto the modified silica ([(≡SiO)₂AliBu.(Et₂O)]) 44

After the synthesis of the nanoparticles **Rh45**, their immobilisation onto the modified silica surface was studied. The amounts of the reagents were calculated to obtain a catalyst loading of 3 weight % of rhodium onto the silica surface.

The triisobutylaluminium modified silica ([(≡SiO)₂Al*i*Bu.(Et₂O)]) **44** was treated with the previously synthesised nanoparticles in diethylether at room temperature during 16h. Washings with diethylether were followed by subsequent elimination of the volatiles under vacuum.

Analysis by TEM microscopy showed a non homogeneous dispersion of the nanoparticles on the support (Figure 5.35). A few nanoparticles of *ca*. 2 nm were observed in the micrograph, although the small number of NPs present did not permit an accurate measurement of their diameter. In this

sample, all the nanoparticles detected were on the support and no free systems were observed.
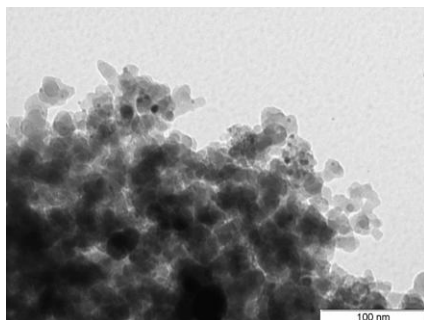
Figure 5.35 TEM micrograph of the supported NPs **51** with a 3% Rh/ SiO$_2$ in weight.

The material **51** was also characterised by DRIFT but no significant difference with the modified support **44** was observed (Figure 5.36). The bands corresponding to the phenyl groups of the phosphine stabilising agents were not detected in this case although alkylic bands were observed, which suggests that hydrogenation of the stabilising agent could have taken place during the synthesis, as observed for the previous P-based stabilised nanoparticles.
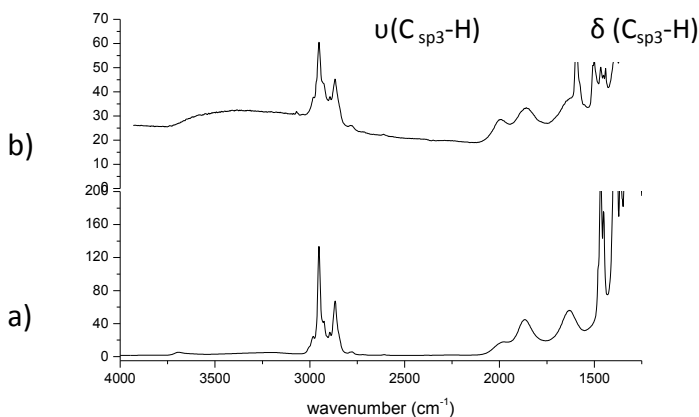
Figure 5.36 Infra-red spectra of a) Si-(700) + AliBu3·Et$_2$O **44**, b) Si-(700) + AliBu3·Et$_2$O + NPs (L= P(Ph$_2$)(PhOH))**51**.

Gas chromatography analysis of the reaction gas phase showed the formation of isobutane, which was quantified by external standard as 0.2 isobutane per aluminum. This observation revealed that reaction between the support and the nanoparticles took place. However, not all the isobutyl-aluminium groups present at the surface were consumed.

This material was also characterised by CPMAS NMR spectroscopy. In the ^{1}H NMR spectrum, the peaks corresponding to the support at -0.2, 0.9 and 1.8 ppm, to the solvent at 1.3 and 3.8 ppm and to aryl moieties at 7.2ppm were observed. Characteristic peak at -0.2 ppm corresponding to the aluminium methylene fragment indicated the presence of these groups in the support, and therefore that the reaction between the aluminium species and the hydroxyl group of the nanoparticles was not complete.

In the CPMAS ^{31}P{^{1}H} NMR spectrum of this material, only a resonance at 41 ppm, with spinning side bands was observed. The previous signal observed for the nanoparticles **Rh45** did not correspond to the oxide derivative of the ligand, as this product was not detected after immobilisation onto the silica support. So the band was attributed to the same signal detected for the stabilising P-ligands at the surface of the nanoparticles, inmobilised in the silica support. However, a shift was observed between both systems, before immobilisation at 29 ppm and after at 41 ppm.

Moreover, Li and co- workers reported a shift between the signal corresponding to the P- Rh bond before and after immobilisation, that could be the case in this study.[37]
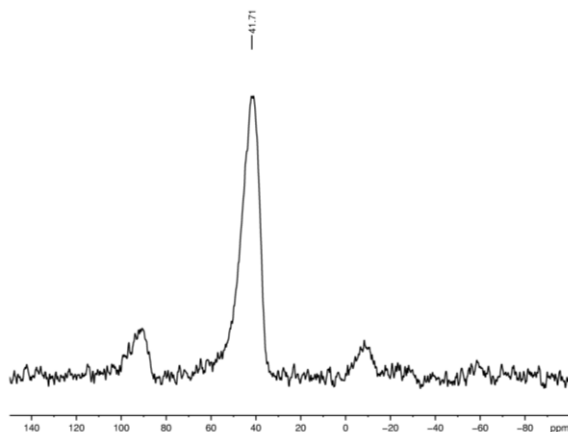
Figure 5.37 ^{31}P{^{1}H} CP-MAS NMR spectrum of the nanoparticles **Rh45** supported on the modified silica **44**.

To summarise this part, nanoparticles stabilised by 4-(diphenylphosphino)phenol **Rh45** were succesfully synthesised and anchored onto the isobutyl modified silica **44**. The detection of isobutane moieties in the gas phase corroborates the successful anchoring of the nanoparticles system. CPMAS NMR showed that isobutyl groups are still present on the support at the end of the reaction and that only one type of ^{31}P environment is present in this material.

5.3 Conclusions

From this preliminary study, a series of conclusions can be drawn:

- A new phosphine modified silica was successfully synthesised and characterised by IR and NMR spectroscopy.

- The [Rh(allyl)$_3$] complex was anchored on two supports: the SiO$_{2-700}$ **43** surface and the phosphine modified surface **46**.

The use of the phosphine derivative as spacer to modify the silica improve the anchoring to this surface.

The subsequent hydrogenation of the rhodium complex anchored onto the silica without modification provides the formation of nanoparticles distributed onto and outside the support while with the material with the complex anchored onto the phosphine modified silica the material turned black, but further TEM analysis are needed to check the species formed under these conditions.

Both surfaces under hydrogen could provide the formation of nanoparticles but in an uncontrolled way, as nanoparticles detached from the support were detected in the first case.

- two methodologies for the anchoring of Rh-NPs onto silica were investigated:

  - First, Rh-NPs stabilised by a mixture of PPh$_3$ **1** and the phosphine modified silica support were successfully synthesised. TEM microscopy revealed strong interaction between the nanoparticles and the support, as no free systems were observed.

  - Next, a 2 step approach was looked at: the colloidal Rh- NPs stabilised by P(Ph$_2$)(PhOH) **45** were first synthesised and subsequently anchored onto the [(≡SiO)$_2$AliBu.(Et$_2$O)] surface. The detection of isobutane after the anchoring indicated that the reaction between the surface Al(isobutyl) groups and the hydroxyls of the nanoparticles took place. As in the previous case, the nanoparticles were only detected on the support, further

experiments are needed to increase the amount of nanoparticles immobilised onto the support.

Promising results were obtained in this work using the techniques derived from surface organometallic chemistry to support the rhodium nanoparticles. These two approaches provided strong interactions between the nanoparticles and the support.

Further catalytic applications of these materials are needed to study the influence of this synthetic design on the activity/selectivity and possible recovery and reuse of the catalysts.

5.4 Experimental part

General conditions

All experiments were carried out under inert atmosphere, either N_2 or Ar. Schlenk and glove-box techniques were used for the synthesis of the organometallic compounds. For the synthesis and treatment of the modified silica materials, a high- vacuum line (about 1 Pa) and a glove box were used. Diethyl ether and pentane were distilled on Na/K-benzophenone and degassed through freeze- pump- thaw cycles.

Elemental analysis was performed at the Mikroanalytisches Labor Pascher, Remagen (Germany). DRIFT spectra were recorded on a Nicolet 6700 FTIR by using airtight cells. Solid- state ^{1}H MAS ^{31}P NMR and ^{13}C CP/MAS-NMR spectra were recorded on a Bruker Avance 500 spectrometer with a conventional double- resonance 4mm CO-MAS probe at the Laboratoire de Chimie Organométallique de Surface of the Ecole Supérieure de Chimie Physique Electronique of Lyon. The samples were loaded under argon atmosphere into a zirconia rotor, which was then tightly closed. Chemical shifts are given with respect to TMS as an external reference for the ^{1}H, ^{13}C and ^{31}P NMR data.

Preparation of SiO$_{2-700}$ 43:

Silica Aerosil (Degussa) with a specific area of 200 m^2g^{-1} was calcined at 500 °C for 4h then dehydroxylated at 700°C for 12h under a high vacuum (10^{-5} mmHg). The DRIFT spectrum features the characteristic isolated SiOH peak at 3747 cm^{-1}.

Preparation of [(≡SiO)$_2$AliBu.(Et$_2$O)] 44:

Using the double Schlenk technique, SiO$_{2-700}$ (3.9g) was treated with 1.2% excess [(Al*i*Bu$_3$) (Et$_2$O)] in diethylether (10ml) for 2h at room temperature. After repeated washings with diethylether (10ml), followed by evacuation

of the volatile under high vacuum (10^{-5} mmHg), the modified silica was afforded as a white powder and characterized by DRIFT, solid- state NMR spectroscopy and mass- balance analysis.

The DRIFT spectrum features the characteristic stretching bands of C-H bond around 2800-3000 cm^{-1}. Phase Gas analysis by GC: 0.87 *i*BuH/Al. Elemental analysis: %Al= 1.6, %C= 7.6, C/Al= 11.

^{1}H solid-state NMR (500Hz, δ in ppm): -0.1 (AlC**H**$_2$CH(CH$_3$)$_2$, 0.9 (AlCH$_2$CH(C**H**$_3$)$_2$, SiC**H**$_2$CH(CH$_3$)$_2$), 1.2 (O(CH$_2$C**H**$_3$)$_2$, 1.8 (MC**H**$_2$CH(CH$_3$)$_2$, 3.8 (O(C**H**$_2$CH$_3$)$_2$.

^{13}C CP-MAS solid-state NMR (500Hz, δ in ppm): 14 (O(CH$_2$**C**H$_3$)$_2$), 22 (Al**C**H$_2$CH(CH$_3$)$_2$, 24-28 (AlCH$_2$**C**H(CH$_3$)$_2$, SiCH$_2$**C**H(CH$_3$)$_2$), 65 (O(**C**H$_2$CH$_3$)$_2$).

*Preparation of the phosphine modified silica **46**:*

Using the double Schlenk technique, [(≡SiO)$_2$Al*i*Bu.(Et$_2$O)] (3g) was treated with1.2% excess of 4-(diphenylphosphino)phenol (0.2296g) in pentane (10ml) for 2h at room temperature. After repeated washings with pentane (10ml), followed by evacuation of the volatile under high vacuum (10^{-5} mmHg), the modified silica was afforded as a white powder.

The DRIFT spectrum features the characteristic stretching bands for C-H bond around 2800-3000 cm^{-1}, the stretching bands for C_{2p2}-H above 3000 cm^{-1} and for C=C around 1700- 1800 cm^{-1}.

Phase gas analysis by GC: 0.87 *i*BuH/Al.

^{1}H solid-state NMR (500Hz, δ in ppm): 0.8 (SiCH$_2$CH(CH$_3$)$_2$), 4.1 (O(CH$_2$CH$_3$)$_2$), 6.8 (Ar-H).

^{13}C CP-MAS solid- state NMR (500Hz, δ in ppm): 12.69 (O(CH$_2$**C**H$_3$)$_2$), 25.69 (Al**C**H$_2$CH(CH$_3$)$_2$, 126.66- 132.81 (Ar-C) .

^{31}P CP-MAS solid-state NMR (500Hz, δ in ppm): (-6.18 P of **46**).

*Anchoring of Rh(η^3-C$_3$H$_5$)$_3$ onto the SiO$_{2-700}$ **47***

SiO$_{2-700}$ (1g) was treated with an excess (1.5%) of Rh(η^3-C$_3$H$_5$)$_3$ (0.062g), in pentane, for 2h at room temperature. Washings with pentane were carried out, followed by the evacuation of the volatiles under high vacuum. The modified silica was afforded as a yellowish solid.

The DRIFT spectrum features the characteristic stretching bands for C-H bond around 2800-3000 cm^{-1}, and for the silanols at 3747 cm^{-1}.

Phase gas analysis by GC: no compounds were detected.

- Treatment under H$_2$

The previously synthesized material was treated under 1 bar of H$_2$ at 40°C overnight. The powder turned black immediately.

The DRIFT spectrum features the characteristic stretching bands for C-H bond around 2800-3000 cm^{-1}, and for the silanols at 3747 cm^{-1}.

Phase gas analysis by GC: C3 and C6 fragments were detected.

TEM: nanoparticles of 1.43± 0.26nm distributed over the support and as "free" colloids.

*Anchoring of Rh(η^3-C$_3$H$_5$)$_3$ onto the phosphine modified SiO$_{2-700}$ **49***

The previously phosphine modified silica (1g) was treated with an excess (1.5%) of Rh(η^3-C$_3$H$_5$)$_3$ (0.102g) in pentane for 2h at room temperature. After repeated washings with pentane, followed by evacuation of the volatile under high vacuum (10^{-5} mmHg), the modified silica was afforded as a yellow solid.

The DRIFT spectrum features the characteristic stretching bands for C-H bond around 2800-3000 cm^{-1}, the stretching bands for C$_{2p2}$-H above 3000 cm^{-1} and for C=C around 1700- 1800 cm^{-1}.

Phase gas analysis by GC: no compounds were detected.

^{1}H solid-state NMR (500Hz): δ (1.5, 2.6, 3.8, 4.8, 7.1 ppm).

^{31}P CP-MAS solid-state NMR (500Hz): δ (-6.18 P of **46**, 19.05, 24.46, 40.16 ppm).

*Synthesis of rhodium nanoparticles stabilized by triphenylphosphine in presence of the phosphine modified SiO$_{2\text{-}700}$ **50***

The desired amount of the previously synthesized phosphine modified silica (250mg), 125mg of the [Rh(η^3-(C$_3$H$_5$)$_3$] and 55 mg of triphenylphosphine, were placed in 125 ml of dry and deoxygenated THF (using freeze-pump-thaw techniques). The Fischer-Porter reactor was then pressurized under 4 bar of H$_2$ and the solution was heated to 40°C overnight. The solution turned black after a few hours. A carbon-covered copper grid for transmission electron microscopy was prepared with a small amount (5 drops approx.) under argon atmosphere. The solution was concentrated under reduced pressure. The black powder was characterized by:
TEM: Nanoparticles of 1.3±0.23nm of mean diameter, distributed only onto the support.
^{1}H solid-state NMR (500Hz, δ in ppm): 0.1, 0.8 (SiCH$_2$CH(CH$_3$)$_2$), 2.1 (alkyl-H), 7.2 (Ar- H).
^{31}P CP-MAS solid-state NMR (500Hz): δ (22.4, 41.0, 60.3 ppm).

*Synthesis of rhodium nanoparticles **Rh45** stabilized by 4-(diphenylphosphino)phenol **45***

In a typical procedure, the [Rh(η^3-(C$_3$H$_5$)$_3$] (0.346 g, 0,28 mmol) was placed into a Fischer-Porter reactor at -110ºC (acetone/ N2 bath) in 342 ml of dry and deoxygenated (using freeze-pump-thaw techniques) THF in the presence of 4- (diphenylphosphino)phenol ligand (0.180g, 0.4 equiv.). The Fischer-Porter reactor was then pressurized under 6 bar of H$_2$ and stirred for 30 minutes at room temperature. The solution was then heated to 60ºC and stirred at this temperature during 24 h. The initial colourless solution became black after 1h. A small amount (5 drops approx.) of the solution

was deposited under argon atmosphere on a carbon-covered copper grid for transmission electron microscopy analysis (TEM). The rest of the solution was concentrated under reduced pressure. Precipitation and washing with pentane (3 x 15ml) was then carried out, obtaining a black precipitate. The pentane washings were analyzed by NMR spectroscopy and GC-MS.

TEM: Nanoparticles of 1.77±0.33nm of mean diameter, sponge-like morphology.

^{1}H solid-state NMR (500Hz, δ in ppm): (0.2, 1.0, 1.5, 3.4, (6.4, 6.7, 7.4) (Ar-H), 8.8 (OH).

^{31}P CP-MAS solid-state NMR (500Hz): δ (29.1, 37.6 ppm).

Anchoring of rhodium nanoparticles stabilised by 4-(diphenylphosphino)phenol into the [(≡SiO)$_2$AliBu.(Et$_2$O)] 51

Using the double Schlenk technique, [(≡SiO)$_2$Al*i*Bu.(Et$_2$O)] (0.4g) was treated with the 3% in weight of NPs **Rh45** (0.032g) in diethyl ether (10ml) for 16h at room temperature. After repeated washings with diethyl ether (10ml), followed by evacuation of the volatile under high vacuum (10^{-5} mmHg), the supported nanoparticles onto the modified silica were obtained as a grey powder.

Phase gas analysis by GC: 0.2 *i*BuH/Al.

TEM: Nanoparticles of *ca*. 2nm of mean diameter, distributed only onto the support.

^{1}H solid-state NMR (500Hz, δ in ppm): (-0.2, 0.9, 1.3, 1.8, 3.8, 7.2 (Ar-H).

^{31}P CP-MAS solid-state NMR (500Hz, δ in ppm): (41 ppm).

5.5 References

[1] J. A. Anderson, M. Fernández Garcia, *Supported metals in catalysis*, Imperial college Press, London, **2005**.

[2] *Pure Appl. Chem*., **1976**, *46*, 71-90.

[3] C.-J. Jia, F. Schüth, *Phys. Chem. Chem. Phys*. **2011**, *13*, 2457- 2487.

[4] a) C. Berger- Karin, M. Sebek, M-M. Pohl, U. Bentrup, V. A. Kondratengo, N. Steinfeldt, E. Kondratenko, *ChemCatChem*, **2012**, *4*, 1368-1375, b) A. Adamczyk, Y. Xu, B. Walaszek, F. Roelofs, T. Pery, K. Pelzer, K. Philippor, B. Chaudret, H.-H. Limbach, H. Breitzke, G. Buntkowsky, *Top. Catal.* **2008**, *48*, 75-83, c) C. Hubert, E. Guyonnet Bilé, A. Denicourt- Nowicki, A. Roucoux, *Green. Chem*. **2011**, *13*, 1766- 1771. d) H-B. Pan, M. Wai., *J. Phys. Chem*. **2010**, *114*, 11364-11369.

[5] J.- M. Basset, R. Psaro, D. Roberto, R. Ugo, *Modern Surface Organometallic Chemistry*, Wiley- VCH, Weinheim, **2009**, pp. 1-697.

[6] J. P. Candy, B. Didillon, E. L. Smith, T. B. Shay, J. M. Basset, *J. Mol. Catal*. **1994**, *86*, 179-204.

[7] D. Astruc (eds), Nanoparticles and Catalysis, Wiley-VCH, Weinheim, **2007**.

[8] K. Pelzer, B. Laleu, F. Lefebvre, K. Philippot, B. Chaudret, J. P. Candy, J. M. Basset, *Chem. Mater*. **2004**, *16*, 4937- 4941.

[9] Julian R. H. Ross, *Heterogeneous catalysis, Fundamentals and application*, Elsevier, Amsterdam, **2012**.

[10] C. Copéret, M. Chabanas, R. P. Saint- Arroman, J.-M. Basset, *Angew. Chem. Int. Ed*. **2003**, *42*, 156-181.

[11] N. Popoff, J. Espinas, J. Pelletier, B. Macqueron, K. C. Szeto, O. Boyron, c. Boisson, I. del Rosal, L. Maron, A. De Mallmann, R. M. Gauvin, M. Taoufik, *Chem. Eur. J*. **2013**, *19*, 964-973.

[12] Legrand, A. P. (eds.), The Surface Properties of Silicas, Wiley- VCH, Chichester, **1998**.

[13] J. P. Thielemann, F. Girgsdies, R. Schlögl, C. Hess, *Beilstein J. Nanotechnol*., **2011**, *2*, 110-118.

[14] a) B. Rhers, A. Salameh, A. Baudoin, E. A. Quadrelli, M. Taoufik, C. Copéret, F. Lefebvre, J.-M. Basset, X. Solants- Monfort, O. Eisenstein, W. W. Lukens, L. Pia H. Lopez, A. Sinha, R. Schrock, *Organometallics*, **2006**, *25*, 3554-3557; b) E. Mazoyer, N. Merle, A. de Mallmann, J.-M. Basset, E. Berrier, L. Delevoye, J.-F. Paul, C. P. Nicholas, R. M. Gauvin, M. Taoufik, *Chem. Commun*. **2010**, *46*, 8944-8946; c) E. Le Roux, M. Chabanas, A. Baudoin, A. de Mallmann, C. Copéret, E. A. Quadrelli, J. Thivolle- Cazat, J.- M. Basset, W. Lukens, A. Lesage, L. Emsley, G. J. Sunley, *J. Am. Chem. Soc*. **2004**, *126*, 13391-13399; d) M. Chabanas, A. Baudoin, C. Copéret, J.- M. Basset, W. Lukens, A. Lesage, S. Hediger, L. Emsley, *J. Am. Chem. Soc*. **2003**, *125*, 492-504.

[15] J.R. Severn, J.C. Chadwick, R. Duchateau, N. Friederichs, *Chem. Rev*. **2005**, *105*, 4073-147. H. Schneider, G.T Puchta, F.A.R Kaul, G. Raudaschl-Sieber, F. Lefebvre, G. Saggio, D. Mihalios, W.A. Herrmann, J.M. Basset, *J Mol Catal A: Chem*. **2001**, *170*, 127-141.

[16] Xiang, S., Zhang, Y., Xin, Q. and Li, C., *Chem. Commun*. **2002**, 2696-2697.

[17] K. B. Klepper, O. Nilsen and H. Fjellvåg, *Dalton Trans.,* **2010**, *39*, 11628-11635.

[18] J. Pelletier, J. Espinas, N. Vu, S. Norsic, A. Baudoin, L- Delevoye, J. Trébosc, E. Le Roux, C. Santini, J.- M. Basset, R. M. Gauvin, M. Taoufik, *Chem. Commun,* **2011**, *47*, 2979-2981.

[19] R. Anwander, C. Palm, O. Groeger, G. Engelhardt, *Organometallics*, **1998**, *17*, 2027-2036.

[20] R. Benn, E. Janssen, H. Lehmkuhl, A. Rufinska, *J. Organomet. Chem*. **1987**, *333*, 155-168.

[21] K. Weichert, B. Carlson, H. Reinke, C. Kremper, *Dalton Trans*. **2010**, *39*, 11513-11515.

[22] N. Popoff, J. Espinas, J. Pelletier, K. C. Szeto, J. Thivolle- Cazat, L. Delevoye, R. M. Gauvin, M. Taoufik, *ChemCatChem*, **2013**, *5*, 1971-1977.

[23] H. Zhang, J. Sun, D. Ma, G. Weinberg, D.S. Su, X. Bao, *J. Phys. Chem. B*, **2006**, *110*, 25908-25915.

[24] J. Pelletier, J. Espinas, N. Vu, S. Norsic, A. Baudoin, L- Delevoye, J. Trébosc, E. Le Roux, C. Santini, J.- M. Basset, R. M. Gauvin, M. Taoufik, *Chem. Commun.* **2011**, *47*, 2979-2981.

[25] M. G. L. Petrucci, A. K. Kakkar, *Chem. Mater*. **1999**, *11*, 269-276.

[26] H. Staub, I. Del Rosal, L. Maron, F. Kleitz, F.- G. Fontaine, *J. Phys. Chem. C*. **2012**, *116*, 25919-25927.

[27] S. Sisodiya, A. Lazar, S. Shylesh, L. Wang, W. R. Thiel, A. P. Singh, *Catalysis communications*, **2012**, *25*, 22-27.

[28] C. R. Hilliard, N. Bhuvanesh, J. A. Gladysz, J. Blümel, *Dalton. Trans*. **2012**, *41*, 1742-1754.

[29] H.C. Foley, S. J. DeCanio, K. D. Tau, K. J. Chao, J. H. Onuferko, C. Dybowski, B. C. Gates, *J. Am. Chem. Soc*. **1983**, *105*, 3074-3082.

[30] P. Dufor, C. Houtman, C. C. Santini, J.- M. Basset, *J. of Mol. Catal*. **1992**, *77*, 257-272.

[31] K. D. John, K. V. Salazar, B. L. Scott, R. T. Baker, A. P. Sattelberger, *Organometallics*, **2001**, *20*, 296-304.

[32] G. A. Slough, J. R. Ashbaugh and L. A. Zannoni, *Organometallics*, **1994**, *13*, 3587-3593.

[33] J. P. Wey, W. C. Neely, S. D. Worley, J. Phys. Chem. **1991**, *95*, 8881-8886.

[34] K. Pelzer, O. Vidoni, K. Philippot, B. Chaudret, V. Collière, *Adv. Funct. Mater*. **2003**, *13*, 118-126.

[35] D. González-Gálvez, P. Nolis, K. Philippot, B. Chaudret, P. W. N. M. van Leeuwen, *ACS Catal*. **2012**, *2*, 317–321.

[36] T. Gutman, E. Bonnefille, H. Breitzke, P.-J. Debouttière, K. Philippot, R. Poteau, G. Buntkowsky, B. Chaudret, *Phys. Chem. Chem. Phys*. **2013**, *15*, 17383-17394.

[37] D. Han, X. Li, H. Zhang, Z. Liu, G. Hu, C. Li, *J. of mol. Cat. A: Chem*. **2008**, *283*, 15-22.

Chapter 6.

Conclusions/ Summary

6.1 General conclusions

Two series of rhodium nanoparticles have been successfully synthesised using mono- and bidentate phosphines and phosphites **1**-**8** as stabilisers. The properties of these ligands were shown to influence the catalytic performance of these NPs in the hydrogenation of arenes and aromatic ketones and allow their grafting onto modified silica.

Detailed conclusions:
- The series of Rh-NPs **Rh1-Rh8** were successfully synthesised by decomposition of the organometallic precursor [Rh(η^3-C$_3$H$_5$)$_3$] under H$_2$ pressure and in THF as the solvent.
- All the nanoparticles synthesized in this work exhibited a small diameter (<2 nm) with narrow size distributions, spherical shape and good dispersion. These crystalline materials present a fcc structure and are mainly composed of Rh in the zero valent state.
- Two families of ligands, namely phosphines and phosphites, were used as stabilizers for these NPs. The ligands triphenylphosphine **1** and triphenylphosphite **5** were used as models for these two series. The amount of stabilizer was varied during the synthesis between 0.1 to 0.6 equivalent of ligand per Rh but no variation in size nor shape were observed when this parameter was varied. Increasing the equivalents of stabilising ligand **5** during the synthesis of the NPs increases the ligand coverage on **Rh5**. However, in the case of ligand **1**, no clear correlation could be observed. In both cases, a higher degree of hydrogenation of the stabilising ligand was observed at low ligand to Rh ratio during the synthesis.
- Nanoparticles bearing the less sterically demanding stabilising ligands PMe$_3$ and P(OMe)$_3$ presented a higher ligand coverage.
- Hydride titration experiments were performed on **Rh1** and **Rh5**, revealing a higher hydride coverage in the case of the phosphine

stabilized **Rh1** (*ca*. 0.8 H/Rh$_s$) than for **Rh5** (*ca*. 0.3H/Rh$_s$). Analysis of the surface of these nanoparticles by infra red spectroscopy revealed the presence of a band at 1950-2000 cm^{-1}, that was attributed to Rh-H stretching based on the analysis of the spectra of the NPs obtained after hydride titration and of these NPs synthesised under D$_2$.

- Using CO adsorption/Infra-red experiments three types of carbonyl signals were observed: bridging (1800-1900 cm^{-1}), terminal (1950-2070 cm^{-1}) and geminal Rh(CO)$_2$ (*ca*. 2100 and 2020 cm^{-1}).

- For the PPh$_3$ system **Rh1**, at higher ligand/Rh ratio, the coordination of the ligand **1** takes also place on the faces of these NPs and the formation of geminal Rh(CO)$_2$ site on edges of the NPs is favoured. The formation of these species is also favoured when the sample is exposed to higher CO pressure (40 bar) or during long reaction times.

- For the systems **Rh5**, at high ligand/Rh ratio, the sites on the edges are occupied by the ligand, similarly to the NPs **Rh3** and **Rh7**, stabilized by the small ligands PMe$_3$ **3** and P(OMe)$_3$ **7**.

- In the ***hydrogenation of arenes***, the hydrogenation of disubstituted arenes **20a-f** was investigated using soluble Rh- NPs as catalysts. Only the triphenylphosphite **5** stabilised nanoparticles **Rh5** were inactive for this reaction.

- The Rh-NPs stabilised by phosphine ligands displayed higher activity than those bearing phosphite ligands and within the series **Rh1-Rh4**, those stabilised by the bidentate ligand dppb were the less active.

- Partially hydrogenated products were detected in most cases and the catalyst **Rh8** stabilised by the diphosphite **8** provided the highest selectivity to this product, up to 39% for *m*- methylanisole **20e**.

- With styrene as substrate, high TOFs up to 13039h^{-1} at room temperature was measured with system **Rh8**. The system **Rh5** was an active catalyst in this reaction and its ligand coverage revealed

critical to either transform this substrate into ethylbenzene and/or ethylcyclohexane.

- Toluene and benzene were successfully hydrogenated using the soluble nanoparticles as catalysts. However no significant amounts of partially hydrogenated products were detected using these substrates.

- The ***comparative study of aryl ketones reduction using Ru and Rh nanoparticles*** was carried out. Acetophenone **31**, was shown to adopt a singular substrate behaviour and two types of substrates have to be distinguished:
  - o with the aryl ketones are not conjugated (**35-36**), a general preference for arene reduction is observed and increases when the number of methylene groups between the arene ring and the keto group increases.
  - o for the acetophenone derivatives **37-42**, the selectivity trends observed were distinct, but were general independently of the substituents present on the phenyl ring.
- In general, it can be considered that in the case of rhodium NPs, the coordination of arene dominates the interaction of the substrate with the nanoparticle, while the coordination of the ketone group with the nanoparticle was not evidenced. The case of acetophenone derivatives is singular, since despite coordination to the nanoparticle takes place through the aromatic ring, the carbonyl group remains at a position very favorable for its reduction.
- For Ru NPs, both arene and ketone moieties coordinate to the NPs surface in a competitive way. The selectivity is strongly affected by the steric hindrance in the ligand and in the substrate, which in both cases increases the ketone reduction.

- two methodologies for the ***anchoring of Rh-NPs onto silica*** were investigated:

  o Rh-NPs stabilised by a mixture of PPh$_3$ **1** and the phosphine modified silica support were successfully synthesised. TEM microscopy revealed strong interaction between the nanoparticles and the support.

  o the colloidal Rh- NPs stabilised by P(Ph)$_2$(C$_6$H$_5$OH) **45** were first synthesised and subsequently anchored onto the [(≡SiO)$_2$Al*i*Bu.(Et$_2$O)] surface.

6.2 Summary

Metal nanoparticles are currently an area of intense scientific research, due to a wide variety of potential applications in biomedical, optical, electronic and catalytic fields. In catalysis, soluble nanoclusters are considered at the frontier between homogeneous and heterogeneous catalysts since they could present the advantages of both: high selectivity by modulation of their surface and catalyst recovery and reuse.

Soluble nanoparticles exhibit several advantages such as higher surfaces areas that confer higher activity and avoid internal mass transfer limitations. Moreover, these systems are freely rotational and three-dimensional in reaction systems. Therefore, their metal- surface active sites are much more accessible for the reactant molecules, which enhance their activity.

Transition-metal nanoclusters are only kinetically stable, since the thermodynamic minimum is the bulk metal. There is therefore a tendency for aggregation which leads to the loss of the properties associated with the colloidal state of these metallic particles. The use of a stabilising agent is required and opens a wide range of possibilities. Polymers, surfactants or ionic liquids are used for instance as stabilisers.

Phosphorus based ligands such as phosphines and phosphites are extensively used in homogeneous catalysis due to their broad coordination chemistry with transition metals and the possibility to fine-tune the electronic and steric properties of the catalysts through structural modifications of the ligands to obtain high activity and selectivity in catalytic processes. In the last decade, these ligands were also shown to efficiently stabilise metal nanoparticles that are catalysts in several catalytic reactions. However, to date, the fine tuning of the properties of this type of catalysts to achieve specific selectivities remains a challenge.

These systems could be applied as catalysts for several transformations such as C-C couplings, oxidations or hydrogenation reactions. The nature of

the real catalyst when dealing with soluble nanoparticles could be in some cases controversial and could required parallel studies.

This thesis focus on the synthesis and characterisation of rhodium nanoparticles stabilised with P-based ligands and their application in selective hydrogenation reactions. A preliminary study on the anchor of these systems onto modified silica will also be explored.

The rhodium nanoparticles were stabilised using mono and bidentate phosphines and phosphites. Triphenylphosphine **1** and triphenylphosphite **5** were used as model for each family. In general terms, the most important difference between these two systems was the observation of ligand hydrogenation during the synthesis for the phosphine stabilised nanoparticles that was not detected in the case of **Rh5** system.

The amount of stabilising ligand during the synthesis was explored for these stabilisers. No direct correlation between the amount of stabiliser used to synthesised the nanoparticles and the content revealed by TGA was observed for the phosphine systems, while the phosphite systems followed the coherent result of more stabilising ligand at the surface of the nanoparticles with more stabilised used during the synthesis.

Moreover, the steric and electronic properties of the ligands were also studied. For that purpose, tricyclohexyl **2** and trimethylphosphine **3** were employed for the phosphine family and triorthotertbutyl **6** and trimethylphosphite **7** for the phosphites. More crowded systems at the surface were observed using the less sterical demand stabilisers.

The hapticity of the ligands was also studied by the use of bidentate ligands. The expected bidentate stabilisation was observed using dppb **4** as stabilising ligand for the phosphine family. However, both triphenylphosphite **5** and the diphosphite **8** could be stabilising the nanoparticles in a monodentate way.

Rhodium nanoparticles stabilised with the PVP K-90 polymer and with the mixture of solvents THF/MeOH were also synthesised for comparative purposes.

IR spectroscopy was also applied to study the surface of the previously synthesised nanoparticles. Moreover, carbon monoxide was adsorbed onto the surface of these systems try to gain information of the nature and position of the stabilising ligands by correlation with the carbonyls observed and consequently of the active sites of the nanoparticles.

The different P- coverage modulated with the different ligands used a stabilising ligands seems to mainly affect the faces of the NPs, as large shifts were observed in the bridging CO region. Two distinct CO environments were detected for both bridging and terminal ligands, which indicates two distinct terminal positions for COs and two surroundings for these ligands on the faces of the NPs. The use of small ligands resulted in high mobility of the CO ligands at the NPs surface and more different active sites and consequently different CO adsorptions were observed with more sterical demanding ligands as stabilisers.

These systems were applied in chapter 3 as catalysts for the hydrogenation of arenes. In a first stage, the disubstituted arenes **20a-f** were used as substrate. The nature and position of the substrates was evaluated using *ortho*, *meta* and *para* xylenes and methylanisoles. System **Rh5** stabilised with triphenylphosphite **5** was not active, maybe due to the crowding of the surface that could inhibit the substrate approach. Higher activities were observed using the phosphine stabilised systems compared to the phosphites. However, system **Rh4** stabilised by dppb **4** was the less active of the series. Partially hydrogenated products were observed with significant amounts in the reactions carried out with system **Rh8** stabilised with the diphosphite 8 as stabiliser. Reactions parameters such as the temperature, pressure, solvent or the use of additives were studied without improving of the amount of these products. No clear effect of the nature of the stabiliser on the cis/ trans selectivity was observed for these substrates.

The substitution of the substrate was also studied. High activities at room temperature and partially hydrogenated products were observed using styrene as substrate. Finally, toluene and benzene were employed as substrate detecting higher activities using the rhodium nanoparticles as

catalysts while no significant amounts of the partially hydrogenated products were detected.

In chapter 4 the hydrogenation of aromatic ketones using the soluble nanoparticles as catalysts were explored. The P-based nanoparticles **Rh1**-**Rh8** were used with acetophenone as model substrate. Moreover, the results obtained for mono and bidentate phosphines stabilised nanoparticles **Rh1** and **Rh4** were compared with the analogous ruthenium systems.

The reduction of non-conjugated aryl ketones and the influence of the alkyl chain length between the phenyl and the ketone and different substituents in the alkyl and phenyl moieties was also studied in this work.

In general, it can be considered that in the case of rhodium NPs, the coordination of arene dominates the interaction of the substrate with the nanoparticle, while the coordination of the ketone group with the nanoparticle was not evidenced, and for alkyl ketones and aromatic compounds containing a carbonyl group far from the ring, the carbonyl remains unaltered and only the aromatic ring is reduced.

The case of acetophenone derivatives is singular, since despite coordination to the nanoparticle takes place through the aromatic ring, the carbonyl group remains at a position very favorable for its reduction, in such a way that it is hydrogenated faster than the arene moiety. The selectivity of this process is scarcely affected by substitution in the alkyl or arene groups, and only the substitution in *para* position of the aromatic ring completely drives the reaction towards the reduction of ketone.

As a whole, this study using two similar metal nanoparticles of similar sizes and bearing two ligands of very similar electronic and steric effects but with different dissociation abilities, leads to different results in terms of activities, selectivities and even capacity to carry out a given reaction, here hydrogenolysis. This therefore demonstrates the interest for tayloring the composition and surface of these organometallic nanoparticles in order to modify their reactivity, in a way comparable to what is commonly achieved for molecular complexes.

The last chapter of this thesis explored the anchor of the rhodium nanoparticles onto silica surface. In a first study, silica support was modified with triisobutyl groups following reported procedures. Moreover, a phosphine ligand was anchored to this modified silica to adapt this support to the methodology employed in this thesis. The anchoring of a rhodium complex to the silica before and after modification and the reactivity under hydrogen was also explored. In both cases, after exposure to hydrogen pressure the solid turns black. In the first case, with the silica without modification the formation of nanoparticles without control was checked by TEM spectroscopy.

The nanoparticles were anchored using two different approaches. In a first study, the triphenylphosphine stabilised **Rh1** nanoparticles were synthesised in situ in presence of the phosphine modified silica. The characterisation techniques revealed the successful anchoring of the systems and a strong interaction between the nanoparticles and the support as no free colloids were detected. Moreover a homogeneous distribution of the nanoparticles onto the support was obtained using this approach.

In order to gain information of the amount of nanoparticles anchored to the support, in a second study, nanoparticles stabilised with 4-(diphenylphosphino)phenol **45** were previously synthesised and later anchored to the isobutyl modified silica **44**. The evacuation of the isobutane groups from the surface provide information of the quantity of nanoparticles anchored.

Both approaches lead with the successfully anchoring of nanoparticles onto the support, while more amount of nanoparticles should be used in further studies for the second aproximation.

These studies formed promising systems that should be used in catalytic reactions in order to study their reuse and recycle.

Resum

Les nanopartícules metàl·liques es troben dins d'una àrea de recerca de gran interés, degut a la gran varietat d'aplicacions d'aquestes en biomedicina, òptica, electrònica i en el camp de la catàlisis. En aquest àmbit, els nanoclusters solubles estan considerats a la frontera entre la catàlisi homogènia i heterogènia ja que presenten els avantatges d'ambdues: una alta selectivitat degut a la modulació de la seva superfície i la possibilitat de ser reciclats i reutilitzats.

Les nanopartícules solubles exhibeixen molts avantatges, entre elles es destaquen la seva gran superfície que els confereix elevada activitat i evita les limitacions de transferències de massa.

En la síntesi dels nanoclusters amb metalls de transició es requereix l'ús d'un agent estabilitzant, el qual obre un gran ventall the possibilitats per al control de les propietats d'aquestes nanopartícules. Polímers, surfactants o lligands s'utilitzen per exemple com estabilitzants. Lligands que contenen fòsfor, com fosfines i fosfits, s'utilitzen àmpliament en catàlisi homogènia degut a la seva habilitat coordinant amb metalls de transició. A més, ofereixen la possibilitat de modular les propietats estereoelectròniques del catalitzador a través de modificacions estructurals dels lligands per així obtenir activitats i selectivitats significants en processos catalítics. En la passada dècada, aquests lligands han demostrat estabilitzar eficientment nanopartícules metàl·liques que s'utilitzen com a catalitzadors en diverses transformacions. No obstant, el modulatge precís de les propietats d'aquest tipus de catalitzadors per aconseguir una bona selectivitat esdevè encara un repte.

Aquesta tesis es basa en la síntesis i la caracterització de nanopartícules de rodi estabilitzades amb lligands fosforats i la seva aplicació en reacciond d'hidrogenació selectiva. Adicionalment, s'ha dut a terme un estudi preliminar sobre l'anclatge d'aquests sistemes en una silica modificada.

Les nanopartícules de rodi van ser estabilitzades mitjançant fosfines i fosfits mono i bidentats. Trifenilfosfina i trifenilfosfit van ser utilitzats com a

models. En termes generals, els lligands de tipus fosfina, que no són tant coordinants, tenen una activitat catalítica diferent.

Durant la síntesis, es va explorar la variació de la quantitat d'estabilitzant va ser explorada. En el cas dels sistemes de tipus fosfines no es va observar una coorrelació directe entre la quantitat d'estabilitzant i el contingut final de lligand determinat per TGA. Per altra banda, en el cas dels fosfits si que es va trobar més contingut de lligand estabilitzant, quan es va augmentar la quantitat d'aquest durant la síntesis.

D'altra banda, l'efecte de les propietats estereoelectròniques dels lligands va ser variada i relacionada amb la estructura i els resultats catalítics d'aquestes nanopartícules. Amb aquest objectiu, triciclohexil i trimetilfosfina també es van utilitzar dins de la familia de les fosfines, mentre que triortotertbutyl i trimetilfosfit es van utilitzar per completar la familia dels fosfits. En termes generals, utilitzant estabilitzants menys impedits es van obtenir sistemes amb superfícies més recobertes.

L'ús de lligands bidentats com ara la dppb van produir activitats catalítiques més baixes que els seus respectius monodentats. Això, va ser atribuït a la seva major coordinació i l'augment de l'impediment estèric induït a la superfície de la nanopartícula.

Les nanopartícules de rodi estabilitzades amb el polímer PVP K-90 i en la barreja de disolvents THF/MeOH van ser sintetitzades l'objectiu de poder comparar.

L'estudi de l'adsorbció de CO per espectroscopia IR es va utilitzar per l'estudi de la superfície de les nanopartícules prèviament sintetitzades i més concretament, per tenir informació sobre la posició dels lligands estabilitzants. Es va veure, que les propietats dels lligands afectaven principalment a les cares de les nanopartícules, ja que es van observar desplaçaments més significatius en la zona de vibració dels carbonils pont. Dos entorns diferents es van detectar pels carbonils ponts i terminals, que indica dos posicions de CO terminals i dos entorns diferents pels lligands situats a les cares de les nanopartícules.

Al capítol 3, es descriu l'aplicació d'aquests sistemes com a catalitzadors per la hidrogenació d'arens. En primer lloc, els arens disubstituits en orto, meta i para xilens i metilanisoles es van utilitzar com a substrats. En termes generals, es van observar activitats més elevades utilitzant sistemes estabilitzats amb fosfina en comparació amb els estabilitzats amb fosfit. En aquestes reaccions, fou destacable que el sistema estabilitzat amb trifenilfosfit no era actiu, el que es va atribuir a l'impediment de la superficie amb aquest lligand. En aquestes reaccions es van obtenir productes d'hidrogenació parcial en quantitats significatives, més concretament quan les reaccions es van dur a terme amb el sistema estabilitzat amb el difosfit. Es va fer un estudi també dels paràmetres de reacció, com temperatura, presió, disolvent o l'ús d'aditius. Tot i així, no es poden extreure conclusions clares de quins són els paràmetres que afecten a la selectivitat cis/ trans durant la hidrogenació.

Utilitzant estirè com a substrat es van obtenir, activitats considerables a temperatura ambient, així com selectivitats apreciables per als productes d'hidrogenació parcial. Finalment, es van usar toluè i benzè com a substrats, obtenint activitats catalítiques considerables. Tot i així, per aquests substrats no es van detectar quantitats significatives de productes d'hidrogenació parcial.

En el capítol 4, es descriu la hidrogenació de cetones aromàtiques emprant les nanopartícules solubles com a catalitzadors. Les nanopartícules que contenen fósfor es van utilitzar amb acetofenona com a model de substrat. També es va estudiar la reducció d'aril cetones no conjugades i la influència de la mida de la cadena alquílica entre el fenil i la cetona, i la presència de diferents substituents en els grups alquil i fenil. En aquesta part, els resultats obtinguts per les nanopartícules estabilitzades amb fosfines mono i bidentades, es van comparar amb sistemes anàlegs de ruteni (aquest estudi utilitzant Ru-NPs forma part de la tesi doctorad d'Emma Bressó Femenia).

En general, es pot considerar que en el cas de les nanopartícules de rodi la coordinació d'arens domina en front de la interacció del substrat amb la

nanopartícula. Per altra banda no s'evidencia la coordinació de la cetona a la nanopartícula, i per cetones alquíliques i aromàtiques que contenen un grup carbonil allunyat de l'anell, aquest carbonil roman inalterat i es redueix únicament l'anell aromàtic.

A grans trets, aquest estudi mostra que les nanopartícules de rodi i ruteni de mides similars i en presència de lligands senzills amb diferent habilitats dissociatives donen lloc a resultats diferents en termes d'activitat, selectivitat i fins i tot de capacitat de dur a terme una reacció específica, en aquest cas, hidrogenòlisis.

En el capítol 5 d'aquesta tesi s'explora l'anclatge de les nanopartícules de rodi en superfícies modificades de silica. En la primera part, el suport de sílica es va modificar amb grups triisobutil seguint procediments ja reportats. El lligand fosfina 4-(difenilfosfinofenol) que conté un grup fenol, es va anclar en silica prèviament modificada per facilitar la interacció del catalitzador amb el suport. Les nanoparticules van ser anclades utilitzant diferents aproximacions. En un primer estudi les nanopartícules estabilitzades amb trifenilfofina van ser sintetitzades in situ, en presencia de la silica modificada amb fosfina. La seva caracterització va evidenciar l'èxit de l'anclatge dels sistemes i una forta interacció entre les nanopartícules i el suport, ja que no es van detectar colloides en suspensió.

En la segona part de l'estudi, les nanopartícules de rodi estabilitzades amb 4-(difenilfosfinofenol) van ser primerament sintetitzades i més endavant anclades en la silica modificada amb isobutil. Les dues aproximacions van donar lloc a un bon anclatge de les nanopartícules de rodi en aquest suport.

Chapter 7.

Appendix

7.1 Congresses and Scientific meetings

2010

- ICIQ- Summer school 2010, Tarragona, Spain.

Assistance

- XXVIII Reunión del grupo especializado química organometálica (GEQO) Huelva, Spain.

Poster contribution: *"Hydrogenation of arenes using Rh- nanoparticles as catalysts."*

- 2nd China- Spain Bilateral Symposium on Catalysis, Tarragona, Spain.

Poster contribution: *"Hydrogenation of arenes using Rh- Nanoparticles as catalysts."*

2011

- EUCOMC2011- Toulouse, France.

Poster contribution: *"Hydrogenation of disubstituted arenes using Rh-nanoparticles stabilized by P-donor ligands as catalysts."*

- GT3: Nanocatalysis, INTERREG IVB SUDOE TRAIN2, Toulouse, France.

Assistance

2012

- VII Trobada Joves investigadors dels països catalans, Mallorca, Spain.

Oral communication: "Hidrogenació d'arens amb nanopartícules de Rh com a catalitzadors.

- CEICS Nobel Campus, Chemistry for life, Tarragona, Spain.

Poster contribution and oral communication: *"Design and synthesis of selective hydrogenation Rh- nanocatalysts bearing P- based stabilisers."*

- XXX Reunión del grupo especializado en química organometálica GEQO Castellón, Spain.

Poster contribution: *"Rhodium nanoparticles stabilised by P-based ligands: structurals modifications and application in selective hydrogenations."*

- XVIII ISHC- Toulouse, France.

Poster contribution: *"Rhodium nanoparticles stabilized by P- based ligands: synthesis, characterization and application in selective hydrogenations."*

2013
- 20th EuCheMS- St Andrews, United Kingdom.

Poster contribution: *"Ligand effects in the rhodium nanoparticles catalysed selective hydrogenation."*

- XXXIV Reunión Bienal Química Santander 2013

Poster contribution: Selective hydrogenation reactions with rhodium nanoparticles: ligand effects.

2014
- VI Journées Franco-catalanes de Chimie Moleculaire, Toulouse, France.

Assistance

- 7th CaRLa Winter School 2014, Heidelberg, Germany.

Poster contribution and oral communication: *"Ligand effects in the rhodium nanoparticles catalysed selective hydrogenation."*

7.2 Stages

- May 2010: short training stage in CAT Catalytic Centre in Aachen, Germany.

- June 2011: short training stage in Institut National des sciences appliqués de Toulouse, France.

- September- December 2012: stage in École Supérieure de chimie physique électronique de Lyon, France.

7.3 Publications based on the content of the thesis

- J. LLop Castelbou, A. Gual, E. Mercadé, C. Claver, C. Godard, **"Ligand effect in the Rh- NP catalysed partial hydrogenation of substituted arenes"**, *Catal. Sci. Technol*., **2013**, *3*, 2828- 2833.

- J. Llop Castelbou, E. Bresó-Femenia, P. Blondeau, B. Chaudret, S. Castillón, C. Claver, C. Godard, , **"Towards the understanding of structure- selectivity relationships in the hydrogenation of aromatic ketones catalysed by organometallic NPs."** *Manuscript in preparation.*

- J. Llop Castelbou, J. A. Delgado, F. Martinez Espinar, C. Claver, C. Godard, **"Selective hydrogenation using metallic nanoparticles"** *Review manuscript in preparation.*